International Atomic Energy Agency

INDC(NDS)-179/G

INDC INTERNATIONAL NUCLEAR DATA COMMITTEE

NUCLEAR DATA FOR RADIATION DAMAGE ESTIMATES FOR REACTOR STRUCTURAL MATERIALS

Proceedings of an IAEA Consultants' Meeting on
Nuclear Data for Radiation Damage Estimates for
Reactor Structural Materials, held in
Santa Fe, New Mexico, USA, 20-22 May 1985

Edited by V. Piksaikin

June 1986

IAEA NUCLEAR DATA SECTION, WAGRAMERSTRASSE 5, A-1400 VIENNA

INDC(NDS)-179/G

NUCLEAR DATA FOR RADIATION DAMAGE ESTIMATES FOR REACTOR STRUCTURAL MATERIALS

Proceedings of an IAEA Consultants' Meeting on
Nuclear Data for Radiation Damage Estimates for
Reactor Structural Materials, held in
Santa Fe, New Mexico, USA, 20-22 May 1985

Edited by V. Piksaikin

June 1986

Reproduced by the IAEA in Austria
June 1986

86-02549

ABSTRACT

The IAEA Consultants' Meeting on Nuclear Data for Radiation Damage Estimates for Reactor Structural Materials was convened by the IAEA Nuclear Data Section in Santa Fe, New Mexico, USA from 20-22 May 1985. The meeting was attended by 17 participants from 10 countries and 2 international organizations.

The main objectives of the meeting were to review the status of displacement cross sections and the requirements for nuclear data needed for radiation damage estimates in reactor structural materials, and to develop recommendations for future activities in this field.

The proposed publication contains the text of all the papers prepared especially for this meeting including the conclusions and recommendations worked out during the meeting.

CONTENTS

CONCLUSIONS AND RECOMMENDATIONS

The Conclusions and Recommendations of the above IAEA Consultant's meeting consist of two separate reports developed by the participants of the two workshops which took place during the meeting:

1. Workshop on Radiation Damage and Gas Production Data

2. Workshop on Dosimetry Data and Transport Calculations

Workshop 1. Radiation Damage and Gas Production Data

Chairman: R. Dierckx

1. It is recommended, for the time being, that radiation exposure be expressed in displacements per atom (dpa) (although other parameters such as fluence should also be given). Dpa should be calculated

   1) for iron in neutron measurements by using the energy dependent displacement cross section as specified in ASTM standard E 693-79;

   2) in other cases by using the energy dependent displacement cross section as calculated as specified in the ASTM-practice and stating the library of the underlying nuclear cross sections and the computer code used to process the data.

   It is noted that further characterizations of the radiation field (such as spectral information and displacement rate) are needed to fully define the environment. However, a specialists' meeting of material scientists should be held to determine whether these measures of neutron exposures are adequate to correlate to important material properties and to propose new models to be used as a standard. In addition, basic studies must continue to help determine a better understanding of the damage process.

2. It is recommended that a Neutron Radiation Damage Nuclear Data File be created having energy dependent cross sections in the 640 group structure following practices stated in recommendation 1 for all major elements which are components of structural materials. The units for these cross sections shall be displacement-barns. The IAEA should consider existing data sets. In the future, researchers needing more basic data should use recoil spectra from evaluations using the ENDF-VI format.

3. It is recommended that the Neutron Radiation Damage Nuclear Data File include hydrogen and helium production cross sections in the 640 group structure for the major elements which are components of structural materials. Also included should be elements having large thermal gas production cross sections as well as reactions involved in multistep reactions such as $^{58}Ni(n,\gamma)^{59}Ni(n,\alpha)^{56}Fe$.

4. It is recommended that documentation of the Neutron Radiation Damage Nuclear Data File shall include comparison with experimental data.

5. It is recommended that the IAEA support the development of damage detectors.

6. It is recognized that better experimental and evaluated nuclear data are needed to support radiation damage assessment. Better experimental and evaluated nuclear data are needed in the future to support radiation damage assessment. The direction of future work should be based on the comparison made in recommendation 4 and on the need by current and future facilities for higher energy data. The need for uncertainty information on nuclear-data based damage parameters is noted.

Workshop 2. Dosimetry Data and Transport Calculations

Chairman: A. Thomas

1. It is recommended that the IAEA circulate a list of known errors and discrepancies in the IRDF data evaluation on a regular basis. The file should be revised as necessary as new evaluations become available.

2. The $^{47}Ti(n,p)^{47}Sc$ and $^{63}Cu(n,\alpha)^{60}Co$ reactions should be re-evaluated in the IRDF file. The $^{93}Nb(n,n')^{93m}Nb$ reaction should also be re-evaluated as new data become available. The $^{59}Co(n,p)^{59}Fe$ and $^{93}Nb(n,\gamma)^{94}Nb$ reactions should be added to the file.

3. The IAEA should support new measurements and evaluations of dosimetry cross sections. In particular, work on the $^{93}Nb(n,n')^{93m}Nb$ reaction is strongly recommended.

4. The IAEA should perform a survey of users of the $^{93}Nb(n,n')^{93m}Nb$ reaction and coordinate and distribute activity standard sources of ^{93m}Nb. For example, this could be done in collaboration with AERE Harwell (UK), CBNM Geel (Belgium), and the Technical Research Centre of Finland.

5. In order to ensure consistency of evaluated neutron cross sections and activity measurements, essential nuclear decay data, isotopic abundances, and selected fission yield data should be included in evaluated dosimetry data files. In particular, this should be implemented in the next version of the IRDF file.

6. There is a strong need to include relevant photonuclear reaction data in evaluated dosimetry data files.

7. The IAEA should make available covariance information for essential benchmark fields including the ^{235}U, ^{252}Cf, CFRMF, and the PCA-LWR simulator.

8. The IAEA should encourage the proper documentation of nuclear data experiments so that covariance information can be obtained. This recommendation is specially important for work done under IAEA research contracts.

9. The IAEA should make available processing codes and data files for dosimetry covariance data. The available codes should be compared to ensure consistency, in a manner similar to the comparison of cross section regrouping codes.

10. This group supports the REAL-84 Exercise and recommends that the IAEA continue to support this project and ensure that it meets the agreed time schedule.

AGENDA AND LIST OF PAPERS

Monday, 20 May 1985

Plenary Session Chairman: L.R. Greenwood

Opening remarks by V. Piksaikin

Radiation Damage

1. Preliminary Damage Production by Primary Recoils of Different Energies
   R. Dierckx
   (oral presentation)

2. SPECTER Computer Code for Radiation Damage Calculations
   L.R. Greenwood

3. Status of Radiation Damage Methods of the Los Alamos Applied Nuclear Science Group
   R.E. MacFarlane
   (oral presentation)

4. Calculated Damage Efficiency for Neutron Spectra
   F.M. Mann
   (oral presentation)

5. Experience with the Use of the $^{93}Nb(n,n')^{93}Nb$ Reaction for Routine Monitoring of Materials Irradiation Experiments
   A.F. Thomas

6. Comparison of Predicted and Measured Charpy NDT Shifts at KRSKO Nuclear Power Plant
   M. Najzer, V. Arnuga, B. Glumac, I. Jencic, I. Kodeli, A. Loose, I. Remec

7. Displacement Model for the Calculation of Radiation Damage
   Jinnan Yu

Gas Production

1. Activation and He-Production in Fusion Reactor Structural Materials, simulated at a Neutron Irradiation Facility at the JRC-ISPRA Cyclotron
   M. Forte, P. Jung, E. Galletti and C. Maranzana

2. He Measurements for the U.S. Fusion Programme
   D.W. Kneff, L.R. Greenwood

Transport Calculations

1. Nuclear Data for High-Energy Neutron Transport and Damage Calculations in Steel
   G. Prillinger

Dosimetry

1. Information on the REAL-84 Exercise
   W.L. Zijp, E.M. Zsolnay and D.E. Cullen

2. Nuclear Data Aspects Encountered in the REAL-80 and REAL-84 Intercomparisons
   H.J. Nolthenius, E.M. Zsolnay, W.L. Zijp, E.J. Szondi

3. On the Influence and Need of Nuclear Data at Relative Standardized Fluence Measurements
   B. Bärs, T. Seren

4. Benchmark Spectra for High Energy Neutron Dosimetry
   R. Dierckx

5. Least-Square Adjustment of a "known" Neutron Spectrum: The Importance of the Covariance Matrix of the Input Spectrum
   W. Mannhart

6. Neutron Dosimetry for Fusion Materials Studies
   L.R. Greenwood

7. Comparison of Two Fine Group Cross-Section Libraries Resulting from the ENDF/B-V Dosimetry File and Gas File (Version 1 and 2)
   H.J. Nolthenius, G.C.H.M. Verhaag

8. Uncertainties and Correlation Data for the ENDF/B-V Dosimetry File (Version 2)
   H.J. Nolthenius, W.L. Zijp

Tuesday, 21 May 1985
morning

Workshop on Radiation Damage and Gas Production (Status, Needs, Recommendations)
Chairman: R. Dierckx

afternoon

Workshop on Dosimetry Data and Transport Calculations (Status, Needs, Recommendations)
Chairman: A. Thomas

Wednesday, 22 May 1985

Formulation of Conclusions and Recommendations of the Meeting

SPECTER Computer Code For Radiation Damage Calculations

L. R. Greenwood
Argonne National Laboratory
Argonne, Illinois 60439 USA

The SPECTER computer code has been developed at Argonne over a number of years to routinely calculate radiation damage parameters for materials irradiations. The code will provide users with spectral-averaged displacement damage, gas production, total energy deposition (Kerma), and recoil atom energy distributions for 38 elements spanning the periodic table. The code is designed with a minimum of user input, basically just the neutron energy spectrum with uncertainties, if available. The computer code has recently been documented in an Argonne report[1] which contains a description of the theory as well as tables and graphs of calculated displacement cross sections. The code is based on the displacement code DISCS [2]. The code has been distributed in the U.S. and Europe and is available to users of the National Magnetic Fusion Energy Computer Center in the U.S. The code can also be obtained from the Radiation Shielding Information Center at Oak Ridge National Laboratory or directly from the author.

SPECTER consists of a master library of group-averaged cross sections for displacement damage, gas production, and total energy deposition. These data are stored in a 100 energy group array up to 20 MeV. Primary recoil atom distributions are further divided into 100 recoil energy groups so that each element has a 100x100 array of recoil distributions. When the user specifies a neutron spectrum, the code performs a spectral-average over the users spectrum and then reports the results. Since only simple averaging is required, the code is quite fast and requires no access to data libraries such as ENDF/B-V [3]. All of the data in the files has been calculated using the basic neutron cross section data in ENDF/B-V.

Users are given several options regarding the types of data which will be reported. Due to the large size of the recoil atom energy distribution files, these data may be omitted if desired. This option greatly reduces the memory required and time to run the code such that calculations can be done on small computers in only a matter of minutes. If recoil energy distributions are desired, then there are also two options, one allowing full distributions for each reaction channel (e g - elastic, inelastic,etc.) and one with only the net atom distribution. Uncertainties in the neutron flux spectrum can also be specified. In this case, the covariance matrices are carried through the calculation in order to provide uncertainties in the calculated damage rates.

Examples of the calculated damage parameters are shown in Figure 1 and Table I. Figure 1 compares helium and damage rates for iron for various fusion materials irradiation facilities. The line marked fusion represents the expected fusion reactor first-wall helium-to-dpa ratio of about 10:1 assuming a wall loading of 1-10 MW/m^2. As can be seen, only the proposed FMIT facility in the U.S.

TABLE I

SPECTRAL-AVERAGED DAMAGE RATES FROM SPECTER

Damage Energy Cross Sections in keV-barns
Multiply by 0.8/2 Ed for Displacements
Values averaged over entire spectrum.

Element	Thermal	Fission	14 MeV	HFIR	EBRII	FFTF	Fusion
Be	0.010	35.3	23.1	11.1	36.1	28.9	27.5
C	0.002	52.0	39.0	14.6	46.8	34.1	36.1
Al	0.156	96.3	177.	23.2	65.1	41.5	83.2
Si	0.097	96.0	191.	22.7	64.4	38.8	85.0
Ti	2.44	92.8	244.	21.9	47.8	30.4	93.7
V	2.27	101.0	270.	24.5	58.2	37.3	105.5
Cr	1.70	94.8	278.	21.6	52.0	30.6	104.0
Mn	5.25	94.6	260.	23.8	54.2	34.6	101.4
Fe	1.01	84.4	290.	19.1	46.3	27.3	101.8
Co	13.38	81.7	294.	24.1	49.0	30.4	102.9
Ni	2.20	85.0	300.	20.6	51.0	32.2	109.4
Cu	1.38	79.2	296.	18.6	46.6	28.5	103.8
Zr	0.026	86.0	259.	20.1	54.3	32.9	98.3
Nb	0.128	79.5	271.	18.5	49.9	29.8	96.9
Mo	0.268	83.5	259.	20.6	53.6	35.4	100.1
Ta	0.401	53.5	216.	12.4	29.5	16.9	72.5
Au	6.51	50.2	218.	15.8	27.7	16.4	72.5

HFIR = High Flux Isotopes Reactor (ORNL) - PTP position
EBRII = Experimental Breeder Reactor II (ANL-W) - Row 2
FFTF = Fast Flux Test Facility (HEDL) - MOTA position
Fusion = First Wall of Fusion Reactor (UWMAK design)

exceeds this fusion goal; however, many of the high flux reactors can achieve the desired damage rates. Furthermore, using the thermal effect in nickel to produce extra helium allows us to achieve fusion-like conditions in stainless steel in about a year in mixed-spectrum reactors such as the High Flux Isotopes Reactor at Oak Ridge.

Examples of calculated displacement damage cross sections are shown in Figure 2 and a calculated primary recoil atom energy distribution is shown in Figure 3 for HFIR. In fission reactors it is apparent that most of the displacements are caused by the elastic and inelastic scattering events, although the highest energy recoils come from the charged particle and (n,2n) reactions.

Table I lists spectral-averaged damage rates for several spectra of interest. One of the innovations in SPECTER is a new treatment of capture damage and beta-decay[4]. This effect is included in column 2 for a thermal neutron spectrum. Other columns list damage energy rates for a fission spectrum, 14 MeV, and selected reactors used in the U.S. fusion program.

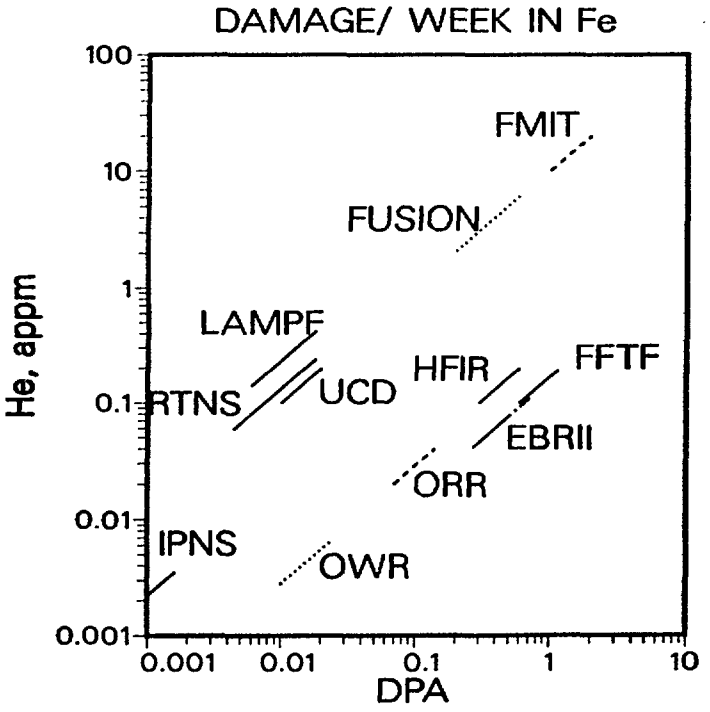

1. Helium (appm) and dpa rates per week for iron are shown for most U.S. fusion materials irradiation facilities. Note that reactors produce high dpa but low helium while accelerators produce a high helium-to-dpa ratio but low rates. The thermal helium effect in nickel can drastically increase the helium production in stainless steel for mixed-spectrum reactors such as HFIR.

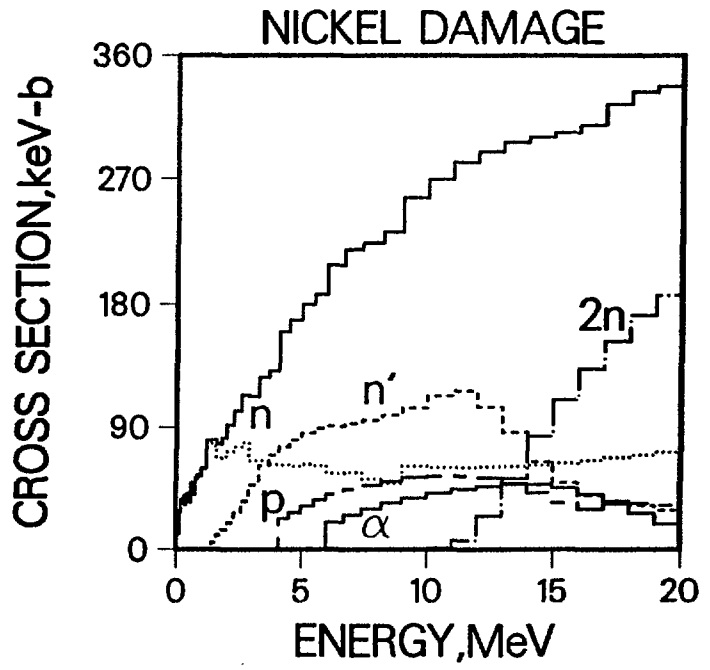

2. Displacement damage energy cross section for nickel showing the contributions from each reaction channel.

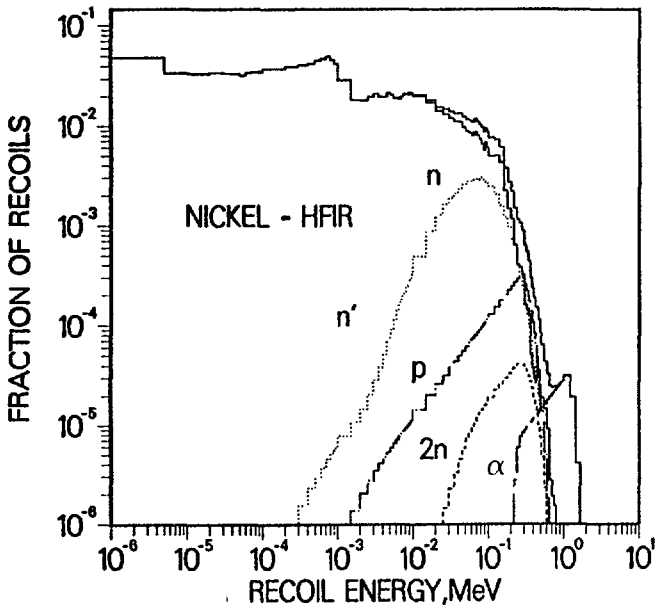

3. A typical recoil atom energy distribution (PKA) is shown for nickel in the HFIR fission reactor spectrum. Note that elastic and inelastic reactions dominate; however, charged particle reactions produce the highest energy recoils.

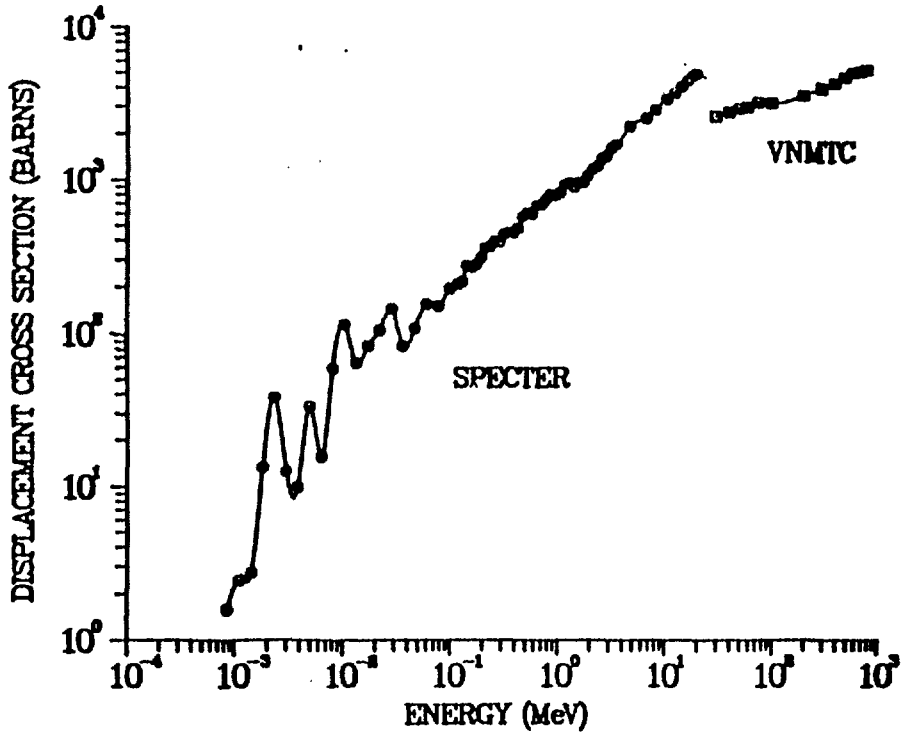

4. Displacement cross sections are shown to 800 MeV for copper. SPECTER was used below 20 MeV and VNMTC was used at higher energies. The apparent discrepancy is not well-understood and further work is needed to adequately define damage for spallation sources.

For the future, SPECTER should be expanded to include higher energies, more elements, and compounds and alloys. Some attempt has been made to extend the calculations above 20 MeV (the highest energy in ENDF); however, nuclear data is generally lacking for such calculations. An effort has been made in the U.S. to develop data up to 50 MeV for the Fusion Materials Irradiation Test Facility (FMIT), a proposed Li(d,n) accelerator neutron source. Recently, we have also tried to use spallation models to develop data for spallation neutron sources [5]. Figure 4 shows displacement damage energy cross sections in copper up to 800 MeV. It is apparent that the displacement damage cross section predicted by SPECTER is far higher than the extrapolation from the high energy code VNMTC. The reasons for this difference are not well understood, although it is clear that neither code works very well in the intermediate energy region between about 40 to 100 MeV since SPECTER neglects multi-particle channels such as spallation and the higher-energy cascade codes neglect channels such as elastic scattering. Further work is needed to provide accurate damage estimates above 20 MeV. The helium cross sections for copper agree rather well[5]; however, this agreement may be somewhat fortuitous since the agreement is rather poor for many other elements.

In summary, the SPECTER computer code package provides users with a fast, simple method for determining radiation damage parameters for a specified neutron irradiation. The code will predict both damage rates and total damage for a specified length of irradiation. The code agrees very well with other programs, such as NJOY [6]; however, SPECTER is not intended to be as comprehensive in its scope. One advantage of SPECTER is that it is completely self-contained and requires no access to ENDF/B-V. Furthermore, since SPECTER contains complete recoil atom energy distributions, users can in principle use these distributions directly to test other damage models if desired. The 100 group energy structure should be completely adequate for most applications, especially since most of the damage cross sections have a rather smooth energy dependence. The only exception to this is in the resonance region; however, this region is usually relatively unimportant since most damage is caused by fast neutrons (>0.1 MeV).

REFERENCES

1. L. R. Greenwood and R. K. Smither, SPECTER: Neutron Damage Calculations for Materials Irradiations, ANL/FPP-TM-197, Argonne National Laboratory, January 1985.

2. G. R. Odette and D. R. Dorion, Nucl. Technol. 29,p.346(1976).

3. Evaluated Nuclear Data File, Part B, Version V, National Neutron Cross Section Center, Brookhaven National Laboratory, 1979.

4. R. K. Smither and L. R. Greenwood, Proc. Fourth ASTM-EURATOM Symp. on Reactor Dosimetry, NUREG/CP-0029,pp793-805(1982).

5. D. R. Davidson, L. R. Greenwood, W. F. Sommer, and M. S. Wechsler, Calculation of Displacement and Helium Production at the LAMPF Irradiation Facility, Proc. Twelfth Int. Symp. on the Effects of Radiation on Materials, Williamsburg, VA, June 1984.

R.E. Mac Farlane, private communication, Los Alamos National Laboratory, USA.

EXPERIENCE WITH THE USE OF THE $^{93}Nb(n,n')^{93m}Nb$ REACTION FOR ROUTINE MONITORING OF MATERIALS IRRADIATION EXPERIMENTS

A F THOMAS

ROLLS-ROYCE AND ASSOCIATES LIMITED, DERBY (UK)

Abstract

The use of the $^{93}Nb(n,n')$ reaction with long half life and low energy threshold holds out much promise as a routine fast neutron and hence damage monitor in materials irradiation dosimetry. Recent UK experience in a large and varied number of metallurgical irradiation experiments using this reaction in conjunction with more conventional activation monitors suggests that there may still be systematic discrepancies in the nuclear data associated with this reaction, particularly in the domain of the reaction cross sections. Experience has shown that previous practical difficulties using this reaction can be simply overcome and therefore impetus should be given quickly to improving our knowledge of its cross section.

1. Introduction

For many years the possibility of using the $^{93}Nb(n,n')^{93m}Nb$ reaction with its wide fast neutron energy response (threshold energy $\sim$ 0.5 Mev) and long lived activation product (half life $\sim$16 years) has been viewed as the 'great white hope' of reactor dosimetrists engaged in determining fast neutron damage exposure parameters for materials irradiations. Over the last three or four years these hopes have taken several more steps towards fulfilment, notably due to:-

a) the work of Tourwé and Maene (1) in establishing counting methods which obviate the problems of self-absorption of the soft X-rays emitted by the ^{93m}Nb isomer in the monitor material and fluorescence activity induced by ^{182}Ta present as a contaminant.

b) improvements to the microscopic energy dependent cross section data due to Strohmaier et al (2) and the appearance of such data in international nuclear data files (eg. IRDF82).

c) improvement in knowledge of the decay scheme data and accuracy of the decay constant for ^{93m}Nb.

These improvements have recently been reviewed by Alberts and Debertin (3).

2. UK Practice

For many years it has been the practice in UK programmes aimed at assessing the irradiation embrittlement of reactor pressure vessel (RPV) steels using the materials test reactors (MTR) DIDO, PLUTO and HERALD (4, 5) and latterly as participants in the USNRC-LWR Surveillance Dosimetry Improvement Programme (6) to incorporate niobium wires in dosimetry capsules in such experiments. Given the long half life and the cheapness involved in so doing, it was anticipated that one day counting methods and nuclear data would be improved to enable the absolute ^{93m}Nb activities in these wires to be determined and hence used to update the fast neutron damage exposure values determined by more conventional but less adequate reactions, eg. $^{58}Ni(n,p)$, $^{54}Fe(n,p)$, $^{46}Ti(n,p)$, $^{63}Cu(n,\alpha)$. Given the high tantalum contamination known to exist in the wires (100 - 500 ppm) long delays in counting the activity were actually beneficial since the ^{182}Ta (half-life 114 days) fluorescence then becomes less of a problem when determining absolute activities of ^{93m}Nb.

2.1 Activity Measurements

In about 1982 AERE Harwell began to undertake routine measurements of ^{93m}Nb activity from niobium monitors irradiated over several years beginning in 1976. Their method of analysis of these and niobium wires in subsequent MTR irradiations has been reported (7) and makes use of a Si (Li) solid state detector. Absolute calibration was originally effected by means of an efficiency curve determined using standard sources of ^{109}Cd, ^{57}Co, ^{133}Ba, ^{139}Ce and ^{241}Am, but recently an absolutely determined standard source of ^{93m}Nb has been produced by AERE Harwell and CBNM Geel, Belgium for calibration purposes. It is estimated that the current state-of-the-art using these methods produces absolute activities of ^{93m}Nb to typically $\pm 5\%$ (1σ) although occasionally problems in source preparation result in uncertainties closer to $\pm 10\%$ (1σ).

Along with the use of the niobium monitor, iron, nickel, titanium and copper fast neutron monitors have also been employed in the dosimetry packages and, when occasion demanded the use of thermal neutron shielding inside the dosimetry capsules, cobalt and iron epithermal monitors have also been incorporated. Absolute activities of the appropriate reaction products were measured using conventional techniques to within $\pm 5\%$ (1σ).

2.2 Damage Rate Estimation

The dosimetry analysis of the AERE Harwell activity measurements is carried out by RR&A using

i) A computer code (ADA) to calculate reaction rates from the measured activities using nuclear data given in (8) and the power history of the rigs to correct for product build-up and decay, and

ii) the least squares data adjustment code SENSAK (9) to produce maximum likelihood neutron flux spectrum and hence damage rates in iron (using ASTM E693 cross sections) from the reaction rates, neutron transport calculated prior estimates of the neutron flux spectrum, and IRDF82 based energy dependent dosimetry cross sections.

3. Results and Observations

A summary of the results for irradiations in DIDO, HERALD and the ORR/PSF (4/12) LWR simulator irradiations is shown in Table 1. Of particular interest in the context of this paper is the systematic tendency for the calculated $^{93}Nb(n,n')$ reaction rate (after spectrum renormalisation but before data adjustment) to overestimate the measured reaction rate with respect to the other fast neutron monitors. This may be ascribed to systematic errors in the measurement of activity and/or decay scheme data and/or cross sections data. Unfortunately, the assigned cross section errors are so large that the process of data adjustment always reconciles these discrepancies by moving the $^{93}Nb(n,n')$ cross section to achieve consistency before making a maximum likelihood estimate of the integral exposure parameters such as damage rate, etc. Until cross section data is improved, therefore, true experimental discrepancies cannot be identified. For the same reason use of the $^{93}Nb(n,n')$ reaction can, at the present, only have a small influence on the estimates of exposure parameters when used in conjunction with more conventional activation monitors.

One further observation is worthy of note. It can be seen that the experience in the monitoring of the DIDO and HERALD rigs indicated an approximately 50% calculated overestimate of the $^{93}Nb(n,n')$ reaction rates with respect to the other monitors, whereas experience with the ORR/PSF experiments varied between 20% - 30%. The reason for this may be in the fact that the prior estimates of neutron spectrum in DIDO and HERALD were based on multiple foil activation (MFA) analysis using various fast fission detectors but notably $^{237}Np(n,f)$ which has an energy response not

TABLE 1 - RATIOS OF CALCULATED TO MEASURED REACTION RATES FOR VARIOUS FAST NEUTRON REACTIONS IN MTR IRRADIATION RIGS

REACTOR	RIG LOCATION	CALCULATED TO MEASURED REACTION RATE RATIO (NORMALISED BUT NOT ADJUSTED)				
		$^{46}Ti(n,p)$	$^{54}Fe(n,p)$	$^{58}Ni(n,p)$	$^{63}Cu(n,\alpha)$	$^{93}Nb(n,n')$
DIDO	2V4	0.80	0.87	0.86	0.76	1.30
	2V9	0.79	0.93	0.81	0.82	1.24
HERALD	D1	0.93	0.96	0.94	0.85	1.49
	D10	0.94	0.89	0.89	-	1.41
	A3	0.94	0.95	0.90	0.95	1.41
	A8	0.91	0.90	0.95	0.99	1.37
ORR/PSF(4/12)	SSC	0.84	0.90	0.89	0.99	1.14
	PVS (0T)	0.83	0.83	0.90	0.88	1.05
	PVS (1/4T)	0.80	0.82	0.84	0.92	1.05
	PVS (1/2T)	0.77	0.79	0.83	0.94	1.18

dissimilar to $^{93}Nb(n,n')$. The ORR/PSF analysis, on the other hand, was based on a 'benchmarked' neutron transport calculation only. The inference here is that due to, for example, uncompensated photo-fission enhancement the initial estimate of neutron spectrum may be exaggerated in the 0.1 to 2 Mev energy region. Recent experience in fission monitoring of surveillance capsules in civil PWRs has cast some doubt on the reliability of fission monitors for this and other reasons. This should add impetus, therefore, to determining all the nuclear data concerned with the $^{93}Nb(n,n')$ reaction and particularly the energy dependent cross section data. If this is the source of most of the discrepancy then the remaining difference is consistent with the results of recent integral measurements of the fission averaged cross section which estimate a value of ~140 millibarns compared to the Strohmaier data averaged out over a Watt fission spectrum of ~160 millibarns (3).

4. Conclusions

Experience of the use of the $^{93}Nb(n,n')$ reaction for routine monitoring of materials irradiation rigs suggests that further improvements to the nuclear cross section data and particularly to the associated variance-covariance data must be made before this reaction can entirely fulfil all its original and potential promise. Work currently being pursued in the UK to this end (10) using monoenergetic neutron sources should be encouraged.

In order to be of use to the dosimetry community involved in determining exposure parameters to meet safety and regulatory requirements such data must also find its way quickly onto the recognised nuclear databases.

Acknowledgements

The author wishes to acknowledge the large amount of experimental work performed by Miss Maureen Foy and Dr Alan Fudge at AERE Harwell which forms the basis of this paper and to Dr S P Walley who performed the computing analysis.

References

1. H Tourwé, N Maene, Proc 3rd ASTM/EURATOM Conference on Reactor Dosimetry 1979 Ispra EUR 6813, p 1245 (1980).

2. B Strohmaier et al, Physik Daten - Physics Data, Nr 13 - 2 (1980).

3. W G Alberts, K Debertin 'Nuclear Data for the Reaction $^{93}Nb(n,n')^{93m}Nb$' presented at 50th EWGRD (23 April 1985) Petten, Holland.

4. T J Williams, A F Thomas et al, Proc 11th ASTM Symposium 'Effects of Radiation on Materials' Brager/Perrin Eds ASTM-STP782 1982, p 343.

5. L M Davies Ed, Analysis of the Behaviour of Advanced RPV Steels under Neutron Irradiation, The UK Programme, UKAEA 1983.

6. C Z Serpan 'NRC-LWR-RPV Surveillance Dosimetry Improvement Programme' Nuclear Safety, Vol 22, No. 4, p 449 (July/August 1981).

7. M Foy, A J Fudge, M Wilkins 'Investigations into the Use of the $^{93}Nb(n,n')^{93m}Nb$ Reaction for Fast Neutron Dosimetry, AERE Harwell Internal Report, September 1983.

8. W L Zijp, J H Baard, Nuclear Data Guide for Reactor Neutron Metrology Retten, Holland (1979) EUR 7164 Parts I and II.

9. A K McCracken, A Packwood, The Spectrum Unfolding Code SENSAK' RPD/AKMcC/682, AEE, Winfrith (UK), December 1981.

10. D B Gayther et al, Interlaboratory Seminary held at Braunschweig (1984).

COMPARISON OF PREDICTED AND MEASURED CHARPY NDT SHIFTS AT KRŠKO NUCLEAR POWER PLANT

M.Najžer, V.Amuga, B.Glumac, L.Jenčič, I.Kodeli, A.Loose, L.Remec

ABSTRACT

Presented are results of impact testing of Charpy specimens irradiated in Krško Nuclear Power Plant, a 632 MWe PWR, during the first two fuel cycles. Neutron fluens E > 1 MeV at specimen position was between 7 to 9.10^{18}cm^{-2} depending on position in the capsule. Neutron fluens was calculated by the transport code DOT and then adjusted, together with the measured reaction rates of neutron monitors, using the code STAYSL. Shift in the Charpy V-notch curve for irradiated material relative to that of unirradiated material was compared with the shifts calculated from different models.

1. INTRODUCTION

The irradiation embrittlement surveillance programme at Krško Nuclear Power Plant meets requirements of RG 1.85/73. Alltogether 6 capsules containing PV material specimen as well as neutron and thermal monitors are irradiated. The first capsule was removed in June last year during the second refueling. The total irradiation time was 1.75 effective full power years. The capsule was dismantled in the hot cell of J.Stefan Institute (IJS), Ljubljana; Charpy tests, neutron dosimetry measurements and calculations were also performed at IJS. Some of the test results are presented in this paper.

Krško NPP is a 632 MWe Westinghouse PWR. The first time it went critical in September 1981. The lower shell plate of the pressure vessel is made of SA 533 Grade B Class 1 steel. Chemical compositions of the plate and the weld metal are given in Table I. The core geometrical configuration leads to quite high azimuthal peaking of the neutron flux supposing standard in-in-out refueling scheme. The distribution calculated by code DOT is shown in Fig. 1. The maximum corresponds to a neutron exposure of about 5 . 10^{19} cm^{-2} neutrons E>1 MeV at the designed plant end-of-life of 32 EFPY.

2. CAPSULES

Capsules were designed and manufactured by the vendor of the plant (1). They are attached to the thermal shield in the gap between the shield and the pressure vessel wall. Capsules are approximately 28 x 28 mm in cross sections and 1500 mm long.

Location and orientation of capsules in the reactor is shown in Fig. 2. Capsules are located at three different azimuthal angles of 13°, 23° and 33°. Respective E >1 MeV neutron exposure lead factors are 2.6; 1.4 and 1.5. Each capsule contains 12 each Charpy V-notch specimens made of base material parallel

Table I.: Chemical composition

Element	Base plate	Weld metal
C	0.22	0.15
S	0.013	0.007
N	0.009	0.013
Co	0.013	0.006
Cu	0.07	0.02
Si	0.29	0.14
Mo	0.58	0.53
Ni	0.60	0.04
Mn	1.31	1.27
Cr	0.05	0.02
V	0.009	0.004
P	0.010	0.007
Sn	0.004	0.002
Al	0.024	0.003
Ti	< 0.01	< 0.01
W	< 0.01	< 0.01
As	0.004	0.001
Zr	< 0.001	< 0.001

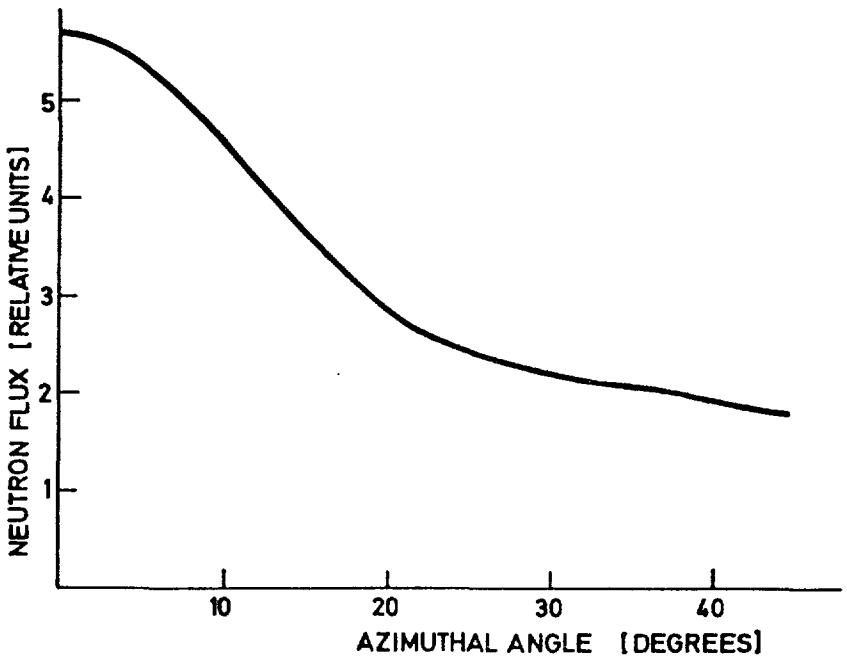

Fig. 1: Azimuthal peaking of neutron flux at the inner wall

to the main working direction, base material perpendicular to the main working direction, weld metal and heat affected zone, 9 each tensile and fracture mechanics specimens, neutron flux wires, neutron fission monitors and thermal monitors. A typical cross-section through Charpy specimens is shown in Fig. 2. It can be seen that Charpy specimens are located at two different distances from the core marked as Charpy I and Charpy II. Neutron flux wires are located at five different heights along the capsule midplane. The following wires are provided: nickel, iron, copper, aluminium - 0.15 % cobalt bare and cadmium shielded.

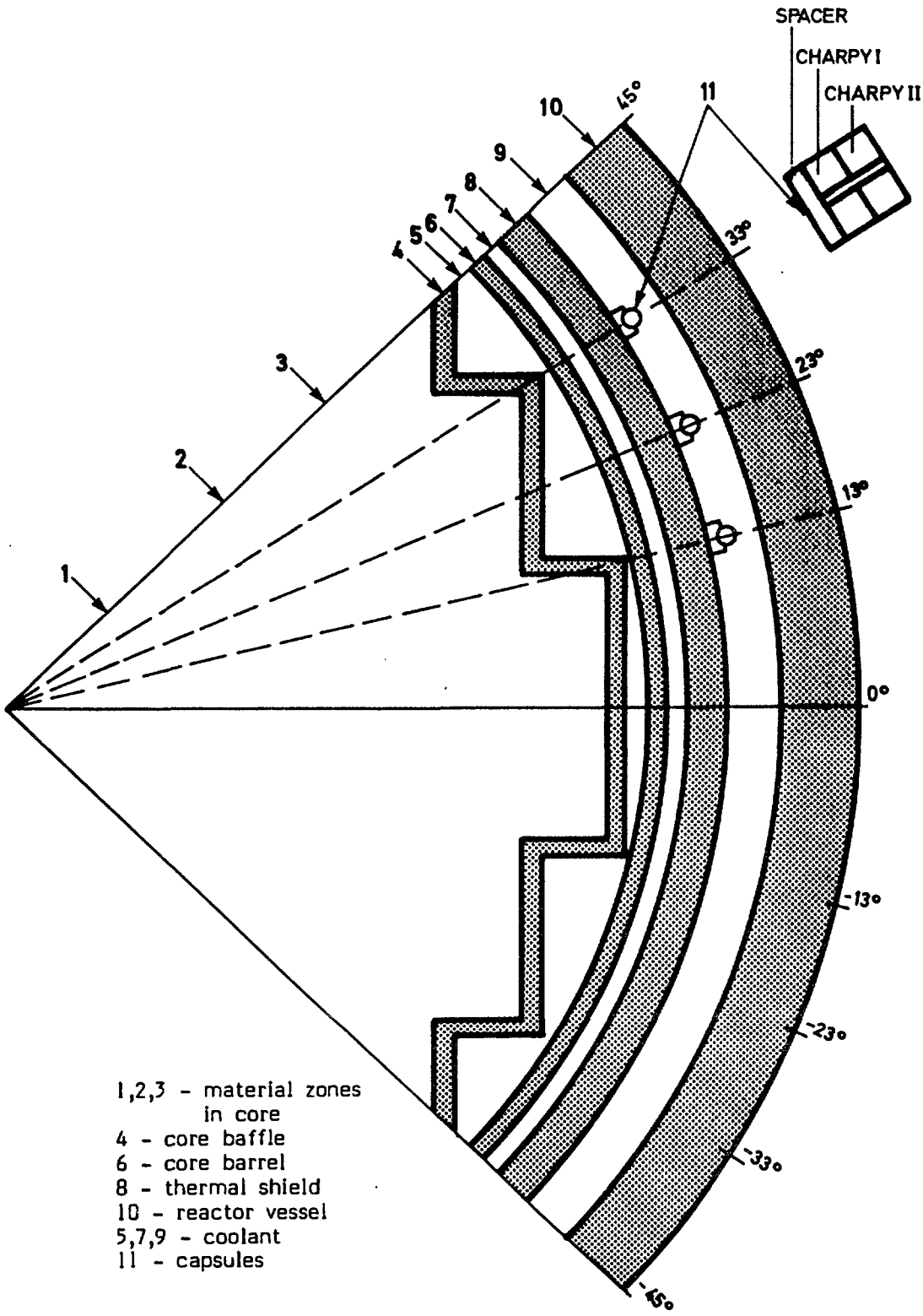

Fig. 2: Location and orientation of capsules

Fission neutron monitors are placed in the middle of the capsule. They are cadmium shielded. Temperature monitors are eutectic alloy wires inserted at the same heights as neutron flux wires but along the axis of the capsule. All parts are placed in a leak tight box. Empty places are filled in with steel spacers to ensure thermal conductivity.

3. MEASUREMENTS

3.1. Temperature monitoring

Two types of eutectic alloy wires were used with melting points of 304°C and 310°C, while the coolant temperature is 287.5°C. Wires were examined and no one was found melted.

3.2. Neutron exposure determination

Neutron transport calculations

Neutron transport code DOT 3.5 was used and cross sections were generated from DLC-2D library. Calculations were performed in two steps. First the whole reactor was calculated using a coarse mesh while the capsules were neglected. Reactor core was described as a fixed fission neutron source in nonmultiplying medium. The fission neutron density was normalized to the nominal core

Table II.: Neutron exposure

	Quantity / Location		Average full power Exposure rate E>1 MeV $cm^{-2}s^{-1}$	Exposure rate dpa s^{-1}	Exposure E>1 MeV cm^{-2}	Exposure dpa
Calculated	Charpy I	*	$1.62.10^{11}$	$2.72.10^{-10}$	$8.92.10^{18}$	$1.50.10^{-2}$
	Charpy II	*	$1.28.10^{11}$	$2.16.10^{-10}$	$7.05.10^{18}$	$1.19.10^{-2}$
	PV wall	**	$5.78.10^{10}$	$9.02.10^{-11}$	$3.19.10^{18}$	$4.98.10^{-3}$
Adjusted	Charpy I	*	$1.70.10^{11}$ ± 8%	$2.85.10^{-10}$ ± 8%	$9.34.10^{18}$ ± 8%	$1.57.10^{-2}$ ± 8%
	Charpy II	*	$1.34.10^{11}$ ± 8%	$2.26.10^{-10}$ ± 8%	$7.39.10^{18}$ ± 8 %	$1.25.10^{-2}$ ± 8%
	PV wall	**	$6.06.10^{10}$ ± 8%	$9.44.10^{-11}$ ± 8%	$3.34.10^{18}$ ± 8%	$5.21.10^{-3}$ ± 8%

* averaged over the capsule height

** at the maximum flux axial and azimuthal location

*** calculated values, corrected by the factor, obtained with unfolding of the neutron spectrum by code STAYSL. Correction factor, calculated for the end of 2nd fuel cycle and centre of the capsule, was used.

Table III.: Activites on 30 June 1984

Reaction	Measured (μCi/g)	Calculated (μCi/g)	M/C
$Cu^{63}(n,\alpha)Co^{10}$	2.58	2.99	0.86
$Fe^{54}(n,p)Mn^{54}$	116	126.4	0.92
$Ni^{58}(n,p)Co^{58}$	2188	1996	1.10
$Np^{237}(n,f)Cs^{137}$ *	82.3	77.7	1.06
Zr^{95}	1890.	1701.	1.11
$Fe^{58}(n,\gamma)Fe^{59}$	296	273	1.09
Co(n,γ)	815	284 (Cd covered) 1004 (bare)	

* No correction for Np(γ,f) reaction was done.

thermal power. Variations in the fission neutron density during the first two fuel cycles as well as the plant power history were taken into account in calculation of the neutron exposure. In the second step the neutron flux distribution in the horizontal section of the capsule was calculated separately using a finer mesh. Neutron flux gradients and neutron exposure gradients in the capsule were determined in this way. More detailed description of transport calculations can be found in (2). Results of calculations are given in Table II.

Neutron dosimetry

Activities of neutron activation and fission detectors were measured by a calibrated Ge-Li detector. Results are given in Table III. together with the calculated activities. Power history and fission neutron density variations during fuel cycles were taken into account in the calculation of activities. No normalization to measured values or other adjustments were performed. It seems that the agreement between measurement and transport calculation is satisfactory except for Al-Co wires.

Neutron flux adjustment

Reaction rates rather than activities are required by adjustment procedure. For the purpose of this analysis reaction rates at the end of the second fuel cycle were calculated as follows: Relative reaction rate variations due to changes in axial power distribution and fuel burnup were taken as obtained from the transport calculations and as determined by the power history. Absolute values of the reaction rates at the end of the 2nd fuel cycle were then calculated from measured activities.

Reaction rates were extrapolated from the detector positions to the centre of the capsule using the reaction rate gradients as obtained from transport calculation of the capsule.

Unfolding of the neutron spectrum was performed by STAYSL (3). Initial spectrum had 27 groups, as calculated by the DOT code. Its covariance matrix was prepared using program FCOV (3). The cross sections were taken from the

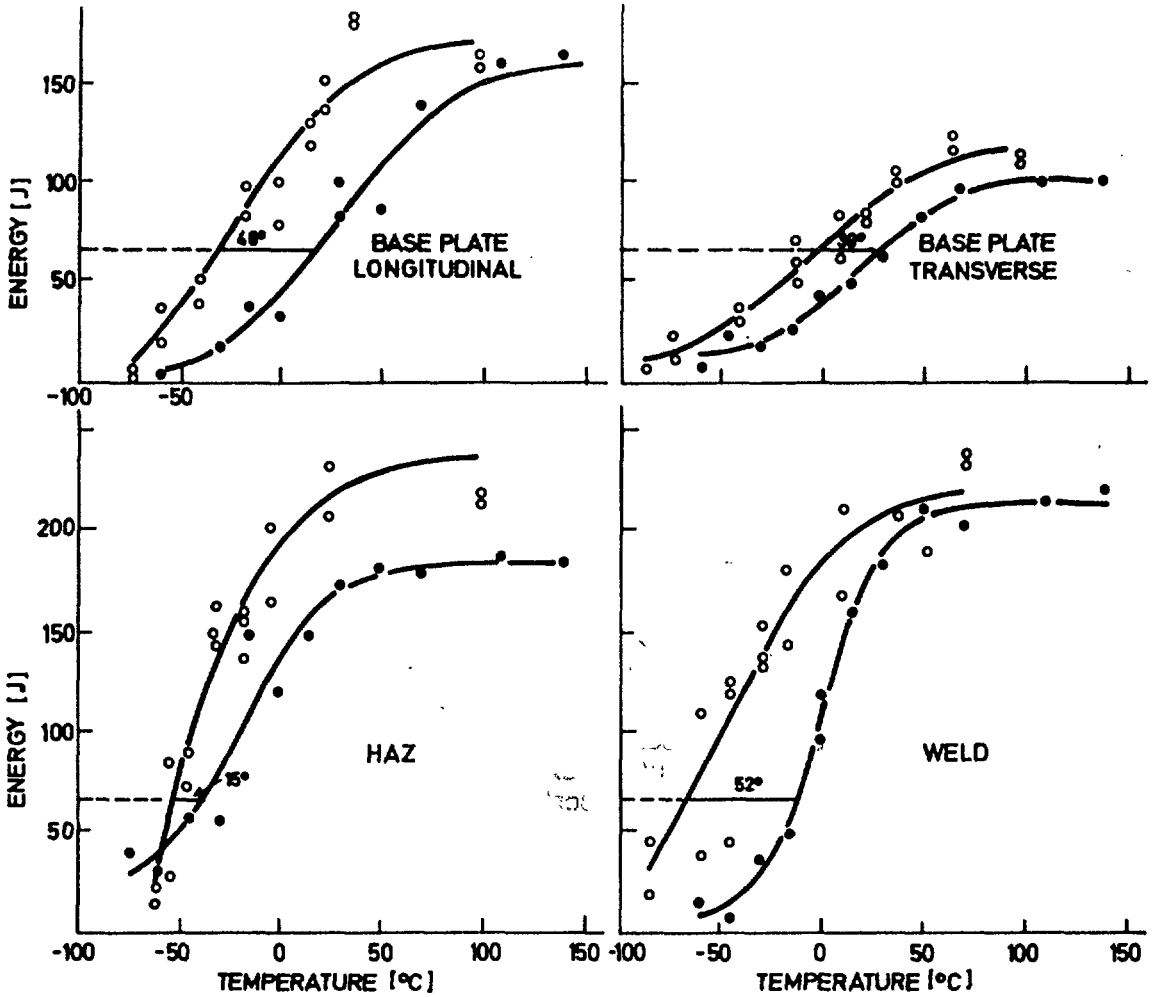

Fig. 3.: Charpy V-notch curves

Circles and dots represent unirradiated and irradiated specimens respectively. Curves represent tanh fit to measured points

Table IV.: Charpy NDT shifts

Material	Exposure E>1 MeV (cm^{-2})	Charpy measured (^{o}C)	NDT RG 1.99/77 (^{o}C)	shifts RG 1.99/ Rev 2 (^{o}C)	Form. Gutrie (^{o}C)	Form. Odette	Form. Enea (^{o}C)	Form. Framatome
Base plate -L	$7.39.10^{18}$	46	24	23	18	23	27	24
Base plate -T	$7.39.10^{18}$	30	24	23	18	23	27	24
HAZ	$9.34.10^{18}$	15	27	25	19	25	30	26
Weld metal	$9.34.10^{18}$	52	22	11	7	11		

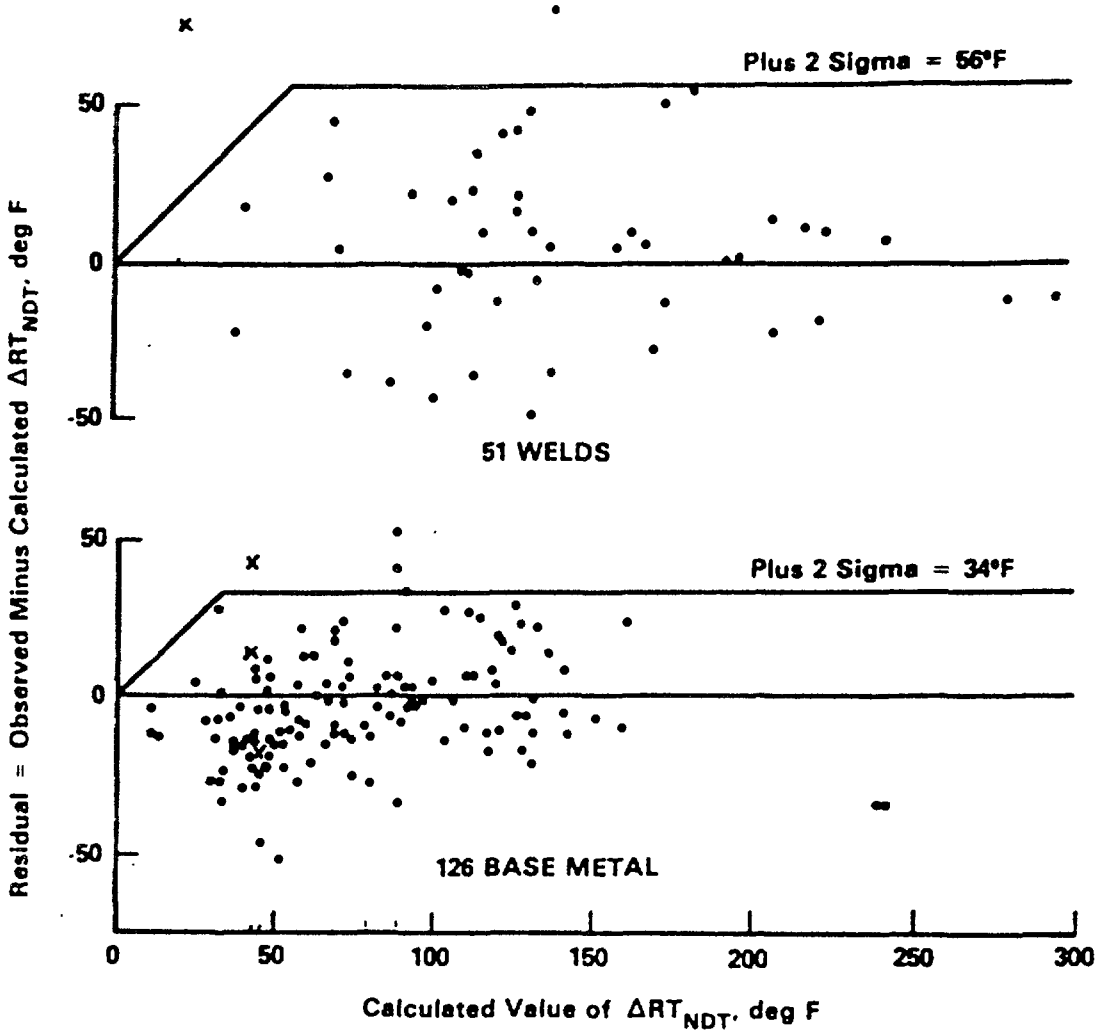

Fig. 4.: Plots of residuals versus calculated value of ΔRT_{NDT} for both welds and base metal, from Ref. (6).
Crosses indicate our results.

IRDF-82 dosimetry file. Their covariance matrix was prepared by the program XCOV (3). The covariance matrix of the measured reaction rates was calculated by the program COVAR (4). Results are given in Table II.

3.3. Charpy V-notch curves determination

Charpy specimens were examined according to ASTM standard E-23/81. Only results of impact testing are presented in this article. Testing was performed by the Wolpert-Amsler Charpy hammer type PW 30/15 equipped with the ASTM blade and abutments. The hammer is instrumented for dynamical testing. A liquid bath was used for temperature control of samples.

Results of impact testing are shown in Fig. 3. Circles and dots represent absorbed energy of unirradiated and irradiated specimens respectively, while curves represent tangens hyperbolicus fit to the measured values. The NDT shifts were determined at 68 J level. Values are given in Table IV.

4. DISCUSSION

Measured NDT shifts are compared with predicted shifts, based on chemistry and fluence factor. Formulas taken from: R.G. 1.99 rev. 1/77(5), proposed R.G. 1.99 rev. 2 (6), and reference (7), were used. All values are given in Table IV. Data show that all materials, except HAZ, exhibit considerably higher NDT shifts than predicted by any of the formula. On the other hand HAZ shift is appreciably lower.

Measured shifts are also shown as crosses in diagram presented in the analysis of Randall (6), Fig. 4. It can be seen, that values are within 2σ error band for HAZ and transverse specimens of the base plate while weld metal and longitudinal base plate specimens are outside 2σ error band.

5. REFERENCES

1. Krško Nuclear Power Station Reactor Vessel Radiation Surveillance Program, WCAP-9441, December 1978

2. A.Kodeli et al, Transport calculation of neutron flux and spectrum in surveillance capsules and pressure vessel of a PWR, Specialists' Meeting on Radiation Embrittlement and Surveillance of Reactor Pressure Vessel Steels, October 1984

3. F.G- Perey, ORNL/TM-6062 (Oct. 1977), Least Squares Dosimetry Unfolding - Program STAYSL

4. B.Glumac: Least Squares Dosimetry Unfolding Package, IJS-DP-3875 (Feb. 1985)

5. U.S. Nuclear Regulatory Commission, Regulatory Guide 1.99, Effects of residual elements on predicted radiation damage to reactor vessel materials, Revision 1, April 1977

6. P.N.Randall, U.S.Nuclear Regulatory Commission, Basis for Revision 2 of U.S. NRC Regulatory Guide 1.99, IAEA Specialists' Meeting on Radiation Embrittlement and Surveillance of Reactor Pressure Vessel Steels, October 1984

7. C. Maricchiolo et al, Prediction of reference transition temperature increase due to neutron irradiation exposure, IAEA Specialists' Meeting on Radiation Embrittlement and Surveillance of Reactor Pressure Vessel Steels, October 1984

DISPLACEMENT MODEL FOR THE CALCULATION OF RADIATION DAMAGE

Jinnan Yu

Institute of Atomic Energy, Beijing, China

ABSTRACT

This paper describes the concept of a multifold displacement threshold energy, which correlates displacement production under electron, proton, and neutron irradiation. An effective threshold energy is derived from a concept of a second-fold threshold energy surface. When details of the time-dependent energy loss of recoils that result from a primary event are considered, the slowing down number of recoils and second-fold threshold energy surface concept adquately describes the correspondence between the cascade process and crystallographic effects.

I. INTRODUCTION

Displacement-per-atom (dpa) irradiation exposure units are widely used for correlating neutron data and as a partial basis for neutron-charged-particle data intercomparison. However, significant uncertainties remain in determining both the differential primary-recoil-atom (PKA) production cross section $\chi(E_p,E)$ (E_p - particles energy, E - PKA energy) and the displacement atom production function, $\nu(E)$. The uncertainties in $\nu(E)$ are thought to be larger than those in $\chi(E_p,E)$.[1] Thus, further investigation of the $\nu(E)$ function is needed.

There is no generalized model for the $\nu(E)$ function which is suitable for the various energy ranges of (E). Upon irradiation of copper at 10K with 1.35 MeV electrons, the increase in resistivity observed experimentally agrees with that calculated theoretically within a factor of two, but the discrepancy between theory and experiment under 12 MeV deuteron irradiation of copper at 12K is about a factor of 4.5, with theory apparently overestimating the number

of displaced atoms. Similar results have been obtained by Blewitt and co-workers, using neutron irradiation at 17K.[2] A continuing trend for the discrepancy between theory and experiment increases with incresing primary recoil energy.[3] The ratio of the number of displaced atoms, theoretical value to experimental value, in germanium is respectively 2.3, 3.9, 6.0 for 1.5 MeV electrons, 9.5 MeV deuteron, and neutron bombardment at 90K.[2]

Use of the concept of a threshold energy surface is suitable for electron irradiation[4], but is unsuitable for deuteron and neutron irradiations[5]. Considering the channeling effect, the Oen and Robinson formula is suitable for the neutron irradiation results[6], but is unable to predict the deuteron and electron irradiation results.

The concept of a threshold energy surface and channeling effect results from the crystal structure, but has not been correlated. A generalized model is developed and described in this paper to relate crystallographic effects to the cascade process.

II. PHYSICAL MODEL

We introduce the concept of multi-fold threshold energy. The n-fold threshold energy $E_{nd}^{hk\ell}$ is the minimum energy required to produce n-displacement atoms if a lattice atom receives $E_{nd}^{hk\ell}$ energy and ejects in the $\langle hk\ell \rangle$ direction. In the following section, it will be shown that the directional dependence of $E_{nd}^{hk\ell}$ for n>2 is very different from that of the simple threshold energy, n=1, but the directional dependence of $E_{nd}^{hk\ell}$ for n>2 are similar. We show below that it is reasonable to base caslculations on the second-fold threshold energy to establish the displacement characteristics for proton, deuteron, and neutron irradiation. Use of the threshold energy and second-fold threshold energy concept allows connection of the results of electron, proton, deuteron, and neutron irradiation.

At low energies, less than a few hundred eV, it is well known that cooperative effects and crystal order criticality affect the structure of a cascade[4,8]. Specifically, the majority of displacements are produced by

focused replacement sequences along close-packed or nearly close-packed crystal directions (i.e., <100> or <110> in face-centered cubic (fcc) and <111> in body-centered cubic (bcc) crystals). The behavior of such a collision sequence is determined by the simultaneous interaction and motion of the atom, Fig.1. The moving atom is repelled by the neighboring atoms as it moves past the equilibrium separation distance and is focused (i.e., the neighboring atoms, by their repulsion of a moving atom as it goes beyond equlibrium seperation, act as a lens and aid in the focusing process). The net result of this process is called assisted focusing.[1,4,7] The energy and momentum transfer are particularly favorable along such close packed directions to form one displaced atom.

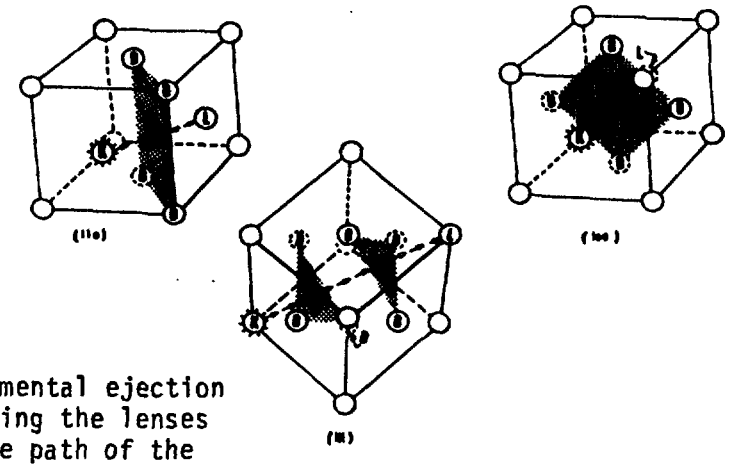

FIG.I Diagram of the three fundamental ejection processes in an fcc lattice showing the lenses formed by the ring atoms B on the path of the knock-on atom K (Sosin, 1962).

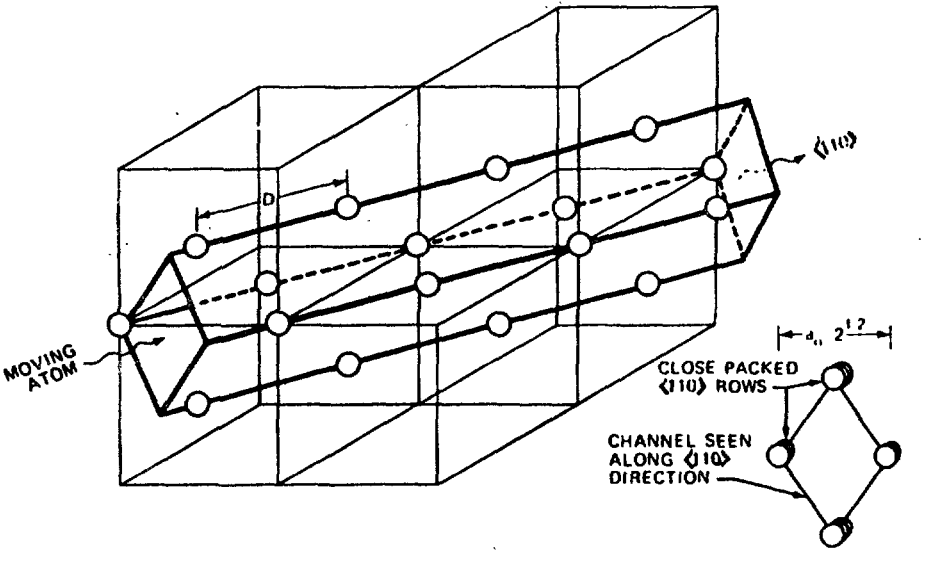

FIG.2 The<110> channel in the fcc lattice.

The threshold energy in these directions is given as the minimum energy to eject an atom which moves 0.5 atomic distance to form one displacement atom. However, for the ejected atom to form two displacement atoms, it must displace a row of atoms, the ejected atom must move at least 1.5 atomic distances. The required recoil energy is more than 4-times the threshold energy in this direction. Thus for the ejected atom to form more than two displacement atoms in this direction, the required recoil energy is much higher. Although at near close packed directions the focusing mechanism is not effective at the higher energies, the channeling effect begins to play a complementary role.[7] Thus, in and near the close packed directions, the recoil atom is more likely to form one displaced atom than it is to form multiple displacement atoms.

Along non-closed packed directions (deviation from focusing or channeling directions), the ejected atom has to overcome more potential barriers to form one displacement atom. Therefore, the threshold energy along non-close packed directions is higher than that in the focusing directions. However, if this ejected atom receives more than $2E_d^{hk\ell}$, the probability of large angle scattering to form more than two displacement atoms in a cascade collision process is large. Part of the ejected atoms' energy is dissipated to form more displacement atoms.

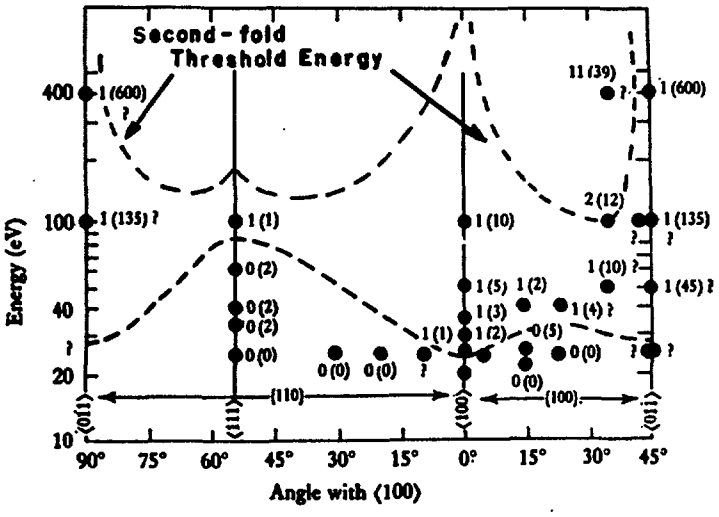

FIG.3 Diagram showing all dynamic events calculated with Cu potential. A dot is shown for each event and indicates kinetic energy and direction of knock-on atom. First figure attached gives number of stable Frenkel pairs created, figure in parentheses gives number of replacements. Dashed line is estimated threshold for creation of at least one stable Frenkel pair. (From Vineyard, I962)

In contrast, the kinetic energy of a focusing or channeling cascade is dissipated in subthreshold atomic collisions, and does not form additional displacement atoms. In summary, if the ejection directions it is difficult to form one displacement atom, it is easier to form more displacement atoms in the collision cascade process and the reverse is also true. Thus, the directional dependence of the second-fold threshold energy is the inverse of the threshold energy.

Experimental evidence supports this idea. Gibbson's computer simulation experiment[8], which has shown that in and near focusing collision row directions, the threshold energy is a saddle point (Fig.3), but in close packed directions, it is more difficult to form multiple displacements and requires higher energy. However, near those directions in which the threshold energy is high (approach maximum), the ejection atom requires more energy, but it is easier to form two displacements than in a close packed direction.

Experiments by Jung et al.[9] have shown that the curves of damage rates normalized to <110> in platinum as a function of crystal orientation changed with the increase of electron energy. For the electron energy of 1.45 MeV and

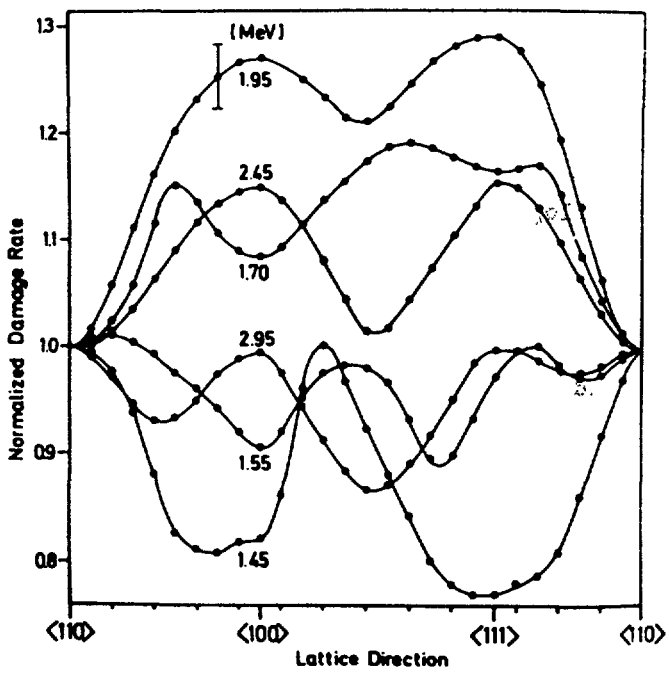

FIG.4 Damage rates normalized to <110> in platium as a function of crystal orientation, for various electron energies (Jung et al., 1973)

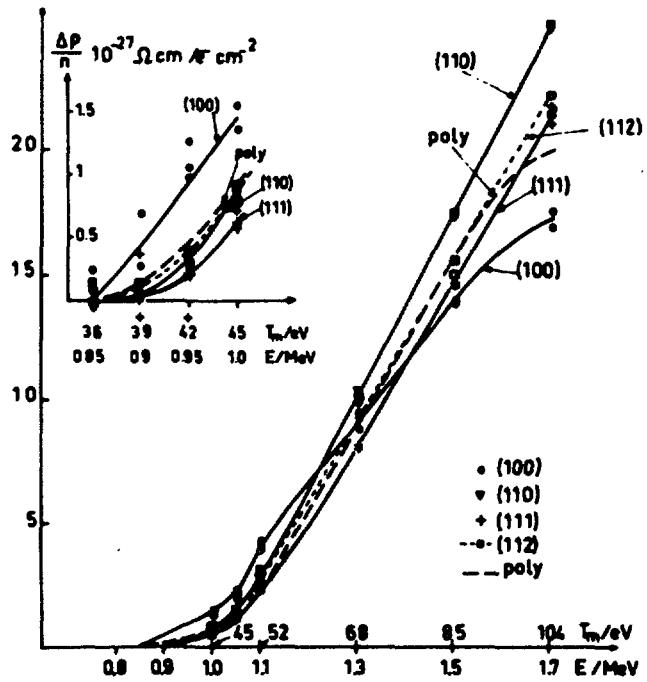

FIG.5 Resistivity change rates of molybdenum in various crystallographic directions as a function of energy (Maury et al., I975)

1.95 MeV, the shape of the curves are reversed (Fig.4). Above 1.70 MeV and below 1.55 MeV, the shape of these curves are similar. (when the energy of the ejected atom increases, the shape of the directionally dependent damage rate reverses).

Maury et al.[10] have shown the resistivity change of molybdenum as a function of various crystallographic directions for electron bombardment in the energy range 0.8 - 1.7 MeV. The lowest threshold energy was in the <100> direction ($Ed^{<100>}$ = 36 ± 1 eV). In this direction the slope of the resistivity curve decreased with high electron energy. The threshold energy in the <110> direction was greater than 72 eV ($Ed^{<110>} > 2\ Ed^{<100>}$). In the <110> direction, the resistivity change with increasing electron energy is a straight-line. Above 1.2 MeV electron energy, the resistivity change in the <110> bombardment direction surpasses that of the <100> direction. This implies that in the <110> direction it is difficult to form a single displacement atom, but, as the ejected atom energy increases, it becomes easier to form multiple displacement atoms. The reverse is true in <100> direction,

where it is easier to form one displacement atom and increasingly difficult to form multiple displacement atoms.

In electron irradiation, one probability function is sufficient to calculate displacement damage rates. For very high electron energies along with deuteron and neutron irradiations, the second-fold threshold energy participates to play a more important role in the cascade process and the evaluation of the displacement damage rate. If the shape of the n-fold threshold energy surface (n>2) is similar to that the second-fold threshold energy surface, it is possible to construct a displacement cascade calculation based on the threshold energy surface and a second-fold threshold energy surface. It is found that the effective threshold energy increases with increasing bombardment particle energy and mass.

III. DISPLACEMENT PRODUCTION FUNCTION $\nu(E)$

The largest source of uncertainty in the displacement production function $\nu(E)$ is the serious failure of the binary-collision approximation (BCA) at low energies combined with the inappropriateness of a single-step displacement function. At low energies, less than a few hundred eV, the cooperative effect and crystal order criticality affect the structure of the cascade. In this region the threshold energy and second-fold threshold energy surfaces (corresponding probability functions $P_1(E)$ and $P_2(E)$) can be used to replace the single-step displacement idea and include the crystallographic order effects.

For recoils at high energy, the binary-collision approximation (BCA) is effective and can be used to calculate the collision cascade. The lower bound in which the binary-collision approximation is inefficient is noted as $\underset{\sim}{E}$. Let each energetic atom with energy E produce $\underline{q}(E,\underset{\sim}{E})$ recoils slowing down through the lower energy level $\underset{\sim}{E}$. The displacement production function $\nu(E)$ can be described by

$$\nu(E) = (P_1(\underset{\sim}{E}) + P_2(\underset{\sim}{E}) + ...)\underline{q}(E,\underset{\sim}{E}) \qquad (1)$$

where $\underline{q}(E,E_v)$ is called as the slowing-down number of recoils*. According to the definition of $\underline{q}(E,E_v)$, it has following boundary conditions:

$$\underline{q}(E,E_v)=\begin{cases}1, & E=E_v\\ 0, & E<E_v\end{cases} \qquad (2)$$

The first condition of equation (2) is $\underline{q}(E,E)=1$. If the E_v is equal to $\hat{E}_{2d}$ (the maximum value of second-fold threshold energy), the displacement production function $\nu(E)$ can be described as follows:

$$\nu=\begin{cases}P_1(E), & 0<E<\hat{E}_d\\ 1+P_2(E), & \hat{E}_d<E<\hat{E}_{2d}\\ (2+P_3(\hat{E}_{2d})+P_4(\hat{E}_{2d}))\underline{q}(E,\hat{E}_{2d}), & E>\hat{E}_{2d}\end{cases} \qquad (1')$$

where the $\hat{E}_d$ is the maximum value of threshold energy surface. If we assume that the multi-fold threshold energy surfaces form similarly shaped surfaces with a constant interspace distance of Δ (different from the threshold energy surface), then Pi(E) can be written as:

$$P_3(E) = P_2(E-\Delta),$$

$$\cdots\cdot,$$

$$P_{n+2}(E) = P_2(E-n\Delta)$$

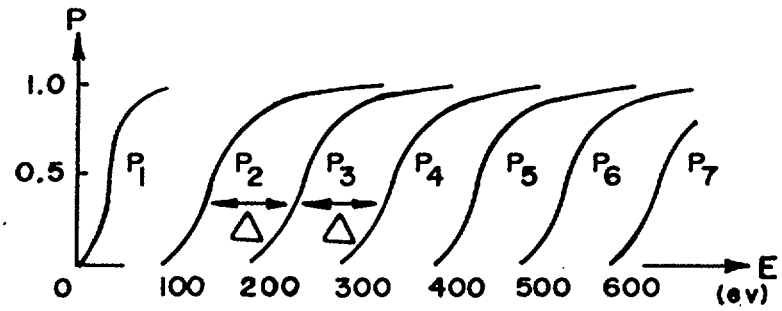

FIG.6 Approximate probability curves of multi-fold threshold energy for copper

where $n = \text{integer}\left[\frac{E-E_{v2d}}{\Delta}\right]$, thus

$$\nu(E) = P_1(E) + \sum_{k=0}^{n} P_2(E-k\Delta), \qquad (3)$$

If the $P_2(E) = 1-e^{-\alpha(E-E_{v2d})}$, where α is a parameter of the material, equation (3) can be writen as:

$$\nu(E) = 2+\text{integer}\left[\frac{E-E_{v2d}}{\Delta}\right] - \frac{e^{-\alpha(E-E_{v2d})}-e^{-\alpha(E-m\Delta-E_{v2d})}}{1-e^{\alpha\Delta}}, \text{ for } E>\hat{E}_{2d} \qquad (3')$$

*The slowing-down number of recoils is similar to the slowing-down density of recoils, but the later is the number of recoils slowing-down past energy E_v per cubic centimeter per second due to a source ofone PKA of energy E per cubic centimeter per second.[7]

In this form, the energy loss in the cascade by electronic excitation has not been considered, for equation (1′) it is possible to consider other energy losses.

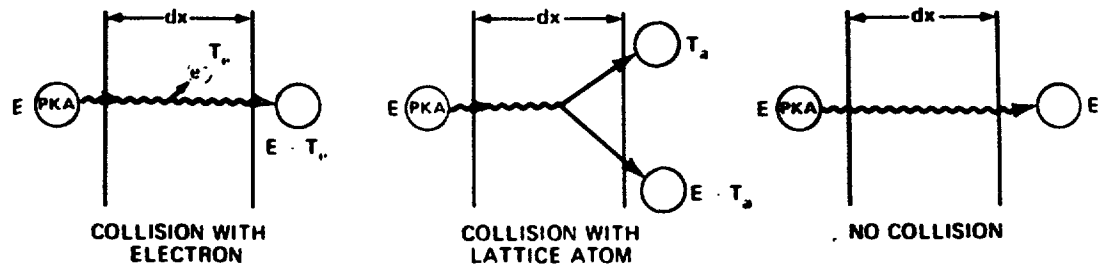

Fig.7 Possible fates of a PKA on passing through a thickness dx of solid.

Possible fates of a PKA passing through a thickness dx in a material are shown in Fig. 7. The probability $p_e dTe$ that a collision between a PKA and an electron in the interval dx which transfers energy in the range (Te, dTe) to the electron is:

$$p_e dT_e = N\sigma_e(E,T_e)dT_e dx \tag{4}$$

Where $\sigma_e(E,Te)$ is the energy-transfer cross section from the PKA to an electron and N is the density of matrix particles. Similarly, the probability of a collision in dx which transfers energy (Ta,dTa) to a lattice atom is:

$$p_a dT_a = N\sigma_a(E,T_a)dT_a dx \tag{5}$$

The probability that nothing happens in dx is given by:

$$p_o = 1-\int_o^{T_{em}} p_e dT_e - \int_o^E p_a dT_a = 1-Ndx\left[\sigma_e(E)+\sigma_a(E)\right] \tag{6}$$

where Tem is the maximum energy transferrable to an electron by a PKA of energy E and $\sigma_e(E)$ and $\sigma_a(E)$ are the total cross sections for collisions of the PKA with electrons and lattice atom, respectively. Thus, the slowing-down number of recoils can be described by

$$\underline{q}(E,\underline{F}) = \int_o^E \left[P_1(E-T_a)\underline{q}(E-T_a,\underline{F})+P_1(T_a)\underline{q}(T_a,\underline{F})\right]p_a dT_a + \\ + \int_o^{T_{em}} \underline{q}(E-T_e,\underline{F})p_e dT_e + p_o\underline{q}(E,\underline{F})$$

It can be rewritten as follows:

$$[\sigma_e(E)+\sigma_a(E)]\underline{q}(E,\underline{E}_v)=\int_0^E[P_1(E-T_a)\underline{q}(E-T_a,\underline{E}_v)+P_1(T_a)\underline{q}(T_a,\underline{E}_v)]\sigma_a(E,T_a)dT_a+$$
$$+\int_0^{T_{em}}\underline{q}(E-T_e,\underline{E}_v)\sigma_e(E,T_e)dT_e \qquad (7)$$

We note that the maximum energy transferrable to an electron is very small compared to E; thus, $\underline{q}(E-Te,\underline{E}_v)$ can be expanded in a Taylor series and truncated after the second term. Using the electronic stopping power of the medium divided by the atom density instead of $\int_0^{tem}Te\sigma_{ep}(E,Te)dTe$, equation (7) becomes:

$$\underline{q}(E,\underline{E}_v)+\frac{(dE/dx)_e}{N\sigma}\frac{d\underline{q}(E,\underline{E}_v)}{dE}=\int_0^E[P_1(T)\underline{q}(T,\underline{E}_v)+P_1(E-T)\underline{q}(E-T,\underline{E}_v)]\frac{\sigma(E,T)}{\sigma}dT \qquad (8)$$

Equation (8) is solved using a hard-sphere approximation and $(\frac{dE}{dx})_e$ is taken to follow the square-root law $(\frac{dE}{dx})_e = kE^{1/2}$, $k=0.3NZ^{2/3}\ eV^{1/2}/A]$. With this simplication, equation (8) reduces to:

$$\underline{q}(E,\underline{E}_v)=\frac{2\underline{E}_v}{E}+\frac{2}{E}\int_{2\underline{E}_v}^E\underline{q}(T,\underline{E}_v)dT-\frac{kE^{1/2}}{N\sigma}\frac{d\underline{q}(E,\underline{E}_v)}{dE} \qquad (8')$$

We now introduce the dimensionless energy variable:

$$y = E/2\underline{E}_v$$

and equation (8') is transformed to

$$\underline{q}=\frac{1}{y}+\frac{2}{y}\int_1^y\underline{q}(y')dy'-Ay^{1/2}\frac{dq}{dy}$$

where $A=\frac{k}{\sigma N(2\underline{E}_v)^{1/2}}=\frac{.3Z^{2/3}}{\sigma(2\underline{E}_v)^{1/2}}$. The solution of Eq. (8") is

$$\underline{q}(E,\underline{E}_v)=\frac{1}{1+4(\frac{k}{\sigma N})/(2\underline{E}_v)^{1/2}+3(\frac{k}{\sigma N})^2/2\underline{E}_v}\cdot\frac{1}{2\underline{E}_v}[E+\frac{3}{2}(\frac{k}{\sigma N})^2+3E^{1/2}(\frac{k}{\sigma N})],E>\underline{E}_v \qquad (9)$$

If $E>>\underline{E}_v$, then $\underline{q}(E,\underline{E}_v)$ is

$$\underline{q}(E,\underline{E}_v)=\frac{\eta E}{2\underline{E}_v},\ E>>\underline{E}_v \qquad (9')$$

where $\eta=(1+\frac{4(k/\sigma N)}{(2\underline{E}_v)^{1/2}}+\frac{3(k/\sigma N)^2}{2\underline{E}_v})^{-1}$

In order to satisfy the condition of $\underline{q}(\underline{E}_v,\underline{E}_v)=1$, the first term of the right side of equation (8′) has to be multiplied by an adjustment factor δ. This is because $\underline{q}(E,\underline{E}_v)$ in the range $[\underline{E}_v,2\underline{E}_v]$ has a finite probability to form $\underline{q}(\underline{E}_v+\delta,\underline{E}_v)$ and another displacements $D(E>\underline{E}_d)$. When using $\underline{q}(E,\underline{E}_v)$ to calculate displacements, those displacements , $D(E>\underline{E}_d)$, are neglected. Thus, we need to add a factor to complement the loss of those displacements in using $\underline{q}(E,\underline{E}_v)$ to calculate displacements. Secondly, $\underline{q}(E,\underline{E}_v)$ at $E=2\underline{E}_v$ has a certain probability to form $2\underline{q}(\underline{E}_v,\underline{E}_v)$. Using the adjustment factor δ, the equation (8′) becomes:

$$\underline{q}(E,\underline{E}_v) = \frac{2\underline{E}_v}{E}\delta + \frac{2}{E}\int_{2\underline{E}_v}^{E} \underline{q}(T,\underline{E}_v)dT - \frac{kE^{1/2}}{N\sigma}\frac{d\underline{q}(E,\underline{E}_v)}{dE}, \qquad (10)$$

The solution of equation (10) is

$$\underline{q}(E,\underline{E}_v)=\frac{\delta}{1+4(\frac{k}{\sigma N})/(2\underline{E}_v)^{1/2}+3(\frac{k}{\sigma N})^2/2\underline{E}_v}\cdot\frac{1}{2\underline{E}_v}[E+\frac{3}{2}(\frac{k}{\sigma N})^2+3E^{1/2}(\frac{k}{\sigma N})], \quad E>\underline{E}_v$$

for this solution to satisfy boundary condition (2), δ must be

$$\delta=\frac{2(1+4(\frac{k}{\sigma N})/(2\underline{E}_v)^{1/2}+3(\frac{k}{\sigma N})^2/2\underline{E}_v)}{1+3\sqrt{2}(\frac{k}{\sigma N})/(2\underline{E}_v)^{1/2}+3(\frac{k}{\sigma N})^2/2\underline{E}_v}$$

therefore, the solution for $\underline{q}(E,\underline{E}_v)$ is

$$\underline{q}(E,\underline{E}_v)=\frac{1}{1+3\sqrt{2}(\frac{k}{\sigma N})/(2\underline{E}_v)^{1/2}+3(\frac{k}{\sigma N})^2/2\underline{E}_v}\cdot\frac{1}{\underline{E}_v}[E+\frac{3}{2}(\frac{k}{\sigma N})^2+3E^{1/2}(\frac{k}{\sigma N})], E>\underline{E}_v \qquad (11)$$

If $E>>\underline{E}_v$, then $q(E,\underline{E}_v)$ is

$$\underline{q}(E,\underline{E}_v) \simeq \frac{n'E}{2\underline{E}_v}, \quad E>>\underline{E}_v \qquad (11')$$

where $\eta'=2/(1+3\sqrt{2}(\frac{k}{\sigma N})/(2E_v)^{1/2} + 3\ (\frac{k^2}{\sigma N}/2E_v))$. The δ only occurs in the $\underline{q}(E,E_v)$, which is in the range $[E_v,2E_v]$ and when $E_v>\hat{E}_{2d}$. For the single step process considering only E_d, δ in the range $[E_d,2E_d]$ is equal to 1. There is no reason to describe $\delta>1$, thus, we obtain $\underline{q}(E,E_d)\simeq\frac{\eta E}{2Ed}$, $E>>E_d$.

IV Conclusion

(1) From the concept of a multi-fold threshold energy, we obtain equations (1'), which unify and describe displacement calculations under electron, proton, and neutron irradiation.

(2) If the energy of the primary knock-on atoms is much higher than $\hat{E}_{2d}$, we obtained from equation (3') the displacement production function $\nu(E)\simeq\frac{E}{\Delta}$ and from equation (9) $\nu(E)\simeq\frac{\eta E}{\hat{E}_{2d}}$ for the condition which considers electronic excitation. These results show that the effective threshold energy does not depend on the threshold energy, but on the interspace between multi-fold threshold energy surfaces and second-fold threshold energy surface.Thus the effective threshold energy is not suitable to characterize the threshold energy surface, except where the crystallographic effect may be unimportant, such as in graphite.

(3) The slowing-down number of recoils and second-fold threshold energy surface is accurate enough to describe the combination cascade process and crystallographic effects.

(4) Further work is necessary to invesitgate the effect of interaction potentials of atom collisions and the character of the second-fold threshold energy surface.

ACKNOWLEDGMENT

The author wishes to thank W. F. Sommer and David Farnum for his editorial efforts in the English version of this paper and for important discussions.

References

1. G. R. Odette, and D. R. Doiron, Nucl. Technol. 29 (1976) 346.

2. J. J. Harwood, et al. "The Effect of Radiation on Materials", Reinhold Publishing Corporation, New York (1968) 14, 23.

3. M. W. Thompson,"Defects and Radiation Damage in Metals", Cambridge University Press (1969) 278-292.

4. Peter Vajda, Rev. Mod. Phys. 49 (1977) 481.

5. Von.Chr. Lehman, Nucleonik 3 (1961) 1.

6. O. S. Oen, et al., J. App. Phys. 34 (1963) 302; Appl. Phys. Lett. 2 (1983) 83.

7. Donald R. Olander TID-26711 (1976) 390-396, 411.

8. J. B. Gibson, et al., Phys. Rev. 120 (1960) 1229.

9. P. Jung, R. L. Chaplin, H. J. Fenzl et al., Phys.Rev.B8(1973) 55.

10. F. Maury, et al., Radiat. Eff. 25 (1975) 175.

ACTIVATION AND He-PRODUCTION IN FUSION REACTOR STRUCTURAL MATERIALS, SIMULATED AT A NEUTRON IRRADIATION FACILITY AT THE JRC-ISPRA CYCLOTRON

M. Forte*, P. Jung**, E. Galletti*** and C. Maranzana*

* Physics Division, JRC-Ispra, Italy

** Institut für Festkörperforschung, KFA-Jülich, W. Germany

*** (Thesis student from Politecnico di Milano, Italy)

ABSTRACT

The characteristics are presented of a neutron source operating at the JRC-Ispra Cyclotron, where the 7Li(p,n) reaction in a thin Li target is used to simulate fusion reactor spectra including a strong quasi-monochromatic 14 MeV component. A particular scintillation spectrometry method, used to determine the neutron energy distribution and intensity, is described and dosimetry problems are discussed. Experiments for the study of neutron activation and He-production are presented, with preliminary results for pure Ni, and for AISI 316 and AMCR 33.

INTRODUCTION

The different radiation effects which are expected to be produced in structural materials exposed to very intense neutron fluxes in fusion reactors are currently evaluated by simulation codes, on the basis of nuclear data. Evaluations are required to predict the behaviour of structural materials and for other specific fusion technology problems and also for the needs of the related material damage studies.
For the simulation and the study of radiation damage in fusion materials, irradiation tests are commonly carried out, using fast neutron fluxes from intense neutron sources or accelerated charged particle beams. However, the intense neutron sources can neither attain the flux levels nor reproduce the spectral distributions of fusion reactors. Typical accelerator sources, using Be(d,n) or spallation reactions, produce a broad neutron spectrum extending to higher energies, well beyond 14 MeV, while the RTNS-I, II produce intense neutron fluxes of approximately monoenergetic T(d,n) neutrons.

The interpretation and the correlation of irradiation tests performed at different facilities require accurate characterization of the radiation fields (neutron flux and spectrum) and of the induced effects, primarily the atomic displacement rate (dpa) and the collateral effects of gas generation and solid transmutation which compete in the damage processes.

Certain experiments, typically with accelerated light particle beams, take advantage from the possibility to arrange the experimental conditions (particle kind and energy, eventually combined with He-injection) to simulate a He/dpa ratio appropriate to a fusion reactor environment and, therefore, this parameter must be characterized for the materials under test. The neutron cross section requirements concern, in addition to fusion technology materials, a variety of elements of interest for the activation and the He-accumulation dosimetry /1,2/.

Evaluations are usually based on differential cross sections and integral cross section testing is performed with a variety of neutron spectra at different facilities /1/.

A novel neutron irradiation facility has been put into operation at the JRC-Ispra cyclotron, where the 7Li(p,n) and, eventually, the 7Li(d,n) reactions can be used to obtain neutron spectra which simulate the features of fusion reactor first-wall and blanket spectra, with a relatively strong 14 MeV component and a broad distribution to lower energies, allowing to perform integral measurements at flux levels of $10^9 \sim 10^{10}$ n $cm^{-2}s^{-1}$ ($\gtrsim 10^{10}$ n $steradian^{-1}s^{-1}$). Measurements have been started of activation and He-generation in different candidate structural materials. As confirmed by preliminary results, similar experiments are suitable to produce integral data required for specific problems and can be useful for integral cross section testing in the energy range of fusion reactor neutrons.

This work is carried out in the frame of the Thermonuclear Fusion Technology Programme of the JRC, which includes various experiments of damage simulation with cyclotron-accelerated particle beams /3/.

EXPERIMENTAL SYSTEM

The neutron source system, schematically represented in Fig. 1, is essentially a channel where the cyclotron beam is suitably collimated, crosses the Li target and is collected, at the end, by a Faraday cup.

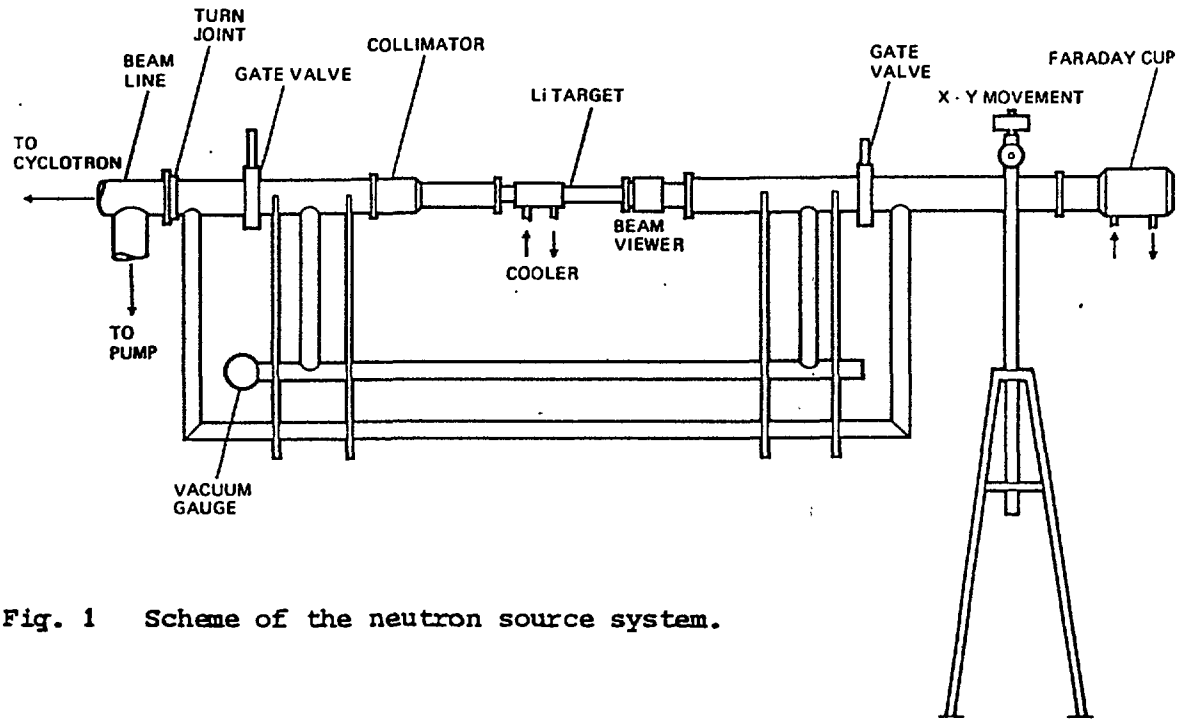

Fig. 1 Scheme of the neutron source system.

The target is made of a Li disc of 2 cm diameter and, usually, $\sim$ 1 mm thickness, fitted in a tube of Al-Mg alloy, which is cooled externally by a water flow (Fig. 2). In a continuous operation, at full proton beam intensity ($\sim$ 60 μA) the target can dissipate a power in excess of 80 W, with no apparent deterioration.

The beam is focused on the target and is guided through a pre-collimator and a centring ring of 10 mm inner diameter, in the target tube. Both this and the collimator are electrically insulated and connected to current meters which help to adjust the beam alignment and profile and to control the stability. In normal operation, at high beam intensity, a very low fraction of proton current ($\lesssim$ 1%) is intercepted and the beam profile width (f.w.h.m.) at the target is estimated to be 3 $\sim$ 4 mm. A simple beam viewer, equipped with a movable ZnS screen, is used to visualize the beam emerging from the Li target, at currents of 10 $\sim$ 100 nA.

Also the main parts of the vacuum system are made of Al-Mg alloy, or other low activation materials, and are maintained under high vacuum, or refilled with pure argon, to reduce the Li-target contamination by residual atmospheric gases.

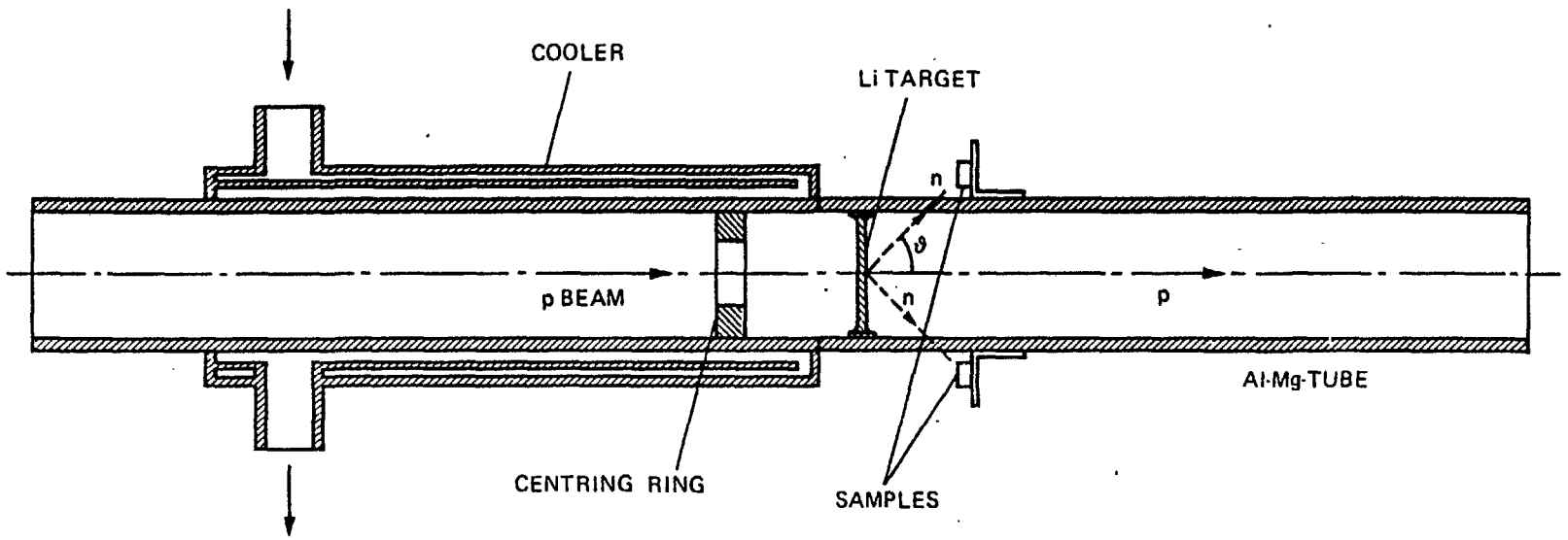

Fig. 2 Scheme of the Li target and disposition for the sample irradiation.

NEUTRON SPECTROMETRY

We have developed a neutron spectrometry method using a pair of recoil proton scintillation detectors, D_1,D_2, made of NE213 liquid scintillator encapsulated in Al containers (Fig. 3). The active volumes have a 4 cm diameter and a different thickness, respectively 1 and 0.5 cm (a little larger than a 20 MeV proton range). An equivalent plastic scatterer in front of the thinner detector allows to symmetrize the neutron attenuation and multiple scattering.

The fast neutron detection efficiency is of the order of a few percent, with a relatively low probability of multiple scattering. The spectrum of single recoil protons completely stopped in the scintillator is related unambiguously to the incident neutron spectrum, and would allow a simple and accurate unfolding procedure with minor corrections. On the other hand, thin detectors have the drawback of wall effects, mainly the energy loss of protons in the glass window and, possibly, the generation of energetic particles from the walls ((n,p) reactions). Such effects can be eliminated by considering the difference spectrum of the two detectors, which represents, essentially, the energy distribution of recoil protons in a scintillator having the difference volume, with no material walls (the contribution of lateral wall effects, only partially subtracted, is practically negligible /4/). The electronics diagram is shown in Fig. 3.

Each scintillator is coupled to a Philips 2202b photomultiplier. Dynode output signals are linearly amplified and fed to a gated peak stretcher, while simultaneous fast anode pulses are analysed by a PSD module which gates the stretcher, for the neutron-gamma discrimination, with a resolving time of 2 μs and conveniently high neutron detection and gamma rejection efficiencies, at gamma pulse levels > 30 keV. The system can operate at low photomultiplier gain (< 10^5), allowing a good gain stability within 2% or better, in the measurements. The stretcher analog output is fed to an ADC interfaced with a PDP11 - 03 computer. The signals are addressed to 1024 memory locations, in the MCA mode. The complete spectra, from both detectors, are finally recorded on floppy disc. The spectrum unfolding program proceeds by the following steps, using the cross section library of /5/.

The proton scintillation amplitudes are converted to a linear energy scale /6,7/.

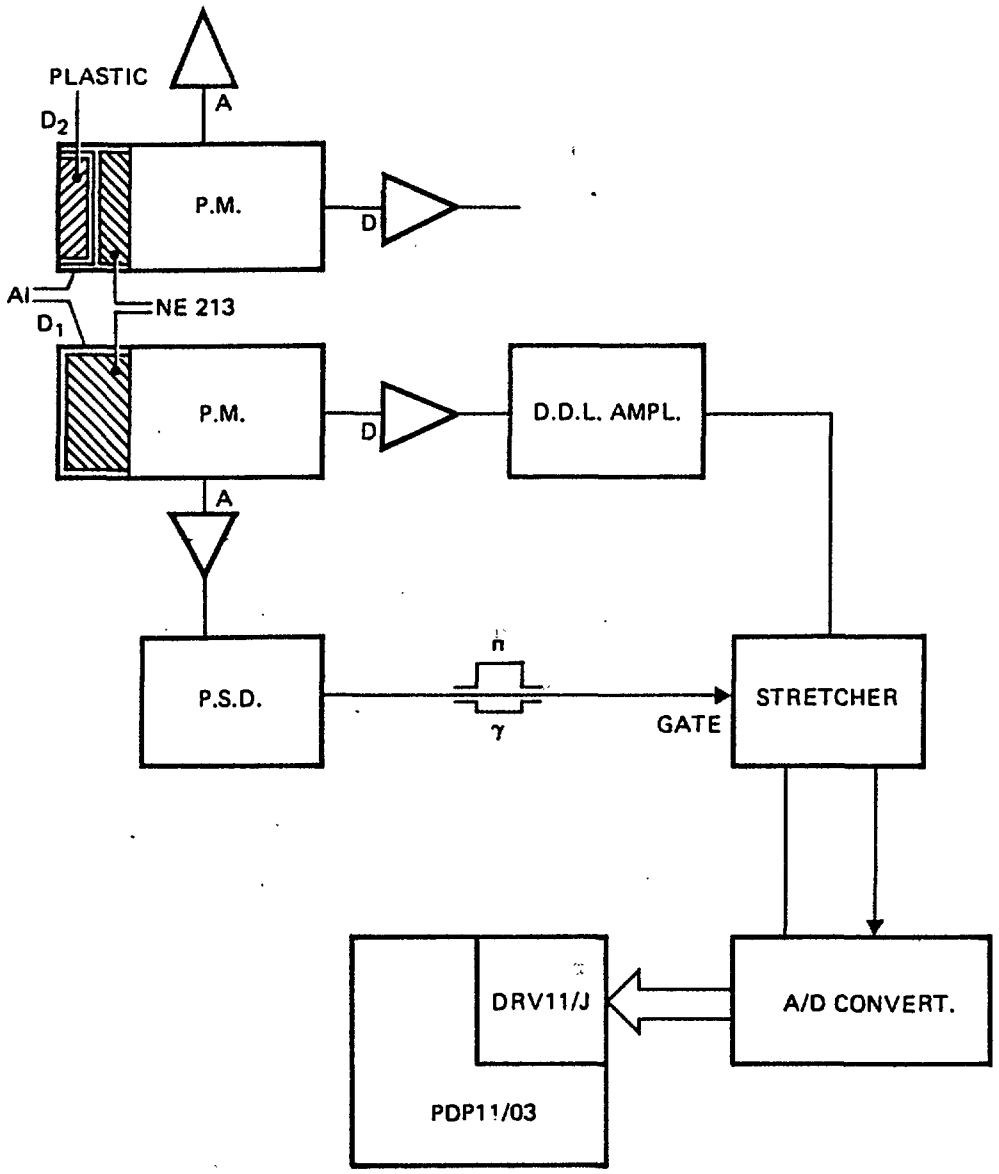

Fig. 3 Scheme of the neutron spectrometer and associated electronics.

The energy spectrum is then differentiated to obtain the detected neutron spectrum.
The latter is corrected by the detector efficiency to obtain the incident neutron spectrum.
Minor corrections for the double n-p scattering /8/ are optionally included.

Neutron spectra from the p-Li target

Neutron spectra were measured at different emission angles, between $\sim 20^{\circ}$ and 80°, using natural Li targets and proton beam energies be-

tween ∿ 16 and 20 MeV, with current of 10 ∿ 100 nA and a source-detector distance of 30 cm.

We consider, for example, the case E_p = 18.25 MeV, emission angle $\vartheta = 60^\circ$. The unfolded neutron spectra of detectors D_1,D_2 and their difference (equivalent to unfolding the difference proton spectrum) are shown in Figs.4,5,6,7. A more or less pronounced distorsion of the single spectra, due to wall effects (depending on detector thickness), is evident in a comparison with the correct difference spectrum. The peak at ∿ 14 MeV is a doublet formed by a stronger and a weaker component, respectively from the $^7Li(p,n)^7Be$ and the $^7Li(p,n)^7Be^*$ (0.43 MeV) /9/. Other monoenergetic components, corresponding to higher $^7Be^*$ excited states, are distinguished over a continuum due to $^7Li(p,n\alpha)$ and $^7Li(p,np)$ break-up reactions.
The observed peak resolution width is mainly due to the finite target thickness (ΔE_n ∿ 1 MeV), the intrinsic detector resolution ($\Delta E/E$ ∿ 5%) and to a minor contribution from the source-detector geometry. The neutron background measured by the spectrometer is generated mainby by reactions in the Al-Mg beam stopper and is practically negligible in the MeV region. A typical background spectrum is shown in Fig. 8, where the intensity scale is expanded by 30, relative to Fig. 7.

For a qualitative simulation of first wall and blanket spectra, we have to consider different combinations of E_p and ϑ which allow to obtain a ∿ 14 MeV neutron peak with a different relative intensity. We compare, for example, the cases E_p = 17.65 MeV, $\vartheta = 45^\circ$ (Fig. 9) and E_p = 20 MeV, $\vartheta = 80^\circ$ (Fig. 10). In the second case, the ∿ 14 MeV component is relatively weaker, corresponding to a steep decay of the two reactions involved , toward large angles /9/, while a strong enhancement is expected at low angles ($\vartheta < 20^\circ$) which, unfortunately, are not easily accessible with our present system (possible modifications are being studied).

In any case, we consider also the possibility of using a linear combination of "physical" spectra to taylor neutron spectra where the relative 14 MeV neutron intensity and, as much as possible, the shape of the softer component meet the requirements. For example, a combination of spectra of Fig. 9 and Fig. 10 allows to simulate a spectrum (Fig. 11) with a higher peak / total ratio with respect to the components.

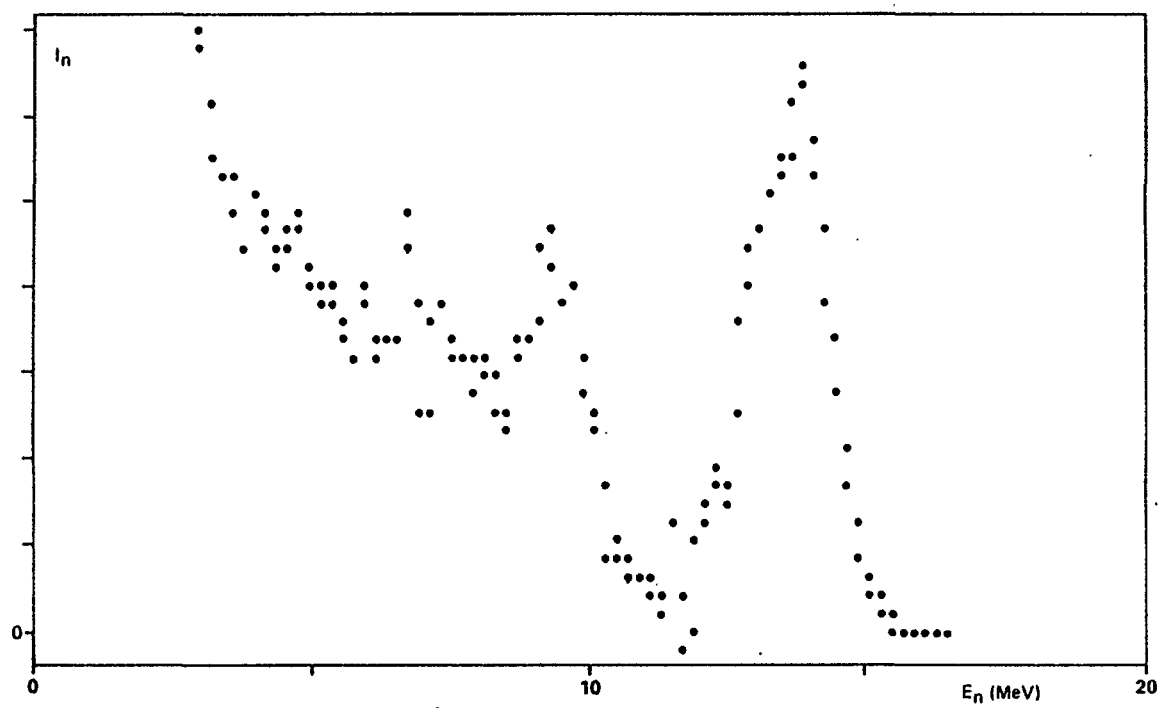

Fig. 4 Energy spectrum of neutrons emitted from the p-Li target, at Ep = 18.25 MeV, $\vartheta = 60^{\circ}$, measured by detector D_1 (1 cm thick). Neutron intensity I_n in arbitrary units.

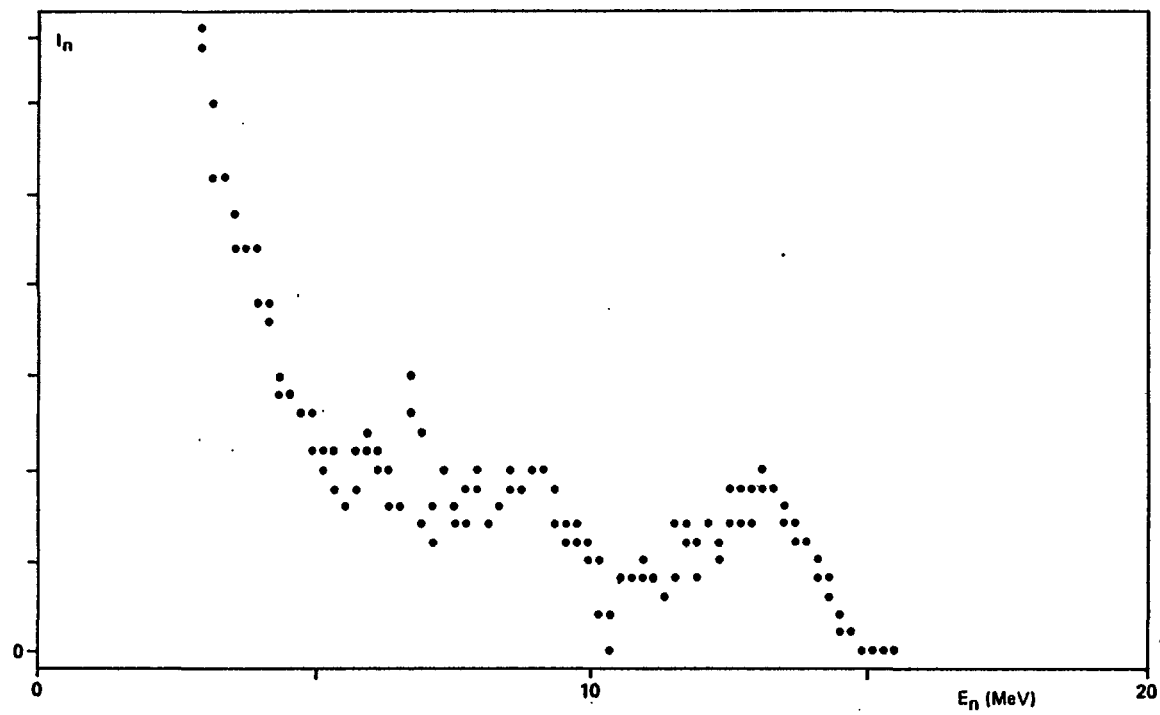

Fig. 5 The same as in Fig. 4, measured by detector D_2 (0.5 cm thick).

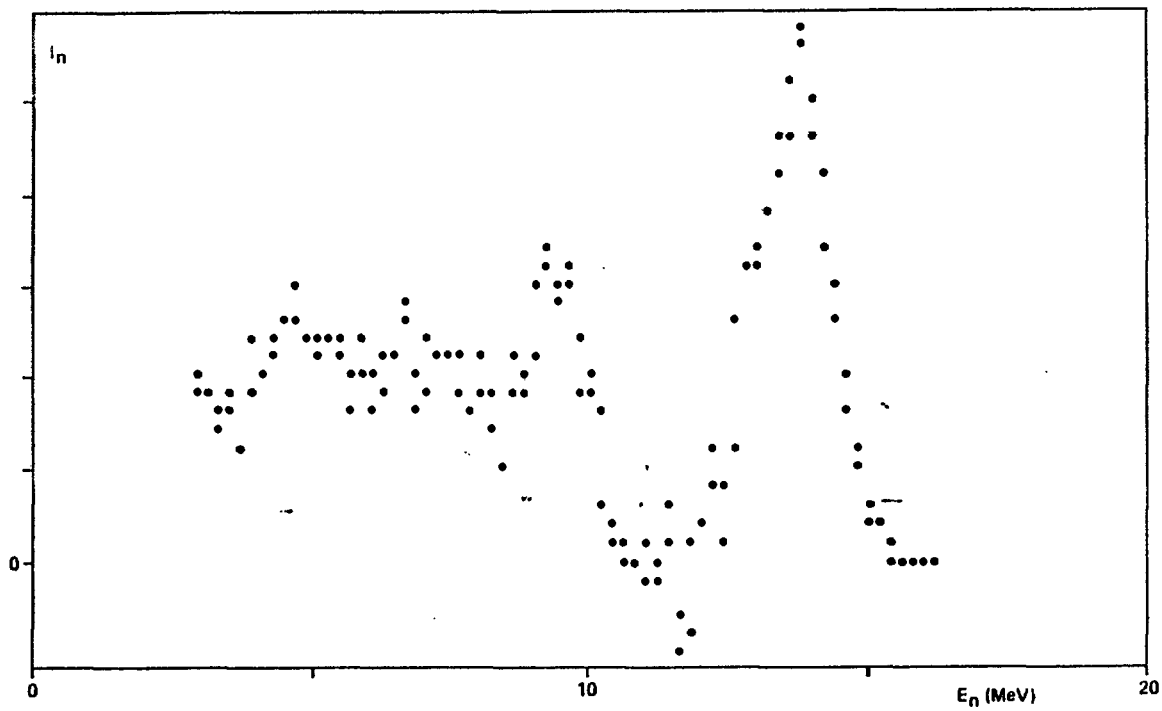

Fig. 6 Difference of spectra of Fig. 4 and Fig. 5, representing the spectrum of a "difference" detector, with no wall effects.

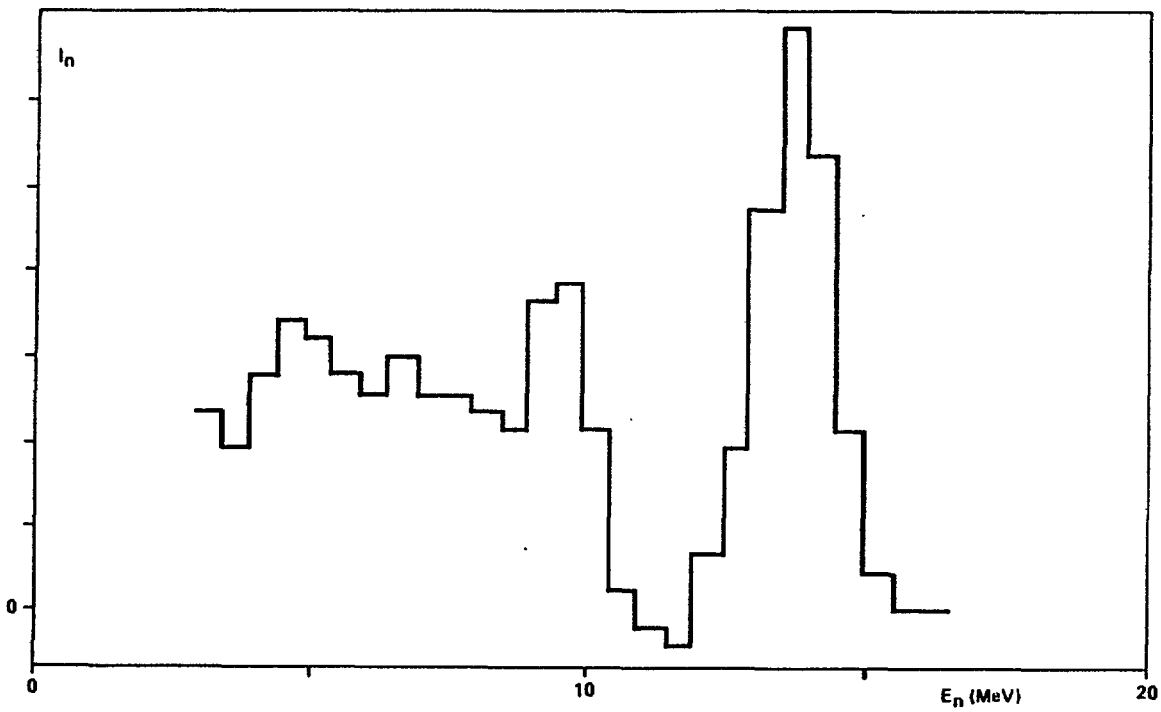

Fig. 7 Histogram of spectrum of Fig. 6.

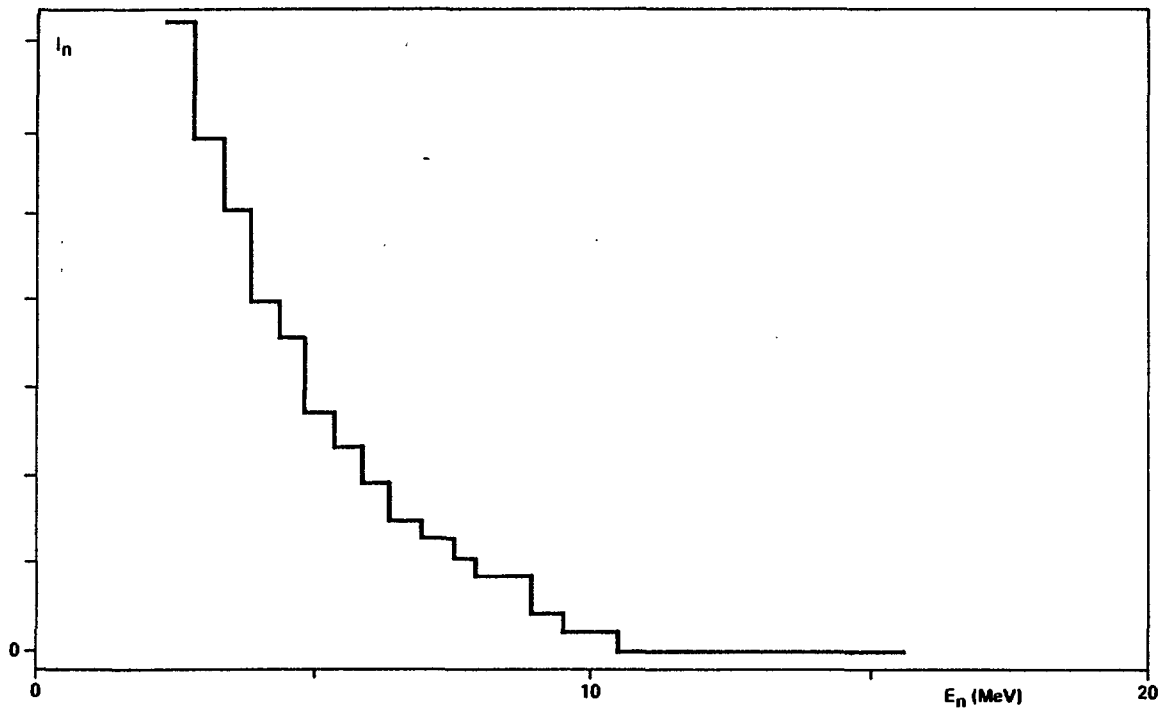

Fig. 8 Histogram of background neutron spectrum, measured without Li target. I_n scale expanded by 30, relative to Fig. 7.

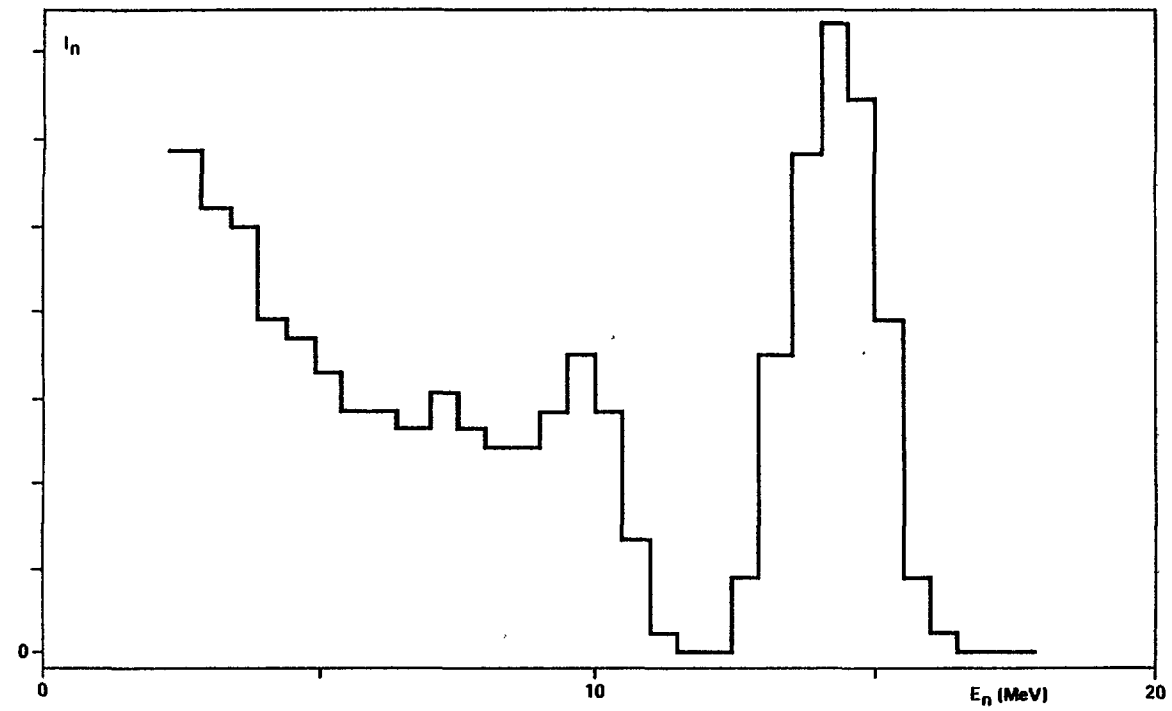

Fig. 9 Histogram of the neutron spectrum, from the p-Li target, at Ep = 17.65 MeV, $\vartheta = 45^{\circ}$.

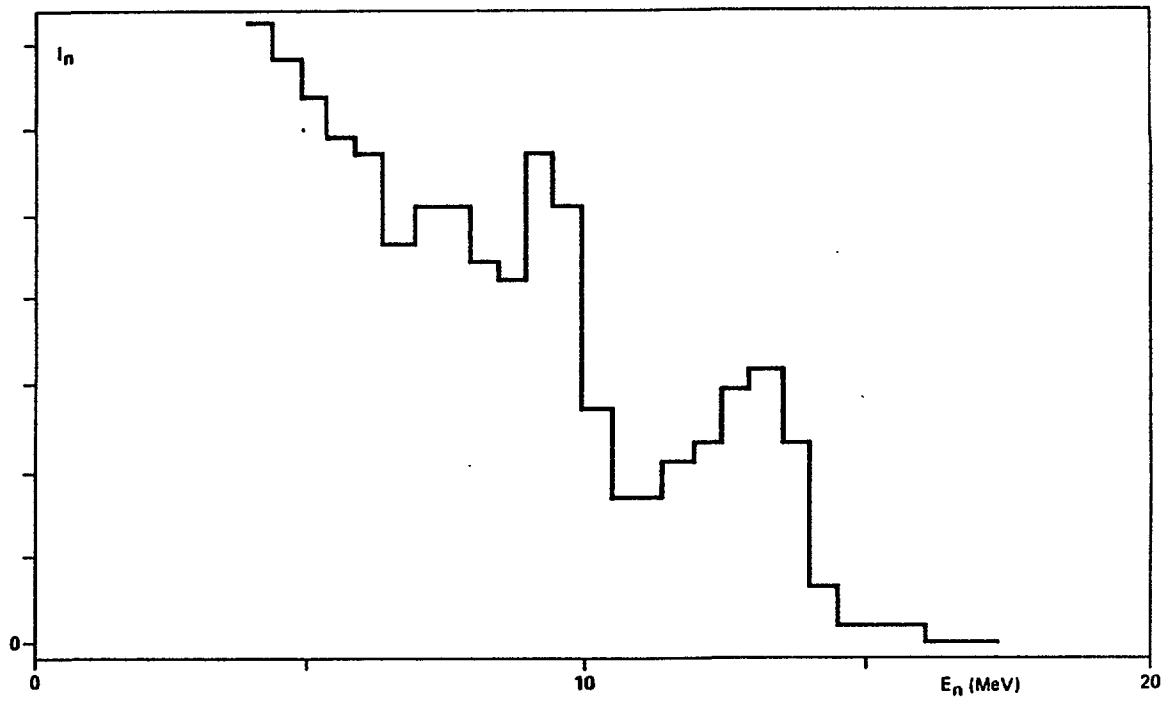

Fig. 10 Histogram of the neutron spectrum from the p-Li target, at Ep = 20 MeV, $\vartheta = 80^{o}$.

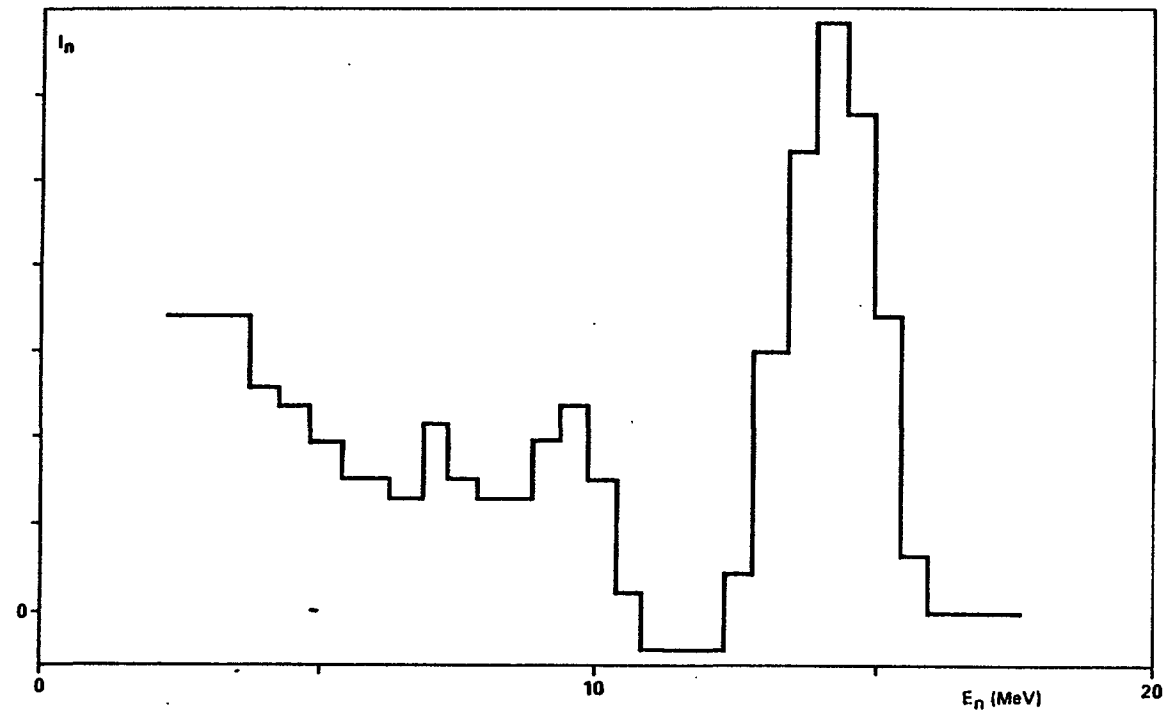

Fig. 11 Linear combination of spectra of Fig. 9 and 10, which shows a higher peak /total ratio.

Following this line, we plan to extend the spectral analysis to angles $\vartheta > 90^{o}$ and to the case of $^{6}Li(d,n)$.

From measurements (of linear effects) obtained with basic spectra, it should be obviously possible to derive integral data for any linear combination spectrum but, for this purpose, accurate fluence dosimetry methods are required.

ACTIVATION AND He GENERATION EXPERIMENTS

A first irradiation experiment has been performed to test the system operation at full beam intensity and to investigate the possibility to obtain accurate relative measurements of the activation and of the He generation in different materials. We are particularly interested in a comparison of the candidate structural materials AISI 316 and AMCR 33, with reference to pure Ni.

The experimental disposition is like in Fig. 2. Tablets of the three materials, of 4x3x1.2 mm, are alternately disposed on a thin Al ring, along a circular zone coaxial with the target tube and are viewed from the Li target centre under a mean angle $\vartheta = 45^{o}$ at a distance of $\sim$ 2 cm. Each of the four equivalent quadrants of the zone is filled with 1 Ni, 2 AISI 316 and 2 AMCR 33 samples, in the sequence ABCBC.
With the actual irradiation geometry and a proton beam energy E_p = 17.65 MeV, the neutron spectral distribution should be well represented by the previous spectrometer measurement (Fig. 9). Indeed, the spread in the incident neutron energy due to a finite source and sample extension is still limited (of the order of the spectrometer spread, in the 14 MeV peak).
The irradiation intensity was measured by the proton current collected by the beam stopper, which was integrated and recorded. We verified a defect in the current collection, probably due to an excessive Coulomb multiscattering in the target (Li and surface contaminations). However, in the irradiation period of $\sim$ 3 days, the measured current ($\sim$ 20-50 μA, interrupted overnight, total collected charge 2.5 C) remained accurately proportional to a neutron monitor current, showing no apparent Li target deterioration.
For reference, the ^{7}Be generated in the Li target was measured after the irradiation using a gamma spectrometer. An order of magnitude esti-

mate of the neutron fluence in the sample is $\sim 2 \cdot 10^{14}$ n cm^{-2}. Fluences of $\sim 10^{15}$ n $cm^{-2}s^{-1}$ or more could be achieved in a current one-week irradiation cycle.

The gamma activity of the irradiated samples has been analysed using a 3"x3" NaI crystal spectrometer and few radioelements have been identified from the gamma energies and decay times.
First, the axial symmetry of the neutron field in the sample region was tested, by comparing the activity of the samples of each material with their respective average value. A variation within ± 15% was found along the irradiation zone. However, the relative activities of the three materials measured in each quadrant were found to be consistent within ± 2% or better. No significant variation was observed in the relative activities of different radioelements in samples of the same material.
The results are consistent with a simple neutron fluence variation (asymmetry of the neutron source profile) with no apparent competition of spectrum variation effects and they assure a good relative accuracy of the average values measured with the sample set of each material.

A few of these results are reported in Table I, indicating only the dominant component of the observed gamma line. The data produced by the experiments will be compared with calculations performed at the JRC-Ispra, by Dr. C. Ponti, with the presently available computing tools, namely the domestic code ANITA (Analysis of Neutron Induced Transmutation and Activation) and the nuclear data library UKCTR III (revised version).
The reported preliminary results and the evaluated data, with a suitable normalization of the neutron fluence, are found in agreement within ± 5%.

The generation of He-atoms in materials by fast neutron irradiation is studied using a mass spectrometer system, at the Institut für Festkörperforschung, KFA-Jülich. This consists essentially of a Balzers QMG 311 quadrupole spectrometer with a secondary electron multiplier, which is connected to a recipient pumped by a titanium-sublimation pump, where the specimens are fused in an Al_2O_3 crucible, to release the He. The sensitivity is better than $5 \cdot 10^8$ He-atoms in a recipient volume of 11.5 litres. The mass spectrometer reading is calibrated against a high

TABLE I - Specific gamma activities in materials, measured after decay periods of 15.5 d (left column) and 54.8 d (right column) from the mean time of neutron irradiation. Standard counting errors < 1%.

Isotope	E_γ (keV)	Specific gamma activity (N_γ $cm^{-3}s^{-1}$)					
		Nickel		AISI 316		AMCR 33	
^{57}Co	122, 136	41,718	38,385	5,495	4,446		
^{51}Cr	320			3,567	1,310	2,196	753
^{58}Co	811	386,996	266,568	49,974	35,295		
^{54}Mn	834					18,871	17,028

vacuum gauge (Leybold IE 211 head), however, this calibration is not actually involved in the determination of relative He contents.
The analysis work has been recently started with the irradiated samples decayed below an acceptable (∿ microcurie) activity level.
Measurements with pure Ni samples seem to be regular and in the correct order of magnitude (∿ 10^{10} He-atoms in a sample). On the other hand, the first few measurements with AISI 316 and AMCR 33 samples were disturbed and failed to give reliable values, relative to Ni, due to an excess of gaseous products released from the fused samples. However, apart from this inconvenience (also due to lack of experience with relatively massive samples, of ∿ 0.1 g) which we expect to avoid in next tests by a suitable material preparation (annealing or, eventually, fusion under high vacuum), this kind of neutron source and the other conditions of these preliminary experiments look quite adequate for an accurate determination of the He produced in the materials in a normal irradiation cycle (fluences of ∿ 10^{15} n cm^{-2}).

In the progress of this work, we plan a few improvements and developments of the experimental methods:

- high resolution gamma spectroscopy, using Ge-Li detectors;
- low background measurements of long-term activation;
- fluence dosimetry for integral cross section measurements.

We consider a method for normalizing integral cross section measurements, where the neutron fluence on the samples is normalized to the

fluence on the spectrometer (viewing the source under the same mean angle) which, in turn, is evaluated in the spectrum unfolding by the well known n-p scattering cross section in the scintillation detectors.

Since the source-sample geometry is not very well defined and the spectrometer cannot work in high intensity runs, the sample activation will be directly intercalibrated with dosimeter foils of the same materials, simultaneously irradiated at the detector position (well defined geometry). The high neutron fluence in the dosimeter foils is normalized to the low fluence used in a spectrometer measurement, by the ratio of the corresponding integrated beam currents (to improve the transmitted beam current collection, we plan to insulate and to use as a collector the entire flight tube after the Li target).

When requested, a relative determination of the neutron/proton yields of different thin targets can be obtained by comparing the respective ^{7}Be activities produced by known integrated beam currents.

ACKNOWLEDGEMENTS

The authors would like to express their appreciation for the efficient collaboration of the Cyclotron staff. In particular, they are grateful to Dr. G. Riccobono for his constant interest and support to this work and useful advise. They would also like to thank Dr. M. Castiglioni for his valuable contribution in defining the beamline configuration and for beam profile evaluations. Many thanks are due to Mr. B. Weckermann for preliminary beam profile measurements and adjustments and for his help in solving various technical problems.

REFERENCES

/1/ L.R. Greenwood, "Neutron flux and spectral measurements to characterize irradiation facilities for fusion reactor materials", Proc. 4th ASTM-EURATOM Symp. on Reactor Dosimetry, Gaithersburg, Maryland, 1982.

/2/ D.M. Kneff, H. Farrar, L.R. Greenwood, "A review of melium accumulation neutron dosimetry for fusion neutron test environments", Proc. 4th ASTM-EURATOM Symp. on Reactor Dosimetry, Gaithersburg, Maryland, 1982.

/3/ EUR-9028EN.

/4/ C.D. Swartz, G.E. Owen, "Recoil detection in scintillators", in: Fast Neutron Physics, Vol.I, Ed. Marion-Fowler, Interscience, N.Y. (1960).

/5/ A. Del Guerra, Nucl. Instr. and Meth., 135, 337 (1976).

/6/ R.A. Cecil et al., Nucl. Instr. and Meth., 161, 439 (1979).

/7/ K. Nakayama, E.F. Pessoa, Nucl. Instr. and Meth., 190, 555 (1981).

/8/ H.W. Broek, C.E. Anderson, The Rev. of Sci. Instr., 31, 1063 (1960).

/9/ K.H. Poppe et al., Phys. Rev., C14, 438 (1976).

Helium Measurements for the U.S. Fusion Program

D. W. Kneff
Rockwell International, Canoga Park, CA, USA
L. R. Greenwood
Argonne National Laboratory,Argonne, IL, USA

In the U.S. we have been engaged in a coordinated program to develop helium and radiometric dosimetry for the fusion materials program. This work is being performed primarily by Rockwell and Argonne. Helium and radiometric monitors have been combined in numerous experiments in all types of irradiation facilities including fission reactors, 14 MeV sources, and new high-energy accelerator neutron sources [1-3]. The goal of this work is not only to measure helium production during specific irradiations, but also to test the helium production cross sections leading to improved helium predictions in materials irradiations.

The helium measurements are performed by mass spectrometry at Rockwell using either prepared helium monitors or simple wires which have also been used for radiometric dosimetry. This latter technique is especially important when space is at a premium in reactor irradiations. For fission reactors, selected comparisons between measured and calculated helium production are shown in Table I. This table summarizes numerous measurements at different fluence levels between 2-15x10^{26} n/m^2 in the High Flux Isotopes Reactor at Oak Ridge National Laboratory. As can be seen, the nickel and iron results show excellent agreement while the titanium and copper results show significant differences. In all cases the calculations are based on the results of adjusted neutron spectra (using radiometric dosimetry and the STAY'SL computer code at Argonne) and the ENDF/B-V Gas Production File [4]. In the case of nickel, we have recently published a new method for calculating the thermal production from ^{58}Ni [5]. This method uses newly evaluated cross sections for 58 and 59 Ni [6]. It is also interesting to note that this thermal process in nickel produces significant extra displacement damage in the ratio of 1 displacement per atom for every 567 appm helium [5]. As is evident in Table I and reference [6], it is now possible to predict helium production in nickel (and stainless steel) with high accuracy.

A new thermal effect has also been discovered in copper, as is evident from the poor disagreement in Table I. We have recently published an explanation of this effect [7]. The helium is produced by a three-stage capture reaction from ^{63}Cu to ^{64}Cu (which decays rapidly to ^{64}Zn) and the ^{64}Zn is then converted to ^{65}Zn which has a high thermal (n,helium) cross section. Using our helium and radiometric data as well as mass spectrometry on irradiated copper samples, it has been possible to deduce the previously unknown cross sections for each stage of the process, as given in Table II. The ^{65}Zn(n,helium) cross section is found to be 4.7 b, much less than reported in ENDF/B-V; however, from the burnup of ^{65}Zn it is clear that the total absorption cross section is about 66 b. The difference is presumably due to capture gammas and protons. From data taken in fast reactors

TABLE I: HELIUM MEASUREMENTS VS. CALCULATIONS FOR HIGH FLUX ISOTOPES REACTOR (HFIR)

MATERIAL	CALCULATED / MEASURED
Ni	0.94
Fe	1.03
Ti	2.37
Cu	0.63 - 0.19 (THERMAL 3-STAGE REACTION)

- FOR TOTAL NEUTRON FLUENCE RANGE 2-15x10^{22} n/cm^2
- CALCULATIONS BASED ON ENDF/B-V; Ni INCLUDES NEW Ni-59 EVALUATION

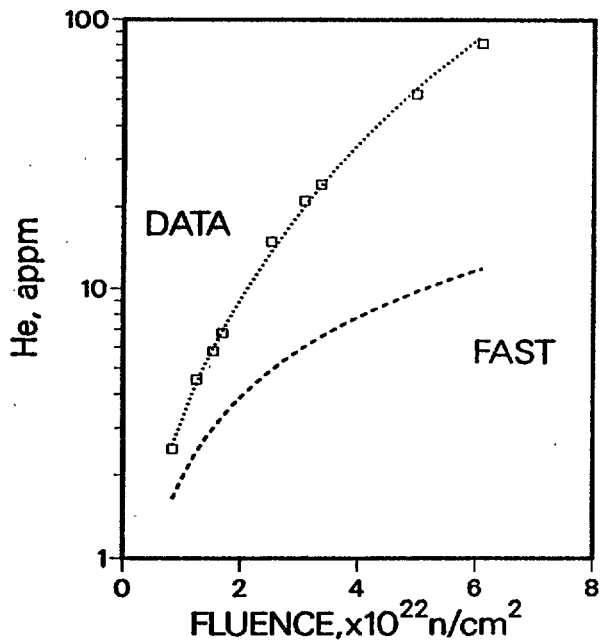

1. Comparison of measured and predicted helium production in copper vs. thermal fluence in the mixed-spectrum reactor HFIR. The dashed line is calculated using ENDF/B-V (fast fluence >.1 MeV is 0.8 times thermal fluence). The data clearly shows a new effect which is well described by our ^{65}Zn process as indicated by the solid line through the data.

it is also clear that the fast neutron helium production cross section in copper is higher than predicted by about 30%. Figure 1 shows a comparison of measured and calculated helium production in copper. The dashed line is the usual fast neutron calculation from ENDF/B-V. The data are well fit using our new thermal and fast cross sections, as listed in Table II. An approximate equation has been developed for these conditions in HFIR, as follows:

$$\text{He(appm)} = 0.67 \times (\text{thermal fluence})^{2.58}$$

where the thermal fluence is in units of 10^{22} neutrons/cm^2. After a thermal

TABLE II

MEASURED HEUTRON CROSS SECTIONS FOR THE THERMAL HELIUM PRODUCTION FROM COPPER

$^{63}Cu(n,\gamma)$ $^{64}Cu(\beta^-)$ $^{64}Zn(n,\gamma)$ $^{65}Zn(n,He)$

Reaction	Data	ENDF/B-V
Thermal Reactions, barns		
$^{65}Zn(n,He)$	4.7 ± 1.5	250 ± 150
$^{65}Zn(n,abs)$	66 ± 8	
$^{64}Cu(n,\gamma)$	270 ± 170	< 6000
Fast Reactions, microbarns		
Cu(n,He)	313 ± 20	238

fluence of 10^{27} n/m^2 in HFIR (about 1.5 years), this will produce about 250 appm extra helium. The fast ^{62}Ni recoils will also produce extra displacement damage in the ratio of 1 dpa for every 492 appm extra helium; however, this will produce only 0.5 extra dpa in the example given above. Certainly, this effect is much less than in nickel, primarily since it requires three reaction stages rather than two. If one started with zinc, then the effects would be comparable. Nevertheless, the helium production is quite substantial and cannot be neglected if mixed-spectrum reactors are used to study radiation effects in copper.

Helium cross sections have been directly measured at about 14.8 MeV for 26 pure elements and 33 separated isotopes and the results are summarized in Table III. These measurements were made at the Rotating Target Neutron Sources I and II at Lawrence Livermore National Laboratory. These data have recently been submitted for publication [8,9] and detailed comparisons with ENDF/B-V and other references are included.

Helium measurements have also been made at higher neutron energies using the Be(d,n) neutron field produced by 30 MeV neutrons at the University of California at Davis. Results are reported for 11 elements and 17 isotopes in Table IV. Comparing these data with the 14 MeV data in Table III shows no unusual effects due to the higher energy neutrons in the Be(d,n) field (up to 34 MeV). These results have also been published [2].

Helium cross section needs can be summarized as follows. At 14 MeV the elements N, Mg, and W, and isotopes of Cr and Ti need to be measured. Few good measurements are available for any materials in the 8-13 MeV region. Monoenergetic data are required for most materials. For fission reactors, measurements for many other elements and isotopes are in progress. However, these measurements need to be supplemented by measurements in other spectra in order to deduce spectral effects. At energies above 15 MeV only one integral measurement has

TABLE III: SUMMARY OF HELIUM GENERATION CROSS SECTION RESULTS FOR 14.8-MeV NEUTRONS (RTNS-I AND RTNS-II)

Material	Cross Section (mb)	Material	Cross Section (mb)	Material	Cross Section (mb)
Li	349 ± 15	Fe	48 ± 3	Mo	14 ± 1
Li-6	512 ± 26	Fe-54	91 ± 6	Mo-92	31 ± 2
Li-7	336 ± 16	Fe-56	46 ± 3	Mo-94	22 ± 2
Be	1018 ± 83	Fe-57	33 ± 2	Mo-95	17 ± 1
B	390 ± 32	Fe-58	20 ± 2	Mo-96	12 ± 1
B-10	693 ± 84	Co	40 ± 3	Mo-97	10 ± 1
B-11	306 ± 21	Ni	99 ± 6	Mo-98	6.7 ± 3.2
C	894 ± 60	Ni-58	121 ± 8	Mo-100	3.8 ± 0.3
O	401 ± 32	Ni-60	79 ± 5	Ag	7.6 ± 0.6
F	501 ± 36	Ni-61	51 ± 4	Sn	1.5 ± 0.1
Al	143 ± 7	Ni-62	22 ± 2	Ta	1.10 ± 0.09
Si	216 ± 11	Ni-64	9 ± 1	Pt	0.71 ± 0.10
Ti	38 ± 2	Cu	51 ± 3	Au	0.50 ± 0.04
V	18.5 ± 1.1	Cu-63	65 ± 4	Pb	0.62 ± 0.05
Cr	34 ± 3	Cu-65	17 ± 1		
Mn	28 ± 2	Y	9.3 ± 0.7	316 SS	56 ± 4
		Zr	10.1 ± 0.7	HT9	55 ± 4
		Nb	14 ± 1	9Cr-1Mo	50 ± 4

TABLE IV: INTEGRAL HELIUM GENERATION CROSS SECTIONS FOR THE 0-32 MeV Be(d,n) NEUTRON SPECTRUM PRODUCED BY 30-MeV DEUTERONS

Material	Average Cross Section (mb)		Material	Average Cross Section (mb)	
	Total Fluence	Fluence >5 MeV[a]		Total Fluence [a]	Fluence >5 MeV[a]
Al	60	121	Cu	18	41
V	8	16	^{63}Cu	22	55
Cr	13	31	^{65}Cu	8	15
Fe	19	41	Zr	4	9
^{54}Fe	34	76	Nb	5	12
^{56}Fe	18	43	Mo	6	14
^{57}Fe	-	-	^{92}Mo	12	26
^{58}Fe	8	21	^{94}Mo	8	20
Co	13	34	^{95}Mo	9	16
Ni	40	98	^{96}Mo	5	9
^{58}Ni	51	127	^{97}Mo	5	10
^{60}Ni	32	73	^{98}Mo		
^{61}Ni	23	47	^{100}Mo	2	4
^{62}Ni	15	36	Au	0.5	1.2
^{64}Ni	-	-			

(a) Cross section uncertainties: ± 35% (total fluence), ± 18% (>5 MeV) due to changing neutron spectrum with source angle

been made in a Be(d,n) field and there are very few measurements for spallation sources. More integral measurements are required at various energies to deduce appropriate helium production data.

REFERENCES

1. D. W. Kneff, H. Farrar IV, and L. R. Greenwood, J. Nucl. Mater. 103, p. 1451-1456(1981).

2. D. W. Kneff, H. Farrar IV, L. R. Greenwood, and M. W. Guinan, Symp. on Neutron Cross Sections for 10-50 MeV, BNL-NCS-51245, pp. 113-132 (1980).

3. B. M. Oliver, D. W. Kneff, and R. P. Skowronski, Damage Analysis and Fund. Studies Quarterly Prog. Rep., DOE/ER-0046-18, August 1984.

4. Evaluated Nuclear Data File, Version V, Part B, National Neutron Cross Section Center, Brookhaven National Laboratory, 1979.

5. L. R. Greenwood, J. Nucl. Mater. 115, pp. 137-142 (1983).

6. L. R. Greenwood, D. W. Kneff, R. P. Skowronski, and F. M. Mann, J. Nucl. Mater. 122, pp. 1002-1010 (1984).

7. D. W. Kneff, L. R. Greenwood, B. M. Oliver, R. P. Skowronski, and E. L. Callis, Proc. Int. Conf. on Nuclear Data for Basic and Applied Sci., Santa Fe, NM, May 1985 (to be published).

8. D. W. Kneff, B. M. Oliver, H. Farrar IV, and L. R. Greenwood, Helium Production in Pure Elements, Isotopes, and Alloy Steels by 14.8 MeV Neutrons, to be published in Nucl. Sci. Eng. (1985).

9. D. W. Kneff, B. M. Oliver, E. Goldberg, and R. C. Haight, Helium Production Cross Sections for 15-MeV Neutrons on ^{6}Li and ^{7}Li, submitted to Nucl. Sci. Eng. (1985).

NUCLEAR DATA FOR HIGH-ENERGY NEUTRON TRANSPORT AND DAMAGE CALCULATIONS IN STEEL

G. Prillinger
Institut für Kernenergetik und Energiesysteme (IKE),
Universität Stuttgart, Pfaffenwaldring 31, D-7000 Stuttgart 80
West Germany

Abstract

For simulating neutron damage in materials needed for the design of fusion reactors the application of high-energetic neutrons from generators and spallation sources up to 1000 MeV is planned. To characterize the radiation damage environment of the various facilities the neutron spectra, primary displacement damage and gas-production rates must be determined.

In contrary to energies below 20 MeV, only few evaluated data sets are available for high energy neutrons. Transport cross-section libraries like HILO or LANL have been compared with a cross-section set calculated with the HETC code. To describe accurately the high scattering anisotropy essential improvements have been performed in the ANISN transport code.

To generate total and differential damage parameters in the medium energy range from 20 - 50 MeV a special code has been written handling also cascade-reactions. For iron and the main additional elements of stainless steel the energy transfer to the heavy recoils and light emitted particles has been calculated.

1 Introduction

For simulating radiation damage in fusion reactor materials irradiation experiments will be performed in different environments of high-energy neutrons. Beside the d-T fusion source around 14 MeV accelerator neutrons from the d-Li or d-Be reaction and finally spallation sources up to 1100 MeV are in operation or will be constructed. To correlate better and compare material property changes

in different neutron spectra a lot of new nuclear data in the high-energy range but also improved computational methods are necessary.

To calculate neutron damage first of all the neutron spectrum must be known. An accurate transport calculation of the neutron flux spectrum starting from a well defined source is essential for the analysis of integral dosimetry measurements and for predicting irradiation damage exposure parameters in reactor structural components. Exposure values like displacement damage and gas-production may be obtained directly from calculations or indirectly from calculations that are adjusted with dosimetry measurements.

The basic input quantities for transport codes are the multigroup cross-section libraries. Available high-energy libraries like HILO /1/ and a second one named LANL in this report /2/ have been analysed and compared with new data calculated with the HETC code /3/. Neutron scattering becomes very anisotropic above 10 MeV especially for medium and heavy elements. To describe the forward peaked scattering more accurately the transport code ANISN /4/ has been improved essentially.

Knowing the neutron spectrum damage parameters like DPA, damage energy and gas-production rates can be calculated. In contrast to fission reactor neutrons where standardized displacement and damage cross-sections already exist new data must be calculated for high-energy neutrons. The computer code SPALL-S has been developed and applied to calculate displacement and damage energy cross-section in a medium energy range for iron and the main additional elements of stainless steel.

2 Multigroup Cross-Section Libraries for High-Energy Neutron Transport

For neutron energies below 20 MeV a large number of multigroup cross-section libraries for different applications exist. To the contrary above 20 MeV there is a lack of evaluated nuclear data files. Consequently there are only few multigroup libraries available. These libraries have several limitations and can not be applied generally. The HILO and LANL library have been analyzed and compared with new data calculated for iron with the HETC code /3/.

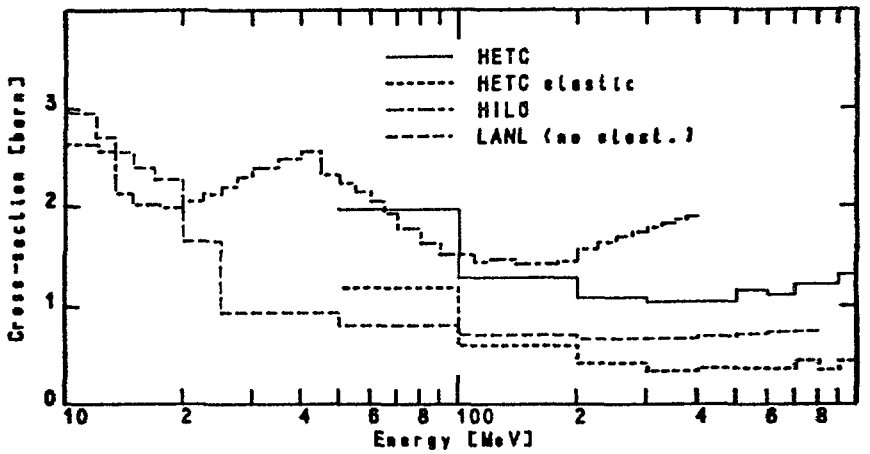

FIG.1 : Total and elastic neutron interaction cross-section in iron

Figure 1 shows the energy dependence of the total cross-section. The LANL library does not contain elastic scattering and is in reasonable agreement with the nonelastic part of the HETC data. The cross-sections in HILO are too high above 100 MeV. In the energy range from 20 to 100 MeV the elastic and nonelastic components are comparable high. Above 100 MeV the elastic part decreases to about 25 % at 1 GeV.

Elastic scattering becomes very anisotropic with increasing energy. High order Legendre expansions of the scattering matrices are ne-

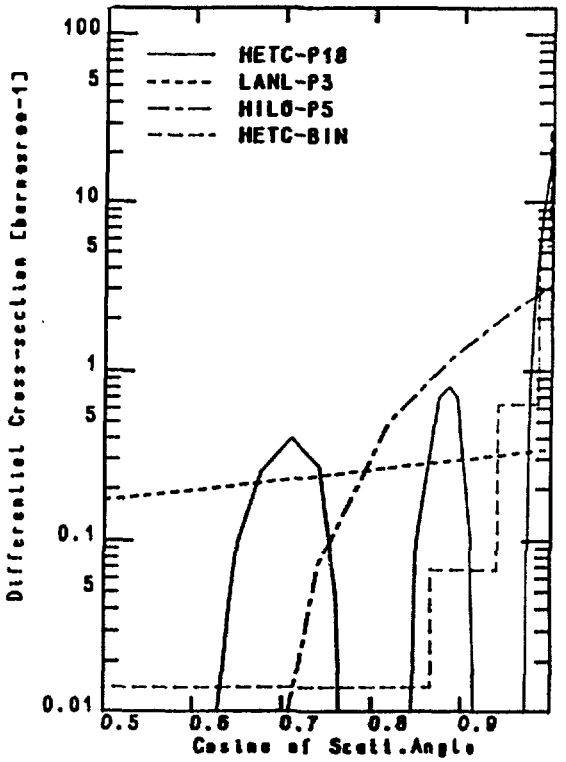

FIG.2 : Scattering cross-section for iron at 75 MeV

cessary in standard transport codes for an accurate treatment of the small changes in angle and energy. In Figure 2 the angular dependence of the total scattering cross-section for iron at 75 MeV, calculated with HETC in discrete angular bins and in P-18 expansion, is shown. Truncated Legendre expansions like P-5 in HILO and P-3 in LANL can not fit the forward peak of the cross-section.

3 ANISN-FP for High Energy Neutron Transport Calculations

In standard transport codes strong anisotropic scattering can not be handled efficiently. High Legendre expansions of the scattering cross-sections are necessary especially for deep penetration problems or if accurate angular fluxes are required. A more efficient treatment can be obtained if the high anisotropic component of the cross-section is separated in the Boltzmann equation. The scattering integral

$$\int\int \Sigma(E' \to E,\ \bar{\Omega}\cdot\bar{\Omega}')\,\phi(E',\Omega')\,dE'\,d\bar{\Omega}'$$

is splitted into two parts, where the anisotropic component is approximated by a linear ansatz leading to Fokker-Planck terms of the form

$$\frac{\partial}{\partial E}\, S(E)\phi + T(E)\, \frac{\partial}{\partial \mu}(1-\mu^2)\, \frac{\partial \phi}{\partial \mu} \quad .$$

The new equation, known also as Boltzmann-Fokker-Planck /5/ equation, can not be solved with transport codes like ANISN directly because the additional parabolic term in μ leads to a coupling of the angular fluxes in the S_N-equations. A new algorithm has therefore been written which is active in ANISN-FP for energy groups where FP-coefficients S and T are given /6/. Approximating the elastic scattering cross-section by an expression of the form

$$\sigma_{el}(\mu) = \alpha\ \beta\ \exp\left[-\beta(1-\mu)\right]$$

the FP-coefficients are defined by

$$T(E) = \pi\ \alpha\left[\frac{1}{\beta}\ (1-\exp(-2\beta)-2\ \exp(-2\beta)\right]$$

$$S(E) = 4\ \frac{E}{A}\ T(E)$$

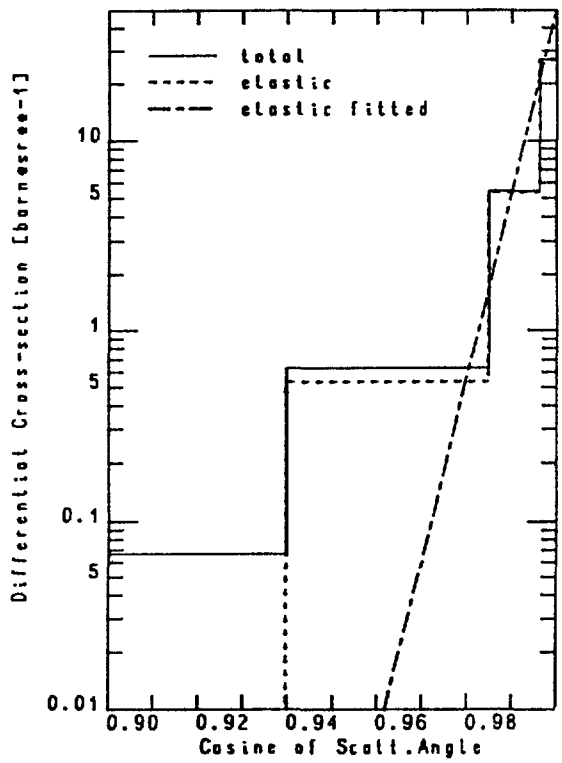

FIG.3 : Scattering cross-section for iron at 75 MeV

Values for α and β are determined by a fitting procedure as can be seen in Figure 3 for 75 MeV neutrons.

To describe neutron scattering in iron FP-coefficients can be effectively used instead of high order Legendre expansions, especially in the energy range from 10 to 100 MeV. Above 100 MeV a straight ahead approximation with transport corrected cross-section is sufficiently accurate.

The amount of nuclear data to be stored can be appreciably reduced. Neutron spectra can be calculated more accurately with less computational effort.

4 Damage Calculations for High-Energy Neutrons

To correlate material damage in different neutron spectra a detailed understanding of the energy transfer from fast neutrons to lattice atoms is necessary. From recoil energy distributions exposure-quantities like displacement or energy damage can be deduced. These quantitites can further serve as input parameters for more sophisticated damage models which take into account also annealing or chemical composition of the irradiated material.

For neutron energies above the fission spectrum a great variety of partial reactions become energetically possible. Since measurements of partial cross-sections above 20 MeV are rare, evaluations are based primarily on predictions of nuclear model codes like GNASH /7/ or STAPRE /8/. Results of both programs have been used to study the energy transfer in iron, nickel and chromium for incident neutron energies up to 40 MeV.

Comparing two cross-section evaluations for iron-56 /8, 9/ and ENDF/B-4 data significant differences have been observed in (n,2n)-, (n,3n)-, (n,n'p)- and (n,n'α)-reactions as can be seen in Figure 4. Inaccurate neutron cross-sections must be regarded as being the major source of uncertainty in calculating neutron damage cross-sections above 20 MeV.

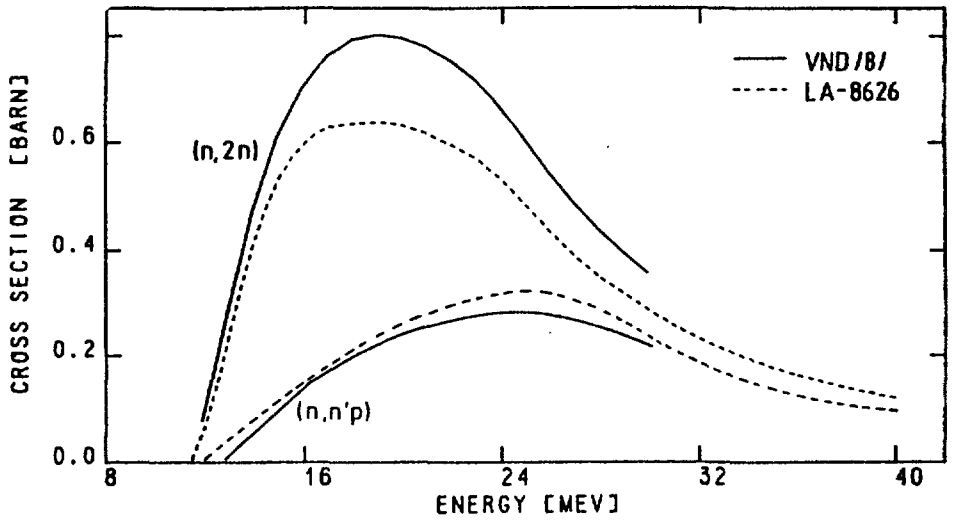

FIG.4: $^{56}Fe(n,2n)$ and $^{56}Fe(n,n'p)$ cross-section

5 The Cascade Processing Code SPALL-S

To calculate neutron damage parameters for energies below 20 MeV several computer codes exist /10, 11, 12/. They all use ENDF/B data input. Above 20 MeV nuclear cascade-reactions become the dominating part, requiring a detailed treatment of their contribution to damage cross-sections.

To study the neutron energy transfer by nuclear cascade-reactions the code SPALL-S has been written. Using the evaporation model the energy spectrum of the heavy recoil atom as well as that of the

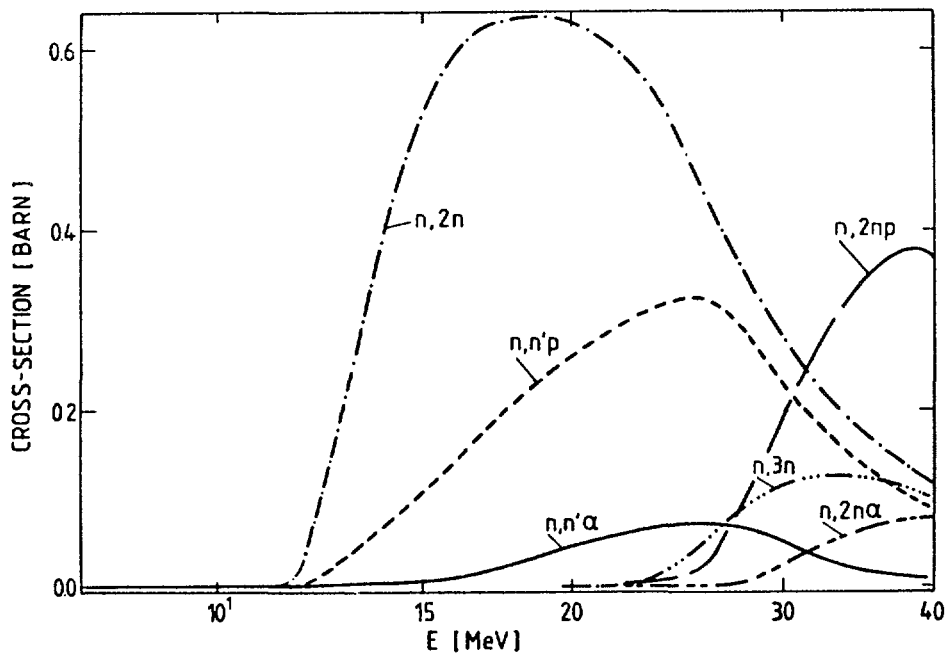

FIG.5: Cascade-reactions of ^{56}Fe up to 40 MeV

smaller emitted particles are calculated with a Monte Carlo procedure. Up to three emitted particles are covered, so that all partial cascade-reactions can be treated, which are of importance up to 40 MeV, as shown for iron-56 in Figure 5.

For charged emitted particles the Coulomb barrier suppresses the lowest energies, and we get for the energy distribution of the evaporated particles in CMS

$$f(E_n \rightarrow T) \cdot dT = C(T-KT_c) \cdot \exp[-(T-KT_c)/\theta] \cdot dT$$

with

E_n = energy of incoming neutron
T = energy of emitted particle
C = normalisation constant
T_c = Coulomb barrier
θ = nuclear temperature
k = fitting constant (0,47 for protons, 0,60 for α-particles)

The code SPALL-S is operating within our modular program system RSYST /13/. The total system applied for processing of kerma and damage data is shown in Figure 6.

To check the SPALL-S code and to see whether the evaporation model is adequate to simulate the energy distribution of the emitted

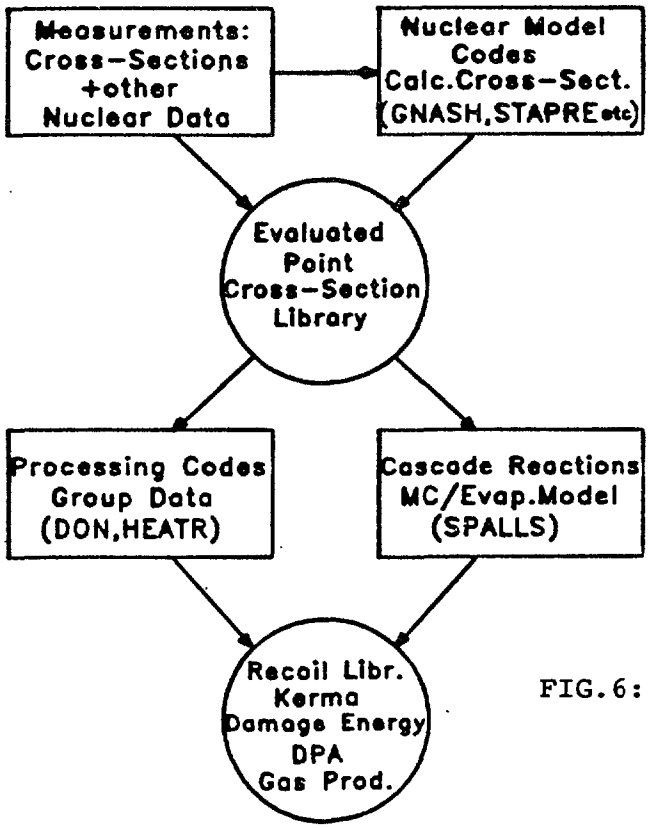

FIG.6: Calculation of neutron damage up to 40 MeV

Table 1: Comparison of the average energies of the emitted protons and alpha particles at 15 MeV incident neutron energy calculated by SPALL-S with measured data /14/

Target	Particle emitted	Average Energy MeV	
		SPALL-S	Measured
Cr-52	p	4.41	4.7 ± 0.2
Cr-52	α	8.44	8.4 ± 0.4
Fe-54	p	4.74	4.8 ± 0.2
Fe-54	α	9.15	8.7 ± 0.4
Fe-56	p	4.55	5.1 ± 0.2
Fe-56	α	8.71	8.8 ± 0.6
Ni-58	p	5.17	5.1 ± 0.2
Ni-58	α	9.67	9.5 ± 0.3
Ni-60	p	4.12	5.0 ± 0.2
Ni-60	α	9.00	9.0 ± 0.3

particles detailed intercomparisons with available data has been performed.

The comparison of the average energies of emitted protons and alpha particles at 15 MeV with measured data /14/ shows excellent agreement for various nuclides as can be seen in Table 1.

The same holds for the neutron emission spectrum. For example ENDF/B-4 data are compared with SPALL-S in Figure 7 for $^{56}Fe(n,2n)$ at 20 MeV. Discrepancies have been observed for energy distributions of the heavy recoils calculated with SPALL-S compared to the RECOIL library DLC-55 /15/. In neutron reactions with emitted charged particles the average recoil energy is strongly underestimated (Figure 8 and 9).

Finally the total damage energy cross-section has been calculated between 10 and 40 MeV for iron shown in Figure 10.

The good agreement of the results achieved up to 20 MeV justifies use of SPALL-S also at higher energies and for other nuclides,

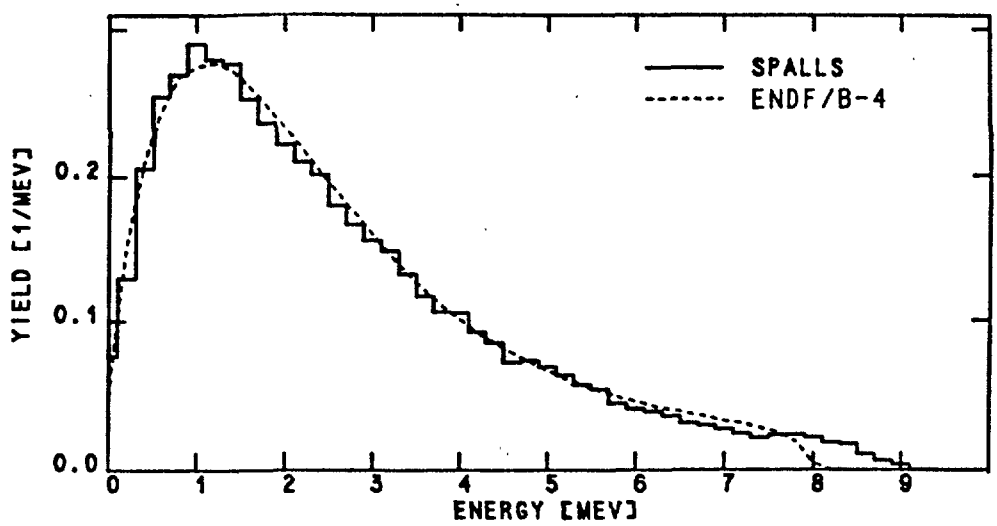

FIG.7: $^{56}Fe(n,2n)$, emitted neutron spectrum at 20 MeV

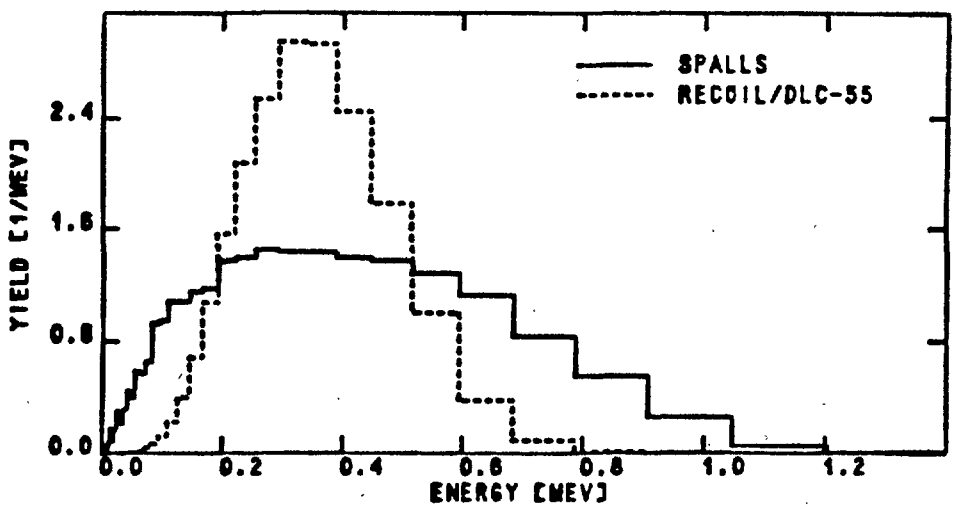

FIG.8: Recoil spectrum $^{56}Fe(n,n'p)$ at 20 MeV

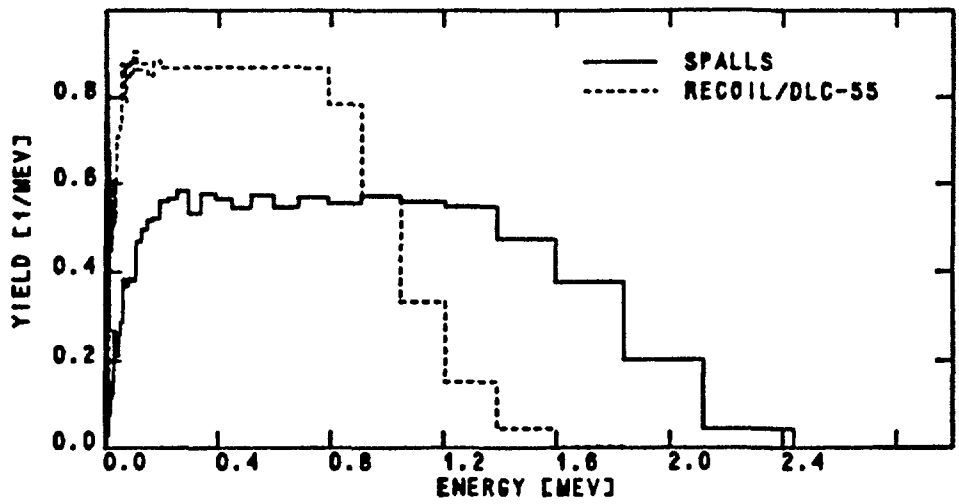

FIG.9: Recoil spectrum $^{56}Fe(n,n'p)$ at 20 MeV

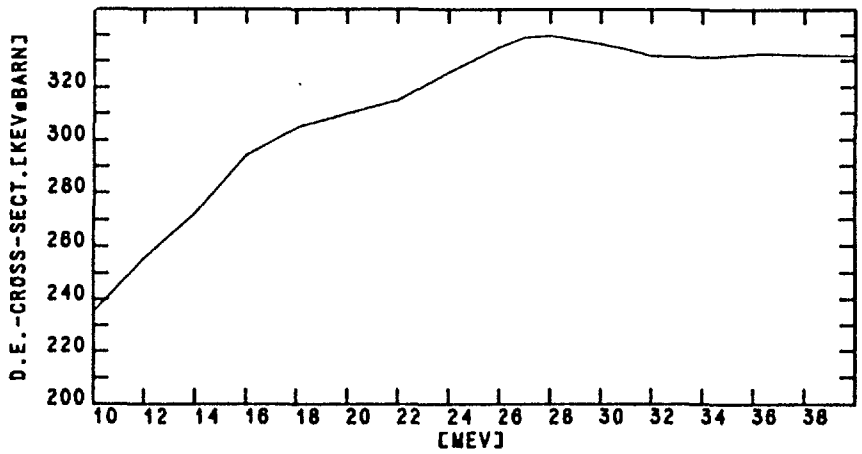

FIG.10: Damage energy cross-section for iron (keV·barn)

provided relevant partial reaction cross-sections are available. For spallation neutrons with several hundred MeV energy improved models and codes are necessary /16/.

References

/1/ R.G. Alsmiller, Jr., J. Barish,
Neutron Photon Multigroup Cross Sections for Neutron Energies < 400 MeV, ORNL/TM-7818 (1981), RSIC, DLC-87

/2/ W.B. Wilson,
Nuclear Data Development and Shield Design for Neutrons Below 60 MeV, LA-7159-T (1978), RSIC, DLC-84

/3/ P. Cloth, D. Filges, G. Sterzenbach, T.W. Armstrong, B.L. Colborn,
The KFA-Version of the High-Energy Transport Code HETC and the Generalized Evaluation Code SIMPLE, Jül-Spez-196 (1983)

/4/ W.W. Engle,
A User's Manual for ANISN, USAEC Report K-1693 (1967)

/5/ M. Caro, J. Ligou,
Treatment of Scattering Anisotropy of Neutrons through the Boltzmann-Fokker-Planck Equation, Nucl. Sc. Eng. 83, p. 242 (1983)

/6/ G. Prillinger,
ANISN-FP, a ANISN Version for High Energy Neutron Transport, to be published

/7/ P.G. Young, E.D. Arthur,
GNASH, A Preequilibrium, Statistical Nuclear Model Code for Calculation of Cross-Sections and Emission Spectra, LA-6947 (1977)

/8/ B. Strohmaier, M. Uhl,
Nuclear Model Calculations of Neutron Induced Cross-Sections for ^{52}Cr, ^{55}Mn, ^{56}Fe, and $^{58+60}Ni$ for Incident Energies up to 30 MeV, in: Nuclear Data for Science and Technology, Ed., K.H. Böckhoff, Reidel Publishing, Dordrecht/Holland 1983

/9/ E.D. Arthur, P.G. Young,
Evaluated Neutron-Induced Cross-Sections for $^{54,56}Fe$ to 40 MeV, LA-8626-MS(ENDF-304) (1980)

/10/ R.E. McFarlane, D.W. Muir, F.M. Mann,
Radiation Damage Calculation with NJOY, 3rd Topical Meeting on Fusion Reactor Materials, Albuquerque, 1983

/11/ G.R. Odette, D.R. Dorion,
Nucl. Technol. 29, 346 (1976)

/12/ D.M. Parkin, A.N. Goland,
Calculation of Radiation Effects as Function of Incident Neutron Spectrum, Radiation Effects, 28 (1976)

/13/ R. Rühle,
RSYST, ein integriertes Modulsystem mit Datenbasis zur automatisierten Berechnung von Kernreaktoren, IKE-4-12 (1973), Universität Stuttgart

/14/ S.M. Grimes, R.C. Haight, K.R. Alvar, H.H. Barschall, R.C. Borchers,
Charged-particle Emission in Reactions of 15 MeV Neutron with Isotopes of Chromium, Iron, Nickel, and Copper, Physical Review C 19, 2127 (1979)

/15/ T.A. Gabriel, J.D. Amburgey, N.M. Greene,
Radiation-Damage Calculations: Primary Recoil Spectra, Displacement Rates, and Gas-Production Rates; RECOIL,
DLC-55, ORNL/TM-5160 (1976)

/16/ L.R. Greenwood, R.K. Smither,
Recent Developments in Neutron Dosimetry and Damage Calculations for Fusion Materials Irradiations, 5th ASTM-EURATOM Symposium on Reactor Dosimetry, Geesthacht, September 1984

Information on the REAL84 exercise

W.L. Zijp, E.M. Zsolnay[1], D.E. Cullen[2]

Abstract

This document gives information on the interlaboratory exercise REAL84. This exercise has as aim the improvement of the assessment of accuracies in radiation damage predictions by using good quality input data and proper calculation methods.
In the exercise integral damage parameters (such as displacements per atom, or produced gas atoms) and spectrum characteristics are calculated for neutron spectra which are adjusted to fit experimental reaction rates obtained with activation spectrometry.
The main difference with the preceding exercise REAL80 is that now improved information can be applied in the input data sets of the exercise. The improvement concerns mainly the availability of uncertainty information for the neutron spectrum and cross-section data.
All parties interested are encouraged to participate in the exercise and to request from the IAEA the magnetic tape R84, which contains all input information.
In order to meet the time schedule (see appendix) fast action is required.

1. BACKGROUND

The REAL84 exercise is a follow-up of the REAL80 exercise, the results of which have been published in a final report [1] and in a summarizing publication [2].
The aim of the REAL80 intercomparison organized by the International Atomic Energy Agency (IAEA) was to determine the state of the art (in 1981) of the capabilities of laboratories to adjust neutron spectrum information on the basis of a series of experimental activation rates,

---

1) Nuclear Reactor of the Technical University Budapest, Hungary.

2) International Atomic Energy Agency, Vienna.

and subsequently to predict the number of displacements in steel together with its uncertainty. The solutions submitted by 13 laboratories (33 solutions for the ORR spectrum and 35 solutions for the YAYOI spectrum) were analyzed by a joint evaluation team from the Technical University in Budapest and from the Netherlands Energy Research Foundation ECN in Petten.

The results of the REAL80 exercise have shown that discrepancies in the prediction of radiation damage parameters and unrealistic values in the uncertainties of these data originate partly from using incomplete and/or unrealistic input data in the calculations, and partly from incorrect (or not optimal) processing of the available data by spectrum adjustment and activity calculation codes.

During the IAEA Consultants' Meeting in Vienna (13-15 June 1983) [3] and in Hamburg (26 September 1984) [4] the benefits and the requirements for a follow-up of the REAL80 exercise have been discussed. At the Hamburg meeting is was recommended that a new exercise, called REAL84, should be organized by the IAEA, and the joint evaluation team was asked to make the necessary preparations for the IAEA and to continue as a team for the analysis of the results.

2. PROJECT NAME AND ORGANIZATION

The exercise will have the code name REAL84 (Reaction Rates Estimates Evaluated by Adjustment Analysis in Leading Laboratories, year 1984). The exercise is organized by the Nuclear Data Section (D.E. Cullen and V. Piksaikin) of the International Atomic Energy Agency (IAEA) in Vienna. The analysis of the responses to the exercise will be performed by a joint evaluation team from the Training Nuclear Reactor of Technical University in Budapest (É.M. Zsolnay and E.J. Szondi) and the Netherlands Energy Research Foundation ECN (W.L. Zijp and H.J. Nolthenius).

3. AIMS OF REAL84

The main aim is improving the assessment of accuracies in radiation damage predictions by various laboratories by using good quality input data and proper calculation methods. The emphasis should be on radia-

tion damage to reactor pressure vessels and related nuclear technology. Therefore the neutron energy range of interest is primarily below 20 MeV. The long term aims of REAL84 will be to strive towards establishment of standardized procedures and recommended data for use in spectrum adjustments and damage parameter calculations.
The short term aims will be improvements in the available data, particularly in spectra and cross-section covariance information.
In addition, the REAL84 exercise will allow the participants to assess and validate the accuracy of the methods and codes they are presently using.
The joint effort of the participants will contribute in solving some basic mathematical and physical problems recently encountered in neutron spectrum adjustments for selected neutron spectra.

4. MEANS AND METHODS

The REAL84 exercise has the form of an international comparison of damage production parameters, calculated for adjusted spectra obtained with adjustment codes which explicitly consider covariance matrices.
The seven spectrum data sets available in REAL84 comprise various representative spectra (see section 13).
Participants don't have to adjust all seven spectrum data sets but for a good success of the exercise the treatment of several spectrum data sets by each participant is highly appreciated.

5. REQUESTED ACTION BY PARTICIPANTS

The participation is open to all laboratories, which are able to perform adjustment with procedures which can take into account available uncertainty information in the form of covariance matrices.
It is essential that the participants should contribute to the exercise not only by giving characteristic parameters of interest etc., but also by reporting the physical information applied to obtain improved results for the given input data. (Improved calculation method, conversion method, reaction set, cross section data, covariance data for activity, cross section and spectrum etc.)

The specific actions which the participants should perform are the following:

- select the spectrum data sets of their own interest for their data treatment;
- make a critical judgement of the input data;
- perform a good neutron spectrum adjustment by means of their laboratory procedure, taking into account the input covariance matrices;
- perform calculations on displacements for steel (and their uncertainties);
- specify where relevant, the procedure for conversion of data from one group structure to another;
- perform, where relevant, calculations on gas production rates per atom (and its uncertainty) for steel;
- give answer to the specific questions mentioned in a questionnaire on procedures followed, decisions taken and values obtained (see section 11);
- submit the questionnaire with solution information before the deadline (see appendix 1);
- submit if possible a magnetic tape with numerical data on output spectra and corresponding output spectrum covariance matrices.

6. INPUT DATA SETS

The magnetic tape, which will be distributed by the IAEA will contain two types of files:

- Files with problem dependent data, describing seven spectrum data sets.

  Each spectrum data set in these files contains:

  a. input spectrum information and a relative spectrum covariance matrix in a multigroup form.

  b. experimentally determined reaction rates and where possible a complete reaction rate covariance matrix.

  For the seven spectrum data sets there will be utility programs to read these files.
- The other type of files contain problem independent data.

These data comprise:

c. a dosimetry cross section library with cross section covariances which the participants may use.
   This library is the IRDF-85 (International Reactor Dosimetry File), which has the ENDF/B-V format. For a number of reactions the contents of the IRDF are the same as those of the ENDF/B-V dosimetry file.

d. several utility programs which may be used in the conversion from library to group values (for cross sections and cross section covariances).

The tape will be accompanied by a report with some extra data and information.

In order to obtain the above mentioned data please contact D.E. Cullen of the IAEA (see chapter 10 for the address) starting your wishes for magnetic tape parameters. For your convenience we have included for this purpose a blank form request which you may use.

7. JUDGEMENTS BY PARTICIPANTS

The exercise is not merely a comparison of the outcome of straightforward calculations with computer codes. It implies scientific judgement by the participants on questions like:

- Which group structure should I use in my calculations?
- Is there consistency in the input data for the spectrum data sets of interest to me?
  If not, what can I do to make these data sets consistent?
- Can improvement be expected, if I use my special laboratory data set or procedure in combination with the REAL84 data?
- Is there reason to delete one or more reaction rates in the analysis?
- Is the input spectrum covariance matrix acceptable from physical and mathematical point of view for the spectrum set of interest?
  If not, what can I do to improve it?
- What do I miss in the input data set?

- What is needed in order to improve the quality of the output information (e.g. weight of certain reactions, better quality cross sections etc.)?
- Which value in the input data set should I like to improve in order to arrive at a better accuracy of the output information?

The participants are requested to make statements on additions, changes, deletions in the input data set, and give short and clear reasons for their decision. With respect to the output data the participants are requested to make statements on the acceptability of the outcome of the calculations.

8. RULES FOR PARTICIPATION

The participants have some possibilities to make changes in the input data of the sets. However, they should stick to some rules.
Participants are requested:

- to take into account the reaction rate variances, or covariances if available;
- to use where relevant the covariance matrices of the input sets.

However, participants are free:

- to select the spectrum data sets of their interest;
- to use any group structure they consider to be suitable;
- to apply a cross section file other than the IRDF-85 for some or all cross sections (it is however recommended to use only cross section libraries which are documented in open literature);
- to delete one or more reaction rate values (if inconsistent);
- to prepare additional solutions for the chosen spectrum data sets for other adjustment conditions (e.g. for other normalization procedures or for other adjustioned codes);
- to prepare additonal solutions for the chosen spectrum data sets for modified input data sets (e.g. referring to other cross section libraries or to deletions of one or more reactions).

However: <u>any change should be documented clearly in the questionnaire.</u>

9. DIFFERENCES IN SOLUTIONS

It is expected that the solutions submitted by the participants will show differences due to one or more effects. At present we think of the following possible effects:

- differences in the procedures for processing of data in the ENDF/B-V format into group values;
- differences in procedures for processing of uncertainty data from the ENDF/B-V format into group values;
- definitions of the detailed shape of the weighting function for calculating new group cross section values;
- participants changes in input values;
- deletion(s) or addition(s) of input values (e.g. cross correlations between different cross section sets etc.);
- differences in group structures;
- different mathematical models (e.g. based on linear or logarithmic normal distributions of uncertainties);
- different numerical procedures in the algorithm (e.g. numerical precision, word length, rounding, number of iterations, interpolation and extrapolation procedures, occurrence of numerical instabilities in the calculations etc.);
- difference in procedures for propagation of variance and covariances in the adjustment (exact or linearized formula);
- differences in procedures for calculating integral parameters and their standard deviations (may be different interpretations of the use of damage cross sections could arise).

10. CORRESPONDENCE

A mailing list of interested persons and prospective participants has been established.

At this stage of the exercise all correspondence with respect to participation should be sent to:

D.E. Cullen
IAEA
P.O. Box 100
A-1400 VIENNA
Austria

Information on physical and technical topics should be addressed directly to:

W.L. Zijp
ECN
P.O. Box 1
1755 ZG PETTEN
The Netherlands

11. QUESTIONNAIRE

It is not intended that by this exercise all numerical information of the calculation results which the participants obtain will be analyzed in detail by the joint team. For this reason a questionnaire has been made, which gives a good overview of the obtained results.
The questionnaires with results from participants should be returned before 31st August 1985.
The returned questionnaires will be reviewed by the team. In case that points will be observed which should need clarification, the participants will be informed at the end of 1985 or early 1986.
For that reason the participants are asked not to discard output information and working papers of the adjustments before publication of the final report.

12. SUBMISSION OF OUTPUT DATA

The questionnaire with selected numerical data should be sent directly to W.L. Zijp (see address under point 10). Magnetic tapes with numerical data on output spectrum and corresponding output spectrum covariance matrices should however be sent directly to D.E. Cullen (see address under point (10)).

13. INPUT DATA SETS

In appendix 4 information is given on the input data sets which can be used in REAL84.
For most of these spectra a complete combination of reaction rates and calculated input spectrum with the covariances is available (see appen-

dix 4 for details). The data will be made available in the original group structure etc.

The reaction rates can be considered to have negligible neutron self-shielding effects; furthermore corrections for any gamma radiation effects have already been incorporated.

No checks on the quality of the data were performed during the preparations for the exercise.

Remark: Only those reaction rates which have uncertainty data in the cross section file were inserted in the input.

The input data sets have been composed from data gathered by the joint team. An important part of these data is not published in open literature. For this reason the input data sets should not be considered as benchmark data, but only as good quality input information for REAL84.

14. REFERENCES

[1] Zijp, W.L., Zsolnay, É.M., Nolthenius, H.J., Szondi, E.J., Verhaag, G.H.C.M., Cullen, D.E., Ertek, C.;
Final Report on the REAL80 exercise;
Report INDC (NED)-7; BME-TR-RES-6/82; ECN-128;
(Netherlands Energy Research Foundation, Petten, 1983.)

[2] Zijp, W.L., Zsolnay, É.M., Nolthenius, H.J., Szondi, E.J., Verhaag, G.H.C.M.;
Intercomparison of predicted displacement rates based on neutron spectrum adjustments (REAL80 exercise);
Nuclear Technology 67 (1984) 282-301.

[3] Minutes of the IAEA consultants meeting on the REAL80 exercise (distributed February 1984).

[4] Minutes of the IAEA consultants meetings on the REAL80 exercise;
Report INDC (NDS) 165.

15. APPENDICES

APPENDIX 1 Time schedule for REAL84

1984	September	Start of preparations.
1985	February	Distribution of information sheet.
1985	March	Distribution of magnetic tapes by the IAEA.
1985 March till 1985 August		Participating laboratories prepare their adjustment results and report.
1985	August	Start of evaluation of the results of the participants.
1985 Fall till 1986 Spring		Communication with participants.
1986	August	Draft report REAL84 available.
1987	April	Presentation of conclusions of the REAL84 exercise at the 6th ASTM-Euratom symposium on Reactor Dosimetry in San Antonio (Texas, USA)

APPENDIX 2 Specification of input data sets

Spectrum data sets are available for the following neutron fields.

Input code	Description
ANO	Pressure-vessel cavity of the Arkansas Power and Light Reactor (Arkansas Nuclear One-1). A sketch of the position of interest in respect to the core is shown in figure 1.
PS1	Oak Ridge Research Reactor Poolside Facility in the metallurgical irradiation experiment. Position simulated surveillance capsule. A sketch is shown in figure 2.
PS2	Oak Ridge Research Reactor Poolside Facility in the metallurgical irradiation experiment. 1/4 T position in the simulated pressure vessel capsule. (See also figure 2.)
RTN	Fusion simulation spectrum measured at the RTNS-II, a 14 MeV neutron source at Lawrence Livermore Laboratory. The spectrum is a pretty fail simulation of a fusion first wall spectrum.
TAN	Accelerator spectrum Be(d,n) with deuteron energies of 16 MeV.
U35	Fission spectrum of ^{235}U.
CFR	Neutron spectrum in the centre of coupled fast reactivity measurement facility (CFRMF). A sketch is shown in figure 3.

Technical details for the input information and references*

Input data	Measured reaction rates	Covariances measured reaction rates	Calculated input spectrum	Covariances calculated input spectrum
ANO	6 reaction rates; no subcadmium responses [1]	available [2]	55 groups [3]	16 groups [3]
PS1	10 reaction rates [4]	only variances [4]	37 groups calculated [4]	37 groups calculated [4]
PS2	6 reaction rates [4]	only variances [4]	37 groups calculated [4]	37 groups calculated [4]
RTN	12 reaction rates [5]	available [5]	60 groups [5]	good estimates 60 groups [5]
TAN	18 reaction rates [5]	available [5]	39 groups [5]	good estimates 39 groups [5]
U35	23 reaction rates [6]	only variances [6]	24 groups [7]	24 groups [7]
CFR	23 reaction rates [6]	only variances [6]	26 groups [8]	26 groups [8]

* The references of this appendix are listed on the next page

REFERENCES for appendix 2

[1] Private communication from R.E. Maerker (1985-01-18).

[2] Wagschal, J.J., Maerker, R.E., Broadhead, B.L., Williams, M.L.;
Unfolded ANO-1 fluences using the Lepricon methodology;
Paper presented at the 5th ASTM-Euratom symposium for reactor dosimetry in Geesthacht (1984 September 24-28).

[3] Maerker, R.E.;
Calculated spectra for ANO-1 and their covariances;
Communication given at the 5th ASTM-Euratom Symposium on Reactor Dosimetry in Geesthacht (1984 September 24-28).

[4] Private communication from F.W. Stallman (1984-09-24...28).

[5] Private communication from L.R. Greenwood (1984-08-31).

[6] Zijp, W.L. et al.;
Comparison of measured and evaluated spectrum averaged cross section data;
Proc. 4th ASTM-Euratom Symposium on Reactor Dosimetry, Gaithersburg, March 22-26, 1982;
Report NUREG/CD-0029 Vol 2; CONF-820321/V2 p. 725;
(National Bureau of Standards, Gaithersburg, Maryland, 1982).

[7] Maerker, R.E., Wagschal, J.J., Broadhead, B.L.;
Development and demonstration of an advanced methodology for LWR dosimetry applications;
Report EPRI NP-2188 (Electric Power Research Institute, Palo Alto, December 1981).

[8] Ryskamp, J.M., Anderl, R.A., Broadhead, B.L., Ford III, W.E., Lucius, J.L., Marable, J.H., Wagschal, J.J.;
Sensitivity and Uncertainty Analysis of the Coupled Fast Reactivity Measurements Facility central flux spectrum;
Nuclear Technology 57 (1982) 20-35.

16. FIGURES

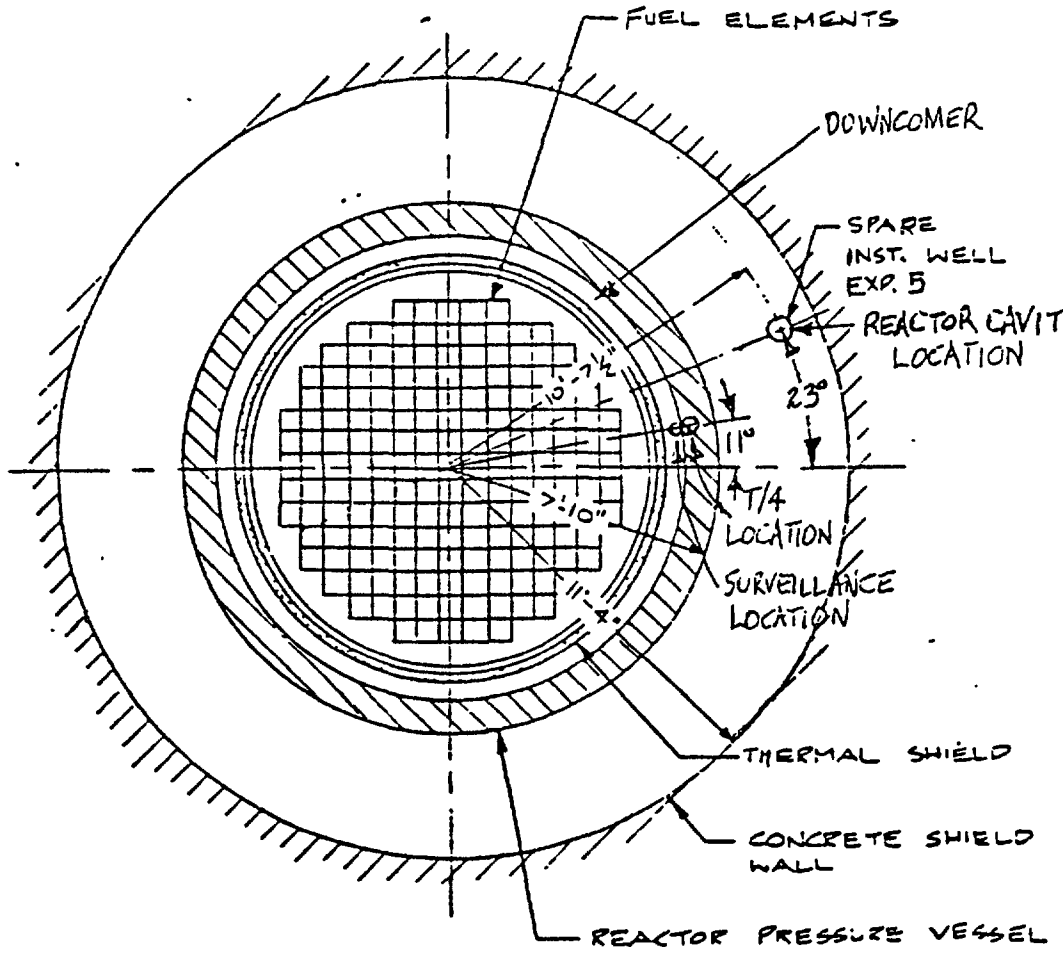

Figure 1 Position sketch for ANO input

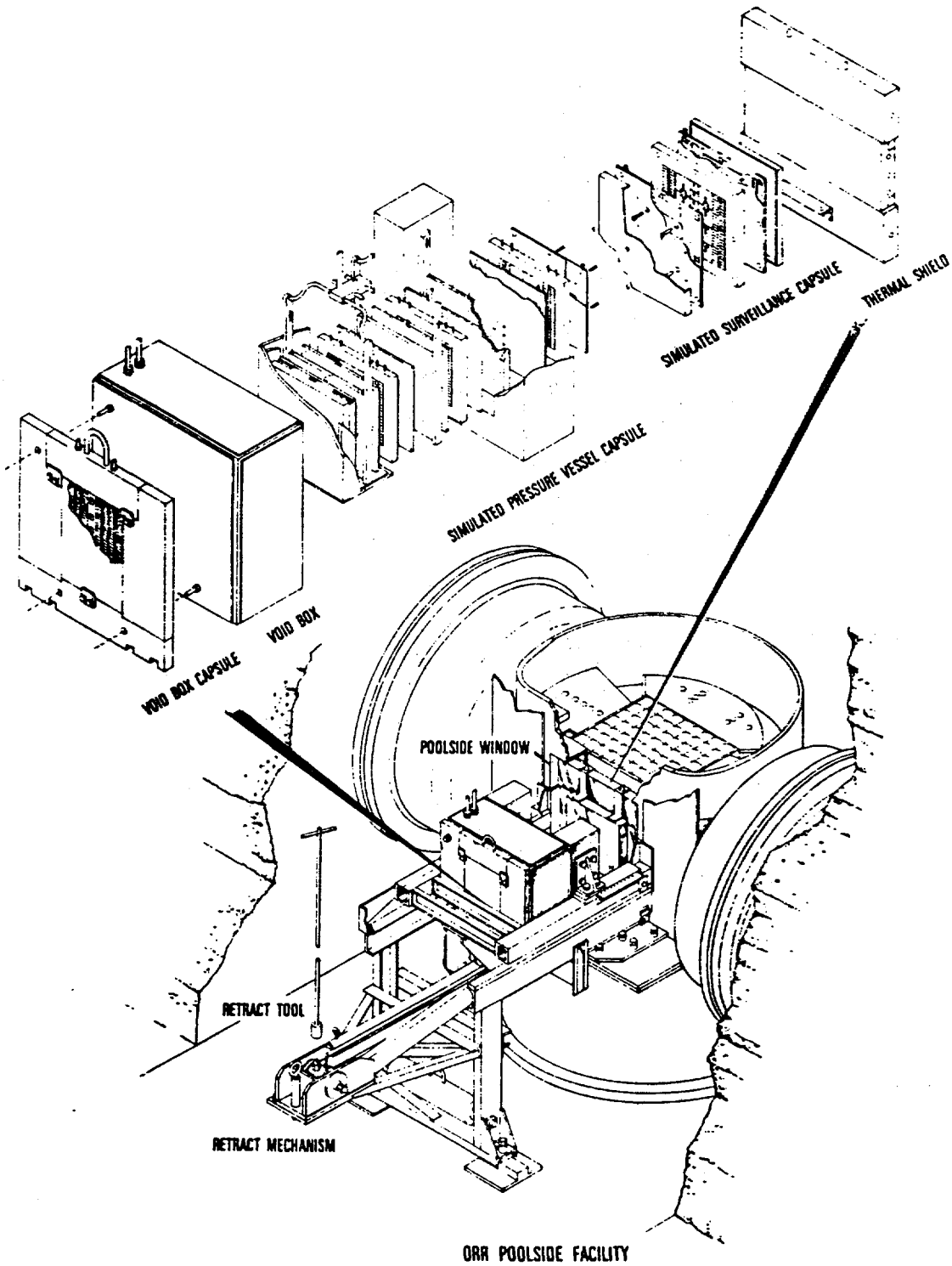

Figure 2 View of the PSF facility

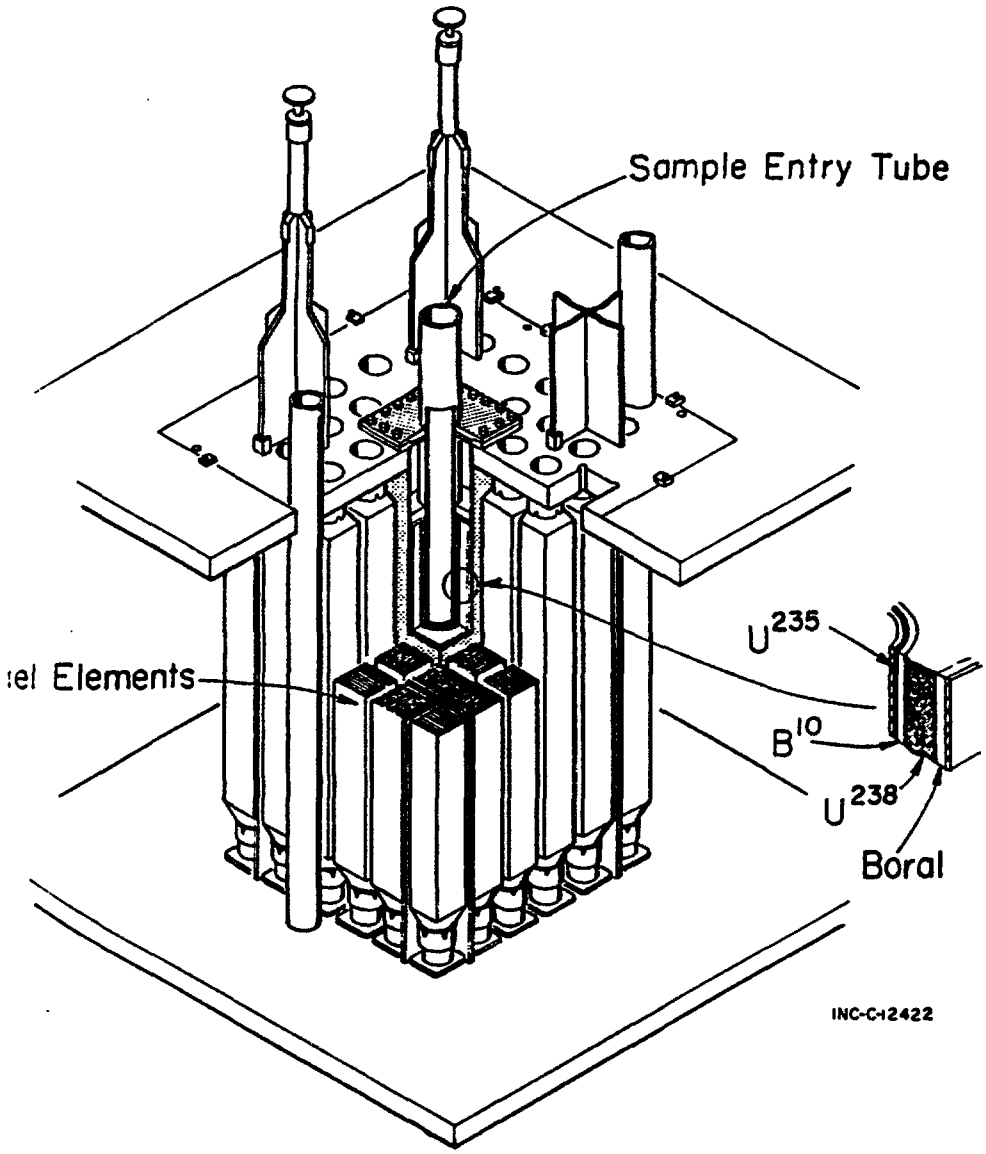

Figure 3 Cutaway pictorial diagram showing general assembly of the CFRMF

Nuclear Data Aspects Encountered in the REAL80 and REAL84 Intercomparisons

H.J. Nolthenius[a], É.M. Zsolnay[b],
W.L. Zijp[a], E.J. Szondi[b]

SUMMARY

A survey is presented of a number of nuclear data aspects encountered in the REAL80/REAL84 intercomparisons.
The aim of the international interlaboratory REAL80 exercise was to determine the state of the art in 1981 to adjust neutron spectrum information, and subsequently predict the number of displacements. This exercise was hampered by lack of good nuclear data. At this moment improved data are available, which are applied in the input for the REAL84 exercise, which is started now.

1. INTRODUCTION

The international interlaboratory exercise REAL80 [1,2] has been executed to determine the state of the art of the capabilities of laboratories to adjust neutron spectrum information and to predict displacement rates in steel. The follow-up of this exercise, called REAL84 [3], is aimed at improving the assessment of accuracies in radiation damage predictions by various laboratories by using good quality input data and proper procedures for adjustment and data treatment.
The basis of the adjustment is a set of experimental reaction rates, the best estimate of the neutron spectrum, and a set of energy dependent cross-section data. These three groups of data should be accompanied by good estimates for the uncertainties and correlations in the form of covariance matrices. With help of a generalized

a) Netherlands Energy Research Foundation ECN, Petten.
b) Nuclear Reactor of the Technical University Budapest.

least-squares procedure the best estimate of the neutron spectrum with its uncertainties can be calculated, which gives the possibilities to obtain parameters with their uncertainties which characterize among others the damage properties of the spectrum of interest.
The characterization parameters are dependent on the input data which are applied in the adjustment procedure. The quality of the input data is among others influenced by the nuclear data values and constants which were applied in deriving them. In this report a number of aspects of these values and constants is discussed.
The topics considered are the availability of data, the quality of the data, and the progress which was observed.
Due to the special conditions of the REAL80 and REAL84 exercises, we are not in a position to consider the situation for other, more general circumstances.
In the REAL80 exercise two input spectrum data sets were applied [1] (i.e. for the material testing reactor ORR and for a typical fast reactor spectrum YAYOI).
For the input of the REAL84 exercise seven input spectrum data sets are available (including a power reactor spectrum, an ORR shielding experiment spectrum, a fission neutron spectrum and a spectrum for the Coupled Fast Reactivity Measurement Facility).
During the preparation of the input data a number of observations was made for the following subjects:
- number of reactions in the input and their uncertainties;
- availability of cross-section data sets and their uncertainties;
- damage characterization and their uncertainties.

In the following parts these subjects will be discussed.

2. INPUT REACTIONS AND THEIR UNCERTAINTIES

In the two exercises the number of input reaction rates for the spectra considered was in the range from 6 to 23. That means, that for practically all input spectra we have the situation that parts of the spectrum are not well covered by detector response. This is partly due to the absence of suitable activation (or fission) re-

actions, and partly due to lack of nuclear data of good quality. The latter remark holds for the reactions ^{93}Nb(n,n'), ^{103}Rh(n,n'), etc., but also other reactions which are not applied due to lack of good quality data (e.g. in the range of the high energy resonances).
The uncertainty of the measured reaction rates used in the exercises is in general of the order of 5 per cent. This value is mainly dependent on the counting and correction procedures for activity measurements, and to a smaller extent dependent on the nuclear data uncertainties.
On the other side, in these activity measurement techniques until now no correlation between various gamma rays of a single radionuclide could be considered. This absence might have a biasing influence on the uncertainty estimates. These correlation coefficients, which are required to obtain a good estimate for the uncertainty assessment, seem to be missing in the nuclear data files, like ENSDF (the Evaluated Nuclear Structure and Decay File).

3. CROSS-SECTION DATA

The quality of the cross-section data has clearly improved with respect to the situation during the preparation of REAL80.
The second version of the ENDF/B-V dosimetry file became available, and in REAL84 also the IRDF85 will be used. Also the software necessary to apply the uncertainty data in these files was developed. Due to this progress improvement can be expected in the results, especially also on the point of judgements on consistency.
With respect to the situation in 1980 the metrology cross-sections for some specific reactions have been improved [4].
The uncertainty data were also changed (see Table 1), but probably more important is the fact that now the correlation data for the successive group values for a given energy dependent cross-section can also be applied in the adjustments; they can be derived from the file data present in ENDF/B-V and/or IRDF85.
In the preparation of the REAL84 exercise nevertheless a number of metrology reactions had to be deleted due to lack of energy

Table 1.
Coefficients of variation for two cross-section libraries.
The calculations have been executed with the original and the second version of the ENDF/B-V dosimetry file.

reaction	coefficient of variation in cross-section averaged over a Watt fission neutron spectrum		reaction	coefficient of variation in cross-section averaged over a Watt fission neutron spectrum	
	original	second version		original	second version
6Li(n,a)	4.98	3.21	59Co(n,a)	4.37	4.29
10B(n,a)	13.05	6.39	58Ni(n,2n)	10.94	10.92
23Na(n,g)	12.69	13.06	58Ni(n,p)	6.56	6.51
27Al(n,a)	5.65	5.47	60Ni(n,p)	7.75	7.47
27Al(n,p)	5.86	5.86	63Cu(n,a)	5.38	5.27
32S(n,p)		8.15	63Cu(n,g)	19.06	19.01
45Sc(n,g)	18.48	3.20	65Cu(n,2n)	6.51	7.31
46Ti(n,p)	12.66	12.61	115In(n,g)	4.25	4.29
47Ti(n,np)	29.70	30.00	115In(n,n')	11.98	11.99
47Ti(n,p)	11.27	11.26	127I(n,2n)	38.39	17.22
48Ti(n,np)	29.60	30.00	197Au(n,g)	8.04	8.36
48Ti(n,p)	10.45	10.30	232Th(n,f)	5.09	5.09
55Mn(n,2n)	13.27	12.95	232Th(n,g)	11.56	11.70
54Fe(n,p)	2.54	3.53	235U(n,f)	1.96	1.97
56Fe(n,p)	4.57	4.48	238U(n,f)	1.11	2.02
58Fe(n,g)	11.78	30.71	238U(n,g)	4.63	5.81
59Co(n,2n)	11.36	10.92	237Np(n,f)	9.33	9.32
59Co(n,g)	13.69	4.61	239Pu(n,f)	1.98	2.86

Remark: The calculations of the standard deviations are not completely comparable due to differences in software and weighting spectra. Furthermore the uncertainties derived from file 32 are not incorporated in the calculations for the original ENDF/B-V version.

dependent cross-section data accompanied by uncertainties.
The deleted reactions are: ^{45}Sc(n,2n), ^{52}Cr(n,p), ^{54}Fe(n,α), ^{59}Co(n,p), ^{89}Y(n,2n), ^{93}Nb(n,2n), ^{169}Tm(n,2n), ^{197}Au(n,2n) and ^{238}U(n,2n).
In Table 2 uncertainty data are given for characteristic values of cross-section sets (i.e. the average cross-section values for a Watt fission spectrum and thermal Maxwellian as well as the resonance integral.
From this table one can observe that only a few reactions yield uncertainties in these values smaller than 4 per cent. These reactions have large statistical weight in the adjustment process. The other reactions contribute only in a reduced way to an adjustment procedure. For good spectrum adjustment procedures a reduction of the uncertainties is important. This holds especially

Table 2.

Coefficients of variation and correlation for three characteristic neutron spectra.
(coefficient of variation given in per cent).

The calculations have been executed with ENDF/B-5 library version 2.

Reaction	coefficient of variation in cross-section averaged over spectrum: (Maxwell) (1)	(1/E) (2)	(Watt)a) (3)	coefficient of correlation in cross-section between spectrum: (1)-(2)	(1)-(3)	(2)-(3)
6Li(n,a)	.40	.40	3.21	1.00	.02	.05
10B(n,a)	.22	.22	6.39	1.00	.00	.00
23Na(n,g)	2.00	4.88	13.06	.95	.00	.00
27Al(n,a)			5.47			
27Al(n,p)			5.86			
32S(n,p)			8.15			
45Sc(n,g)	.89	1.14	3.20	.95	.00	.00
46Ti(n,p)			12.61			
47Ti(n,np)			30.00			
47Ti(n,p)		11.31	11.26			
48Ti(n,np)			30.00			
48Ti(n,p)			10.30			
55Mn(n,2n)			12.95			
54Fe(n,p)		7.31	3.53			
56Fe(n,p)			4.48			
58Fe(n,g)	5.96	14.34	30.71	.34	.00	-.03
59Co(n,2n)			10.92			
59Co(n,g)	.67	.77	4.61	.95	.00	.00
59Co(n,a)			4.29			
58Ni(n,2n)			10.92			
58Ni(n,p)		9.57	6.51			
60Ni(n,p)			7.47			
63Cu(n,a)			5.27			
63Cu(n,g)	2.00	2.76	19.01	.06	.00	.25
65Cu(n,2n)			7.31			
115In(n,g)	6.00	5.99	4.29	1.00	.00	.00
115In(n,n')		12.87	11.99			
127I(n,2n)			17.22			
197Au(n,g)	.78	3.05	8.36	.27	.00	.00
232Th(n,f)		6.56	5.09			
232Th(n,g)	5.08	10.95	11.70	.01	.00	.11
235U(n,f)	.32	2.14	1.97	.14	.00	.01
238U(n,f)	25.04	6.29	2.02	.01	.04	.55
238U(n,g)	.74	3.45	5.81	.00	.00	.01
237Np(n,f)	46.59	16.22	9.32	.00	.00	.93
239Pu(n,f)	.41 b)	5.62	2.86	.00	.00	.28

a) 235-U fission spectrum from ENDF/B-5 version 2.
b) Negative variances observed for the first group.

Remark 1:The following computer programs,operational at ECN, have been used:UNC33,STAYNL and FITOCO.
Remark 2:The weighting spectrum for UNC33 and FITOCO was determined in the FLUX81 experiment and refers to HFR pos.C3.
Remark 3:The 1/E spectrum originated from SAND-2.

Table 3.

CROSS-SECTION NAME : AU197652 MAT-NUMBER : 6379

X-SECTION CORRELATION MATRIX (27 X 27) UPPER TRIANGLE

GROUP NO	ENERGY (EV)																								
1	.73	1.000E-04																							
	100	92	82	82	78	25	24	26	25	26	26	13	8	8	8	8	8	9	11	13	28	3	0	0	0	0	0
2	1.67	2.150E-01																							
		100	100	93	31	31	31	31	31	31	12	10	10	10	10	10	11	14	16	33	3	0	0	0	0	0
3	1.67	4.650E-01																							
			100	100	93	31	31	31	31	31	31	12	10	10	10	10	10	11	14	15	33	3	0	0	0	0	0
4	1.92	1.000E+00																							
				100	93	31	31	31	31	31	31	12	10	10	10	10	10	11	14	16	33	3	0	0	0	0	0
5	2.94	2.150E+00																							
					100	100	100	100	100	100	100	11	3	3	4	3	3	4	5	6	12	1	0	0	0	0	0
6	3.15	4.650E+00																							
						100	100	100	100	100	100	10	3	3	3	3	3	4	4	5	11	1	0	0	0	0	0
7	3.18	1.000E+01																							
							100	100	100	100	100	10	3	3	3	3	3	4	4	5	11	1	0	0	0	0	0
8	3.19	2.150E+01																							
								100	100	100	100	10	3	3	3	3	3	4	4	5	11	1	0	0	0	0	0
9	3.19	4.650E+01																							
									100	100	100	10	3	3	3	3	3	4	4	5	11	1	0	0	0	0	0
10	3.19	1.000E+02																							
										100	100	10	3	3	3	3	3	4	4	5	11	1	0	0	0	0	0
11	3.19	2.150E+02																							
											100	10	3	3	3	3	3	4	4	5	11	1	0	0	0	0	0
12	6.37	4.650E+02																							
												100	100	100	5	1	1	1	2	2	4	0	0	0	0	0	0
13	10.05	1.000E+03																							
													100	100	5	1	1	1	1	2	3	0	0	0	0	0	0
14	10.05	2.150E+03																							
														100	5	1	1	1	1	2	3	0	0	0	0	0	0
15	9.69	4.650E+03																							
															100	100	100	99	1	2	4	0	0	0	0	0	0
16	10.05	1.000E+04																							
																100	100	99	1	2	3	0	0	0	0	0	0
17	10.05	2.150E+04																							
																	100	99	1	2	3	0	0	0	0	0	0
18	9.97	4.650E+04																							
																		100	2	2	4	0	0	0	0	0	0
19	7.67	1.000E+05																							
																			100	2	5	0	0	0	0	0	0
20	6.06	2.150E+05																							
																				100	72	1	0	0	0	0	0
21	2.93	4.650E+05																							
																					100	19	11	0	0	0	0
22	12.28	1.000E+06																							
																						100	99	93	85	85	76
23	20.40	1.400E+06																							
																							100	97	88	88	78
24	20.29	2.500E+06																							
																								100	88	88	79
25	22.38	4.000E+06																							
																									100	100	72
26	22.32	6.500E+06																							
																										100	72
27	24.99	1.000E+07																							
																											100

Table 4.

CROSS-SECTION NAME : PU239F52 MAT-NUMBER : 6399

X-SECTION CORRELATION MATRIX (27 X 27) UPPER TRIANGLE

GROUP NO	REL.SDEV (PT)	ENERGY (EV)																								
1	.39	1.000E-04																								
	100	1.7	93	0	0	0	0	0	0	0	0	0	0	0	0	0	0	0	0	0	0	0	0	0	0	0
2	.66	2.150E-01																								
		-100	-102	0	0	0	0	0	0	0	0	0	0	0	0	0	0	0	0	0	0	0	0	0	0	0
3	.91	4.650E-01																								
			-100	0	0	0	0	0	0	0	0	0	0	0	0	0	0	0	0	0	0	0	0	0	0	0	0
4	7.62	1.000E+00																								
				100	100	100	100	100	100	100	82	12	12	12	12	12	14	10	9	14	13	17	17	14	13	13	11
5	7.62	2.150E+00																								
					100	100	100	100	100	100	82	12	12	12	12	12	14	10	9	14	13	17	17	14	13	13	11
6	7.62	4.650E+00																								
						100	100	100	100	100	82	12	12	12	12	12	14	10	9	14	13	17	17	14	13	13	11
7	7.62	1.000E+01																								
							100	100	100	100	82	12	12	12	12	12	14	10	9	14	13	17	17	14	13	13	11
8	7.62	2.150E+01																								
								100	100	100	82	12	12	12	12	12	14	10	9	14	13	17	17	14	13	13	11
9	7.62	4.650E+01																								
									100	100	82	12	12	12	12	12	14	10	9	14	13	17	17	14	13	13	11
10	7.62	1.000E+02																								
										100	82	12	12	12	12	12	14	10	9	14	13	17	17	14	13	13	11
11	6.13	2.150E+02																								
											100	66	66	66	66	66	43	13	11	18	16	21	21	18	16	16	13
12	8.94	4.650E+02																								
												100	100	100	100	100	55	9	7	12	11	14	15	12	11	11	9
13	8.94	1.000E+03																								
													100	100	100	100	55	9	7	12	11	14	15	12	11	11	9
14	8.94	2.150E+03																								
														100	100	100	55	9	7	12	11	14	15	12	11	11	9
15	8.94	4.650E+03																								
															100	100	55	9	7	12	11	14	15	12	11	11	9
16	8.94	1.000E+04																								
																100	55	9	7	12	11	14	15	12	11	11	9
17	7.41	2.150E+04																								
																	100	88	9	15	13	17	18	15	13	13	11
18	10.30	4.650E+04																								
																		100	6	11	9	12	13	11	9	10	8
19	12.04	1.000E+05																								
																			100	21	19	17	13	11	8	8	7
20	3.57	2.000E+05																								
																				100	72	64	46	40	26	27	22
21	4.09	4.000E+05																								
																					100	82	53	44	27	28	20
22	3.11	8.000E+05																								
																						100	87	60	45	46	28
23	3.04	1.400E+06																								
																							100	83	56	57	37
24	3.67	2.500E+06																								
																								100	58	55	40
25	4.17	4.000E+06																								
																									100	95	52
26	4.08	6.500E+06																								
																										100	58
27	6.70	1.050E+07																								
																											100

Table 5.

CROSS-SECTION NAME : NP237F52 MAT-NUMBER : 6337

X-SECTION CORRELATION MATRIX (27 X 27) UPPER TRIANGLE

GROUP NO	ELE.SOLV (PT)	ENERGY (EV)																								
1	.00	1.000E-04	0	0	0	0	0	0	0	0	0	0	0	0	0	0	0	0	0	0	0	0	0	0	0	0
2	46.54	2.150E-01	100	93	2	1	0	0	0	0	0	0	0	0	0	0	0	0	0	0	0	0	0	0	0	0
3	34.80	4.650E-01	100	2	1	0	0	0	0	0	0	0	0	0	0	0	0	0	0	0	0	0	0	0	0	0
4	30.33	1.000E+00	100	3	0	0	0	0	0	0	0	0	0	0	0	0	0	0	0	0	0	0	0	0	0	0
5	12.47	2.150E+00	100	0	0	0	0	0	0	0	0	0	0	0	0	0	0	0	0	0	0	0	0	0	0	0
6	******	4.650E+00	100	0	0	0	0	0	0	0	0	0	0	0	0	0	0	0	0	0	0	0	0	0	0	0
7	30.00	1.000E+01	100	100	100	100	100	100	100	100	100	100	100	100	0	0	0	0	0	0	0	0	0	0	0	0
8	30.00	2.150E+01		100	100	100	100	100	100	100	100	100	100	100	0	0	0	0	0	0	0	0	0	0	0	0
9	30.00	4.650E+01			100	100	100	100	100	100	100	100	100	100	0	0	0	0	0	0	0	0	0	0	0	0
10	30.00	1.000E+02				100	100	100	100	100	100	100	100	100	0	0	0	0	0	0	0	0	0	0	0	0
11	30.00	2.150E+02					100	100	100	100	100	100	100	100	0	0	0	0	0	0	0	0	0	0	0	0
12	30.00	4.650E+02						100	100	100	100	100	100	100	0	0	0	0	0	0	0	0	0	0	0	0
13	30.00	1.000E+03							100	100	100	100	100	100	0	0	0	0	0	0	0	0	0	0	0	0
14	30.00	2.150E+03								100	100	100	100	100	0	0	0	0	0	0	0	0	0	0	0	0
15	30.00	4.650E+03									100	100	100	100	0	0	0	0	0	0	0	0	0	0	0	0
16	30.00	1.000E+04										100	100	100	0	0	0	0	0	0	0	0	0	0	0	0
17	30.00	2.150E+04											100	100	0	0	0	0	0	0	0	0	0	0	0	0
18	30.00	4.650E+04												100	0	0	0	0	0	0	0	0	0	0	0	0
19	10.00	1.000E+05													100	0	0	0	0	0	0	0	0	0	0	0
20	10.00	2.500E+05														100	100	100	100	100	100	73	0	0	0	0
21	10.00	4.000E+05															100	100	100	100	100	73	0	0	0	0
22	10.00	8.000E+05																100	100	100	100	73	0	0	0	0
23	10.00	1.400E+06																	100	100	100	73	0	0	0	0
24	10.00	2.500E+06																		100	100	73	0	0	0	0
25	8.44	4.000E+06																			100	73	0	0	0	0
26	15.00	7.500E+06																				100	69	69	0	0
27	15.00	1.050E+07																					100	100	0	0
																								100	0	0

Table 6.

CORRELATION MATRIX (39 X 39) for ^{93}Nb(n,n').   UPPER TRIANGLE

1		128.84																											
																					100	81	28	362	41	65	324	38	139
89	207	35	71	64	59	111	36	19	36	56	15	71	5	25	12	35	17	6	59	9	9	31	21	15	10	5	23	4	6
2		27.39																											
																						100	169	148	69	56	73	234	69
91	86	82	61	41	32	30	47	71	22	80	28	53	17	31	12	33	19	10	127	16	19	58	44	32	22	12	8	8	10
3		15.30																											
																							100	441	42	100	126	92	125
55	45	41	45	54	60	69	430	16	72	103	43	59	17	36	16	57	46	25	71	67	95	47	83	65	69	32	17	14	13
4		13.11																											
																								100	87	104	156	120	229
365	53	129	107	110	75	54	89	21	46	103	46	95	43	112	56	449	39	43	99	94	32	77	48	42	44	38	34	37	40
5		20.32																											
																									100	104	155	202	67
100	84	92	62	39	33	33	70	23	52	96	39	78	34	85	41	313	27	30	69	66	22	54	33	29	31	26	23	25	27
6		20.69																											
																										100	152	193	187
114	271	38	91	72	77	57	75	16	29	55	27	60	27	71	36	116	72	33	87	75	67	42	75	59	62	29	15	13	12
7		14.46																											
																											100	87	183
121	127	132	135	127	124	131	246	60	265	60	57	90	42	75	25	66	37	20	71	72	38	142	107	103	98	54	49	43	47
8		22.18																											
																												100	339
31	79	65	73	50	34	31	54	16	43	82	33	67	29	74	36	112	68	31	81	69	33	235	21	53	40	31	18	12	11
9		12.53																											
																													100
77	103	119	124	122	123	135	261	66	129	213	79	147	60	145	126	47	79	29	93	62	22	65	43	52	68	51	41	43	45
10		20.81																											
100	49	130	98	90	86	90	168	41	79	153	5	34	9	36	15	34	18	7	30	40	23	87	66	64	62	40	31	31	31
11		21.77																											
	100	94	95	87	84	89	132	1	19	13	13	23	8	16	7	39	38	21	60	55	28	100	72	69	65	62	32	31	31

for the various reactions in titanium, the $^{115}In(n,n')$ and $^{237}Np(n,f)$ reactions which have standard deviations in the characteristic values larger than 10%. Therefore, the influence of these reactions in combination with reactions with lower uncertainties is clearly limited.

4. DAMAGE CHARACTERIZATION

The output spectrum with its covariance matrix can be used to calculate a number of characteristic values which can be applied in the description of the damage processes. The characteristic values are calculated with special cross-section sets. In the REAL84 exercise cross-section sets are available to calculate the displacement rates for a few pure metals.* One can doubt whether the required damage cross-section of a steel alloy can be derived from the damage cross-section of the constituent single metals. In any case the damage cross-section for the specified steel alloy was not made available in the REAL84 exercise.

In the REAL80 exericse the displacement cross-section was available only for iron. In the REAL84 exercise also gas production cross-section sets are incorporated, while in addition cross-section sets* are included for the He production by the double reaction in nickel: $^{58}Ni(n,\gamma)^{59}Co$ and $^{59}Ni(n,\alpha)^{56}Fe$.

Most of these "damage" cross-sections have been calculated with aid of ENDF/B-V data.

Uncertainty data for the damage cross-sections based on the physics of the process and on uncertainties of the cross-section values are completely lacking. These lacking data are needed in particular if damage parameters determined e.g. in a materials testing reactor spectrum are used to predict the situation for a totally different fusion reactor blanket spectrum.

For the REAL84 exercise uncertainties have been chosen which are only useful for comparison of two or more calculation methods; these estimates, however, should not be interpreted as physics based uncertainties for the damage characteristics.

---

* based on a private communication by L.R. Greenwood from ANL.

5. REFERENCES

[1] Zijp, W.L., et al.: "Final report on the REAL80 exercise", Report ECN-128 (Netherlands Energy Research Foundation ECN, Petten, February 1983).

[2] Zijp, W.L., Zsolnay, É.M., Nolthenius, H.J., Szondi, E.J., Verhaag, G.C.H.m.: "Intercomparison of predicted displacement rates based on neutron spectrum adjustments (REAL80 exercise)", Nuclear Technology 67 (1984), p. 282-301.

[3] Zijp, W.L., et al.: "Information sheet for the REAL84 exercise" Report INDC(NDS)-166 (Netherlands Energy Research Foundation ECN, Petten, March 1985).

[4] Nolthenius, H.J., Verhaag, G.C.H.M.: "Comparison of two fine group cross-section libraries resulting from the ENDF/B-V dosimetry and gas file (version 1 and version 2)", Report ECN-85- (Netherlands Energy Research Foundation ECN, Petten, May 1985).

ON THE INFLUENCE AND NEED OF NUCLEAR DATA AT RELATIVE STANDARDIZED FLUENCE MEASUREMENTS

BRUNO BÄRS AND TOM SEREN
Technical Research Centre of Finland
Reactor Laboratory, SF-02150 Espoo 15, Finland

ABSTRACT

The quality of the fast neutron fluence estimates to be used at the prediction of pressure vessel (PV) steel embrittlement may be significantly improved by the combined use of PV cladding dosimetry (Fe,Ni,Nb), by applying relative standardized measurements and by utilizing the low energy threshold reaction $^{93}Nb(n,n')^{93m}Nb$. In this way the influence of the relatively large systematic (correlated) errors in the reaction cross sections (and possibly other nuclear data) and in the spectrum shapes at the surveillance chain (SC) and at the PV may be significantly suppressed.

The influence and need of nuclear data at these types of measurements is discussed and is exemplified by the use of the $^{54}Fe(n,p)^{54}Mn$ and $^{93}Nb(n,n')^{93m}Nb$ reactions. Iron is a common reactor structural material, which also may be used for dosimetric purposes by the sampling or scraping technique. The Nb-reaction is of special importance due to its low threshold energy (≈1 MeV) and long half-life (16.1 y) and due to practical problems with the low threshold energy fission reactions.

The quality of the dose estimates, especially the absolute ones, may be further improved if the uncertainties in some Nb data (cross section and γ to X conversion probability), and the relatively large discrepancies between the measured and calculated (Nb) cross sections could be reduced.

1. INTRODUCTION

The safe and economical use of nuclear power plants would benefit from an improved quality of the fast neutron dose estimates at the estimation of the embrittlement of the pressure vessel steel. In fast neutron fluence measurements by the commonly used threshold detectors the biggest fluence uncertainties arise from:

1) The relatively large uncertainties in the reaction cross sections ($\Delta\sigma_T \approx$ 5-30 %). Table 1 gives the uncertainties and the discrepancies between the measured and calculated cross sections for the reactions (almost two extreme cases)

$^{54}Fe(n,p)^{54}Mn$ (R1)

$^{93}Nb(n,n')^{93m}Nb$ (R2).

2) For reactions with high threshold energies (like Fe, Ni, Ti and Cu with $E_T \gtrsim 3$ MeV) a large uncertainty arises at the extrapolation ($\Delta f(E_T \rightarrow E_o \approx \pm 10\text{-}30$ %) of the fluence to the needed cut-off energy ($E_o \approx 1$ MeV). This uncertainty arises from the uncertainty in the shape of the neutron spectra, which mainly originates from the limited number of suitable threshold reactions, from the cross section uncertainties and from incomplete theory and calculations.

TABLE 1. Uncertainties [%] in A) absolute fluence measurements and in B) combined PV cladding dosimetry, relative measurements and the use of the Fe- and Nb-reactions at Loviisa NPP,unit 1.

A) UNCERTAINTIES [%] IN ABSOLUTE FLUENCES $\Phi(>1\ MeV)$

		$\Phi(>1\ MeV)$ TOTAL	= R	$\frac{1}{\sigma_T}$	t	$f(E_T \rightarrow E_o)$	$\frac{ROD}{FOIL}$	$f(SC \rightarrow PV)$
Fe	SC	26	7	15	2	20		
Fe	PV	27	10	15	2	20		x)
Nb	SC	18	8-9.5	15	2	0	3	
Nb	PV	19	9-11	15	2	0		x)

x) Applicable at indirect measurements and computations.

B) UNCERTAINTIES [%] IN RELATIVE FLUENCES (>1 MeV)

		$\frac{\Phi_{PV}}{\Phi_{SC}}$	= $\frac{(A/m)_{PV}}{(A/m)_{SC}}$	$\frac{\sigma_{TSC}}{\sigma_{TPV}}$	$\frac{f_{PV}(E_T \rightarrow E_o)}{f_{SC}(E_T \rightarrow E_o)}$	$\frac{1}{ROD/FOIL}$
Fe	SC	12	4	6	4	10
Fe	PV		4			
Nb	SC	7-11	3-5	5-8.6	4	0
Nb	PV		4-7			3

3) Mostly there are no direct fluence measurements at the pressure vessel (PV) and the fluence has to be based on extrapolations or on computer calculations, which are fitted to the measurements at the surveillance chain (SC). The distance and the calculations themselves introduce uncertainties and it may also be difficult to assign proper error estimates to the computed fluences. Without error estimates the dose- and embrittlement estimates have limited value.

2. MEANS TO IMPROVE THE QUALITY OF DOSE ESTIMATES

The quality i.e. the accuracy of the neutron fluence estimates may be improved e.g. by the following means

a) Direct fluence measurements at the PV by scraping samples from the corrosion shield at the inner surface of the PV and by using them as dosimeters [4,5,6],

b) Relative measurements at two positions (e.g. SC/PV) and standardization based on the same reactions, same set of nuclear data etc. In this method one takes advantage of of an available analytic model, which under specific conditions can be based on only relative values. One refined form for the the embrittlement parameter ΔT (shift in the nil-ductility transition temperature) is [3]

$$\Delta T = C(P,Cu,..)\ \Phi^{(b' + a \ln\Phi)} \qquad (1)$$

where $C(P,Cu,..)$ is a material dependent chemical factor, a and b' are fluence related constants and $\Phi \equiv \Phi(>1\ MeV)$ is the fast-neutron dose above the commonly used cut-off energy E_o = 1 MeV.

If similar SC and PV materials (such as base, weld and HAZ), similar irradiation conditions and roughly equal doses are app-

lied then the PV embrittlement can be approximated by the relation [4,7]

$$\Delta T_{PV} = \Delta T_{SC}\left(\frac{\Phi_{PV}}{\Phi_{SC}}\right)^{b} \qquad (2).$$

The subindexes refer to the surveillance chain and pressure vessel and the exponent b ≈ 1/3.

Since only relative (PV/SC) fluence estimates are needed the influence of the systematic (correlated) errors, e.g. in the cross sections may be significantly suppressed [4,5]. In addition, by standardization a part of the uncorrelated errors are converted to correlated errors and their influence cancelled.

c) The use of low energy threshold reactions reduces the errors arising from spectrum extrapolations. The Nb-reaction (R2) has been successfully used both for absolute and relative fluence measurements [5,6] but requires demanding, destructive material purification and sample preparation techniques. The use of the the low threshold energy fission reactions (^{232}Th, ^{238}U, ^{237}Np) seems to be in an immature state. Due to practical problems (thermal neutron and gamma radiation induced fission, fission yield uncertainty, relatively large probes) the obtained dose estimates have mostly a poor quality.

It has been demonstrated [4,5,7] that the combined use of (a) PV corrosion shield dosimetry, (b) relative standardized measurements and (c) the low-threshold Nb-reaction (R2) provide a possibility to significantly reduce the main uncertainties at dose estimation. This subject is treated in more detail in sections 3 and 4 with special emphasis on the influence and need of nuclear data.

A number of other methods to improve the quality of the dose estimates are given in the literature [e.g.1,2,3,7].

It seems that the improvement of the nuclear data is a long range task where on the average no immediate big improvement are expected. The half-life (16.11 ±0.19 a) of the product nuclide at Nb activation (R2) is well known [8]. The standardization of the data [9] and procedures obviously provide some immediate possibilities to improve the quality of the dose estimates.

The use of many nuclear reactions leads to error reduction through smoothing but involves practical problems due to the limited number of reactions available.

3. COMBINED USE OF PV CLADDING DOSIMETRY, RELATIVE STANDARDIZED MEASUREMENTS AND THE Fe- AND Nb-REACTIONS

A significant improvement in the quality of the fast neutron dose estimates was recently obtained by the combined use of a) PV cladding dosimetry, b) relative measurements and c) the low threshold energy Nb-reaction (R2) [5,7].

After three operating cycles 23 samples were scraped from the corrosion shield of the Loviisa NPP, unit 1 (PWR of the Soviet type VVER 440). The samples contain several elements (Fe,Ni,Nb) whose neutron induced reactions may be used to experimentally estimate the fast neutron flux.

In the first stage [4] these PV samples and the steel specimens from the SC were used as dosimeters to obtain absolute and relative fluence estimates (Φ_{PV}/Φ_{SC}) for the SC and the PV above the threshold energy E_T = 2.8 MeV based on the Fe-reaction (R1). The estimated uncertainty in the absolute threshold flux was

16-18 % (SC-PV) and in the relative flux (SC/PV) about 6 %. The estimated uncertainty in the threshold cross section was reduced from ±15 % to about ±4 %. The estimated uncertainty in the (PV/SC) fluence ratio (>1 MeV) was ± 12 % (in absolute fluence ≈±27 %). The biggest uncertainties (≈10 %) in the relative fluences Φ(>1 MeV) arise from the extrapolation of the flux from the threshold energy to the cut-off energy (≈1 MeV).

In the second stage of development [5,7] the Nb-reaction (R2) with a low threshold energy (≈ 0.9 MeV) was used, which provides a possibility to reduce the uncertainty at the spectrum extrapolations, $f(E_T \rightarrow E_o)$. The Nb-foils in the SC provided by the Soviet reactor supplier and the separated Nb from the steel samples scraped from the welded austenitic cladding of the PV were used as dosimeters. The PV samples contain 0.5-1 % Nb, which was separated with ion exchange liquid chromatography and then electrodeposited on copper plates. The X-ray (16.6 + 18.6 keV) emission rate was measured with a calibrated Si(Li) spectrometer.

The statistical standard deviations in the obtained emission rates were in the range 0.2-7 %. An additional systematic error of 5 % (SC) or 6 %(PV) was added to the absolute fluence estimates (3 and 4 % in relative measurements) due to estimated or assumed additional bias effects from calibration efficiency and distance (3%), Nb-mass (3-4%), ^{182}Ta-activity (2-3%), unsymmetry in depositions (1%) and the measured shape correction (1.032±1 %). The estimated uncertainty in the absolute fluence Φ(>1 MeV) was 18-19 % and in the relative fluence (PV/SC) 7-11 % [5,7].

Table 1 gives the basic relations used in absolute and relative measurements and rough estimates for the uncertainties. By using the relative method the uncertainties in the fluence estimates could be reduced more than a factor of two. The use of the Fe-reaction (R1) for fast neutron dosimetry by application of relative measurements at SC and PV is simple as compared to the Nb-reaction (R2). Neither the activity nor the mass of niobium can be determined non-destructively. However, the accuracy both in absolute (18-19 %) and in relative (7-11 %) fluences obtained from Nb was better than for the Fe-reaction (26-27 %, 12 %).

4. ON THE INFLUENCE AND USE OF NUCLEAR DATA IN RELATIVE STANDARDIZED FLUENCE MEASUREMENTS

Table 2 gives the uncertainties (1σ), the discrepancies and consistency of measured (σ_m) and calculated (σ_c) spectrum averaged cross sections for the Fe- (R1) and Nb- (R2) reactions in ^{252}Cf and ^{235}U fields [10,11/Kobayashi]. The results for these two reactions represent almost two extreme cases, the consistency is good or excellent between the measured and calculated average Fe cross sections and very poor for the Nb reaction. Consequently the Nb cross section used (from IRDF-82) based on the results of Strohmaier et al. [12] is obviously biased giving too high estimates (σ_c). Since the measurements in ^{235}U fields show larger discrepancies than measurements in ^{252}Cf fields this indicates that the shape (i.e. the energy dependence) of the Nb-cross section may be wrong. E.g. a lowering of the cross section in the 0.5-2 MeV region would lead to a better agreement with the experimental estimates. There are no integral cross section measurements for the Nb-reaction in some other neutron fields as is the case for many other reactions [10,13].

TABLE 2. Uncertainties (1σ, %), discrepancies [%] and consistency (χ^2) of measured (σ_m) and calculated (σ_c) average cross sections for the $^{54}Fe(n,p)^{54}Mn$ and $^{93}Nb(n,n')^{93m}Nb$ reactions in ^{252}Cf and ^{235}U fields [10,13].

REACTION	STAND.DEV. in $\langle\sigma_m\rangle$ [%]	$\langle\sigma_c\rangle$	DISCREPANCY $(\langle\sigma_m\rangle-\langle\sigma_c\rangle/\langle\sigma\rangle$ [%]	CONSISTENCY χ^2 xx)	FIELD	REF
$^{54}Fe(n,p)^{54}Mn$	2.83	3.47	-3.56	0.65	^{252}Cf	[13]
	2.12		-2		^{252}Cf	[10]
	5		-3.7...0.4		^{235}U	[10]
	4.74	3.54	0.27	0.002	^{235}U	[13]
$^{93}Nb(n,n')^{93m}Nb$	7		-8.5		^{252}Cf	[10]
	7		-27.3..-31.3		^{235}U	[10]
	7.38		-21.5	13.76	^{235}U	[13]

xx) The consistency, which takes into account both the uncertainty (stand.dev.) and the discrepancy is very good if $\chi^2<1.5$, good if $1.5<\chi^2<3$, moderate if $3<\chi^2<4.5$, bad if $4.5<\chi^2<6$ and very bad if $\chi^2>6$.

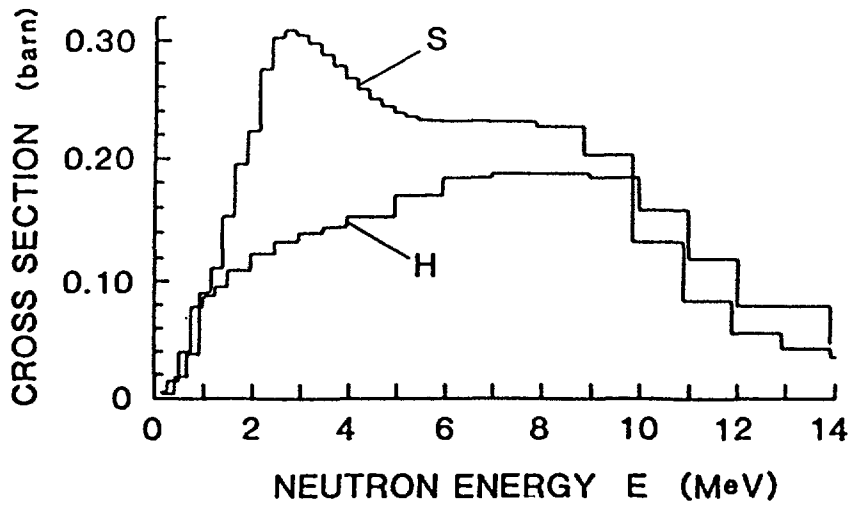

FIG. 1. Cross section for the reaction $^{93}Nb(n,n')^{93m}Nb$ given by H) Hegedüs [14] and by S) Strohmaier et al. [12].

Figure 1 displays the energy dependent cross sections for the Nb-reaction (R2) as given by Strohmaier et al. [12] and by Hegedüs [14]. In later computations by Strohmaier [15] the Nb cross section was almost the same as the previously computed one [12].

Table 3 provides data for sensitivity analysis of the spectrum shape on the threshold cross section for the Fe and Nb reactions. It gives the calculated threshold cross sections for the Fe- and Nb-reactions in a number of neutron spectra: a) OLDSC, b) OLDPV, c) NEWSC, d) NEWPV, e) NEWCAVITY, f) WATT, g) and an irradiation position in a research reactor. "OLD" and "NEW" refer to neutron spectra for two different loading configurations of the Loviisa reactors. The threshold cross section for the Nb-reaction was taken from DOSCROS-81 [11, same as IRDF-82] and was normalized to agree with with integral measurements by

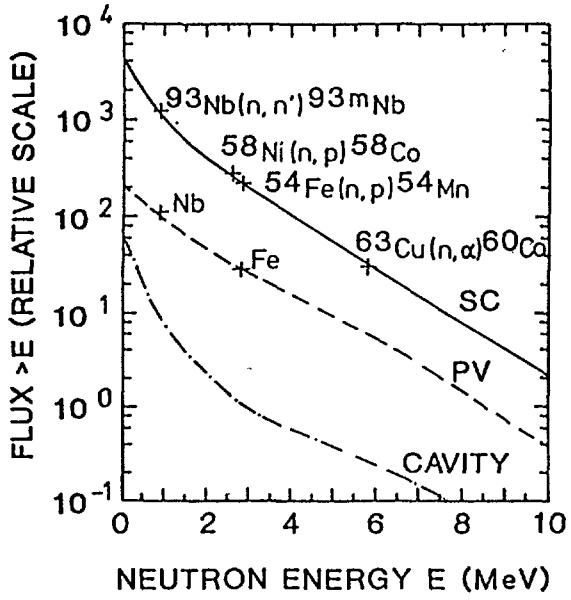

FIG. 2. Sketch of the relative neutron fluxes $\phi(>E)$ (OLDSC, OLDPV, NEWCAVITY) at the SC, PV inner surface and cavity of the Loviisa reactors. Some measured points are indicated [4,5].

Alberts et al. [16], $\langle\sigma\rangle$=149 ±10 mb in a ^{252}Cf field and is 0.92 times the result obtained from the calculated cross section based on the data of Strohmaier et al. [11,12].

The research group of Alberts has given a notice [private communication 1984] that their previously reported γ to X-ray conversion probability in Nb (p_k=0.107±0.003) probably is 5-10 % too small. Since the used p_k - σ pair obviously is coupled [16] an increased p_k estimate does not change the absolute (Nb) fluence estimates.

A very important conclusion is that the p_k estimate and the absolute value of the Nb cross section have no influence on the relative measurements provided that the shape of the cross section is unchanged.

Figure 2 is a sketch of the relative neutron fluxes $\Phi(>E)$ at the SC (OLDSC), PV (OLDPV) and cavity (NEWCAVITY) at the Loviisa NPP with some measured points indicated. The neutron spectra above 0.5 MeV were constructed from data provided by the Soviet reactor supplier and in the range ≈0.1-0.5 MeV an 1/E dependence was assumed. Winkler's [17] Cu-cross sections were used.

The ratios of the cut-off fluxes $\phi(>1$ MeV) obtained from the Nb-, Ni-, Fe- and Cu-reactions during the three first operating cycles at the SC and by utilizing the mentioned spectrum and cross section information are 1.06 : 1.036 : 1 : 0.92. The flux ratio obtained at the PV from the Nb- and Fe-reactions is 1.068 :1. If we use the 8.7 per cent higher calculated Nb cross section (based on Strohmaier et al. data [12] and the same p_k estimate) instead of the data adjusted to the ^{252}Cf field measurements then the agreement with the Fe-results would be still better (Nb : Fe = 0.975 : 1 at SC).

Fig. 3 shows the normalized response $\sigma(E)\phi(E)$ of the Nb-reaction at the PV (spectrum OLDPV) together with the dpa response $\sigma_{dpa}(E)\phi(E)$ in the same spectrum.

Threshold flux measurements in a 30 MW research reactor (No 2 in Table 3) gave the following ratios for the cut-off fluxes

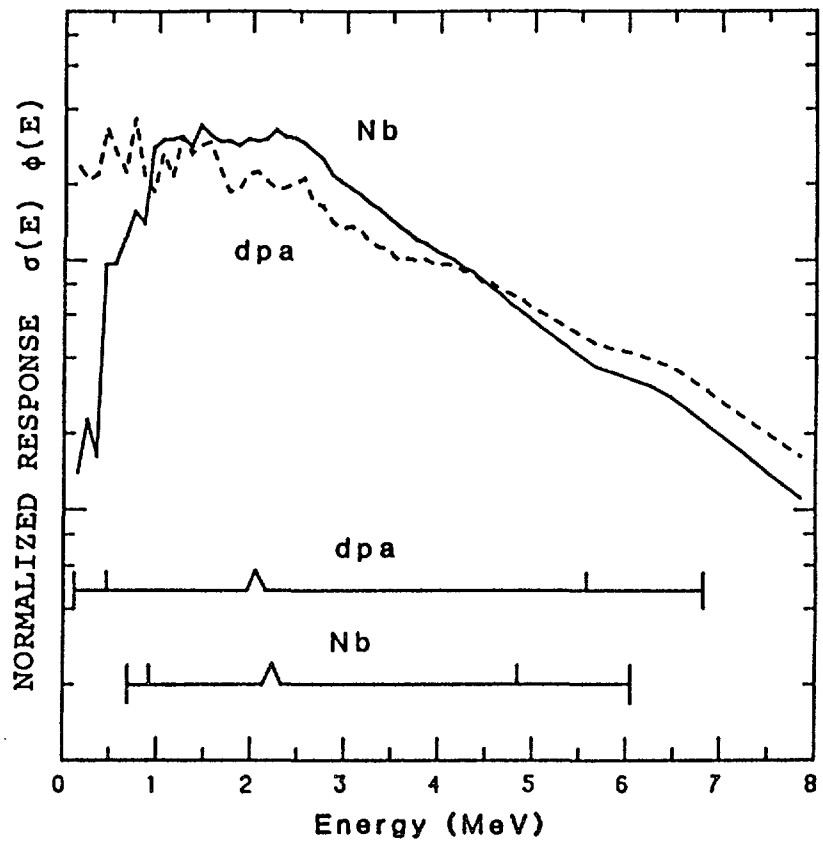

FIG. 3. Normalized responses $\sigma(E)\ \phi(E)$ (log scale) of the reactions $^{93}Nb(n,n')^{93m}Nb$ ($\sigma(E)$ from DOSCROS-81) and dpa ($\sigma(E)$ from ASTM, E>10 keV) at the PV of the Loviisa-1 reactor (VVER-440). Spectrum: OLDPV. The range charts are shown (for 95%, 90%, 50%, 10% and 5% lower integral response limits).

TABLE 3. Sensitivity analysis: the influence of the neutron spectra (Loviisa NPP spectra, a WATT and a research reactor spectrum) on the threshold cross section σ_T for the Fe- and Nb-reactions (m= adjusted to ^{252}Cf measurements [16], c= calculated cross section, new p_k and $t_{1/2}$ data). σ-data: S=Strohmaier [12], H=Hegedüs [14], Fig.1.

	THRESHOLD CROSS SECTION σ_T [mb] FOR		
REACTION →	$^{93}Nb(n,n')^{93m}Nb$	Nb σ	$^{54}Fe(n,p)^{54}Mn$
THRESHOLD ENERGY →	E_T=0.9 MeV	DATA	E_T=2.8 MeV
SPECTRUM ↓			
OLDSC/Lo	190.16	S,m	338.8
OLDPV/Lo	190.78	S,m	428.8
NEWSC/Lo	172.7	S,m	372.6
NEWPV/Lo	193.3	S,m	382.3
NEWCAVITY/Lo	194.1	S,m	382.4
WATT	200.7	S,m	325.4
RES. REACTOR 2	206.86 (>1 MeV)	S,m	
RES. REACTOR 2	192.03 (>1 MeV)	H,c	

above 1 MeV obtained from the Nb-, Ni-, Fe-, Ti- and Cu-reactions 0.900: 1.044: 1: 1.001: 1.148. Similar to the Loviisa case the (Nb) threshold cross section (206.86 mb, >1 MeV) was calculated from data [12] adjusted to the measured Nb cross section (149 mb, ref. 11) in a ^{252}Cf field. If the calculated Nb cross section is used the bias (0.82 : 1) to the Fe-based flux is still higher but in the same direction as for the Loviisa NPP. Biased (too soft) neutron spectra may also contribute to the difference. For this specific case (research reactor No 2 in Table 3) the the threshold cross section (192.03 mb) obtained from Hegedüs [14] cross section data adjusted to new $t_{1/2}$ and $p_k$data is 7.2 per cent lower.

These results can also be compared to those of Sakurai [18]. At an irradiation in the JMTR reactor he obtained 23 % larger flux values using Nb compared to Fe (R1). He normalized the cross section of Hegedüs [14] to the half-life 13.6 a and the γ to X-ray conversion probability 0.116. If the more recent values 16.11 a and 0.107 are used, the Nb results will be 4.6 % below the Fe results. If in addition the cross section data of Strohmaier et al. [12,=IRDF-82, Fig.1 and Table 3] are used the negative bias between the Nb- and the Fe- based cut-off fluences is obviously still bigger.

A systematic feature is that all comparisons based on the calculated cross section (IRDF-82/Strohmaier et al.) and on the other side on measurements in ^{235}U and ^{252}Cf fields, on the comparative use of the Fe-reaction (R1) (at Loviisa NPP and at two research reactors) indicate that the calculated Nb cross section used gives too high estimates for the average and threshold cross sections. Consequently the flux estimates based on these data and on Nb measurements are too low. However, due to the large uncertainties the flux estimates are within the error limits and no definite conclusions can be drawn.

5. CONCLUSIONS

1. It has been demonstrated that the combined use of PV cladding dosimetry, relative standardized measurements and the low threshold energy Nb-reaction (R1) may significantly improve the quality of the dose estimates (uncertainty from 20-30 % to less than 10 %) to be used at the estimation of the PV embrittlement. The great advantage of the relative standardized measurements is that the influence of some large systematic (correlated) errors in the nuclear data (especially in the cross sections), in the spectrum shapes etc. may be cancelled or much suppressed. In fact no absolute data are needed, no absolute cross sections (shape of σ and flux needed), no conversion factors, no absolute detector efficiencies etc.

The standardization of data and procedures, which is an essential part of the relative measurements is used in order to convert uncorrelated errors into correlated errors and in order to suppress their influence. In addition to the cross sections a similar philosophy or procedure is of course applicable to the other quantities as well.

The relative standardized measurements may be regarded as a further extension of the "flux transfer" method in the sense that they include standardizations at the estimation of all quantities but no absolute fluence estimates are needed, no reference field, no absolute calibrations etc.

2. Due to the low threshold energy (≈1 MeV), the relatively large low-energy fast neutron flux, the long half-life (16.1 a) of the product nuclide (^{93m}Nb), the problems encountered with the fission reactions etc. the use of the Nb-reaction is of great importance in fast neutron metrology. Although the large systematic errors in the Nb-cross section and possibly also in other quantities may be strongly suppressed by standardized relative measurements at embrittlement estimations, there is also a need to obtain accurate absolute flux data. These demands arise from the need to check or adjust the shape of the neutron spectrum to absolute flux estimates obtained from several threshold reactions with special emphasis on the low energy region (≈1-3 MeV). In such absolute measurements estimates for the absolute nuclear data are needed.

The presently available cross section data and the γ to X-ray conversion coefficient for Nb reaction include larger inconsistencies than most other reactions. The available results and our experiences (sections 3 and 4) indicate that the calculated Nb cross section used [12,=IRDF-82] gives too high (^{252}Cf, ^{235}U) spectrum averaged and threshold cross sections. Secondly in the available test cases the Nb-based fluxes (using the calculated Nb-cross section [12]) are lower than the Fe-based fluxes. These results also indicate that the applied calculated Nb-cross section [12] is too large. The important fast neutron metrology would benefit from more consistent nuclear cross section and γ to X-ray conversion data for the Nb-reaction.

ACKNOWLEDGEMENTS

The work on relative standardized neutron dose measurements has been financially supported by Imatran Voima Oy (Imatra Power Company Ltd) and by the Ministry of Trade and Industry.

REFERENCES

[1] Proceedings of the Third ASTM-Euratom Symposium on Reactor Dosimetry, Ispra (Varese), Italy, Oct. 1-5, 1979. EUR 6813 (1980).

[2] Proceedings of the Fourth ASTM-Euratom Symposium on Reactor Dosimetry, Gaithersburg, Maryland, USA, March 22-26, 1982. NUREG/CP-0029 (1982).

[3] Proceedings of the Fifth ASTM-Euratom Symposium on Reactor Dosimetry, Geesthacht, FRG, Sept. 24-28, 1984. EUR Report (to be published).

[4] BÄRS, B. et al., A Method for Improving the Accuracy in Neutron Fluence Measurements in Power Reactors and its Application to a WWER-440 Nuclear Power Plant, Kernenergie 27 (1984) 342.

[5] BÄRS, B. and KARNANI, H., Use of Niobium for Accurate Relative Fast Neutron Fluence Measurements at the Pressure Vessel in a VVER-440 NPP. In Ref. [3].

[6] HEGEDUES, F., Fast Neutron Dosimetry by means of the Scraping Sampling Method. In Ref. [3].

[7] BÄRS B. et al., Modern methods to improve the accuracy in fast neutron dosimetry. IAEA Specialists' Meeting on "New Instrumentation of Water Cooled Reactors", Dresden, GDR, 23 to 25 April 1985.

[8] LLORET, R., Complement à la mesure de la période de décroissance radioactive du ^{93m}Nb, Radiochem. Radioanal. Lett. 50 (1981) 113.

[9] Nuclear Data Standards for Nuclear Measurements. IAEA Technical Reports Series No. 227 (1983).

[10] CULLEN, D.E. et al., Comparison of Experimental and Calculated Spectrum-Averaged Neutron Cross Sections for the IAEA International Reactor Dosimetry File (IRDF-82), Nucl. Sci. Eng. 83 (1983) 497.

[11] ZIJP, W.L. et al., Cross Section Library DOSCROS81, ECN-111 (1981).

[12] STROHMAIER B., et al., Physics Data 13 (1980).

[13] ZIJP, W.L. et al., Comparison of measured and evaluated spectrum-averaged cross-section data. Ref.[2], p. 725.

[14] HEGEDUES, F. Détecteur de fluence de neutrons rapides basé sur la réaction ^{93}Nb(n,n')^{93m}Nb, EIR-Bericht Nr. 195 (1971).

[15] STROHMAIER B., Nuclear model calculations of cross section for neutron-induced reactions on ^{93}Nb to 20 MeV, Ann. Nucl. Energy 9 (1982) p. 397-407.

[16] ALBERTS, W.G. et al., Measurements with the Niobium Neutron Fluence Detector at the PTB. Ref. [2], p. 433.

[17] WINKLER, G. et al., Measurement of Cross Sections for the ^{63}Cu(n,α)^{60}Co Reaction from Threshold to 10 MeV, Nucl. Sci. Eng. 76 (1980) p. 30.

[18] SAKURAI, K., Measurement of neutron fluence above 0.1 MeV with the the dosimeter ^{93}Nb(n,n')^{93m}Nb, Nucl. Technol. 57 (1982) p. 436-441.

BENCH MARK SPECTRA FOR HIGH-ENERGY NEUTRON DOSIMETRY

R.DIERCKX
Commission of the European Communities
JRC Ispra, 21020 Ispra, Italy

ABSTRACT

To monitor radiation damage experiments, activation detectors are commonly used. The precision of the results obtained by the multiple foil analysis is largely increased by the intercalibration in bench-mark spectra. This technique is already used in dosimetry measurements for fission reactors.

To produce neutron spectra similar to fusion reactor and high-energy high-intensity neutron sources (d-Li or spallation), accelerators can be used. Some possible solutions as p -Be and d-D_2O neutron sources, useful as bench-mark spectra are described.

1. INTRODUCTION

The monitoring of radiation damage experiments for fusion application requires special attention due to the high neutron-energy nature of the spectra to be measured. The first-wall spectrum of a fusion reactor has a peak at 14 MeV. The accelerator neutron sources used to simulate fusion irradiation environments, d-Li or spallation sources, have neutron spectra extending to about 40 MeV.
Experience from fission reactor dosimetry has shown that the use of Bench Mark spectra is not only useful but necessary to obtain reliable results and to keep the uncertainties below the 10% level [1,2].
Bench mark spectra useful for fusion oriented dosimetry can be realized at a cyclotron. With a beam current (protons or deuterons) of 65 uA it is possible to obtain a medium-intensity high-energy neutron source of about 5.10^{12} n/s.sr in the forward direction.

Such a source can be used for different research activities :

1. fusion dosimetry studies
2. cross-section testing up to 40 MeV

2. THE NEUTRON SOURCE [3-6]

Different targets and bombarding ions have to be used in function of the different experiments executed. All sources have about the same output, 5.10^{12} n/s.sr in the forward direction and 10^{13} n/s total neutron output for normal cyclotron operation conditions of 65 uA beam current. The source should be operated in two ways, a D-C mode and a pulsed mode. In the D-C mode of operations, the full cyclotron current is used and the maximum neutron output obtained. For the pulsed mode, a pulsed ion source will be used delivering a 1 ns pulse, necessary for time of flight experiments.

2.1. 19 MeV deuterons on a D_2O target

This source delivers a spectrum which is a good simulation of a first wall-neutron spectrum. It has a low energy part, peaking around 6 MeV and about 20% of the neutrons have energies greater than 12 MeV (fig.1). The difference between the spectrum and a first-wall neutron spectrum is that instead of having a peak at 14 MeV, the neutrons are equally distributed between 12 and 21 MeV.

Using 12 MeV deuterons as bombarding particles on a D_2O target, the spectrum of fig.2 is obtained. The maximum neutron energy is 15 MeV but the source intensity is about one thirth relative to the 19 MeV deuterons. By changing the deuteron energy different spectra are obtained.

2.2. 19 MeV deuterons on a Be target

This source has a broad peak around 6 MeV, with a half width of 10 MeV. This means that most neutrons lies between 2 MeV and 12 MeV (fig.1).

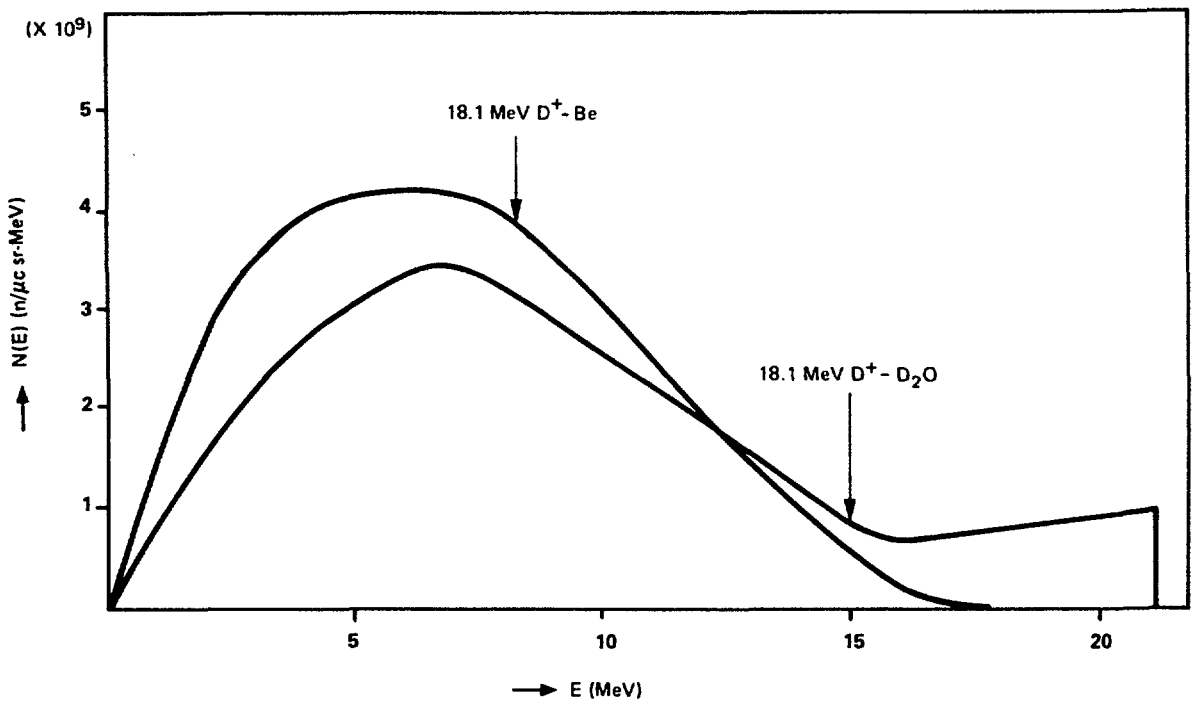

Fig. 1. 0° neutron spectra from 18.1 MeV deuterons on beryllium and D_2O

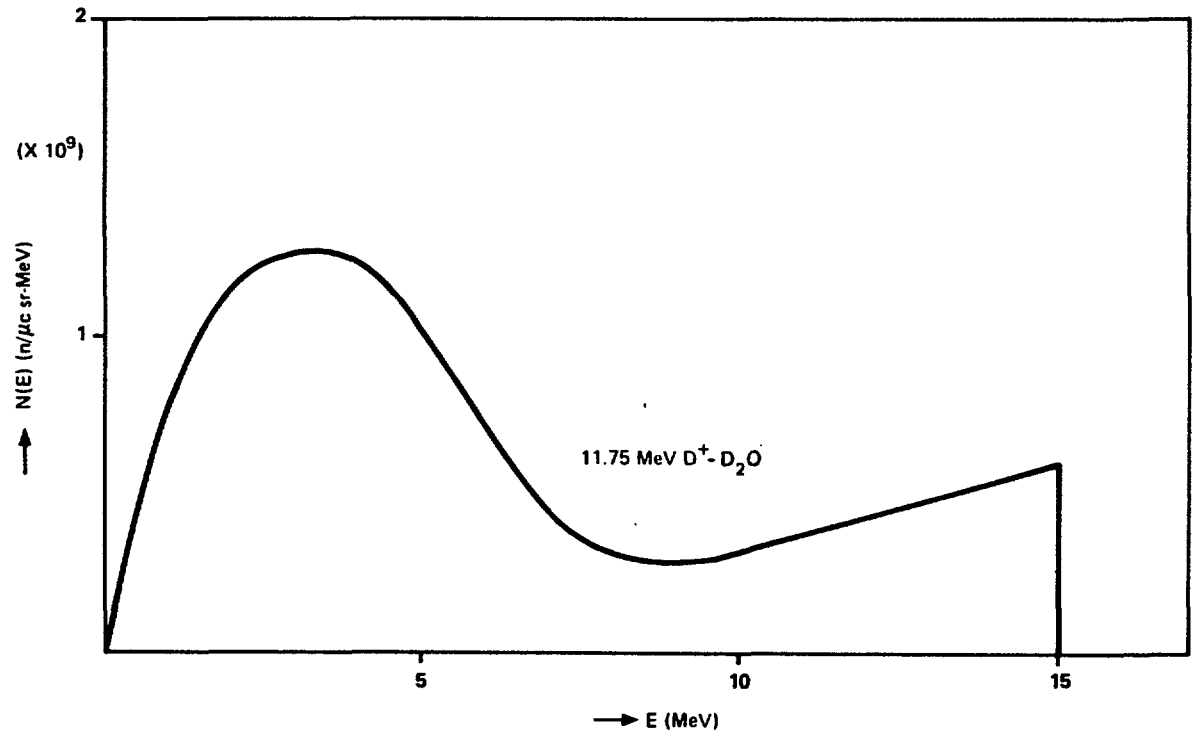

Fig. 2. 0° neutron spectrum from 11.75 MeV deuterons on D_2O

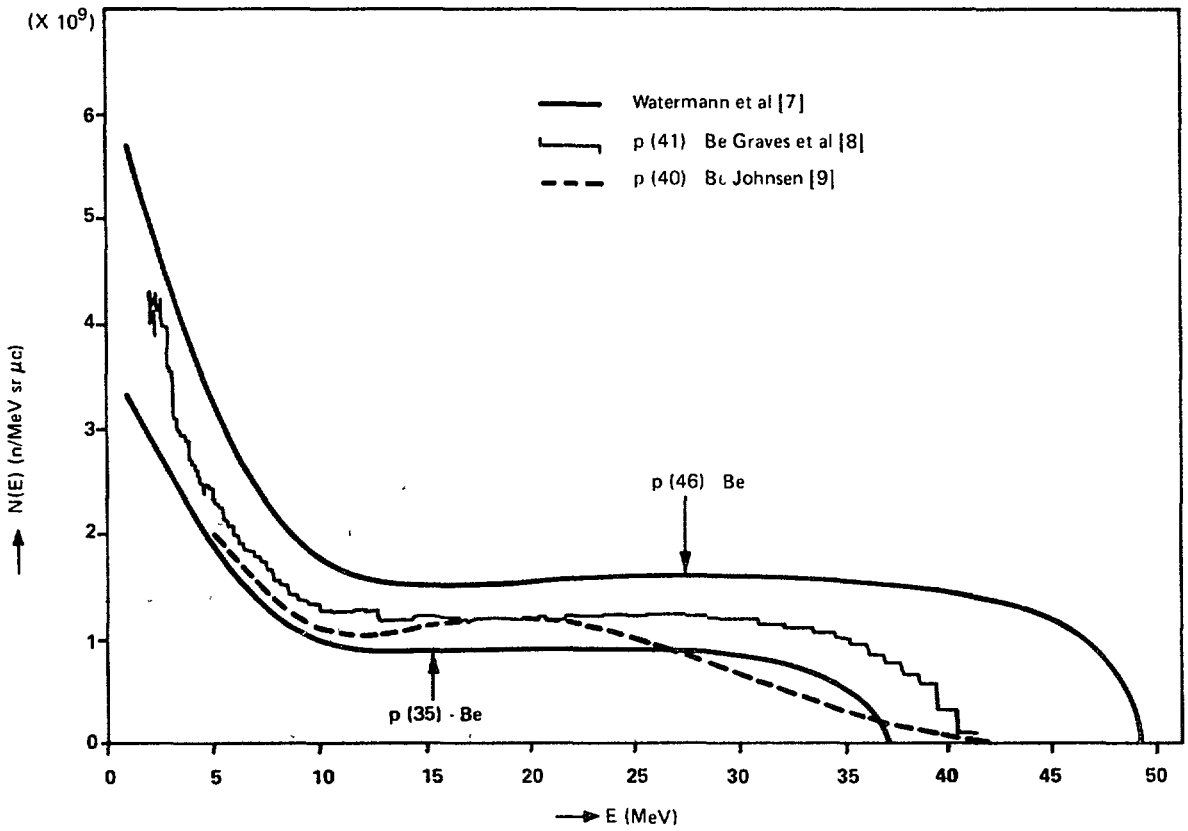

Fig. 3. 0° neutron spectra from protons on beryllium

2.3. 20 to 40 MeV protons on Be /7,8,9/

The maximum neutron energy is equal to the bombarding proton energy, and the neutron spectrum is quite flat from a few MeV up to the maximum neutron energy with a rise at small neutron energies. Thus bombarding with 40 MeV protons, neutrons up to 40 MeV are produced (fig.3).

3. RESEARCH ACTIVITIES

3.1. Fusion-dosimetry studies

Neutron dosimetry for Radiation-damage irradiation is of primordial necessity. These irradiations have to be monitored with enough precision to predict mechanical properties of the materials used for fusion-reactor design and construction. Only with a good neutron monitoring, it is possible to extrapolate and predict end-of-life of these materials under irradiation.

Therefore it is necessary to develop the neutron dosimetry for fusion and high-intensity high-energy neutron sources (such as the d-Li source, and spallation sources).

The neutron dosimetry is done with activation foils and the measured activities are analysed with unfolding techniques. For energies greater than 20 MeV only calculated cross-sections exist and these have to be tested (see next Section). Further unfolding techniques give reliable results when intercalibrated in calibration spectra or Bench-Mark spectra.

The research programme to develop the dosimetry for fusion and high-energy neutrons sources looks as follows :

- setting up of Bench-Mark spectra
- measuring these spectra with time of flight (TOF) and other techniques
- calibrating the foils in these TOF spectra
- testing of the methods in other spectra

3.2. Cross-section testing

It will take a long time before the first fusion reactor will work, and radiation damage experiments can be done in a real fusion environment. In the mean time the materials will be irradiated in the high-energy neutron sources such as d-Li and spallation sources. These sources have a significant part of the neutron spectrum up to 30-40 MeV. Cross sections are measured up to 20 MeV and some transmission measurements at higher energies.

Above 20 MeV, most used cross-sections are calculated, and need experimental verification. Differential measurements are difficult and very time consuming, such that only a few key cross-sections are and will be measured differentially. The other needed cross-sections have to be tested by integral experiments.

Both techniques, differential cross-section measurements and integral cross-section testing is possible at the proposed neutron sources.

A recommendation in this sense is put forward by the IAEA Advisory Committee "Nuclear data for radiation damage assessment and related safety aspects" held at Vienna in 1981 [10]. Some of the recommendations are :

1. Integral cross section measurements for dosimetry reactions in well-known neutron fields should be considered during the evaluation of neutron cross sections. These data should then be included in the data files.

2. It is recommended to supplement the future International Reactor Radiation Damage File, for Fe, Cr and Ni up to 40 MeV, and to include the data for Al up to 40 MeV with the first priority. The data for graphite, O, Ti, V, Mn, Cu, Zr, Mo, W up to 40 MeV and for Nb, Sn up to 20 MeV should be included in the file with second priority.

3. Few experimental data above 20 MeV exist. More experimental data are wanted, but in their absence one has to recur to theoretical calculations. Theoretical calculations of H and He production cross-sections show that at higher incident energies the contributions of reactions of the type (n,pp) and (n,pα) cannot be neglected for target nuclei with small neutron excess. Evaluations of needed changes in the energy dependence of the damage function should be considered in future theoretical and experimental research.

4. For the calculations of gas production and solid transmutation accurate excitation functions would be necessary from thereshold up to about 30 MeV for (n,γ); (n,xn); (n,tot.H) and (n,tot He)

mostly between 9 and 15 MeV. The list of important materials (e.g. Li, C, N, O, Al, Si, Ti, V, Cr, Mn, Fe, Ni, Cu, Zr, Nb, Mo, Pb) can be found in the IAEA biennial publication WRENDA.

5. It is further recommended that the Nuclear Data Section encourage measurements of total cross-sections up to 40 MeV for the above mentioned reactions.
   Such measurements are extremely useful for parametrization of nuclear model calculations.

4. EXPERIMENTAL LAY-OUT (fig.4)

A possible lay out of such a Bench Mark facility is given in fig.4. As reference the Ispra cyclotron is taken. The neutron source is located in a target-cell, constructed outside the actual cyclotron building. The ion beam will pass the existing cyclotron wall through an existing penetration, pass a 90° bending magnet and is lead into the target cell of 2 x 2 x 2 m^3. The target cell is shielded heavely (about 2 m of iron in the forward direction) and has beam holes to extract the neutron beam for TOF measurements either from the source itself either from a mock-up placed inside the target cell. Through the sliding door mock-ups for integral measurements can be brought into the target cell.
Around the target cell, an experimental hall is foreseen, in which a collimator, detector and electronics are placed. The experimental hall measures about 11 x 21 m^2.

This lay-out permits the measurement of the neutron output of the source and of the scattered neutrons in the mock-up from 0° to 180°.

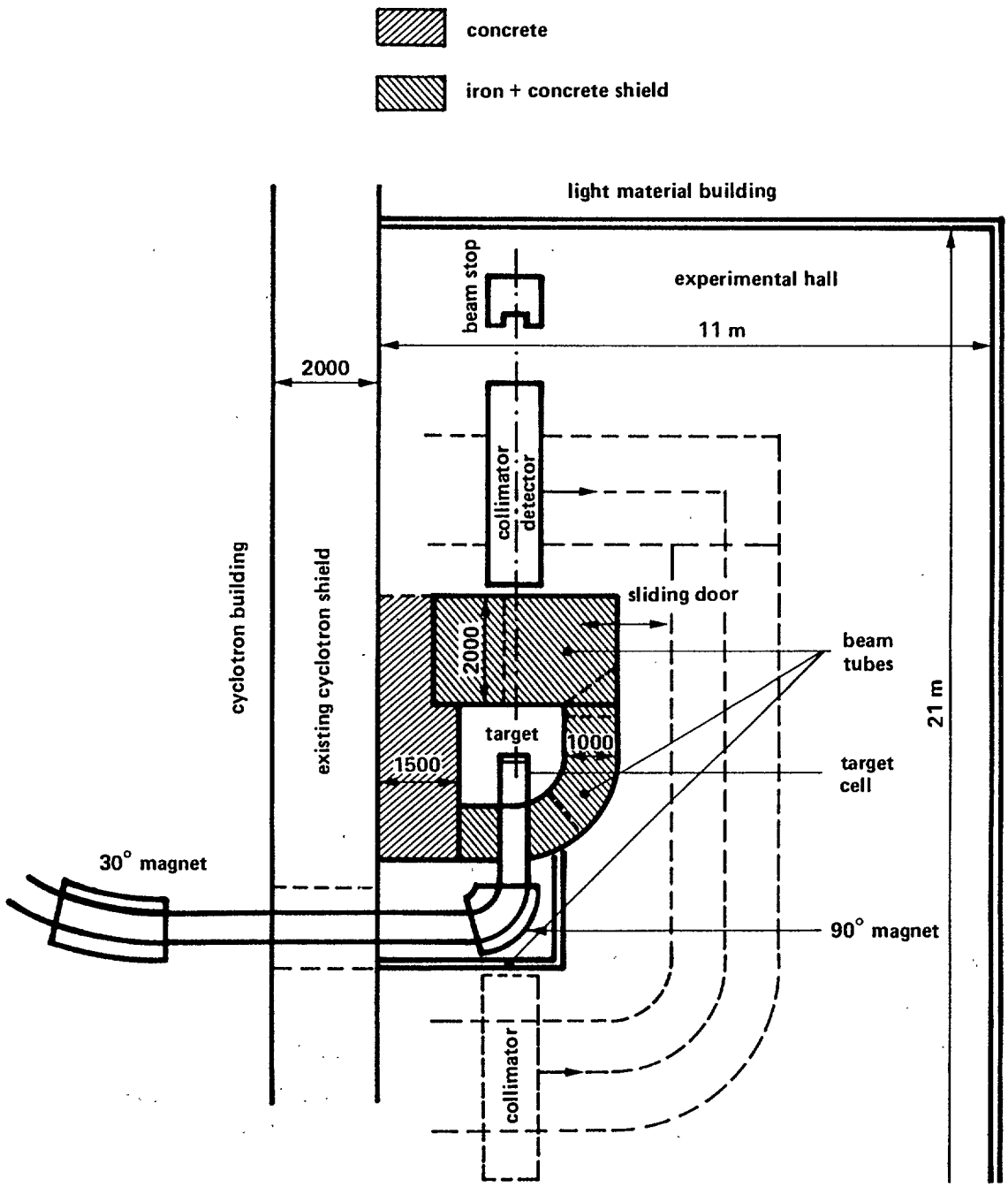

Fig. 4. Lay-out of target cell and experimental hall

REFERENCES

1. W.N.McELROY et al
Surveillance dosimetry of operating power plants
Proc. of 4° ASTM-EURATOM Symposium on reactor dosimetry NBS-Gaitherburg (Maryland) March 22-26, 1982
p.3 vol.I NUREG/CP-0029, Conf.820321/V1

2. R.DIERCKX
Uncertainties on the neutron spectra measured by activation technique
Neutron measurements metrology for nuclear physical facilities (p.167, vol.I) edited by R.D.Vasiliev, Moscow (1976)

3. K.A.WEAVER et al
Neutron spectra from deuteron bombardement of D, Li, Be and C
Nucl. Sci. and Eng. 52, 35-45 (1973)

4. G.J.BATRA et al
Neutron production from hydrogen isotopes
Nucl. Instr. & meth. 100, 135-139 (1972)

5. G.A. SCHWEIMER
Fast neutron production with 54 MeV deuterons
Nucl. Physics A-100, 537-544, 1967

6. M.A.LONE et al
Thick target neutron yields and spectral distributions from the $^{7}Li(_{p}^{d}n)$ and $^{9}Be(_{p}^{d}n)$ reactions
Nucl. Instr. & Meth. 143, 331-344 (1977)

7. F.M.WATERMANN et al
Neutron spectra
Med. Phys. vol.6, p.160 (1979)

8. R.G.GRAVES et al
Med. Phys. 5, 451 (1978)

9. S.W. JOHNSEN
Med. Phys. 5, 452 (1978)

10. IAEA
TECDOC-263 (April 1982)

Least-Squares Adjustment of a 'Known' Neutron Spectrum: The Importance of the Covariance Matrix of the Input Spectrum

W. Mannhart
Physikalisch-Technische Bundesanstalt
3300 Braunschweig, FRG

Abstract

Based on the responses of 25 different neutron activation detectors, the neutron spectrum of Cf-252 has been adjusted with least-squares methods. For a fixed input neutron spectrum, the covariance matrix of this spectrum has been systematically varied to investigate the influence of this matrix on the final result. The investigation showed that the adjusted neutron spectrum is rather sensitive to the structure of the covariance matrix for the input spectrum.

1. Introduction

Radiation damage estimates are of limited use unless they are accompanied by realistic estimates of their inaccuracy. Besides damage modeling, for the determination of neutron-induced material changes the radiation environment must be determined as accurately as possible, i.e., the calculation of any neutron damage requires the knowledge of the neutron spectrum. This information is often obtained by spectrum adjustment procedures based on the experimentally determined responses of various neutron detectors. Such adjustment codes when based on the least-squares principle allow a correct uncertainty propagation of all the quantities involved in the procedure.

Every spectrum "unfolding" or adjustment code needs a "guess" or input spectrum to work properly. In the case of least-squares adjustment, additional information in the form of the input spectrum uncertainties is mandatory. At present, there is scarcely any realistic covariance information for input spectra available /1/.

To investigate the influence of this deficit in a systematic way in the case of the relatively well-known neutron spectrum of spontaneous fission of Californium-252, least-squares adjustment was done with various assumptions of the covariance matrix of the input spectrum within realistic limits.

2. The neutron spectrum of Californium-252

For a long period, this spectrum was described in the literature by a simple Maxwellian:

$$\chi(E) = \frac{2}{\sqrt{\pi}} \frac{1}{T_M^{3/2}} \sqrt{E} \quad \exp\ (-E/T_M) \qquad (1)$$

The temperature parameter T_M deduced from spectrum measurements approximated a value of T_M = 1.42 MeV. While the description of Eq. (1) fitted well the spectrum data up to a few MeV, recent integral experiments with high-threshold neutron reactions /2, 3/ and also time-of-flight experiments /4 - 6/ indicated the inadequacy of Eq. (1) at higher neutron energies. Taking this information into account resulted in the following modification of Eq. (1):

$$\chi(E) = 0.6680 \sqrt{E} \exp\ (-E/1.42) \quad \text{for } 0 \leq E \leq 6 \text{ MeV} \qquad (2)$$
$$\chi(E) = 0.7997 \sqrt{E} \exp\ (-E/1.362) \quad \text{for } 6 \leq E \leq 20 \text{ MeV}$$

The approximation of Eq. (2) describes fairly well the available spectrum data. A comparison of the result of Eq. (2) with recent time-of-flight spectrum experiments and with nuclear evaporation theory models is given elsewhere /7/. Eq. (2) was chosen for the input spectrum of the least-squares adjustment shown in the next section. Eq. (2) is essentially identical with an earlier NBS evaluation /8/. This evaluation parameterized the spectral distribution by a Maxwellan of T_M = 1.42 MeV. The deviations from the Maxwellian were taken into account by five continous energy-dependent segment corrections. Based on recent spectrum data the corrections below 6 MeV neutron energy were neglected in Eq. (2). In addition a slight rescaling was done to conserve the normalization of Eq. (2). The value of T_M = 1.362 MeV valid for E > 6 MeV of Eq. (2) is in good agreement with T_M = (1.374 ± 0.020) MeV obtained by Märten et al. /5/ from spectrum data between 9 MeV and 20 MeV and with T_M = (1.355 ± 0.015) MeV obtained by Böttger et al. /6/ from data between 3 MeV and 13 MeV.

3. Least-squares adjustment of the Cf-252 neutron spectrum

This step is described in detail elsewhere /9/. Only a few essential points and results are repeated here. The responses of 25 different neutron reactions were used in the adjustment procedure.

Table 1: Reaction rates used in the adjustment procedure

Reaction	$\langle\sigma\rangle^{EXP}$ (barn)	Rel.Std. Dev. %	$\langle\sigma\rangle^{CALC}$ (barn)	EXP/CALC	χ^2_{part}
F-19(n,2n)	1.628E-5	3.33	1.628E-5	1.000	0.00
Mg-24(n,p)	2.005E-3	2.39	2.160E-3	0.928	2.62
Al-27(n,p)	4.892E-3	2.16	5.140E-3	0.952	0.61
Al-27(n,α)	1.021E-3	1.42	1.013E-3	1.008	0.10
Ti-46(n,p)	1.420E-2	1.68	1.347E-2	1.054	0.16
Ti-48(n,p)	4.275E-4	1.81	4.096E-4	1.044	0.17
Mn-55(n,2n)	4.079E-4	2.26	4.462E-4	0.914	0.47
Fe-54(n,p)	8.729E-2	1.29	8.823E-2	0.989	0.17
Fe-56(n,p)	1.471E-3	1.73	1.415E-3	1.039	0.66
Ni-58(n,p)	1.176E-1	1.25	1.138E-1	1.034	0.19
Ni-58(n,2n)	8.965E-6	3.32	8.471E-6	1.058	0.72
Co-59(n,α)	2.221E-4	1.78	2.164E-4	1.027	0.32
Co-59(n,2n)	4.058E-4	2.49	4.107E-4	0.988	0.02
Cu-63(n,γ)	1.055E-2	3.08	9.772E-3	1.080	0.37
Cu-63(n,α)	6.897E-4	1.88	6.767E-4	1.019	0.08
Cu-63(n,2n)	1.866E-4	3.82	1.982E-4	0.941	2.96
Zn-64(n,p)	4.047E-2	1.85	3.922E-2	1.032	0.13
Zr-90(n,2n)	2.211E-4	2.78	2.058E-4	1.075	3.73
In-115(n,γ)	1.261E-1	2.19	1.222E-1	1.032	0.47
In-115(n,n')	1.981E-1	1.31	1.819E-1	1.089	0.52
Au-197(n,γ)	7.711E-2	1.54	7.720E-2	0.999	0.00
U-235(n,f)	1.210E+0	1.19	1.238E+0	0.978	1.89
Np-237(n,f)	1.356E+0	1.65	1.353E+0	1.003	0.00
U-238(n,f)	3.234E-1	1.72	3.134E-1	1.032	2.89
Pu-239(n,f)	1.811E+0	1.37	1.792E+0	1.010	0.05

The reactions are listed in Table 1. The experimental reaction rates normalized by the neutron fluence rate are given in the form of spectrum-averaged cross sections, $\langle\sigma\rangle^{EXP}$. The corresponding relative standard deviations of these data are shown in column 3 of the table. The full covariance matrix is shown in ref. /9/. The experimental data are compared with those calculated based on the spectral representation of Eq. (2) and appropriate σ(E) data. The energy-dependent cross section data and their covariances were taken mainly from ENDF/B-V. (For details, see ref. /9/). The last two columns of Table 1 list the ratio between experiment and calculation and the specific contribution of each reaction to the final chi-square value. The agreement between the experimental and calculated reaction rates confirms the appropriateness of the

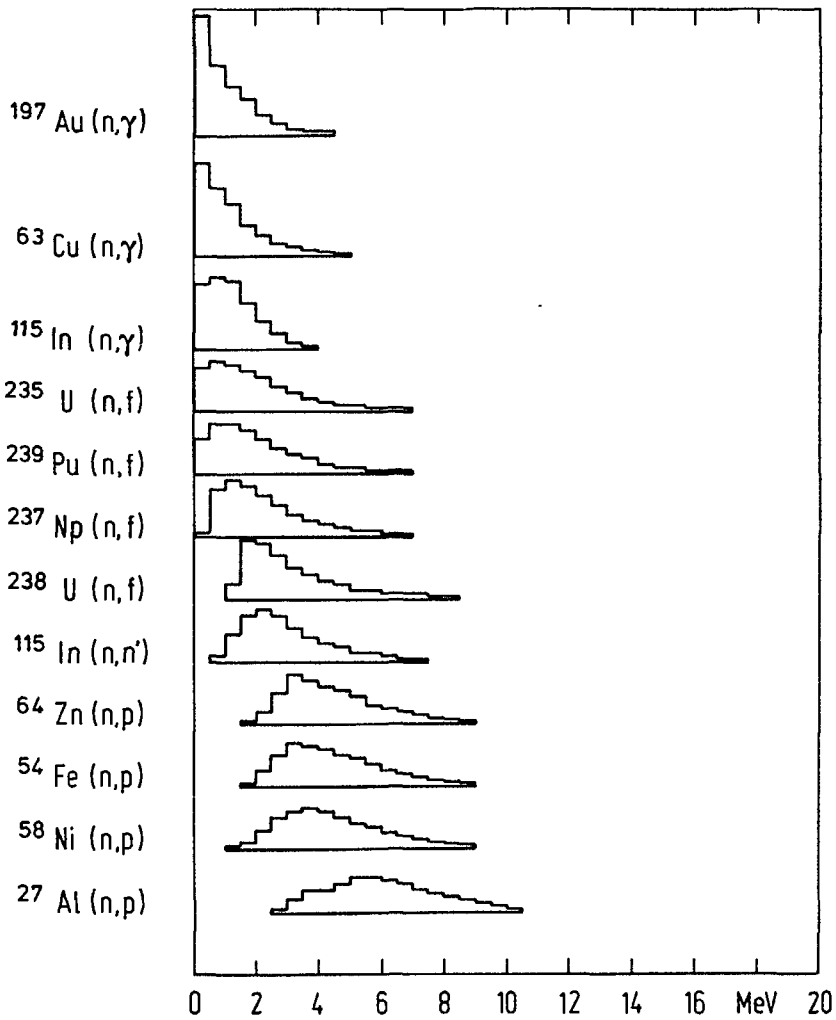

Fig. 1: Response of the various activation neutron detectors in the Cf-252 neutron spectrum. The responses are normalized to the same energy integrated value.

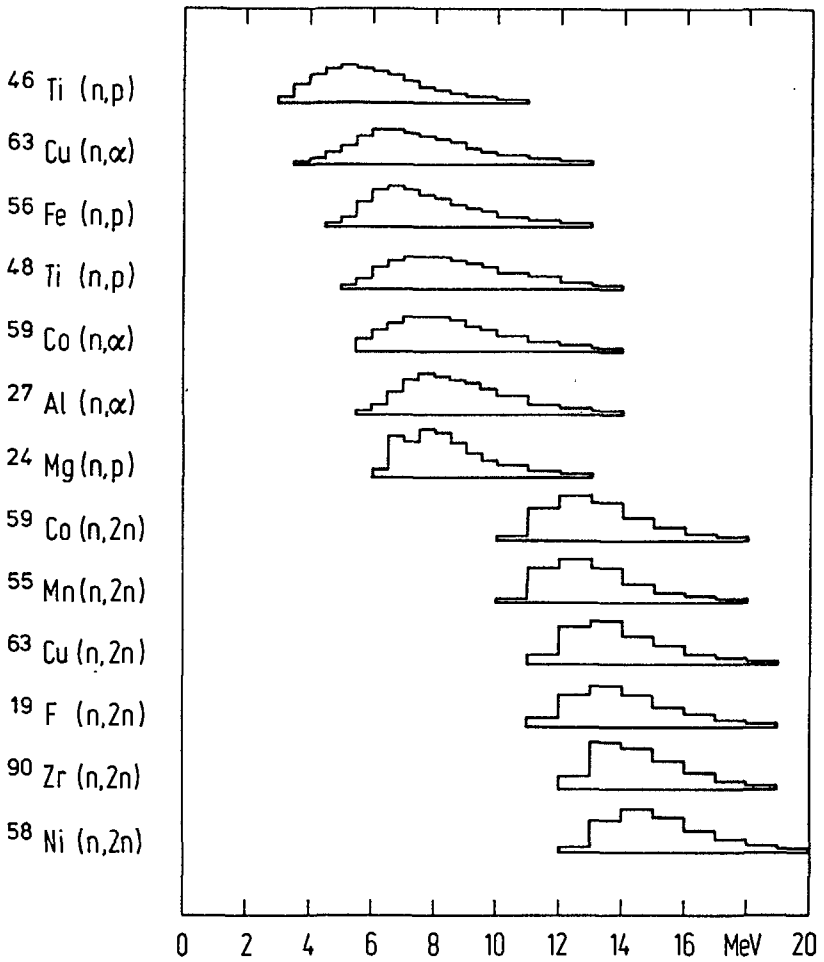

Fig. 2: Same as Fig. 1.

spectral representation of Eq. (2) and of the $\sigma(E)$ data. The contributions to the final chi-square automatically take into account the covariances of $\langle\sigma\rangle^{EXP}$, of $\chi(E)$ and of $\sigma(E)$. Therefore an EXP/CALC value strongly deviating from unity does not have to automatically result in a large contribution to the chi-square.

The least-squares adjustment of the spectrum was done in 30 energy groups. The group bins were 0.5 MeV between 0 MeV and 10 MeV and 1 MeV between 10 MeV and 20 MeV. The energy responses of the various neutron reactions normalized to the same area are shown in Fig. 1 and 2. The reactions cover the neutron energy range between a few keV and about 18 MeV.

Besides the energy group delimiters, Table 2 shows the group averages of Eq. (2) used for the input. The corresponding relative standard deviations are also given. The data used for the complete covariance matrix of the input spectrum are discussed in the next section. The last two columns of Table 2 list the output of the adjustment procedure and its standard deviations. The correlation matrix of the output, shown in Table 3, contains correlations as well as anticorrelations. This is due to the normalization of the energy integral of Eq. (2) which must be unity over the whole energy range. The ratio of the output of the adjustment procedure relative to the input is plotted in Fig. 3. The error bars quoted correspond to the uncertainties of the output data. The figure shows that within the uncertainties, the output is fully consistent with the input. This is also reflected in a chi-square value of 19.3 which should be considered at 25 degrees of freedom. The pronounced structure above 12 MeV is probably due to a deficit in the energy-dependent $\sigma(E)$ data. At present, for this data the covariance matrices comprise only autocorrelations but no cross-correlations between the various neutron reactions. However, it is known that such cross-correlations must exist due to the measurement procedures of $\sigma(E)$ data /10/. It must also be considered that not more than 0.06 % of the total spectrum intensity is above 12 MeV neutron energy.

4. Variation of the input spectrum covariances

In the following, all parameters of the adjustment procedure, the reaction rates and their covariances, the $\sigma(E)$ data and their covariances and particularly the input spectrum data of Eq. (2)

Table 2: Input and output of the least-squares adjustment

E_L (MeV)	E_U (MeV)	$\bar{x}_{IN}$	Rel.Std. Dev. %	$\bar{x}_{OUT}$	Rel.Std.* Dev. %
0.0	0.5	1.280E-1	4.51	1.253E-1	3.79
0.5	1.0	1.689E-1	1.03	1.691E-1	1.01
1.0	1.5	1.545E-1	1.65	1.544E-1	1.63
1.5	2.0	1.288E-1	1.21	1.294E-1	1.16
2.0	2.5	1.029E-1	1.05	1.034E-1	0.95
2.5	3.0	8.003E-2	1.86	8.056E-2	1.75
3.0	3.5	6.121E-2	1.87	6.160E-2	1.76
3.5	4.0	4.625E-2	1.40	4.650E-2	1.25
4.0	4.5	3.464E-2	2.09	3.480E-2	1.95
4.5	5.0	2.575E-2	2.09	2.587E-2	1.96
5.0	5.5	1.904E-2	2.10	1.913E-2	1.96
5.5	6.0	1.402E-2	2.10	1.408E-2	1.97
6.0	6.5	1.020E-2	2.24	1.025E-2	2.15
6.5	7.0	7.347E-3	2.25	7.376E-3	2.15
7.0	7.5	5.275E-3	2.25	5.296E-3	2.15
7.5	8.0	3.778E-3	2.25	3.793E-3	2.15
8.0	8.5	2.701E-3	8.49	2.675E-3	5.32
8.5	9.0	1.927E-3	8.49	1.912E-3	5.37
9.0	9.5	1.372E-3	8.49	1.363E-3	5.46
9.5	10.0	9.761E-4	8.49	9.695E-4	5.53
10.0	11.0	1.185E-3	8.49	1.177E-3	5.39
11.0	12.0	5.954E-4	8.49	5.863E-4	5.60
12.0	13.0	2.979E-4	15.02	2.839E-4	7.40
13.0	14.0	1.486E-4	15.02	1.502E-4	6.39
14.0	15.0	7.392E-5	15.02	7.663E-5	6.48
15.0	16.0	3.668E-5	15.02	3.790E-5	7.07
16.0	17.0	1.816E-5	15.02	1.860E-5	7.64
17.0	18.0	8.978E-6	16.02	9.150E-6	7.97
18.0	19.0	4.430E-6	15.02	4.503E-6	8.15
19.0	20.0	2.183E-6	15.02	2.215E-6	8.24

*Correlation matrix in Table 3

were fixed. Only the covariance matrix of the input spectrum has been varied in the course of the work.

To give a clearer picture of what has been done, the generation of the input spectrum covariance matrix of the original adjustment (section 3) is briefly reviewed. As mentioned above, the spectral distribution of Eq. (2) is essentially based on an NBS evaluation /8/. For this evaluation some uncertainty estimates are given which

Table 3: Correlation matrix of the adjusted spectral distribution $\bar{\chi}_{OUT}$

Energy range (MeV)	Correlation matrix (x100)
0.0 - 0.5	100
0.5 - 1.0	-57 100
1.0 - 1.5	-48 44 100
1.5 - 2.0	-44 19 -3 100
2.0 - 2.5	-53 6 -15 57 100
2.5 - 3.0	-29 -17 -20 -11 40 100
3.0 - 3.5	-29 -16 -19 -10 41 68 100
3.5 - 4.0	-36 -10 -19 -4 18 27 27 100
4.0 - 4.5	-20 -3 -9 1 -11 -19 -18 53 100
4.5 - 5.0	-20 -2 -9 1 -10 -18 -18 54 72 100
5.0 - 5.5	-20 -2 -9 2 -9 -18 -17 54 72 72 100
5.5 - 6.0	-20 -2 -9 2 -9 -17 -17 54 72 72 72 100
6.0 - 6.5	-18 13 1 15 10 -4 -4 -2 -1 -0 -0 -0 100
6.5 - 7.0	-18 13 1 16 10 -4 -3 -2 -0 -0 -0 -0 76 100
7.0 - 7.5	-18 13 1 16 11 -4 -3 -1 -0 -0 0 0 76 76 100
7.5 - 8.0	-18 13 1 16 11 -4 -3 -1 -0 0 0 0 76 76 76 100
8.0 - 8.5	7 -6 -3 -6 -6 -2 -2 -4 -3 -3 -4 -4 -20 -20 -21 -21 100
8.5 - 9.0	6 -6 -3 -6 -6 -2 -2 -4 -3 -3 -3 -3 -19 -20 -20 -20 36 100
9.0 - 9.5	6 -5 -3 -5 -5 -1 -1 -4 -3 -3 -3 -3 -18 -19 -19 -19 37 37 100
9.5 - 10	6 -5 -3 -5 -5 -1 -1 -3 -3 -3 -3 -3 -18 -18 -19 -19 38 38 39 100
10 - 11	6 -5 -3 -5 -5 -1 -1 -3 -3 -3 -3 -3 -19 -19 -19 -20 36 37 38 39 100
11 - 12	6 -5 -3 -5 -5 -1 -1 -3 -3 -3 -3 -3 -17 -18 -18 -18 38 39 40 41 39 100
12 - 13	1 -1 -1 -0 -1 -0 -0 0 1 1 1 1 1 1 1 1 -5 -5 -5 -5 -5 -8 100
13 - 14	1 -1 -1 -0 -1 -1 -1 0 1 1 1 1 1 1 1 1 2 2 2 2 2 -0 -17 100
14 - 15	1 -1 -1 -0 -1 -1 -0 0 1 1 1 1 1 1 1 1 4 4 4 3 4 3 -6 -26 100
15 - 16	0 -1 -1 -0 -0 -0 -0 0 1 1 1 1 1 1 1 1 3 3 3 3 3 2 3 -15 -14 100
16 - 17	0 -0 -1 -0 -0 -0 -0 0 1 1 1 1 1 1 1 1 2 2 2 2 2 1 7 -6 -5 2 100
17 - 18	0 -0 -1 0 -0 -0 -0 0 1 1 1 1 1 1 1 1 2 2 2 2 2 1 10 -2 -0 6 12 100
18 - 19	0 -0 -1 0 -0 -0 -0 0 1 1 1 1 1 1 1 1 2 1 1 1 1 0 12 0 2 9 14 17 100
19 - 20	0 -0 -1 0 -0 -0 -0 0 1 1 1 1 1 1 1 1 1 1 1 1 1 0 12 2 4 10 15 17 19 100

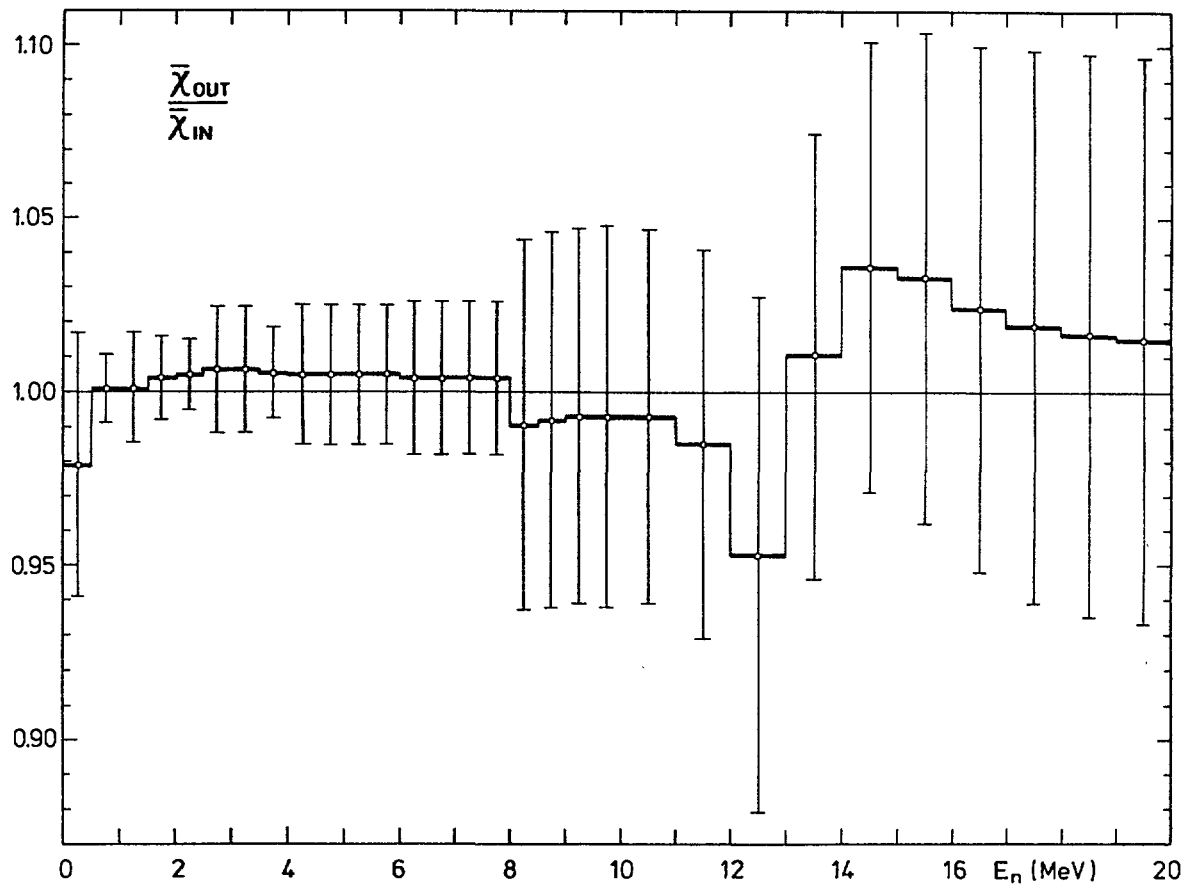

Fig. 3: Ratio of the output of the adjustment relative to the input for the spectral distribution of Cf-252.

Table 4: Uncertainty of the NBS spectrum evaluation /8/ in different energy ranges

Energy range (in MeV)	Rel. Std. Dev.
0 - 0.25	13.0 %
0.25 - 0.8	1.1 %
0.8 - 1.5	1.8 %
1.5 - 2.3	1.0 %
2.3 - 3.7	2.0 %
3.7 - 6.0	2.1 %
6.0 - 8.0	2.1 %
8.0 - 12.0	8.5 %
12.0 - 20.0	15.0 %[a)]

a) This value is based on an estimate of the author.

are listed in Table 4. After the generation of a group structure containing the energy delimiters in Table 4 and those in Table 2, the diagonal elements of the covariance matrix in this structure were filled with the data from Table 4 in the various energy ranges. All data within one of the energy ranges shown in Table 4 were assumed to be correlated by 75 %. However, no correlations between the different energy ranges were used. With regard to a correct uncertainty propagation /11/, this matrix was then collapsed to the group structure of Table 2. The side condition of the normalization of Eq. (2), i.e. the sum of $\bar{\chi}_{IN}$ in Table 2 being unity over the whole energy range, was taken into account by a transformation of the matrix according to Eqs. (17) and (18) of ref. /11/.

For the different versions used of the input spectrum covariance matrix, the same procedure was applied with modifications of the diagonal elements of the matrix and of the degree of correlation. Nine different matrices were generated and tested in the present investigation. The data sets used for the generation of these matrices are summarized in Table 5. In the last column of Table 5 the resulting chi-square value is also given. In the case of a relative standard deviation quoted as a "constant" one, this quantity was assumed to be equal over the whole neutron range from 0 MeV to 20 MeV. Those relative standard deviations quoted as "variable" were different in the different energy ranges. Correlations quoted as "partial" ones were constant within one of the energy ranges and were zero outside it. In a few cases a Gaussian correlation pattern was also used. Here the correlation was described by:

$$\mathrm{Corr}\ (\bar{E}_1, \bar{E}_2) = \exp\left[- (\ln 2) \times (\bar{E}_1 - \bar{E}_2)^2 / W^2 \right] \qquad (3)$$

$\bar{E}_i$ stands for the mean energy of one of the energy groups in Table 2. Within the same group the correlation is 1. The width of the Gaussian W is the energy difference which reduces the correlation from 1 to 0.5. The data set H in Table 5 is identical with that used in the original adjustment in section 3.

The result of the present investigation is summarized in Figs. 4 - 11. The output of the adjustment of the group-averaged spectral distribution is plotted relative to the input spectrum given in

Table 5: Different versions of the covariance matrix of the input spectrum

	Rel. Std. Dev.	Correlation	χ^2 (f = 25)
Set A	50 %, const.	0 %	9.7
Set B	15 %, const.	0 %	15.3
Set C	15 %, const.	Gaussian, width: 1 MeV	15.0
Set D	15 %, const.	Gaussian, width: 2 MeV	16.1
Set E	15 %, const	Gaussian, width: 4 MeV	18.0
Set F	NBS[a)], var.	0 %, partial	17.6
Set G	NBS[a)], var.	50 %, partial	18.6
Set H	NBS[a)], var.	75 %, partial	19.3
Set I	NBS[a)], var.	100 %, partial	20.3

a) see data in Table 4

Table 2. In all cases the input data for the spectral distribution were the same. The results obtained with the different versions of the covariance matrix listed in Table 5 are plotted. To ease the comparison each figure gives the result of two different covariance matrices. Attention should be paid to the different scalings of the vertical axis of the figures.

Fig. 4 shows that two covariance matrices of the same structure which differ only by a multiplicative factor produce essentially the same structure in the output spectrum. An increase in the magnitude of the relative standard deviations of the input spectrum enhances the structure of the output. Fig. 4 also clearly demonstrates the tendency of the least-squares adjustment procedures to keep the variations of the output spectrum within the standard deviations used for the input spectrum. Fig. 5 gives the result obtained with two strongly differing covariance matrices. The difference of the relative standard deviations between set H (see Table 4) and set B (15 % over the whole range) is reflected in the variation of the output relative to the input. The covariance matrix of the NBS type (Table 4 and sets F to I) contains relative standard deviations of 15 % above 12 MeV neutron energy. This

explains the similarity of the structure in Fig. 5 above this energy for the output data of the data sets B and H.

In Figs. 6 to 8 a Gaussian-like correlation pattern is compared with the uncorrrelated case. The Gaussian structure has the tendency to shift the structure of the uncorrelated input data (set B) to higher neutron energies. With the increasing width of the Gaussian a pronounced smoothing effect of the structure of the output becomes apparent.

Figs. 9 to 11 compare the influence of a different degree of the partial correlations of the input spectrum based on the NBS data on the resulting output spectrum. Increasing correlations show the tendency to reduce the variations of the output especially at high neutron energies. The small relative standard deviations of the NBS input data (Table 4) at lower energies result in only small differences between input and output data. An extreme is the partial correlation of 100 % (set I) shown in Fig. 11. The full correlation within each of the energy ranges in Table 4 forces the adjustment procedure to adjust such an energy range as a whole, i.e. by a constant factor for the energy range. It should be mentioned that such 100 % correlations are very unlikely and are shown here only for demonstration purposes.

The chi-square values given in the last column of Table 5 show that each of the data sets used in the generation of the covariance matrix of the input spectrum is compatible with the remainder of the information (experimental reaction rates and $\sigma(E)$ data). The resulting chi-square value is therefore only a weak indicator of the correctness of the covariance matrix of the input neutron spectrum.

5. Conclusions

The present investigation showed that a variety of different covariance matrices for the input spectrum in the least-squares adjustment procedure gave reasonable results for the output spectrum. The structures observed in the output spectra dependent on the magnitude and the correlation pattern of the input spectrum covariance matrix indicate a strong need for such matrices which

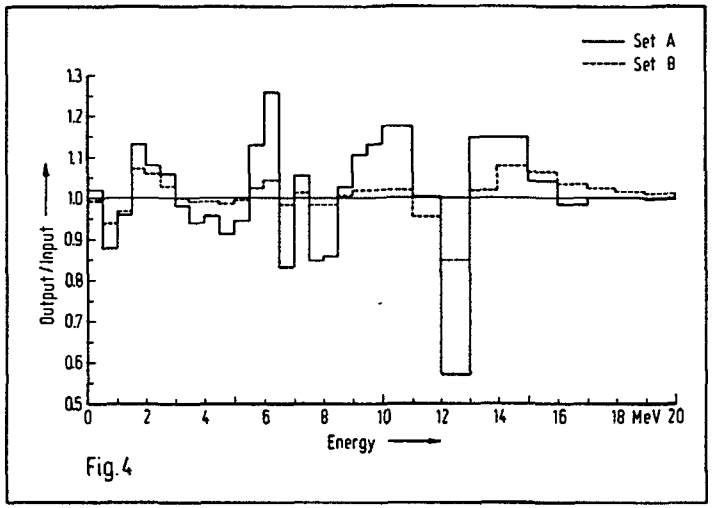

Fig.4

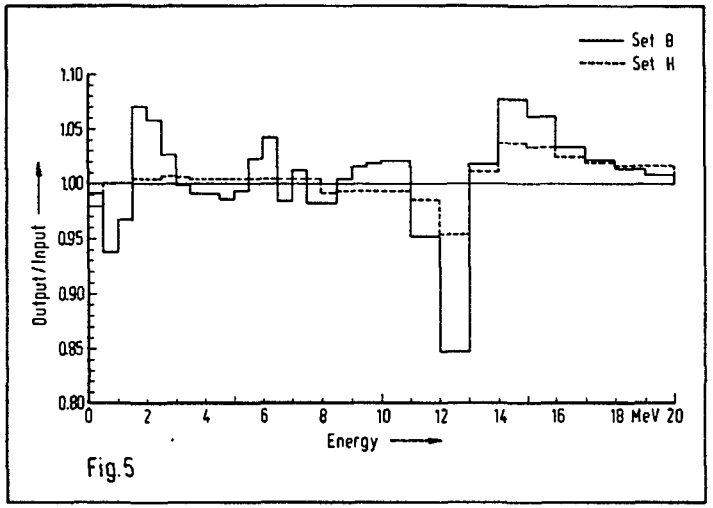

Fig.5

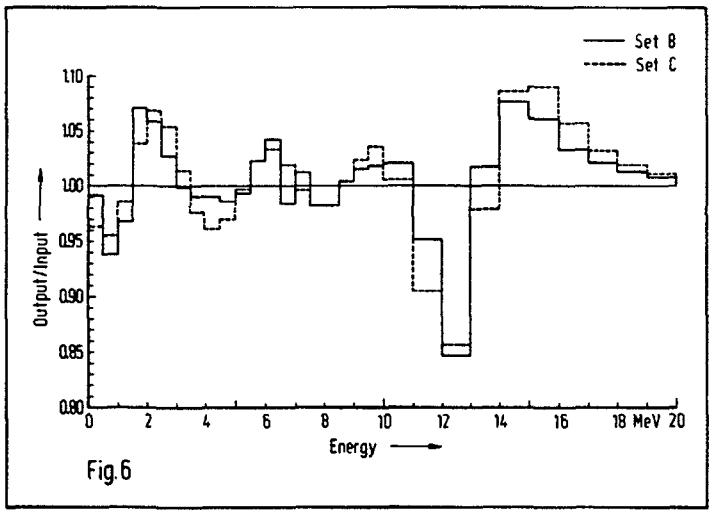

Fig.6

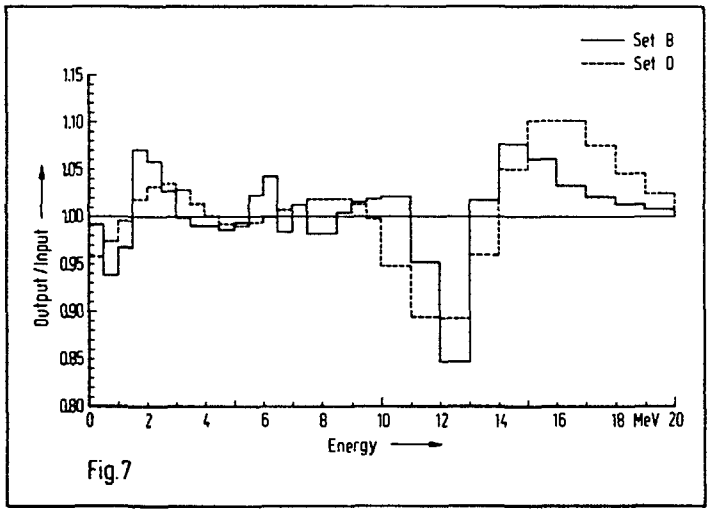

Fig.7

Figs. 4 - 7: Ratio of the output of the adjustment relative to the input for various input covariance matrices. The data sets used in the generation of the covariance matrices are listed in Table 5. The input spectrum itself is in all cases the same.

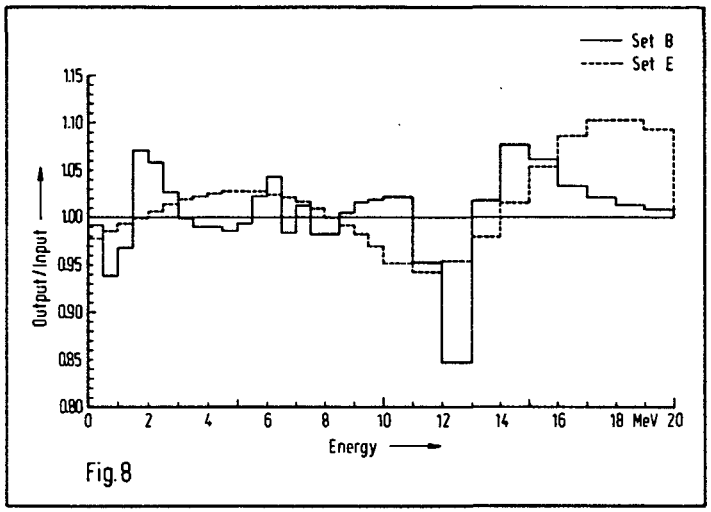

Fig.8

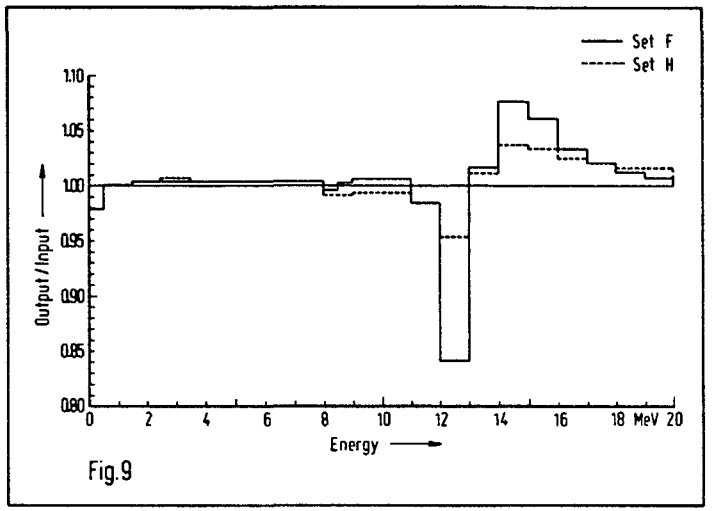

Fig.9

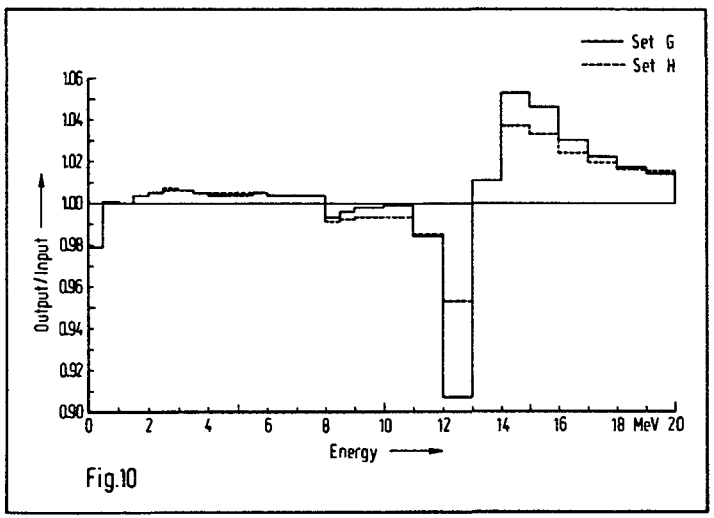

Fig.10

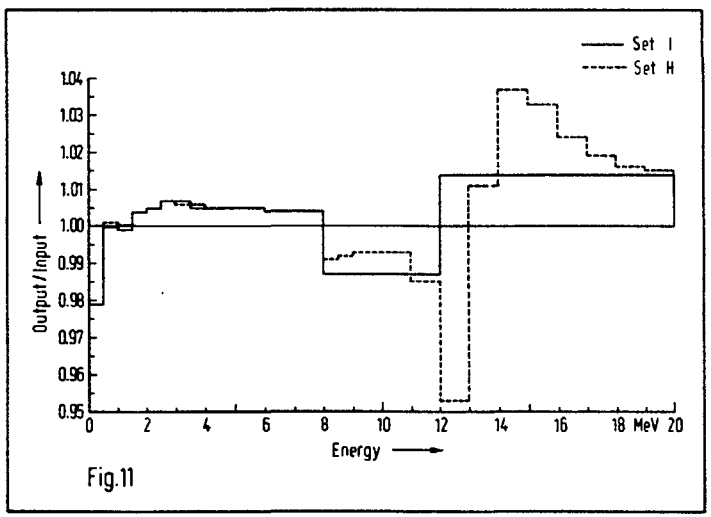

Fig.11

Figs.8 - 11: Same as Figs. 4 - 7.

are as reasonable as possible. To improve the quality of least-squares adjusted neutron spectra and to objectify the radiation damage estimates based upon such spectra, additional effort must be concentrated on obtaining more qualified data for neutron spectra and their covariances based on neutron transport calculations.

References:

/1/ W.L. Zijp, E.M. Zsolnay, E.J. Szondi, H.J. Nolthenius, D.E. Cullen: "Reactor Dosimetry", (J.P. Genthon, H. Röttger, eds.) D. Reidel Publ. Comp., Dordrecht (1985) 729

/2/ W. Mannhart: "Nuclear Data for Science and Technology", (K.H. Böckhoff, ed.), D. Reidel Publ. Comp., Dordrecht (1983) 429

/3/ W. Mannhart: Proc. IAEA Consultants' Meeting on the Cf-252 Fission Neutron Spectrum, Smolenice (CSSR), March 1983, Report INDC (NDS) - 146/L (1983) 213

/4/ H. Märten, D. Seeliger, B. Stobinski: "Nuclear Data for Science and Technology", (K.H. Böckhoff, ed.), D. Reidel Publ. Comp., Dordrecht (1983) 488

/5/ H. Märten, D. Richter, D. Seeliger: Report INDC (GDR) - 28/L (September 1984)

/6/ R. Böttger, H. Klein, A. Chalupka, B. Strohmaier: "Nuclear Data for Science and Technology", (K.H. Böckhoff, ed.) D. Reidel Publ. Comp., Dordrecht (1983) 484

/7/ W. Mannhart: IAEA Handbook on Nuclear Activation Data, chapter I, C-2 (to be published)

/8/ H.T. Heaton II, D.M. Gilliam, V. Spiegel, C. Eisenhauer, J.A. Grundl: Proc. NEANDC/NEACRP Specialist Meeting, Argonne National Laboratory, June 1976, Report ANL-76-90 (1976) 333

/9/ W. Mannhart: "Nuclear Standard Reference Data", Proc. IAEA Advisory Group Meeting, Geel (Belgium), November 1984, IAEA-TECDOC-335 (1985) 294

/10/ W. Mannhart: "Nuclear Data for Radiation Damage Assessment and Related Safety Aspects", Proc. IAEA Advisory Group Meeting, Vienna, October 1981, IAEA-TECDOC-263 (1982) 47

/11/ W. Mannhart: Proc. IAEA Consultants' Meeting on the Cf-252 Fission Neutron Spectrum, Smolenice (CSSR), March 1983, Report INDC (NDS) - 146/L (1983) 229

Neutron Dosimetry for Fusion Materials Studies

L. R. Greenwood
Argonne National Laboratory
Argonne, Illinois 60439 USA

We are engaged in a program to characterize irradiaition facilities for the U.S. fusion materials program. In lieu of an operating high-flux fusion reactor, experiments are being performed in a variety of facilities, including fission reactors, 14 MeV T(d,n) sources, and accelerator-based neutron sources. Our goal is to develop techniques to characterize each source in terms of neutron exposure and induced damage, gas production, and other transmutation. Papers concerning radiation damage calculations and helium production measurements are also included in these proceedings. The present paper summarizes our efforts to measure neutron fluences and energy spectra during materials irradiations.

The neutron environment can be sampled during an irradiation by measuring the induced activation in carefully selected materials These integral activities can then be used to adjust calculated neutron spectra. This technique relies on our knowledge of neutron activation cross sections. Consequently, neutron cross sections are being measured at various facilities in order to improve this technique and to extend it to higher neutron energies. This work has been well-summarized in recent publications [1,2] and only a brief summary will be given here.

By necessity most fusion materials irradiations are being conducted in fission reactors since present accelerator sources lack the fluxes and irradiation volumes required to study the large variety of fusion materials. In the U.S. two types of reactors are in use, namely fast and mixed-spectrum reactors. The mixed-spectrum (part thermal, part fast) facilities are being used in order to take advantage of the high thermal helium production in nickel (and hence in stainless steel). In this way we can induce the fusion-like helium-to-displacements ratio of about 10-1 in stainless steel. Fast reactors simply don't produce sufficient helium to simulate the higher production from the 14 MeV neutrons in a fusion reactor; however, they do produce higher damage rates than presently available mixed-spectrum reactors, they have large irradiation volumes, and they avoid the high thermal transmutation rates in some elements. At the present time, U.S. experiments are mainly performed in the High Flux Isotopes Reactor and the Oak Ridge Research Reactor at Oak Ridge National Laboratory and the Experimental Breeder Reactor II at Argonne National Laboratory (Idaho).

Integral and differential cross section measurements are being conducted at a variety of facilities including 14 MeV sources[3], Be(d,n) fields at deuteron energies between 7 and 40 MeV [4,5], and higher energy spallation facilities[6]. Combining all of these measurements with previous data allows us to adjust discrepant data and to establish poorly known cross sections. Some of our measurements at 14 MeV are listed in Table I. An example of a cross section adjustment is shown in Figure 1. In this case, the adjusted data is in excellent agreement

TABLE I

CROSS SECTIONS MEASURED AT RTNS II

Values normalized to ^{93}Nb(n,2n) = 463 mb
Zero degrees; En = 14.9 MeV; Accuracy 2% unless noted
ENDF/B-V Values are spectral-averaged at each angle

Reaction		Cross Section, mb		
	Data	ENDF/B-V	ENDF/Data-1, %
^{27}Al(n,a)^{24}Na	108.	113.	+ 4.6
^{45}Sc(n,2n)^{44}Sc	128.	124.	- 3.1
^{46}Ti(n,x)^{46}Sc	297.	324.	+ 9.1
^{47}Ti(n,x)^{47}Sc	317.	246.	-22.4
^{48}Ti(n,x)^{48}Sc	66.3	61.9	- 6.6
^{55}Mn(n,2n)^{54}Mn	840.	786.	- 6.4
^{54}Fe(n,p)^{54}Mn	296.	289.	- 2.4
^{54}Fe(n,a)^{51}Cr	92.7	95.8 [B]	+ 3.3
^{59}Co(n,p)^{59}Fe	45.9	62.2 [B]	+35.5
^{59}Co(n,2n)^{58}Co	803.	819.	+ 2.0
^{58}Ni(n,p)^{58}Co	295.	335.	+13.6
^{58}Ni(n,2n)^{57}Ni	40.9	36.7	-10.3
^{60}Ni(n,p)^{60}Co	132.	108.	-18.2
^{63}Cu(n,a)^{60}Co (3%)	40.1	38.4	- 4.2
^{89}Y(n,2n)^{88}Y	991.	942. [L]	- 4.9
^{89}Zr(n,x)^{89}Zr	846.	799. [L]	- 5.6
^{96}Zr(n,2n)^{95}Zr	1593.	-	-
^{107}Ag(n,2n)^{106}Ag	567.	612. [L]	+ 7.9
^{169}Tm(n,2n)^{168}Tm	1946.	2034. [L]	+ 4.5
^{197}Au(n,2n)^{196}Au	2174.	2109.	- 3.0

[B] = BNL-325, (1976)
[L] = LANL, B. P. Bayhurst, et. al., Phys. Rev. C12,451(1975).

with new measurements[7]. A number of other reactions are being measured in this way including ^{54}Fe(n,α)^{51}Cr, ^{60}Ni(n,p)^{60}Co, ^{59}Co(n,p)^{59}Fe, ^{58}Ni(n,2n)^{57}Ni, ^{63}Cu(n,α)^{60}Co, ^{65}Cu(n,p)^{65}Ni, and ^{93}Nb(n,n')^{93m}Nb. Selected differential measurements are planned using the Li(p,n) source at Argonne.

For fusion reactors we are developing nuclear data for plasma diagnostics, dosimetry, and waste management. Long-lived isotope production cross sections are being measured at 14 MeV and results have been published for ^{26}Al(7.3x10^5 y) and ^{53}Mn(3.7x10^6 y)[8]. The (n,2n) reactions on ^{27}Al and ^{54}Fe have also been shown to be particularly useful for plasma diagnostics as demonstrated in Figure 2. We are collaborating with Princeton Plasma Physics Laboratory to measure these reactions and to test them when the Tokamak Fusion Test Reactor commences d-t operation. Measurements of other long-lived isotopes such as ^{92}Nb, ^{94}Nb, ^{93}Zr, ^{93}Mo, and ^{59}Ni are currently in progress using lengthy irradiations at the

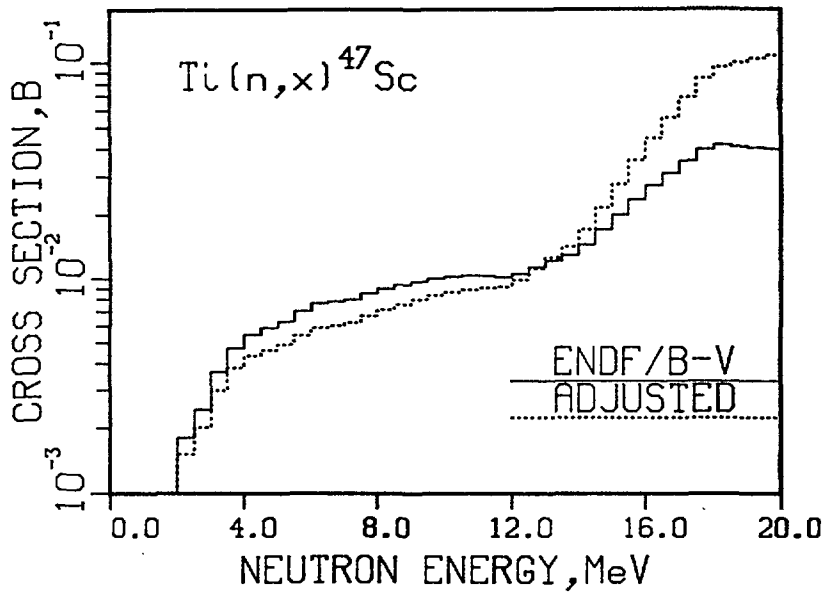

1. Cross section adjustment for the $^{47}Ti(n,p)^{47}Sc$ reaction using integral and differential data. The ENDF/B-V data was adjusted using the STAY'SL computer code.

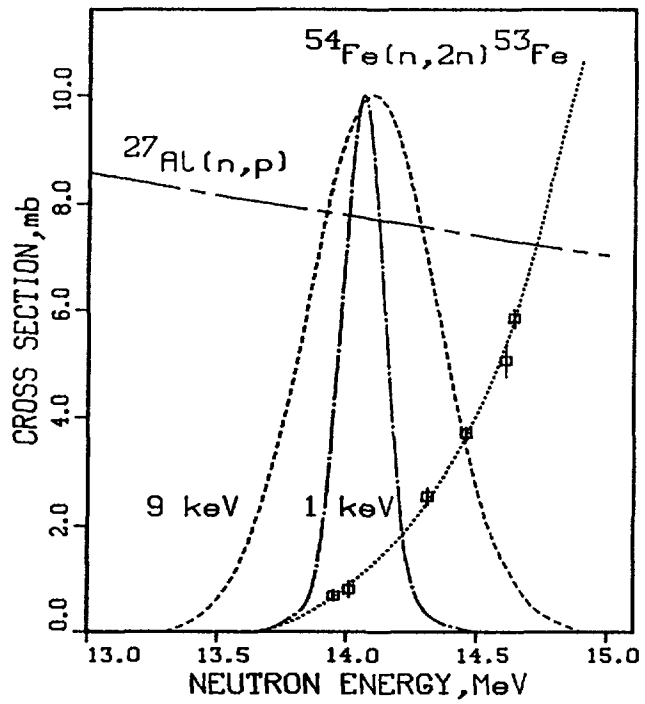

2. Cross section measurements are shown for the $^{54}Fe(n,2n)^{53}Fe$ reaction near 14 MeV. Superimposed on the data are neutron energy distributions for d-t fusion plasmas operating at 1 and 9 keV ion temperatures. The $^{27}Al(n,p)$ reaction shows the typical energy dependence of other reactions.

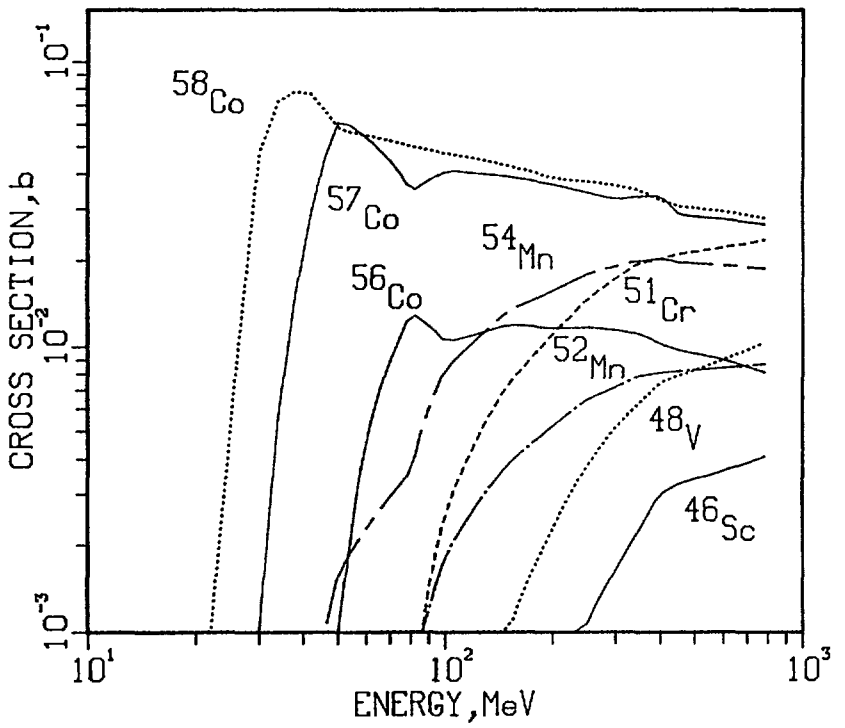

3. Spallation cross sections used for neutron spectral adjustment at IPNS and LAMPF. The radioisotopes shown were produced by monoenergetic proton irradiation of copper targets.

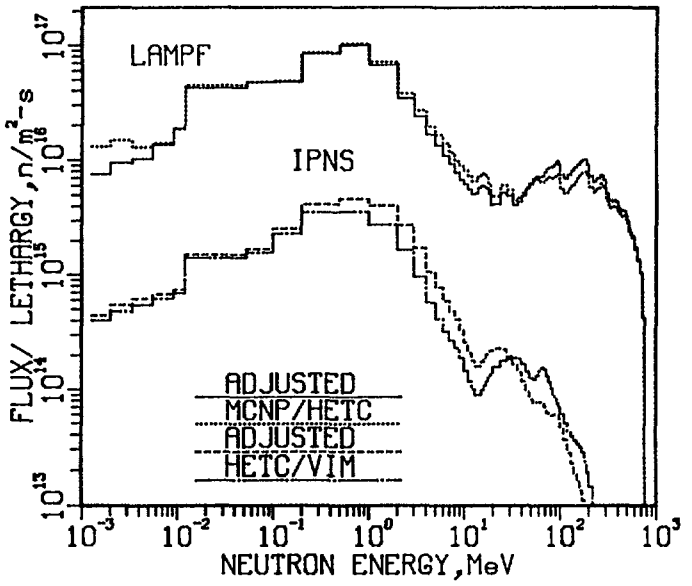

4. Calculated and adjusted neutron spectra are compared for IPNS and LAMPF. Note that our new spallation yield data can be used to extend the spectral adjustment technique to 800 MeV.

Rotating Target Neutron Source II at Lawrence Livermore National Laboratory followed by gamma spectroscopy, radiochemical separations and the relatively new technique of accelerator mass spectrometry This latter technique can also be used to study transmutation to stable isotopes.

Higher energy accelerator neutron sources require the development of new nuclear data for dosimetry. Integral measurements have been performed at Be(d,n) facilities to study (n,xn) reactions up to about 50 MeV[4,5]. At higher energies spallation reactions appear to be ideal for this purpose since one target material such as copper can produce a large number of lower mass radioisotopes, each having a different threshold in the 40-600 MeV energy range. We have measured production data for copper and aluminium [9], and have tested these data for spectral adjustments at the new Intense Pulsed Neutron Source at Argonne National Laboratory and the Los Alamos Meson Physics Facility at Los Alamos National Laboratory[6]. Preliminary results are shown in Figures 3 and 4.

Further work is needed to develop these data for routine use during materials irradiations. A combination of integral and differential measurements and nuclear model calculations are needed to improve the nuclear data needed for dosimetry measurements and damage calculations. Attention is also needed to define uncertainties and covariances used in the spectral adjustment computer codes to improve the reliability of fluence and damage estimates during materials irradiations. Damage and gas production measurements and calculations are discussed in separate papers in these proceedings.

REFERENCES

1. L. R. Greenwood and R. K. Smither, Reactor Dosimetry, Proc. Fifth ASTM-EURATOM Symp. on Reactor Dosimetry, Geesthacht, FRG, pp. 251-261 (1985).

2. L. R. Greenwood, Review of Source Characterization for Fusion Materials Studies, Symp. on Neutron Cross Sections From 0-50 MeV, BNL-NCS-51245, p. 75 (1980).

3. L. R. Greenwood, J. Nucl. Mater. 108, pp. 21-27 (1982).

4. L. R. Greenwood, R. R. Heinrich, R. J. Kennerley, and R. Medrzychowski, Nucl. Technol. 41, pp. 109-128 (1978).

5. L. R. Greenwood, R. R. Heinrich, M. J. Saltmarsh, and C. B. Fulmer, Nucl. Sci. Eng. 72, pp. 175-190 (1979).

6. D. R. Davidson, L. R. Greenwood, R. C. Reedy, and W. F. Sommer, Proc. Twelfth Int. Symp. on Effects of Radiation on Materials, Williamsburg, VA, June 1984.

7. D. L. Smith, private communication, Argonne National Laboratory.

8. R. K. Smither and L. R. Greenwood, J. Nucl. Mater. 122, pp. 1071- 1077 (1984).

9. L. R. Greenwood and R. K. Smither, Damage Analysis and Fund. Studies Quarterly Progress Report, DOE/ER-0046/14, August 1983.

Comparison of Two Fine Group Cross-section Libraries resulting from the ENDF/B-V Dosimetry File and Gas File (Version 1 and Version 2)

H.J. Nolthenius, G.C.H.M. Verhaag
(Physics Department)

Abstract

Some results are presented for the comparison of two versions of the ENDF/B-V dosimetry file.
The comparison is made for a fine group structure of the SAND-II type.

1. INTRODUCTION

The ENDF/B-V dosimetry and gas file with neutron cross-section information contains point cross-section data, resonance parameters, and prescribed interpolation schemes.
Rather complicated calculations have to be performed to obtain fine group cross-sections which can be used for neutron metrology purposes.
Probably the most simple conversion of the ENDF/B-V dosimetry file data is obtained if a fine group cross-section set is calculated.
In the latter case the weighing neutron spectrum can be approximated by a constant neutron spectrum without loss of information. A suitable fine group structure for this purpose is a SAND-II type structure with about 620 groups. The applied group structure contains 45 groups per energy decade between 10^{-10} and 1 MeV and a group width of 100 keV above 1 MeV. The maximum upper bound of the total energy range is 20 MeV for 640 groups.
The group structure applied in these calculations has been described in [1].
The ENDF/B-V files obtained from the NEA data bank (Gif-sur-Yvette, France) have been converted to the fine group cross-section values using the Fortran-IV computer program ENTOSAN [2], developed by ECN Petten.
In this report the second version of the ENDF/B-V dosimetry and gas file (TAPE531 and TAPE533) are compared with the first version.

---

* The work described in this report has been carried out under contract to the European Commission and has been financed by the JRC budget.

Table 1a. Characteristic cross-section data for the metrology tape.
The serial number is the same as the figure number of the cross-section plot.

ENDF/B-V version	reaction	code	$\langle\sigma\rangle$ (in m^2)		resonance integral (in m^2)	σ_{2200} (in m^2)		g
			Maxwell	Watt		Maxwell	point value	
0	TI47(N,P)SC47	TI47P5	5.183E-45	2.191E-30	2.085E-33	5.848E-45	2.506E-45	2.334
2	TI47(N,P)SC47	TI47P52	0.000E+00	2.191E-30	2.035E-33	0.000E+00	0.000E+00	
0	FE54(N,P)MN54	FE54P5	1.923E-43	7.875E-30	2.196E-33	2.170E-43	9.297E-44	2.334
2	FE54(N,P)MN54	FE54P52	0.000E+00	7.875E-30	2.172E-33	0.000E+00	0.000E+30	
0	NI58(N,P)CO58	NI58P5	1.417E-41	1.021E-29	2.476E-32	1.599E-41	6.851E-42	2.334
2	NI58(N,P)CO58	NI58P52	0.000E+00	1.023E-29	1.359E-31	0.000E+00	0.000E+00	
0	IN115(N,G)IN116M	IN115G5	1.502E-26	1.259E-29	3.229E-25	1.695E-26	1.663E-26	1.019
2	IN115(N,G)IN116	IN115G52	1.901E-26	1.594E-29	3.265E-25	2.146E-26	2.105E-26	1.01
0	AU197(N,G)AU198	AU197G5	8.789E-27	7.948E-30	1.562E-25	9.917E-27	9.869E-27	1.005
2	AU197(N,G)AU198	AU197G52	8.789E-27	7.948E-30	1.562E-25	9.917E-27	9.869E-27	1.00
0	TH232(N,G)TH233	TH232G5	6.545E-28	9.315E-30	8.346E-27	7.385E-28	7.402E-28	0.998
2	TH232(N,G)TH233	TH232G52	6.545E-27	9.317E-30	8.558E-27	7.385E-28	7.402E-28	0.99
2	NP237(N,F)F.P.	NP237F52	1.606E-30	1.339E-28	1.263E-28	1.813E-30	1.846E-30	0.98
0	NP237(N,F)F.P.	NP237F5	1.419E-30	1.339E-28	1.265E-28	1.601E-30	1.668E-30	0.960
0/2	PU239(N,F)F.P.	PU239F5	6.942E-26	1.790E-28	2.788E-26	7.833E-26	7.413E-26	1.057
0/2	U238(N,F)F.P.	U238F52	4.678E-34	3.003E-29	6.037E-31	5.279E-34	5.280E-34	1.00

Table 1b. Characteristic cross-section data for the gas tape.

0	3LI7-D-TOTAL	D-LI7-B5	0.	1.466E-33	0.	0.	0.	
2	3LI7-D	D-LI7-V2	0.000E+00	1.589E-33	0.000E+00	0.000E+00	0.000E+00	
0	3LI7-HE-TOTAL	HE-LI7B5	6.348E-30	2.406E-30	3.134E-30	7.163E-30	7.195E-30	0.996
2	3LI7-HE	HE-LI7V2	0.000E+00	2.037E-30	0.000E+00	0.000E+00	0.000E+00	
0	3LI7-T-TOTAL	T-LI7-B5	0.	2.399E-30	0.	0.	0.	
2	3LI7-T	T-LI7-V2	0.000E+00	2.036E-30	0.000E+00	0.000E+00	0.000E+00	
2	3LI7-H	H-LI7-V2	0.000E+00	3.523E-35	0.000E+00	0.000E+00	0.000E+00	

The comparison is made after conversion to a 640 group structure, which is standard practice in our laboratory.

2. THE CROSS-SECTION LIBRARIES

The two sets of two fine group cross-section libraries with ENDF/B-V dosimetry file information have the same group structure up to 20 MeV. The second version of the ENDF/B-V files TAPE531 and TAPE533 were received in April 1984 from the OECD.
These data were converted with aid of the program ENTOSAN. The results of this program have been compared with the fine cross-section library obtained for the original version of the two ENDF/B-V files TAPE531 and TAPE533.

3.COMPARISON

With a modified version of a small utility program, SIGRATI, the ratio of the corresponding group cross-section values of the two libraries were calculated and plotted vs. energy (see figs. 1-12).
The numerator of the ratio is formed by the version 2 data and the denominator by the old version.
For the reactions which show differences also some characteristic data are presented in table 1. The Westcott g-value, listed in the last column, is calculated as the ratio of the average cross-section in a Maxwellian spectrum multiplied by $2/\sqrt{\pi}$, and the 2200 $m.s^{-1}$ point cross-section value.

4. RESULTS

The plots indicate that for 9 reactions of the metrology tape the results of the two versions were different. These reactions are:
$^{47}Ti(n,p)$, $^{54}Fe(n,p)$, $^{58}Ni(n,p)$, $^{115}In(n,\gamma)$, $^{197}Au(n,\gamma)$, $^{232}Th(n,\gamma)$, $^{237}Np(n,f)$, $^{239}Pu(n,f)$ and $^{238}U(n,\gamma)$.
Figs.5, 8 and 9 show that the differences for the reactions $^{197}Au(n,\gamma)$, $^{239}Pu(n,f)$ and $^{238}U(n,\gamma)$ are very small.
It is not completely sure that these differences are due to modifications in the ENDF/B-V tapes. They may be due to a small change in the program ENTOSAN.

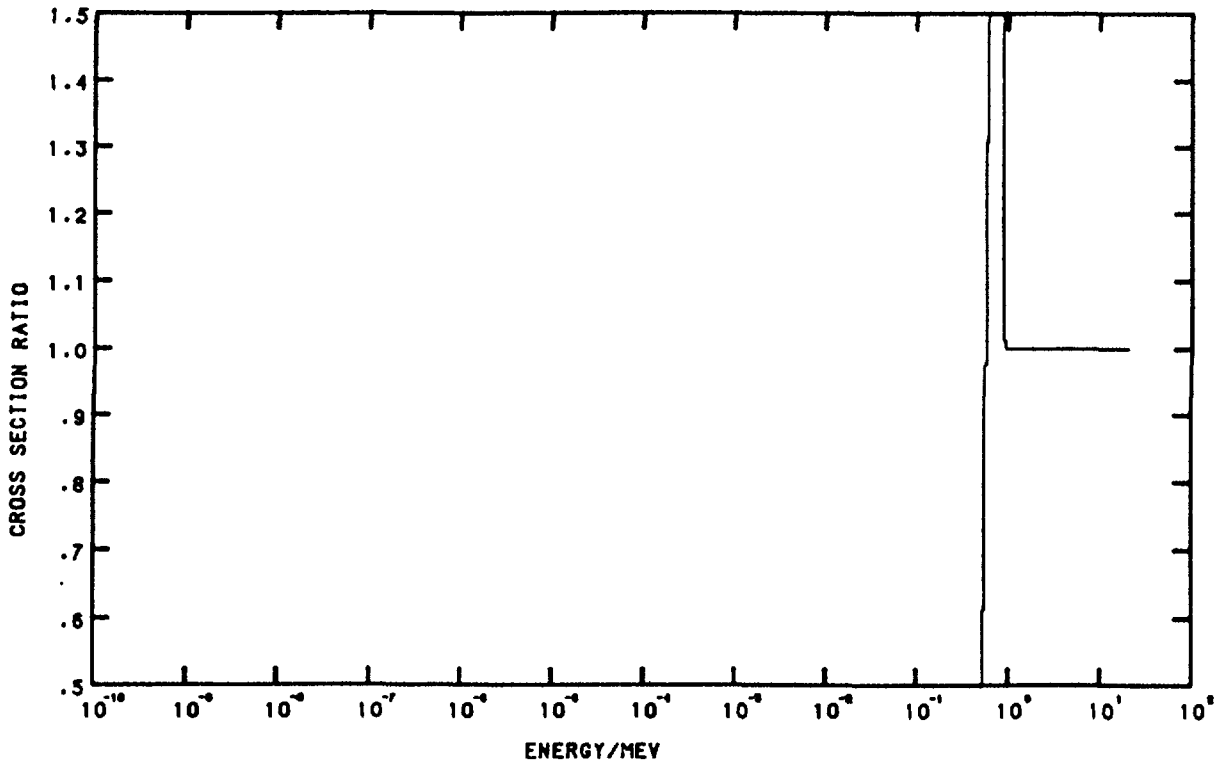

Fig.1. CROSS SECTION RATIO FOR THE REACTION TI47(N,P)SC47

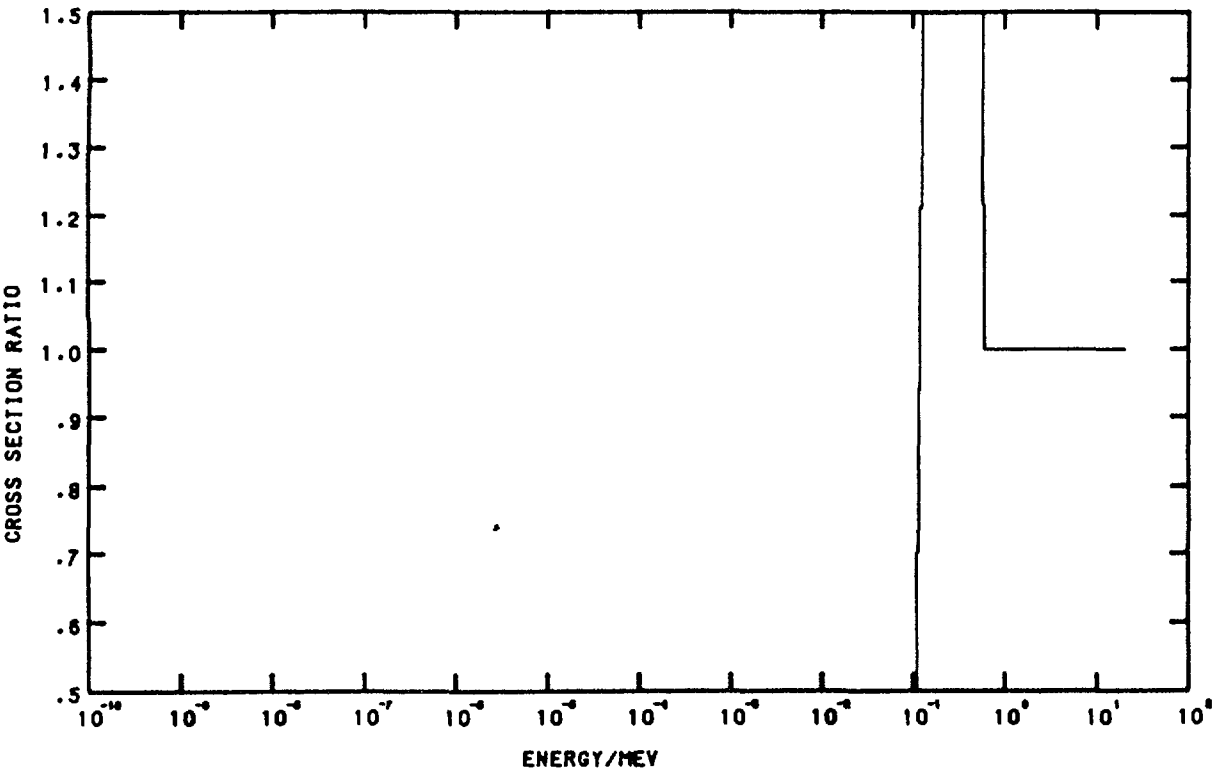

Fig.2. CROSS SECTION RATIO FOR THE REACTION FE54(N,P)MN54

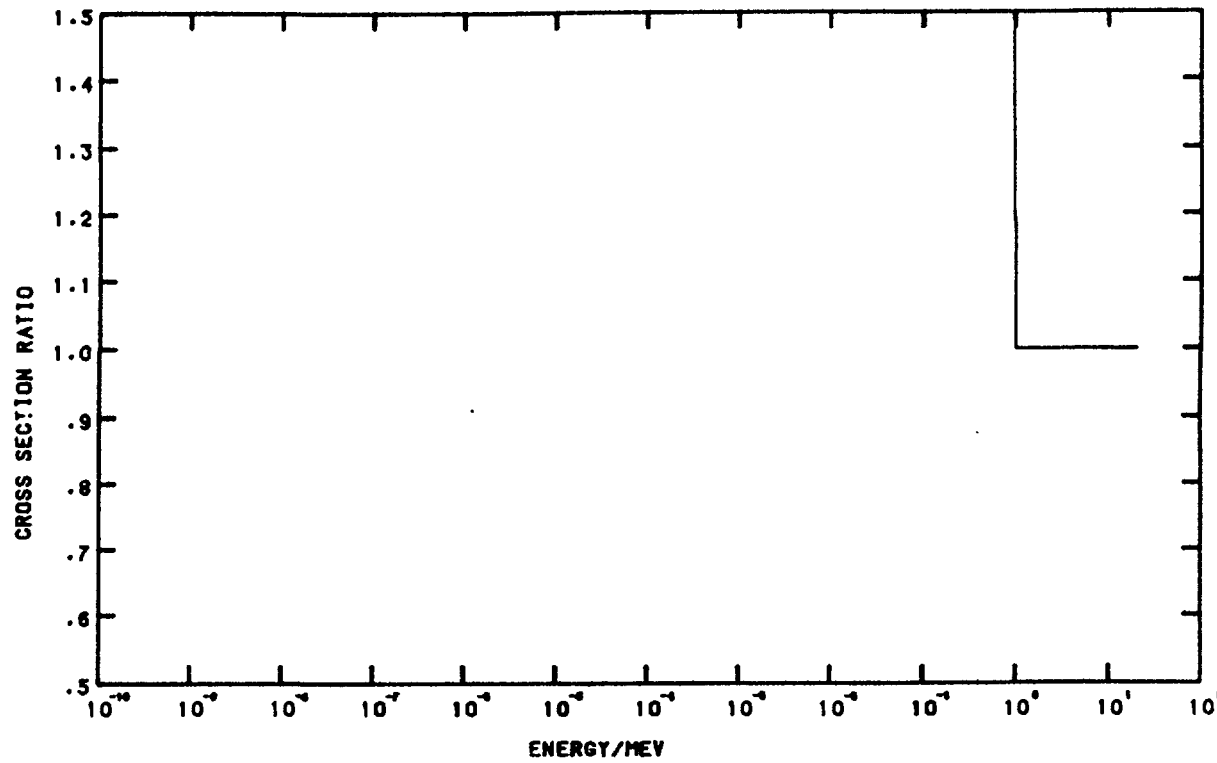

Fig.3. CROSS SECTION RATIO FOR THE REACTION NI58(N,P)CO58

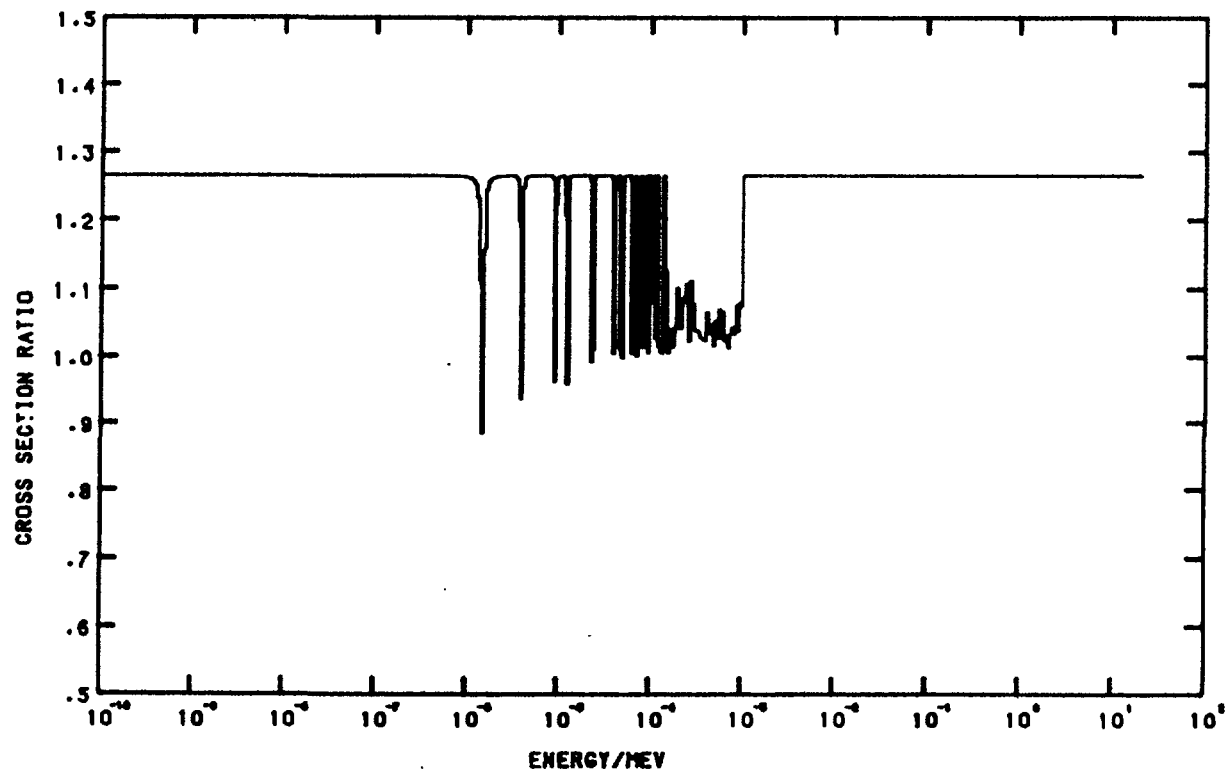

Fig.4. CROSS SECTION RATIO FOR THE REACTION IN115(N,G)IN116M

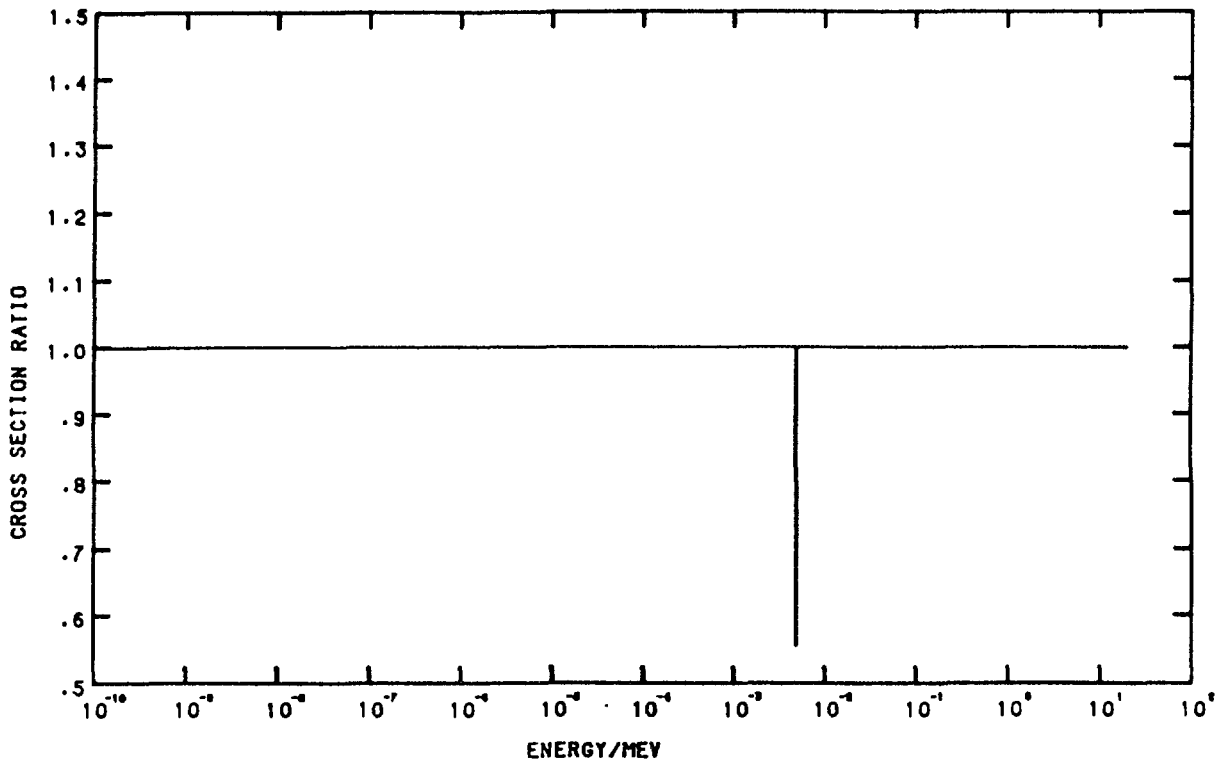

Fig.5. CROSS SECTION RATIO FOR THE REACTION AU197(N,G)AU198

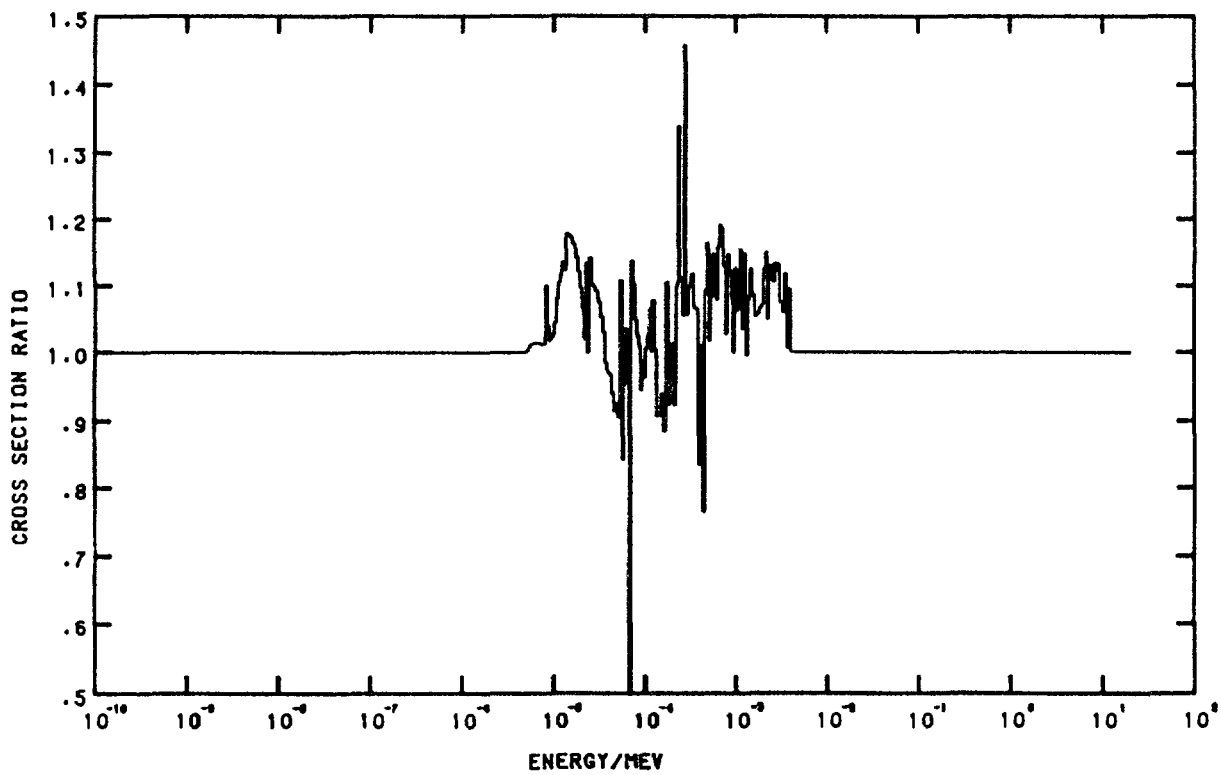

Fig.6. CROSS SECTION RATIO FOR THE REACTION TH232(N,G)TH233

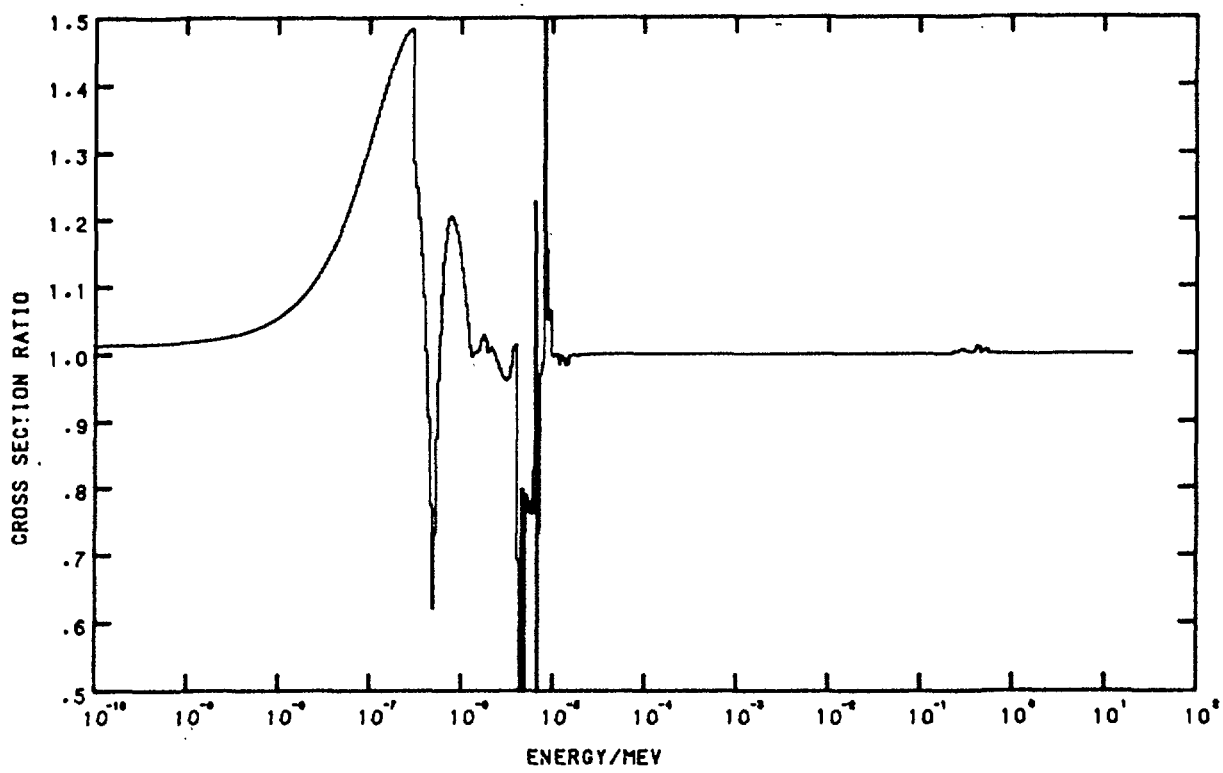

Fig.7. CROSS SECTION RATIO FOR THE REACTION NP237(N.F)F.P.

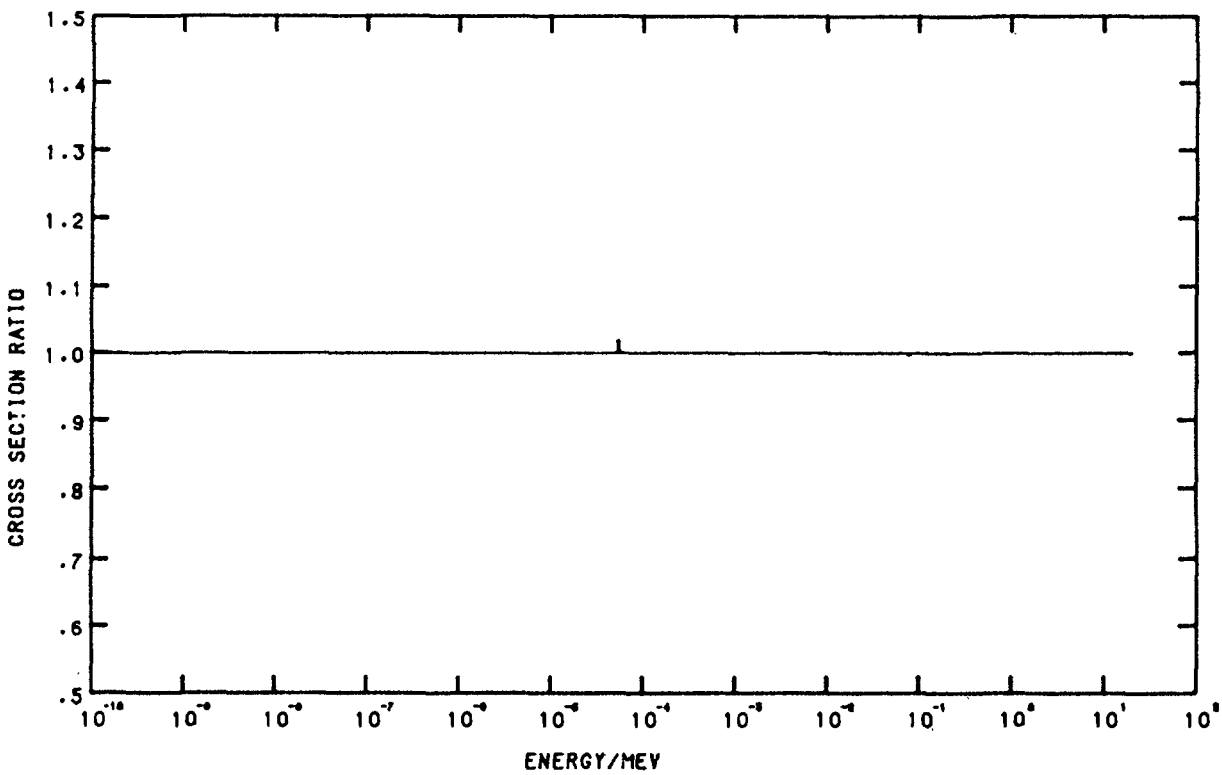

Fig.8. CROSS SECTION RATIO FOR THE REACTION PU239(N.F)F.P.

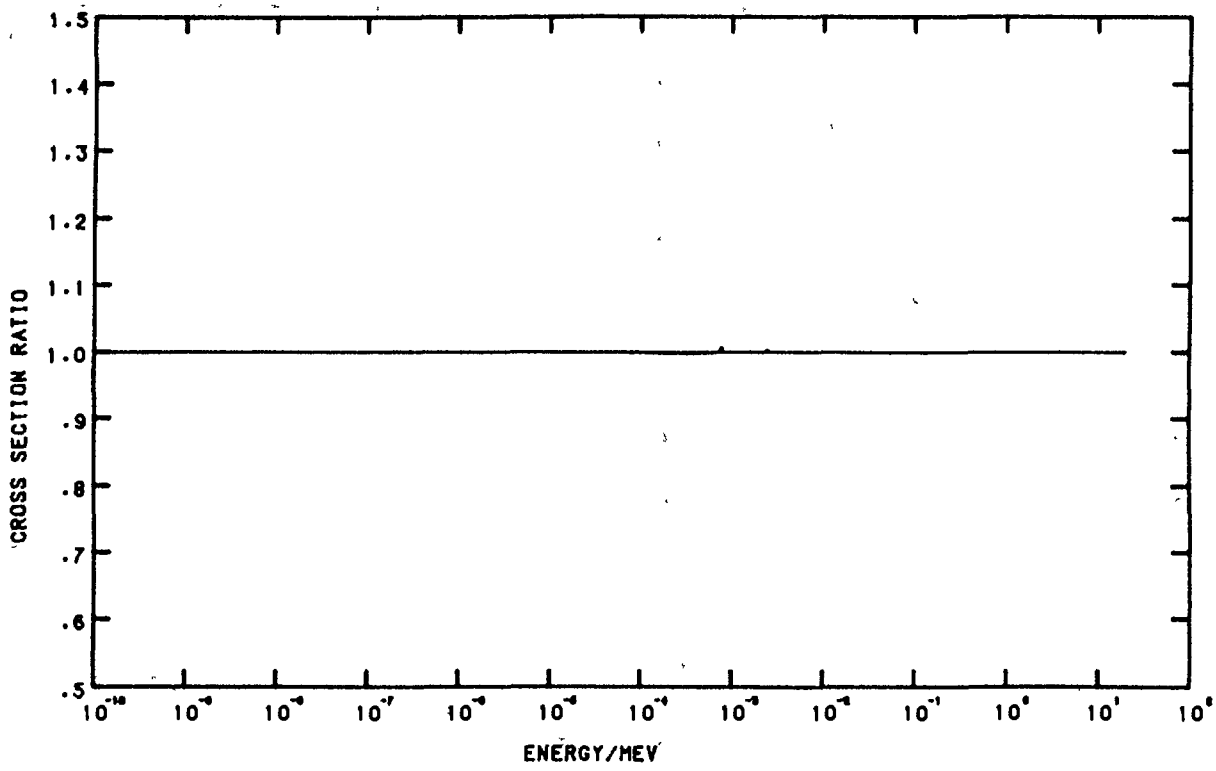

Fig.9. CROSS SECTION RATIO FOR THE REACTION U238(N,G)U239

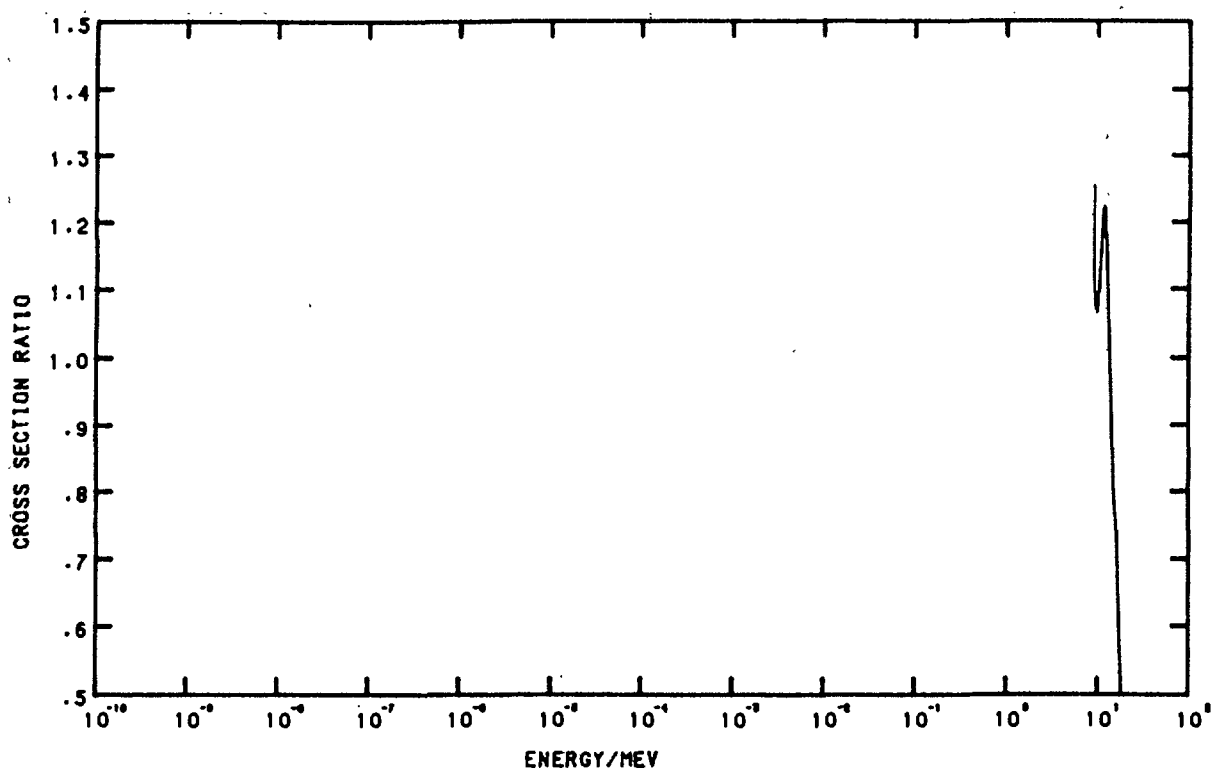

Fig.10. CROSS SECTION RATIO FOR THE REACTION 3LI7-D-TOTAL

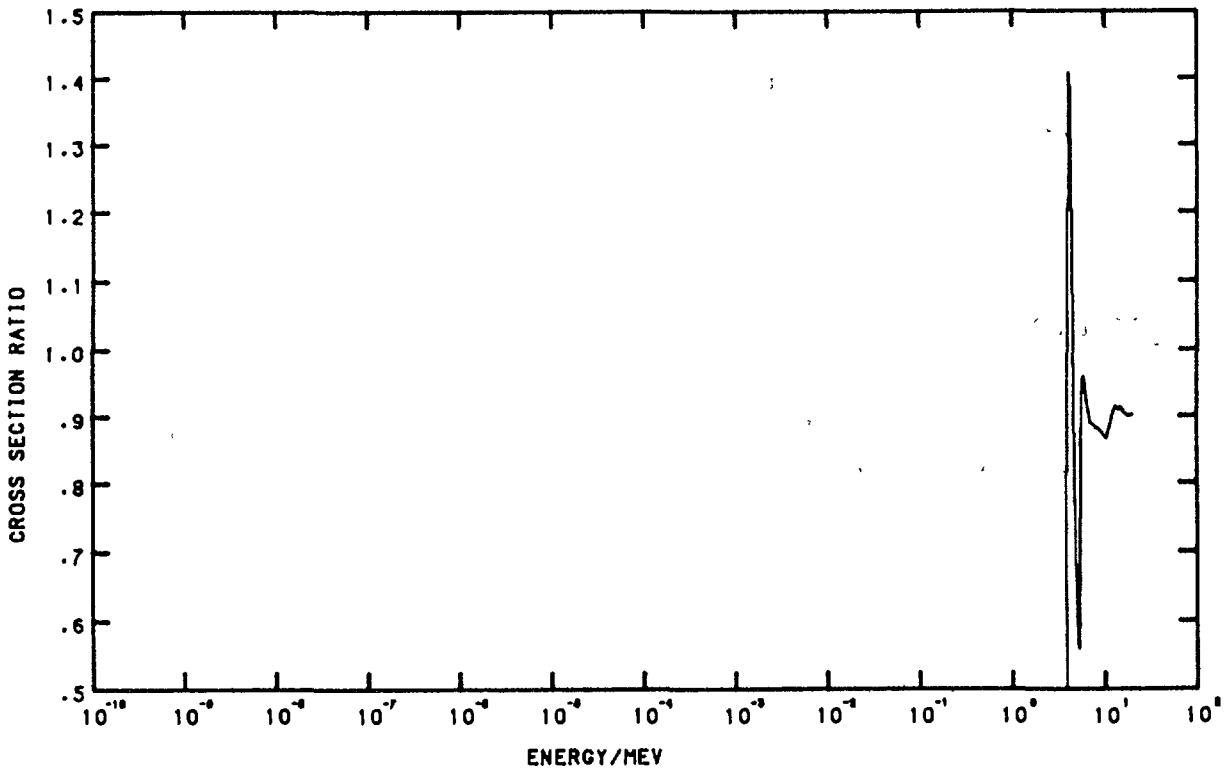

Fig.11. CROSS SECTION RATIO FOR THE REACTION 3LI7-HE-TOTAL

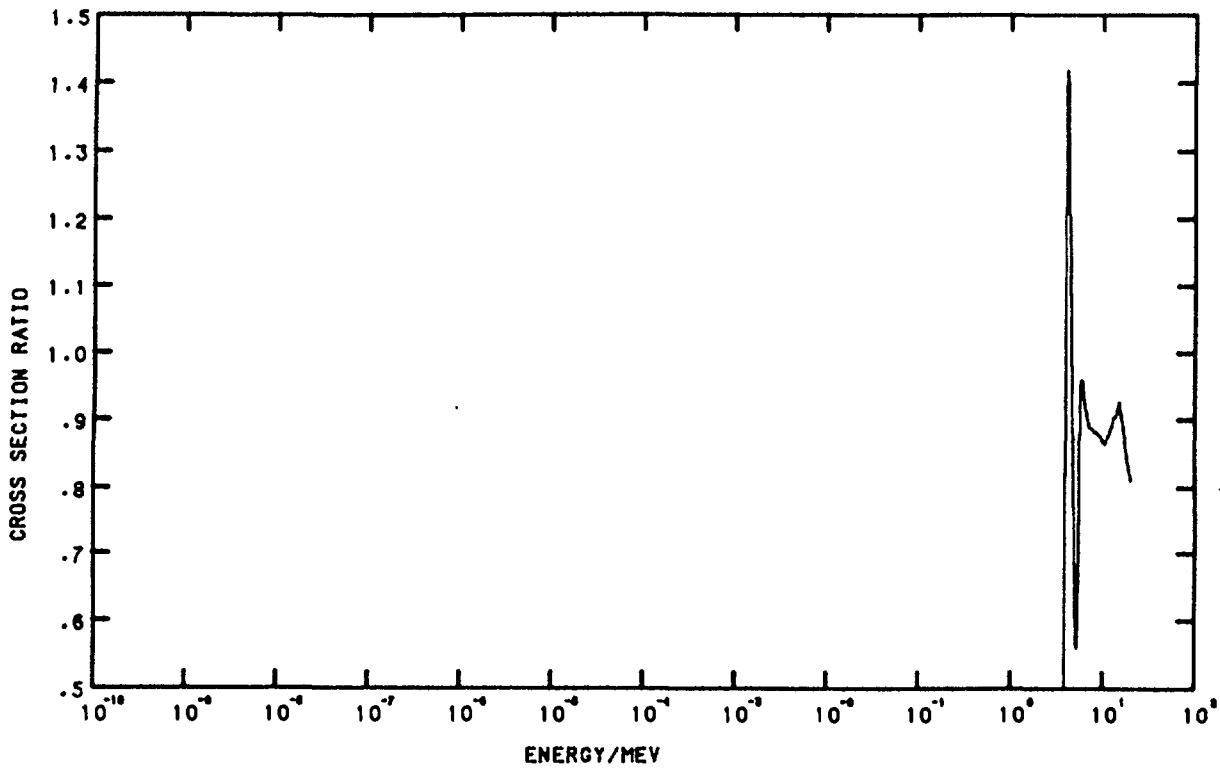

Fig.12. CROSS SECTION RATIO FOR THE REACTION 3LI7-T-TOTAL

For the gas tape differences between the original and the second version were found for the reactions: $^{7}_{3}Li(n,d)$, $^{7}_{3}Li(n,\alpha)$ and $^{7}_{3}Li(n,total)$.
In the second version also the reaction $^{7}_{3}Li(n,p)$ is present.
Ratios for the differences in the cross-section are shown in figs.10...12.
In table 1 the characteristic cross-section data are shown.

5. REFERENCES

[1] Simons, R.L., and McElroy, W.N.: "Evaluated reference cross-section library",
BNWL-1312 (Richland, May 1970).

[2] Rieffe, H.Ch., Nolthenius, H.J., and Zijp, W.L.:
"ENTOSAN. A program for the calculation of fine group cross section values from ENDF/B data",
ECN-93 (Petten, April 1981).

Uncertainty and correlation data for the ENDF/B-V dosimetry file (version 2)

H.J. Nolthenius and W.L. Zijp
(Physics Department)

ABSTRACT

This document presents a compilation of standard deviations and correlations for group cross-sections derived from TAPE531 version 2 of the ENDF/B-V.
The group structure chosen for the presentation of the triangular matrices is the ABBN group structure, supplemented with a thermal group.

INTRODUCTION

A compilation was made of standard deviations and correlations for group cross-sections, derived from TAPE531 version 2 of the ENDF/B-V. This tape contains data for 36 activation or fission reactions applied in reactor neutron metrology.
The group structure chosen for the presentation of the triangular matrices is the ABBN group structure supplemented with a thermal group.
The results are obtained with aid of the computer programs UNC32 and UNC33, developed in our laboratory ([1],[2]).
In deriving the coarse group data from the TAPE531 data, we used as weighting spectrum a typical spectrum for a steel irradiation experiment in the fuel region of a materials testing reactor (HFR core position C3).
Each page corresponds to a particular reaction, characterized by a shortened reaction code and ENDF/B-V material number.
The first column lists the group number, going from thermal to fast.

The work described in this report has been carried out under contract to the European Commission and has been financed by the JRC budget.

The second column lists the coefficient of variation (relative standard deviation - rel.sdev) in per cent.
The third column lists the lower energy boundary of the energy group considered. The upper energy of group 27 is 20 MeV.
The correlation information is given as an upper triangle matrix of correlation coefficients, multiplied by 100.

REFERENCES

[1] Verhaag, G.C.H.M., Rieffe, H.Ch., and Nolthenius, H.J.:
"UNC32. A computer program for calculating group cross-section covariances from ENDF/B-V resonance parameter uncertainties", Report ECN-84-132 (Netherlands Energy Research Foundation ECN, Petten, August 1984).

[2] Verhaag, G.C.H.M., Rieffe, H.Ch., and Nolthenius, H.J.:
"UNC33. A computer program for calculating group cross-section covariances from uncertainty parameters in the ENDF/B-V format", Report ECN-85-030 (Netherlands Energy Research Foundation ECN, Petten, February 1985).

CROSS-SECTION NAME : LI6A52 MAT-NUMBER : 6424

X-SECTION CORRELATION MATRIX (27 X 27) UPPER TRIANGLE

GROUP NO	REL.SDEV (PT)	ENERGY (EV)																								
1	.40	1.000E-04	100	100	100	100	100	100	100	100	100	100	100	100	94	94	58	42	31	26	7	-1	4	4	1	0	0	0
2	.40	2.150E-01		100	100	100	100	100	100	100	100	100	100	100	94	94	58	42	31	26	7	-1	4	4	1	0	0	0
3	.40	4.650E-01			100	100	100	100	100	100	100	100	100	100	94	94	58	42	31	26	7	-1	4	4	1	0	0	0
4	.40	1.000E+00				100	100	100	100	100	100	100	100	100	94	94	58	42	31	26	7	-1	4	4	1	0	0	0
5	.40	2.150E+00					100	100	100	100	100	100	100	100	94	94	58	42	31	26	7	-1	4	4	1	0	0	0
6	.40	4.650E+00						100	100	100	100	100	100	100	94	94	58	42	31	26	7	-1	4	4	1	0	0	0
7	.40	1.000E+01							100	100	100	100	100	100	94	94	58	42	31	26	7	-1	4	4	1	0	0	0
8	.40	2.150E+01								100	100	100	100	100	94	94	58	42	31	26	7	-1	4	4	1	0	0	0
9	.40	4.650E+01									100	100	100	100	94	94	58	42	31	26	7	-1	4	4	1	0	0	0
10	.41	1.000E+02										100	100	100	94	94	58	42	31	26	7	-1	4	4	1	0	0	0
11	.50	2.150E+02											100	100	96	96	72	47	36	30	6	-2	4	4	1	0	0	0
12	.50	4.650E+02												100	96	96	72	47	36	30	6	-2	4	4	1	0	0	0
13	.50	1.000E+03													100	97	97	74	49	38	31	6	-3	4	4	1	0	0	0
14	.50	2.150E+03														100	100	89	69	59	49	2	-13	5	6	2	0	0	0
15	.50	4.650E+03															100	89	69	52	49	2	-13	5	6	2	0	0	0
16	1.00	1.000E+04																100	94	89	75	-5	-31	6	8	2	0	0	0
17	1.54	2.150E+04																	100	99	88	-3	-41	1	4	1	0	0	0
18	2.00	4.650E+04																		100	90	-3	-43	0	3	1	0	0	0
19	1.93	1.000E+05																			100	29	-31	-4	-1	0	0	0	0
20	2.28	2.000E+05																				100	53	22	18	5	0	0	0
21	3.72	4.000E+05																					100	80	72	19	0	0	0
22	4.98	8.000E+05																						100	93	24	0	0	0
23	5.37	1.400E+06																							100	43	3	1	0
24	6.72	2.500E+06																								100	27	13	1
25	10.00	4.000E+06																									100	58	6
26	11.30	6.500E+06																										100	42
27	14.75	1.000E+07																											100

CROSS-SECTION NAME : B10A52 MAT-NUMBER : 6425

X-SECTION CORRELATION MATRIX (27 X 27) UPPER TRIANGLE

GROUP NO	REL.SDEV (PT)	ENERGY (EV)																							
1	.22	1.000E-04	100	100	100	100	100	100	100	100	100	100	100	100	100	100	100	96	91	82	46	47	2	0	0	0	0	0
2	.22	2.150E-01	100	100	100	100	100	100	100	100	100	100	100	100	100	100	100	96	91	82	46	47	2	0	0	0	0	0
3	.22	4.650E-01	100	100	100	100	100	100	100	100	100	100	100	100	100	100	100	96	91	82	46	47	2	0	0	0	0	0
4	.22	1.000E+00	100	100	100	100	100	100	100	100	100	100	100	100	100	100	100	96	91	82	46	47	2	0	0	0	0	0
5	.22	2.150E+00	100	100	100	100	100	100	100	100	100	100	100	100	100	100	100	96	91	82	46	47	2	0	0	0	0	0
6	.22	4.650E+00	100	100	100	100	100	100	100	100	100	100	100	100	100	100	100	96	91	82	46	47	2	0	0	0	0	0
7	.22	1.000E+01	100	100	100	100	100	100	100	100	100	100	100	100	100	100	100	96	91	82	46	47	2	0	0	0	0	0
8	.22	2.150E+01	100	100	100	100	100	100	100	100	100	100	100	100	100	100	100	96	91	82	46	47	2	0	0	0	0	0
9	.22	4.650E+01	100	100	100	100	100	100	100	100	100	100	100	100	100	100	100	96	91	82	46	47	2	0	0	0	0	0
10	.22	1.000E+02	100	100	100	100	100	100	100	100	100	100	100	100	100	100	100	96	91	82	46	47	2	0	0	0	0	0
11	.22	2.150E+02	100	100	100	100	100	100	100	100	100	100	100	100	100	100	100	96	91	82	46	47	2	0	0	0	0	0
12	.22	4.650E+02	100	100	100	100	100	100	100	100	100	100	100	100	100	100	100	96	91	82	46	47	2	0	0	0	0	0
13	.22	1.000E+03	100	100	100	100	100	100	100	100	100	100	100	100	100	100	100	96	91	82	46	47	2	0	0	0	0	0
14	.22	2.150E+03	100	100	100	100	100	100	100	100	100	100	100	100	100	100	100	96	91	82	46	47	2	0	0	0	0	0
15	.22	4.650E+03	100	100	100	100	100	100	100	100	100	100	100	100	100	100	100	96	91	82	46	47	2	0	0	0	0	0
16	.22	1.000E+04	100	100	100	100	100	100	100	100	100	100	100	100	100	100	100	96	91	82	46	47	2	0	0	0	0	0
17	.39	2.150E+04	100	100	100	100	100	100	100	100	100	100	100	100	100	100	100	96	91	82	46	47	2	0	0	0	0	0
18	.56	4.650E+04	100	100	100	100	100	100	100	100	100	100	100	100	100	100	100	96	91	82	46	47	2	0	0	0	0	0
19	.77	1.000E+05	100	100	100	100	100	100	100	100	100	100	100	100	100	100	100	96	91	82	46	47	2	0	0	0	0	0
20	1.56	2.150E+05	100	100	100	100	100	100	100	100	100	100	100	100	100	100	100	96	91	82	46	47	2	0	0	0	0	0
21	1.22	4.650E+05	100	100	100	100	100	100	100	100	100	100	100	100	100	100	100	96	91	82	46	47	2	0	0	0	0	0
22	8.93	8.610E+05	100	100	100	100	100	100	100	100	100	100	100	100	100	100	100	96	91	82	46	47	2	0	0	0	0	0
23	15.00	1.400E+06	100	100	100	100	100	100	100	100	100	100	100	100	100	100	100	96	91	82	46	47	2	0	0	0	0	0
24	13.13	2.500E+06	100	100	100	100	100	100	100	100	100	100	100	100	100	100	100	96	91	82	46	47	2	0	0	0	0	0
25	12.01	4.000E+06	100	100	100	100	100	100	100	100	100	100	100	100	100	100	100	96	91	82	46	47	2	0	0	0	0	0
26	11.77	6.500E+06	100	100	100	100	100	100	100	100	100	100	100	100	100	100	100	96	91	82	46	47	2	0	0	0	0	0
27	10.24	1.950E+07	100	100	100	100	100	100	100	100	100	100	100	100	100	100	100	96	91	82	46	47	2	0	0	0	0	0

CROSS-SECTION NAME : NA23G52 MAT-NUMBER : 6311

X-SECTION CORRELATION MATRIX (27 X 27) UPPER TRIANGLE

GROUP NO	REL.SDEV (PT)	ENERGY (EV)																							
1	2.00	1.000E-04	100	100	100	100	100	100	100	5	0	0	0	0	0	0	0	0	0	0	0	0	0	0	0
2	2.00	2.150E-01		100	100	100	100	100	100	5	0	0	0	0	0	0	0	0	0	0	0	0	0	0	0
3	2.00	4.650E-01			100	100	100	100	100	5	0	0	0	0	0	0	0	0	0	0	0	0	0	0	0
4	2.00	1.000E+00				100	100	100	100	5	0	0	0	0	0	0	0	0	0	0	0	0	0	0	0
5	2.00	2.150E+00					100	100	100	5	0	0	0	0	0	0	0	0	0	0	0	0	0	0	0
6	2.00	4.650E+00						100	100	5	0	0	0	0	0	0	0	0	0	0	0	0	0	0	0
7	2.00	1.000E+01							100	5	0	0	0	0	0	0	0	0	0	0	0	0	0	0	0
8	2.00	2.150E+01								5	0	0	0	0	0	0	0	0	0	0	0	0	0	0	0
9	4.26	4.650E+01									100	100	100	11	0	0	0	0	0	0	0	0	0	0	0
10	4.74	1.000E+02										100	100	11	0	0	0	0	0	0	0	0	0	0	0
11	4.74	2.150E+02											100	11	0	0	0	0	0	0	0	0	0	0	0
12	12.77	4.650E+02												100	98	98	61	95	10	15	21	38	12	0	0
13	19.52	1.000E+03													100	95	56	90	9	14	20	36	11	0	0
14	17.86	2.150E+03														100	64	99	10	16	22	39	12	0	0
15	21.33	4.650E+03															100	66	9	13	18	33	10	0	0
16	15.77	1.000E+04																100	12	27	25	45	14	0	0
17	54.69	2.150E+04																	100	6	7	13	4	0	0
18	35.57	4.650E+04																		100	11	20	6	0	0
19	25.55	1.000E+05																			100	28	9	0	0
20	14.19	2.000E+05																				100	17	0	0
21	14.43	4.000E+05																					100	95	95
22	20.00	8.000E+05																						100	100
23	20.00	1.400E+06																							100
24	20.00	2.500E+06																							
25	15.62	4.000E+06																							
26	25.00	6.500E+06																							
27	25.00	1.050E+07																							

CROSS-SECTION NAME : AL27A52 MAT-NUMBER : 6313

X-SECTION CORRELATION MATRIX (4 X 4)

GROUP NO	REL.SDEV (PT)	ENERGY (EV)	UPPER TRIANGLE			
24	44.72	2.500E+06	100	76	86	73
25	7.63	4.000E+06		100	95	69
26	5.94	6.500E+06			100	79
27	3.94	1.050E+07				100

CROSS-SECTION NAME : AL27P52 MAT-NUMBER : 6313

X-SECTION CORRELATION MATRIX (5 X 5)

GROUP NO	REL.SDEV (PT)	ENERGY (EV)	UPPER TRIANGLE				
23	25.26	1.400E+06	100	76	67	0	0
24	12.84	2.500E+06		100	68	0	0
25	6.68	4.000E+06			100	27	0
26	7.55	6.500E+06				100	60
27	11.55	1.050E+07					100

CROSS-SECTION NAME : S32P52 MAT-NUMBER : 6439

X-SECTION CORRELATION MATRIX (6 X 6)

GROUP NO	REL.SDEV (PT)	ENERGY (EV)	UPPER TRIANGLE					
22	.00	8.300E+05	0	0	0	0	0	0
23	14.80	1.400E+06	100	36	0	0	0	
24	13.99	2.500E+06		100	27	0	0	
25	9.49	4.000E+06			100	15	0	
26	9.31	6.500E+06				100	15	
27	10.82	1.050E+07					100	

CROSS-SECTION NAME : SC45G52 MAT-NUMBER : 6426

X-SECTION CORRELATION MATRIX (27 X 27) UPPER TRIANGLE

GROUP NO	REL.SDEV (PT)	ENERGY (EV)																									
1	.82	1.000E-04	100	95	95	95	95	95	95	95	95	95	95	95	95	38	20	12	11	27	28	21	5	0	0	0	0	0
2	1.14	2.150E-01	100	100	100	100	100	100	100	100	100	100	100	100	100	43	25	15	14	33	34	26	7	0	0	0	0	0
3	1.14	4.650E-01	100	100	100	100	100	100	100	100	100	100	100	100	100	43	25	15	14	33	34	26	7	0	0	0	0	0
4	1.14	1.000E+00	100	100	100	100	100	100	100	100	100	100	100	100	100	43	25	15	14	33	34	26	7	0	0	0	0	0
5	1.14	2.150E+00	100	100	100	100	100	100	100	100	100	100	100	100	100	43	25	15	14	33	34	26	7	0	0	0	0	0
6	1.14	4.650E+00	100	100	100	100	100	100	100	100	100	100	100	100	100	43	25	15	14	33	34	26	7	0	0	0	0	0
7	1.14	1.000E+01	100	100	100	100	100	100	100	100	100	100	100	100	100	43	25	15	14	33	34	26	7	0	0	0	0	0
8	1.14	2.150E+01	100	100	100	100	100	100	100	100	100	100	100	100	100	43	25	15	14	33	34	26	7	0	0	0	0	0
9	1.14	4.650E+01	100	100	100	100	100	100	100	100	100	100	100	100	100	43	25	15	14	33	34	26	7	0	0	0	0	0
10	1.14	1.000E+02	100	100	100	100	100	100	100	100	100	100	100	100	100	43	25	15	14	33	34	26	7	0	0	0	0	0
11	1.14	2.150E+02	100	100	100	100	100	100	100	100	100	100	100	100	100	43	25	15	14	33	34	26	7	0	0	0	0	0
12	1.14	4.650E+02	100	100	100	100	100	100	100	100	100	100	100	100	100	43	25	15	14	33	34	26	7	0	0	0	0	0
13	1.14	1.000E+03	100	100	100	100	100	100	100	100	100	100	100	100	100	43	25	15	14	33	34	26	7	0	0	0	0	0
14	1.14	2.150E+03	100	100	100	100	100	100	100	100	100	100	100	100	100	43	25	15	14	33	34	26	7	0	0	0	0	0
15	2.32	4.650E+03	100	100	100	100	100	100	100	100	100	100	100	100	100	43	25	15	14	33	34	26	7	0	0	0	0	0
16	3.55	1.000E+04	100	97	7	7	16	17	13	3	0	0	0	0	0													
17	5.92	2.150E+04	100	22	6	11	11	8	2	0	0	0	0	0	0													
18	6.47	4.650E+04	100	12	6	7	5	1	0	0	0	0	0															
19	2.64	1.000E+05	100	6	6	5	1	0	0	0	0	0																
20	2.60	2.150E+05	100	36	11	3	0	0	0	0	0																	
21	3.40	4.000E+05	100	38	3	0	0	0	0	0																		
22	6.03	8.000E+05	100	2	0	0	0	0	0																			
23	8.89	1.400E+06	100	81	81	80	12	12																				
24	8.89	2.500E+06	100	100	100	15	15																					
25	8.36	4.000E+06	100	100	15	15																						
26	10.68	6.500E+06	100	24	24																							
27	10.65	1.050E+07	100	100																								
			100																									

CROSS-SECTION NAME : TI46P52

MAT-NUMBER : 6427

X-SECTION CORRELATION MATRIX (5 X 5)

GROUP NO	REL.SDEV (PT)	ENERGY (EV)
23	12.79	1.400E+06
24	12.81	2.500E+06
25	12.81	4.000E+06
26	12.63	6.500E+06
27	14.14	1.050E+07

UPPER TRIANGLE

100	100	100	100	55	
	100	100	100	55	
		100	100	55	
			100	58	
				100	

CROSS-SECTION NAME : TI47NP52

MAT-NUMBER : 6428

X-SECTION CORRELATION MATRIX (1 X 1)

GROUP NO	REL.SDEV (PT)	ENERGY (EV)
27	30.00	1.050E+07

UPPER TRIANGLE

100

CROSS-SECTION NAME : TI47P52

MAT-NUMBER : 6428

X-SECTION CORRELATION MATRIX (7 X 7)

GROUP NO	REL.SDEV (PT)	ENERGY (EV)
21	.00	4.000E+05
22	11.31	8.500E+05
23	11.31	1.400E+06
24	11.31	2.500E+06
25	11.31	4.000E+06
26	11.13	6.500E+06
27	12.81	1.050E+07

UPPER TRIANGLE

0	0	0	0	0	0	0
100	100	100	100	100	44	
	100	100	100	100	44	
		100	100	100	44	
			100	100	44	
				100	47	
					100	

CROSS-SECTION NAME : TI48NP52

MAT-NUMBER : 6429

X-SECTION CORRELATION MATRIX (1 X 1)

GROUP NO	PEL.SDEV (PT)	ENERGY (EV)	UPPER TRIANGLE
27	30.00	1.050E+07	100

CROSS-SECTION NAME : TI48P52

MAT-NUMBER : 6429

X-SECTION CORRELATION MATRIX (4 X 4)

GROUP NO	PEL.SDEV (PT)	ENERGY (EV)	UPPER TRIANGLE
24	11.30	2.500E+06	100 100 100 44
25	11.31	4.000E+06	100 100 44
26	10.91	6.500E+06	100 51
27	12.81	1.050E+07	100

CROSS-SECTION NAME : MN55252

MAT-NUMBER : 6325

X-SECTION CORRELATION MATRIX (2 X 2)

GROUP NO	PEL.SDEV (PT)	ENERGY (EV)	UPPER TRIANGLE
26	27.37	6.500E+06	100 66
27	12.91	1.050E+07	100

CROSS-SECTION NAME : FE54P52

MAT-NUMBER : 6430

X-SECTION CORRELATION MATRIX (10 X 10)

UPPER TRIANGLE

GROUP NO	REL.SDEV (PT)	ENERGY (EV)									
18	15.81	4.650E+04									
19	15.81	1.000E+05	100	100	100	100	63	24	5	13	10	11
20	15.81	2.000E+05		100	100	100	63	24	5	13	10	11
21	15.81	4.000E+05			100	100	63	24	5	13	10	11
22	7.30	8.100E+05				100	63	24	5	13	10	11
23	4.44	1.400E+06					100	61	31	29	23	18
24	4.69	2.500E+06						100	94	56	40	29
25	3.75	4.000E+06							100	55	38	27
26	3.53	6.500E+06								100	69	38
27	4.30	1.050E+07									100	70
												100

CROSS-SECTION NAME : FE56P52

MAT-NUMBER : 6431

X-SECTION CORRELATION MATRIX (4 X 4)

UPPER TRIANGLE

GROUP NO	REL.SDEV (PT)	ENERGY (EV)				
24	10.01	2.500E+06				
25	6.36	4.000E+06	100	47	28	21
26	4.68	6.500E+06		100	63	47
27	3.36	1.050E+07			100	81
						100

CROSS-SECTION NAME : FE58G52

X-SECTION CORRELATION MATRIX (27 X 27) UPPER TRIANGLE

GROUP NO	REL.SDEV (PT)	ENERGY (EV)																								
1	5.97	1.000E-04	100	100	100	100	100	100	100	99	91	26	21	14	2	0	0	0	0	0	1	1	1	0	0	0	0	0	0
2	5.95	2.150E-01		100	100	100	100	100	100	99	91	27	21	14	2	0	0	0	0	0	1	1	1	0	0	0	0	0	0
3	5.94	4.650E-01			100	100	100	100	100	99	91	27	21	14	2	0	0	0	0	0	1	1	1	0	0	0	0	0	0
4	5.93	1.000E+00				100	100	100	100	99	91	27	21	15	2	0	0	0	0	0	1	1	1	0	0	0	0	0	0
5	5.91	2.150E+00					100	100	100	99	91	27	22	15	2	0	0	0	0	0	1	1	1	0	0	0	0	0	0
6	5.89	4.650E+00						100	100	99	92	29	23	15	2	0	0	0	0	0	1	1	1	0	0	0	0	0	0
7	5.84	1.000E+01							100	100	93	31	26	16	2	0	0	0	0	0	1	1	1	0	0	0	0	0	0
8	5.81	2.150E+01								100	96	38	33	19	2	0	0	1	0	0	1	1	1	0	0	0	0	0	0
9	6.24	4.650E+01									100	58	53	26	2	0	0	1	0	0	0	0	0	0	0	0	0	0	0
10	39.93	1.000E+02										100	64	14	1	-1	-2	-1	-1	-1	0	0	0	0	0	0	0	0	-1
11	24.33	2.150E+02											100	40	1	-4	-11	-9	-5	-5	-1	-1	-1	-2	-1	-1	-1	-1	-3
12	15.16	4.650E+02												100	88	83	41	33	22	21	-26	-26	-26	-22	-12	-12	-12	-12	-2
13	15.17	1.000E+03													100	97	50	41	26	26	-30	-30	-30	-25	-14	-14	-14	-14	-1
14	14.71	2.150E+03														100	70	57	26	25	-33	-39	-39	-31	-17	-17	-17	-17	-1
15	21.28	4.650E+03															100	80	15	13	-49	-49	-49	-38	-20	-20	-20	-20	0
16	26.33	1.000E+04																100	12	11	-39	-39	-39	-31	-17	-17	-17	-16	0
17	17.75	2.150E+04																	100	100	0	0	0	-18	-21	-21	-21	-21	0
18	17.89	4.650E+04																		100	0	0	0	-17	-21	-21	-21	-21	0
19	30.82	1.000E+05																			100	100	100	58	17	17	17	16	1
20	30.82	2.000E+05																				100	100	58	17	17	17	16	1
21	30.82	4.000E+05																					100	58	17	17	17	16	1
22	33.38	6.000E+05																						100	90	90	90	90	23
23	52.92	1.400E+06																							100	100	100	100	27
24	52.92	2.500E+06																								100	100	100	27
25	52.92	4.000E+06																									100	100	27
26	92.11	6.500E+06																										100	30
27	78.10	1.050E+07																											100

CROSS-SECTION NAME : C059252 MAT-NUMBER : 6327

X-SECTION CORRELATION MATRIX (1 X 1) UPPER TRIANGLE

GROUP NO	REL.SDEV (PT)	ENERGY (EV)	
27	20.92	1.05CE+07	100

CROSS-SECTION NAME : C059G52 MAT-NUMBER : 6327

X-SECTION CORRELATION MATRIX (27 X 27) UPPER TRIANGLE

GROUP NO	REL.SDEV (PT)	ENERGY (EV)																								
1	.65	1.000E-04	100	94	94	94	94	94	94	94	94	94	94	94	94	35	7	4	4	11	10	8	2	0	0	0	0	0
2	.77	2.150E-01	100	100	100	100	100	100	100	100	100	100	100	100	100	39	10	6	6	15	15	12	2	0	0	0	0	0
3	.77	4.650E-01		100	100	100	100	100	100	100	100	100	100	100	100	39	10	6	6	15	15	12	2	0	0	0	0	0
4	.77	1.000E+00			100	100	100	100	100	100	100	100	100	100	100	39	10	6	6	15	15	12	2	0	0	0	0	0
5	.77	2.150E+00				100	100	100	100	100	100	100	100	100	100	39	10	6	6	15	15	12	2	0	0	0	0	0
6	.77	4.650E+00					100	100	100	100	100	100	100	100	100	39	10	6	6	15	15	12	2	0	0	0	0	0
7	.77	1.000E+01						100	100	100	100	100	100	100	100	39	10	6	6	15	15	12	2	0	0	0	0	0
8	.77	2.150E+01							100	100	100	100	100	100	100	39	10	6	6	15	15	12	2	0	0	0	0	0
9	.77	4.650E+01								100	100	100	100	100	100	39	10	6	6	15	15	12	2	0	0	0	0	0
10	.77	1.000E+02									100	100	100	100	100	39	10	6	6	15	15	12	2	0	0	0	0	0
11	.77	2.150E+02										100	100	100	100	39	10	6	6	15	15	12	2	0	0	0	0	0
12	.77	4.650E+02											100	100	100	39	10	6	6	15	15	12	2	0	0	0	0	0
13	.77	1.000E+03												100	100	39	10	6	6	15	15	12	2	0	0	0	0	0
14	.77	2.150E+03													100	39	10	6	6	15	15	12	2	0	0	0	0	0
15	1.58	4.650E+03														100	39	10	6	6	15	15	12	2	0	0	0	0	0
16	3.69	1.000E+04															100	95	3	3	8	7	6	1	0	0	0	0	0
17	5.86	2.150E+04																100	10	2	3	3	3	0	0	0	0	0	0
18	6.25	4.650E+04																	100	12	2	2	2	0	0	0	0	0	0
19	2.44	1.000E+05																		100	2	2	1	0	0	0	0	0	0
20	2.52	2.000E+05																			100	29	4	1	0	0	0	0	0
21	3.19	4.000E+05																				100	39	1	0	0	0	0	0
22	6.19	8.000E+05																					100	1	0	0	0	0	0
23	8.64	1.400E+06																						100	89	89	88	10	10
24	8.66	2.500E+06																							100	100	100	11	11
25	8.15	4.000E+06																								100	100	11	11
26	10.49	6.500E+06																									100	20	20
27	10.47	1.050E+07																										100	100
																													100

CROSS-SECTION NAME : C059A52

MAT-NUMBER : 6327

X-SECTION CORRELATION MATRIX (3 X 3)

UPPER TRIANGLE

GROUP NO	REL.SDEV (PT)	ENERGY (EV)			
25	8.94	4.000E+06	100	45	21
26	4.58	6.500E+06		100	46
27	4.87	1.050E+07			100

CROSS-SECTION NAME : NI58252

MAT-NUMBER : 6433

X-SECTION CORRELATION MATRIX (1 X 1)

UPPER TRIANGLE

GROUP NO	REL.SDEV (PT)	ENERGY (EV)	
27	10.92	1.050E+07	100

CROSS-SECTION NAME : NI58P52

MAT-NUMBER : 6433

X-SECTION CORRELATION MATRIX (10 X 10)

UPPER TRIANGLE

GROUP NO	REL.SDEV (PT)	ENERGY (EV)									
18	1.00	4.650E+04	100	100	100	1	0	0	0	0	0	0
19	1.00	1.000E+05		100	100	1	0	0	0	0	0	0
20	1.00	2.000E+05			100	1	0	0	0	0	0	0
21	14.45	4.000E+05				100	59	22	0	0	0	0
22	13.22	8.000E+05					100	55	0	0	0	0
23	8.33	1.400E+06						100	83	30	32	19
24	10.30	2.500E+06							100	36	39	23
25	6.74	4.000E+06								100	64	35
26	6.23	6.500E+06									100	41
27	9.38	1.050E+07										100

CROSS-SECTION NAME : NI60P52

MAT-NUMBER : 6434

X-SECTION CORRELATION MATRIX (5 X 5)

GROUP NO	REL.SDEV (PT)	ENERGY (EV)
23	7.65	1.400E+06
24	7.65	2.500E+06
25	7.42	4.000E+06
26	7.76	6.500E+06
27	8.83	1.050E+07

UPPER TRIANGLE

100	100	89	51	0
	100	89	51	0
		100	80	0
			100	13
				100

CROSS-SECTION NAME : CU63A52

MAT-NUMBER : 6435

X-SECTION CORRELATION MATRIX (5 X 5)

GROUP NO	REL.SDEV (PT)	ENERGY (EV)
23	14.89	1.400E+06
24	14.75	2.500E+06
25	6.93	4.000E+06
26	5.58	6.500E+06
27	5.97	1.050E+07

UPPER TRIANGLE

100	54	31	17	7
	100	44	25	11
		100	66	27
			100	55
				100

CROSS-SECTION NAME : CU63352 MAT-NUMBER : 6435

X-SECTION CORRELATION MATRIX (27 X 27) UPPER TRIANGLE

GROUP NO	REL.SDEV (PT)	ENERGY (EV)																									
1	2.00	1.000E-04	100	100	100	0	0	0	0	0	0	0	0	0	0	0	0	0	0	0	0	0	0	0	0	0	0
2	2.00	2.150E-01		100	100	0	0	0	0	0	0	0	0	0	0	0	0	0	0	0	0	0	0	0	0	0	0
3	2.00	4.650E-01			100	0	0	0	0	0	0	0	0	0	0	0	0	0	0	0	0	0	0	0	0	0	0
4	5.00	1.000E+00				100	100	100	0	0	0	0	0	0	0	0	0	0	0	0	0	0	0	0	0	0	0
5	5.00	2.150E+00					100	100	0	0	0	0	0	0	0	0	0	0	0	0	0	0	0	0	0	0	0
6	5.00	4.650E+00						100	0	0	0	0	0	0	0	0	0	0	0	0	0	0	0	0	0	0	0
7	1.65	1.000E+01							100	100	98	91	62	17	61	12	6	2	0	0	0	0	0	0	0	0	0
8	1.70	2.150E+01								100	99	93	65	19	65	12	7	2	0	0	0	0	0	0	0	0	0
9	1.85	4.650E+01									100	97	72	23	73	14	7	2	0	0	0	0	0	0	0	0	0
10	2.27	1.000E+02										100	83	34	81	15	8	2	0	0	0	0	0	0	0	0	0
11	3.79	2.150E+02											100	76	60	11	5	1	0	0	0	0	0	0	0	0	0
12	5.16	4.650E+02												100	0	0	0	0	0	0	0	0	0	0	0	0	0
13	12.14	1.000E+03													100	15	0	0	0	0	0	0	0	0	0	0	0
14	6.62	2.150E+03														100	1	0	0	0	0	0	0	0	0	0	0
15	4.55	4.650E+03															100	2	0	0	0	0	0	0	0	0	0
16	4.78	1.000E+04																100	78	5	0	0	0	0	0	0	0
17	10.00	2.150E+04																	100	6	0	0	0	0	0	0	0
18	17.82	4.650E+04																		100	100	100	100	100	100	100	100
19	20.00	1.000E+05																			100	100	100	100	100	100	100
20	20.00	2.000E+05																				100	100	100	100	100	100
21	20.00	4.000E+05																					100	100	100	100	100
22	20.00	8.000E+05																						100	100	100	100
23	20.00	1.400E+06																							100	100	100
24	20.00	2.500E+06																								100	100
25	20.00	4.000E+06																									100
26	20.00	6.500E+06																									
27	20.00	1.050E+07																									

CROSS-SECTION NAME : CU65252 MAT-NUMBER : 6436

X-SECTION CORRELATION MATRIX (2 X 2)

GROUP NO	REL.SDEV (PT)	ENERGY (EV)	UPPER TRIANGLE
26	.00	6.500E+06	0 0
27	7.41	1.350E+07	100

CROSS-SECTION NAME : IN115G52 MAT-NUMBER : 6437

X-SECTION CORRELATION MATRIX (27 X 27) UPPER TRIANGLE

GROUP NO	ELL.SDEV (PI)	ENERGY (EV)																								
1	5.00	1.000E-04	100	100	100	100	100	100	100	100	100	100	100	100	0	0	0	0	0	0	0	0	0	0	0	0
2	5.00	2.150E-01	100	100	100	100	100	100	100	100	100	100	100	100	0	0	0	0	0	0	0	0	0	0	0	0
3	6.00	4.650E-01		100	100	100	100	100	100	100	100	100	100	100	0	0	0	0	0	0	0	0	0	0	0	0
4	5.00	1.000E+00			100	100	100	100	100	100	100	100	100	100	0	0	0	0	0	0	0	0	0	0	0	0
5	6.00	2.150E+00				100	100	100	100	100	100	100	100	100	0	0	0	0	0	0	0	0	0	0	0	0
6	6.00	4.650E+00					100	100	100	100	100	100	100	100	0	0	0	0	0	0	0	0	0	0	0	0
7	6.00	1.000E+01						100	100	100	100	100	100	100	0	0	0	0	0	0	0	0	0	0	0	0
8	6.00	2.150E+01							100	100	100	100	100	100	0	0	0	0	0	0	0	0	0	0	0	0
9	5.00	4.650E+01								100	100	100	100	100	0	0	0	0	0	0	0	0	0	0	0	0
10	5.00	1.000E+02									100	100	100	100	0	0	0	0	0	0	0	0	0	0	0	0
11	5.00	2.150E+02										100	100	100	0	0	0	0	0	0	0	0	0	0	0	0
12	5.00	4.650E+02											100	100	0	0	0	0	0	0	0	0	0	0	0	0
13	15.00	1.000E+03												100	0	0	0	0	0	0	0	0	0	0	0	0
14	15.00	2.150E+03													100	100	100	0	0	0	0	0	0	0	0	0
15	15.00	4.650E+03														100	100	0	0	0	0	0	0	0	0	0
16	9.00	1.000E+04															100	0	0	0	0	0	0	0	0	0
17	9.00	2.150E+04																100	100	100	0	0	0	0	0	0
18	9.00	4.650E+04																	100	100	0	0	0	0	0	0
19	5.00	1.000E+05																		100	0	0	0	0	0	0
20	5.00	2.000E+05																			100	100	100	42	0	0
21	5.00	4.000E+05																				100	100	42	0	0
22	4.60	8.000E+05																					100	42	0	0
23	7.00	1.400E+06																						100	91	91
24	7.00	2.500E+06																							100	100
25	13.00	4.000E+06																								100
26	13.00	6.500E+06																								
27	13.00	1.950E+07																								

CROSS-SECTION NAME : IN115N52

MAT-NUMBER : 6437

X-SECTION CORRELATION MATRIX (8 X 8)

GROUP NO	REL.SDEV (PT)	ENERGY (EV)
20	31.62	2.000E+05
21	15.84	4.000E+05
22	13.05	8.000E+05
23	14.14	1.400E+06
24	11.97	2.500E+06
25	12.62	4.000E+06
26	11.66	6.500E+06
27	11.40	1.050E+07

UPPER TRIANGLE

100	35	24	22	26	25	27	28
	100	71	45	53	50	54	55
		100	94	90	61	66	67
			100	92	56	61	62
				100	84	72	73
					100	69	70
						100	99
							100

CROSS-SECTION NAME : I127252

MAT-NUMBER : 6438

X-SECTION CORRELATION MATRIX (2 X 2)

GROUP NO	REL.SDEV (PT)	ENERGY (EV)
26	17.96	6.500E+06
27	17.45	1.050E+07

UPPER TRIANGLE

100	89
	100

CROSS-SECTION NAME : AU197G52 MAT-NUMBER : 6379

X-SECTION CORRELATION MATRIX (27 X 27) UPPER TRIANGLE

GROUP NO	REL.SDEV (PT)	ENERGY (EV)																							
1	.73	1.000E-04	100	82	82	82	28	26	26	26	25	26	26	10	8	8	8	8	8	9	11	13	28	3	0	0	0	0	0
2	1.02	2.150E-01		100	100	100	33	31	31	31	31	31	31	12	10	10	10	10	10	11	14	16	33	3	0	0	0	0	0
3	1.02	4.650E-01			100	100	33	31	31	31	31	31	31	12	10	10	10	10	10	11	14	16	33	3	0	0	0	0	0
4	1.02	1.000E+00				100	33	31	31	31	31	31	31	12	10	10	10	10	10	11	14	16	33	3	0	0	0	0	0
5	2.94	2.150E+00					100	100	100	100	100	100	100	10	3	3	4	3	3	4	5	6	12	1	0	0	0	0	0
6	3.16	4.650E+00						100	100	100	100	100	100	10	3	3	3	3	3	4	4	5	11	1	0	0	0	0	0
7	3.16	1.000E+01							100	100	100	100	100	10	3	3	3	3	3	4	4	5	11	1	0	0	0	0	0
8	3.16	2.150E+01								100	100	100	100	10	3	3	3	3	3	4	4	5	11	1	0	0	0	0	0
9	3.16	4.650E+01									100	100	100	10	3	3	3	3	3	4	4	5	11	1	0	0	0	0	0
10	3.16	1.000E+02										100	100	10	3	3	3	3	3	4	4	5	11	1	0	0	0	0	0
11	3.16	2.150E+02											100	10	3	3	3	3	3	4	4	5	11	1	0	0	0	0	0
12	6.37	4.650E+02												100	10	3	3	3	3	4	4	5	11	1	0	0	0	0	0
13	10.05	1.000E+03													100	100	100	5	1	1	1	2	2	4	0	0	0	0	0
14	10.05	2.150E+03														100	100	5	1	1	1	1	2	3	0	0	0	0	0
15	9.69	4.650E+03															100	5	1	1	1	1	2	3	0	0	0	0	0
16	10.05	1.000E+04																100	100	100	99	1	2	4	0	0	0	0	0
17	10.05	2.150E+04																	100	100	99	1	2	3	0	0	0	0	0
18	8.97	4.650E+04																		100	99	1	2	3	0	0	0	0	0
19	7.07	1.000E+05																			100	2	2	4	0	0	0	0	0
20	6.06	2.150E+05																				100	2	5	0	0	0	0	0
21	2.93	4.000E+05																					100	72	1	0	0	0	0
22	12.28	8.000E+05																						100	19	11	0	0	0
23	20.40	1.400E+06																							100	99	93	85	95	76
24	20.29	2.500E+06																								100	97	88	88	78
25	22.30	4.000E+06																									100	88	88	79
26	22.32	6.500E+06																										100	100	72
27	24.99	1.050E+07																											100	72
																														100

CROSS-SECTION NAME : TH232F52 MAT-NUMBER : 6390

X-SECTION CORRELATION MATRIX (7 X 7) UPPER TRIANGLE

GROUP NO	REL.SDEV (PT)	ENERGY (EV)						
21	30.53	4.000E+05	100	8	8	9	7	5	5
22	6.59	8.000E+05		100	38	46	36	23	23
23	6.32	1.400E+06			100	86	37	23	23
24	5.30	2.500E+06				100	45	28	28
25	6.76	4.000E+06					100	37	37
26	10.77	6.500E+06						100	100
27	10.77	1.050E+07							100

CROSS-SECTION NAME : TH232G52 MAT-NUMBER : 6390

X-SECTION CORRELATION MATRIX (27 X 27) UPPER TRIANGLE

GROUP NO	REL.SDEV (PT)	ENERGY (EV)																						
1	4.17	1.000E-04	100	99	99	99	99	99	1	0	0	0	0	0	0	0	0	0	0	0	0	0	0	0
2	8.00	2.150E-01	100	100	100	100	100		1	0	0	0	0	0	0	0	0	0	0	0	0	0	0	0
3	8.00	4.650E-01	100	100	100	100			1	0	0	0	0	0	0	0	0	0	0	0	0	0	0	0
4	8.00	1.000E+00	100	100	100				1	0	0	0	0	0	0	0	0	0	0	0	0	0	0	0
5	8.00	2.150E+00	100	100					1	0	0	0	0	0	0	0	0	0	0	0	0	0	0	0
6	8.00	4.650E+00	100						1	0	0	0	0	0	0	0	0	0	0	0	0	0	0	0
7	11.18	1.000E+01							100	100	100	100	100	100	100	100	100	100	100	100	48	11	11	11	11	11
8	11.18	2.150E+01								100	100	100	100	100	100	100	100	100	100	100	48	11	11	11	11	11
9	11.18	4.650E+01									100	100	100	100	100	100	100	100	100	100	48	11	11	11	11	11
10	11.18	1.000E+02										100	100	100	100	100	100	100	100	100	48	11	11	11	11	11
11	11.18	2.150E+02											100	100	100	100	100	100	100	100	48	11	11	11	11	11
12	11.18	4.650E+02												100	100	100	100	100	100	100	48	11	11	11	11	11
13	11.18	1.000E+03													100	100	100	100	100	100	48	11	11	11	11	11
14	11.18	2.150E+03														100	100	100	100	100	48	11	11	11	11	11
15	11.18	4.650E+03															100	100	100	100	48	11	11	11	11	11
16	11.18	1.000E+04																100	100	100	48	11	11	11	11	11
17	11.18	2.150E+04																	100	100	48	11	11	11	11	11
18	11.18	4.650E+04																		100	48	11	11	11	11	11
19	11.18	1.000E+05																			48	11	11	11	11	11
20	11.18	2.000E+05																			48	11	11	11	11	11
21	11.18	4.650E+05																			48	11	11	11	11	11
22	12.95	8.000E+05																			48	11	11	11	11	11
23	20.62	1.400E+06																			100	92	92	92	92	92
24	20.62	2.500E+06																				100	100	100	100	100
25	20.62	4.000E+06																					100	100	100	100
26	20.62	6.500E+06																						100	100	100
27	20.62	1.050E+07																							100	100
																										100

CROSS-SECTION NAME : 0235F52 MAT-NUMBER : 6395

X-SECTION CORRELATION MATRIX (27 X 27) UPPER TRIANGLE

GROUP NO	FLL.SDEV (PT)	ENERGY (EV)																								
1	.32	1.000E-04																								
	100	100	39	14	14	12	12	11	10	10	10	10	5	6	6	9	7	5	0	0	0	0	0	0	0	0
2	.32	2.150E-01																								
		100	39	14	14	12	12	11	10	10	10	10	5	6	6	9	7	5	0	0	0	0	0	0	0	0
3	.82	4.650E-01																								
			100	64	62	53	53	50	45	44	45	44	24	26	28	38	33	23	0	0	0	0	0	0	0	0
4	2.19	1.000E+00																								
				100	84	70	70	65	57	58	59	58	31	34	37	50	43	31	0	0	0	0	0	0	0	0
5	2.24	2.150E+00																								
					100	69	68	64	58	57	57	57	31	34	36	49	42	30	0	0	0	0	0	0	0	0
6	2.62	4.650E+00																								
						100	87	81	73	72	73	72	39	43	45	62	53	38	0	0	0	0	0	0	0	0
7	2.62	1.000E+01																								
							100	84	75	74	74	73	40	44	46	63	54	39	0	0	0	0	0	0	0	0
8	2.79	2.150E+01																								
								100	85	83	84	83	45	49	52	71	61	44	0	0	0	0	0	0	0	0
9	3.11	4.650E+01																								
									100	94	93	92	50	54	58	78	68	49	0	0	0	0	0	0	0	0
10	3.14	1.000E+02																								
										100	93	91	49	54	57	78	67	48	0	0	0	0	0	0	0	0
11	3.12	2.150E+02																								
											100	93	49	54	58	78	68	49	0	0	0	0	0	0	0	0
12	3.16	4.650E+02																								
												100	49	54	57	77	67	48	0	0	0	0	0	0	0	0
13	5.83	1.000E+03																								
													100	99	95	84	82	69	0	0	0	0	0	0	0	0
14	5.91	2.150E+03																								
														100	99	89	89	76	0	0	0	0	0	0	0	0
15	5.00	4.650E+03																								
															100	99	93	81	0	0	0	0	0	0	0	0
16	3.69	1.000E+04																								
																100	91	70	33	36	0	0	0	0	0	0
17	3.02	2.150E+04																								
																	100	93	40	44	0	0	0	0	0	0
18	2.97	4.650E+04																								
																		100	41	45	0	0	0	0	0	0
19	3.28	1.000E+05																								
																			100	40	44	31	10	7	0	0
20	3.00	2.150E+05																								
																				100	50	44	18	16	0	0
21	3.50	4.650E+05																								
																					100	77	33	25	5	5	0
22	2.32	1.000E+06																								
																						100	78	41	23	22	3
23	2.26	1.400E+06																								
																							100	77	40	40	16
24	3.00	2.500E+06																								
																								100	40	40	25
25	3.50	4.000E+06																								
																									100	100	45
26	3.45	6.500E+06																								
																										100	48
27	4.04	1.050E+07																								
																										100

CROSS-SECTION NAME : U238F52 MAT-NUMBER : 6398

X-SECTION CORRELATION MATRIX (27 X 27) UPPER TRIANGLE

GROUP NO	REL.SDEV (PT)	ENERGY (EV)																									
1	25.04	1.000E-04	100	100	100	6	6	6	6	6	6	6	6	0	0	0	0	0	0	1	1	1	3	4	4	3	3
2	25.04	2.150E-01		100	100	6	6	6	6	6	6	6	6	0	0	0	0	0	0	1	1	1	3	4	4	3	3
3	25.04	4.650E-01			100	6	6	6	6	6	6	6	6	0	0	0	0	0	0	1	1	1	3	4	4	3	3
4	1.50	1.000E+00				100	100	100	100	100	100	100	100	5	5	5	5	5	5	11	14	20	51	61	64	47	56
5	1.50	2.150E+00					100	100	100	100	100	100	100	5	5	5	5	5	5	11	14	20	51	61	64	47	56
6	1.50	4.650E+00						100	100	100	100	100	100	5	5	5	5	5	5	11	14	20	51	61	64	47	56
7	1.50	1.000E+01							100	100	100	100	100	5	5	5	5	5	5	11	14	20	51	61	64	47	56
8	1.50	2.150E+01								100	100	100	100	5	5	5	5	5	5	11	14	20	51	61	64	47	56
9	1.50	4.650E+01									100	100	100	5	5	5	5	5	5	11	14	20	51	61	64	47	56
10	1.50	1.000E+02										100	100	5	5	5	5	5	5	11	14	20	51	61	64	47	56
11	1.50	2.150E+02											100	5	5	5	5	5	5	11	14	20	51	61	64	47	56
12	1.50	4.650E+02												5	5	5	5	5	5	11	14	20	51	61	64	47	56
13	1.50	1.000E+03													100	100	5	5	5	11	14	20	51	61	64	47	56
14	30.03	2.150E+03														100	5	5	5	11	14	20	51	61	64	47	56
15	30.04	4.650E+03															100	100	100	100	100	100	98	1	1	3	3	3	2	3
16	30.04	1.000E+04																100	100	100	100	100	98	1	1	3	3	3	2	3
17	30.04	2.150E+04																	100	100	100	100	98	1	1	3	3	3	2	3
18	30.04	4.650E+04																		100	100	100	98	1	1	3	3	3	2	3
19	30.04	1.000E+05																			100	100	98	1	1	3	3	3	2	3
20	13.49	2.300E+05																				100	98	1	1	3	3	3	2	3
21	10.61	4.000E+05																					100	48	2	6	7	7	5	6
22	7.65	8.000E+05																						100	3	7	9	9	7	8
23	2.93	1.490E+06																							100	53	12	13	9	11
24	2.47	2.500E+06																								100	31	33	24	29
25	2.33	4.000E+06																									100	39	29	34
26	3.16	6.500E+06																										100	45	36
27	2.66	1.350E+07																											100	29
																														100

CROSS-SECTION NAME = U238G52 MAT-NUMBER = 6398

X-SECTION CORRELATION MATRIX (27 X 27) UPPER TRIANGLE

GROUP NO	E(LO)EV (PT)	ENERGY (EV)																							
1	.74	1.000E-04	100	100	100	0	0	0	0	0	0	0	0	0	0	0	0	0	0	0	0	0	0	0	0
2	.74	2.150E-01		100	100	0	0	0	0	0	0	0	0	0	0	0	0	0	0	0	0	0	0	0	0
3	.74	4.650E-01			100	0	0	0	0	0	0	0	0	0	0	0	0	0	0	0	0	0	0	0	0
4	4.60	1.000E+00				100	100	99	97	98	97	99	100	100	100	97	14	13	17	16	15	19	19	5	0	0	0	0	0
5	4.96	2.150E+00					100	99	96	98	96	98	100	100	100	97	13	12	16	15	14	18	17	5	0	0	0	0	0
6	3.64	4.650E+00						100	99	100	99	100	99	99	99	96	18	16	22	21	19	24	24	7	0	0	0	0	0
7	3.14	1.000E+01							100	100	100	100	96	96	96	94	20	19	25	24	22	28	27	8	0	0	0	0	0
8	3.37	2.150E+01								100	100	100	98	98	98	95	19	17	24	23	20	26	25	7	0	0	0	0	0
9	3.07	4.650E+01									100	100	96	96	96	94	21	19	26	25	22	28	26	8	0	0	0	0	0
10	3.44	1.000E+02										100	98	98	98	96	19	17	23	22	20	25	25	7	0	0	0	0	0
11	5.66	2.150E+02											100	100	100	97	13	12	16	15	14	17	17	5	0	0	0	0	0
12	5.00	4.650E+02												100	100	97	13	12	16	15	14	17	17	5	0	0	0	0	0
13	5.00	1.000E+03													100	97	13	12	16	15	14	17	17	5	0	0	0	0	0
14	4.56	2.150E+03														100	97	13	12	16	15	14	17	17	5	0	0	0	0	0
15	6.26	4.650E+03															100	35	20	27	26	23	30	29	13	5	5	4	2	2
16	5.84	1.000E+04																100	47	63	61	55	70	68	40	25	24	19	9	9
17	5.05	2.150E+04																	100	61	55	50	64	62	37	23	22	17	8	8
18	5.27	4.650E+04																		100	79	69	86	85	50	32	30	24	11	11
19	5.83	1.000E+05																			100	65	83	81	48	30	28	23	10	10
20	4.58	2.000E+05																				100	75	73	43	27	26	20	9	9
21	4.68	4.000E+05																					100	93	55	35	33	26	12	12
22	7.02	8.000E+05																						100	54	34	32	25	11	11
23	10.02	1.400E+06																							100	89	81	65	29	29
24	10.72	2.500E+06																								100	95	75	34	34
25	13.46	4.000E+06																									100	80	36	36
26	29.98	6.500E+06																										100	85	85
27	29.98	1.050E+07																											100	100
																														100

CROSS-SECTION NAME : NP237F52 MAT-NUMBER : 6337

X-SECTION CORRELATION MATRIX (27 X 27) UPPER TRIANGLE

GROUP NO	SIL.SOEV (PI)	ENERGY (EV)																								
1	.00	1.000E-04	0	0	0	0	0	0	0	0	0	0	0	0	0	0	0	0	0	0	0	0	0	0	0	0
2	46.59	2.150E-01	100	93	2	1	0	0	0	0	0	0	0	0	0	0	0	0	0	0	0	0	0	0	0	0
3	94.80	4.650E-01	100	2	1	0	0	0	0	0	0	0	0	0	0	0	0	0	0	0	0	0	0	0	0	0
4	38.33	1.000E+00	100	3	0	0	0	0	0	0	0	0	0	0	0	0	0	0	0	0	0	0	0	0	0	0
5	12.47	2.150E+00	100	0	0	0	0	0	0	0	0	0	0	0	0	0	0	0	0	0	0	0	0	0	0	0
6	******	4.650E+00	100	0	0	0	0	0	0	0	0	0	0	0	0	0	0	0	0	0	0	0	0	0	0	0
7	30.00	1.000E+01	100	100	100	100	100	100	100	100	100	100	100	100	0	0	0	0	0	0	0	0	0	0	0	0
8	30.00	2.150E+01		100	100	100	100	100	100	100	100	100	100	100	0	0	0	0	0	0	0	0	0	0	0	0
9	30.00	4.650E+01			100	100	100	100	100	100	100	100	100	100	0	0	0	0	0	0	0	0	0	0	0	0
10	30.00	1.000E+02				100	100	100	100	100	100	100	100	100	0	0	0	0	0	0	0	0	0	0	0	0
11	30.00	2.150E+02					100	100	100	100	100	100	100	100	0	0	0	0	0	0	0	0	0	0	0	0
12	30.00	4.650E+02						100	100	100	100	100	100	100	0	0	0	0	0	0	0	0	0	0	0	0
13	30.00	1.000E+03							100	100	100	100	100	100	0	0	0	0	0	0	0	0	0	0	0	0
14	30.00	2.150E+03								100	100	100	100	100	0	0	0	0	0	0	0	0	0	0	0	0
15	30.00	4.650E+03									100	100	100	100	0	0	0	0	0	0	0	0	0	0	0	0
16	30.00	1.000E+04										100	100	100	0	0	0	0	0	0	0	0	0	0	0	0
17	30.00	2.150E+04											100	100	0	0	0	0	0	0	0	0	0	0	0	0
18	30.00	4.650E+04												100	0	0	0	0	0	0	0	0	0	0	0	0
19	10.00	1.000E+05													0	0	0	0	0	0	0	0	0	0	0	0
20	10.00	2.300E+05													100	100	100	100	100	100	73	0	0	0	0	0
21	10.00	4.300E+05														100	100	100	100	100	73	0	0	0	0	0
22	10.00	8.400E+05															100	100	100	100	73	0	0	0	0	0
23	10.00	1.400E+06																100	100	100	73	0	0	0	0	0
24	10.00	2.500E+06																	100	100	73	0	0	0	0	0
25	8.44	4.000E+06																		100	73	0	0	0	0	0
26	15.00	6.500E+06																			100	69	69	69	69	69
27	15.00	1.050E+07																				100	100	100	100	100
																							100	100	100	100

CROSS-SECTION NAME : PU239F52 MAT-NUMBER : 6399

X-SECTION CORRELATION MATRIX (27 X 27) UPPER TRIANGLE

GROUP NO	REL.SDEV (PT)	ENERGY (EV)																								
1	.35	1.000E-04	100	127	93	0	0	0	0	0	0	0	0	0	0	0	0	0	0	0	0	0	0	0	0	0
2	.66	2.150E-01	-100	-102	0	0	0	0	0	0	0	0	0	0	0	0	0	0	0	0	0	0	0	0	0	0
3	.91	4.650E-01		-100	0	0	0	0	0	0	0	0	0	0	0	0	0	0	0	0	0	0	0	0	0	0
4	7.62	1.000E+00			100	100	100	100	100	100	100	82	12	12	12	12	12	14	10	9	14	13	17	17	14	13	13	11
5	7.62	2.150E+00				100	100	100	100	100	100	82	12	12	12	12	12	14	10	9	14	13	17	17	14	13	13	11
6	7.62	4.650E+00					100	100	100	100	100	82	12	12	12	12	12	14	10	9	14	13	17	17	14	13	13	11
7	7.62	1.000E+01						100	100	100	100	82	12	12	12	12	12	14	10	9	14	13	17	17	14	13	13	11
8	7.62	2.150E+01							100	100	100	82	12	12	12	12	12	14	10	9	14	13	17	17	14	13	13	11
9	7.62	4.650E+01								100	100	82	12	12	12	12	12	14	10	9	14	13	17	17	14	13	13	11
10	7.62	1.000E+02									100	82	12	12	12	12	12	14	10	9	14	13	17	17	14	13	13	11
11	6.13	2.150E+02										100	66	66	66	66	66	43	13	11	18	16	21	21	18	16	16	13
12	8.94	4.650E+02											100	100	100	100	100	55	9	7	12	11	14	15	12	11	11	9
13	8.94	1.000E+03												100	100	100	100	55	9	7	12	11	14	15	12	11	11	9
14	8.94	2.150E+03													100	100	100	55	9	7	12	11	14	15	12	11	11	9
15	8.94	4.650E+03														100	100	55	9	7	12	11	14	15	12	11	11	9
16	8.94	1.000E+04															100	55	9	7	12	11	14	15	12	11	11	9
17	7.41	2.150E+04																100	88	9	15	13	17	18	15	13	13	11
18	10.30	4.650E+04																	100	6	11	9	12	13	11	9	10	8
19	12.04	1.000E+05																		100	21	19	17	13	11	8	8	7
20	3.67	2.000E+05																			100	72	64	46	40	26	27	22
21	4.09	4.000E+05																				100	82	53	44	27	28	20
22	5.11	8.000E+05																					100	87	60	45	46	28
23	3.06	1.490E+06																						100	83	56	57	37
24	3.67	2.500E+06																							100	58	55	40
25	4.17	4.000E+06																								100	95	52
26	4.09	6.500E+06																									100	58
27	4.70	1.050E+07																										100

List of Participants

1. Dr. Bärs, B.
   Technical Research Centre of Finland
   Reactor Laboratory
   Otakaari 3A
   SF-02150 Espoo 15
   Finland

2. Dr. Dierckx, R.
   C.E.C. - Joint Research Centre
   Physics Division
   Ispra Establishment
   I-21020 Ispra (Varese)
   Italy

3. Dr. Greenwood, L.R.
   Chemical Technology Division
   Argonne National Laboratory
   9700 South Cass Avenue
   Argonne, Illinois 60439
   U.S.A.

4. Dr. Jin-Nan Yu
   Institute of Atomic Energy
   Beijing
   People's Rep. of China

5. Prof. Kanda, Y.
   Department of Energy Conversion Engineering
   Kyushu University
   33 Sakamoto, Kasuga
   Kasuga-Shi 816
   Japan

6. Dr. Mann, F.
   Hanford Engineering Development Laboratory
   P.O. Box 1970
   Richland, Washington 99352
   U.S.A.

7. Dr. Mannhart, W.
   Physikalisch Technische Bundesanstalt
   Abteilung 6
   Bundesallee 100
   D-3300 Braunschweig
   Fed. Rep. of Germany

8. Dr. Mattes, M.
   Institut fuer Kernenergetik der Universitaet Stuttgart
   Postfach 80 1140
   Pfaffenwaldring 31
   D-7000 Stuttgart 80
   Fed. Rep. of Germany

9.	Dr. MacFarlane, R.J.	Los Alamos National Laboratory P.O. Box 1663 Los Alamos, New Mexico 87545 U.S.A.
10.	Dr. Mizumoto, M.	Nuclear Physics II Laboratory Japan Atomic Energy Research Institute (JAERI) Tokai-Mura, Naka-Gun Ibaraki-Ken 319-11 Japan
11.	Dr. Najzer, M.	Institut Jozef Stefan Jamova 39 P.O. Box 199-4 YU-61001 Ljubljana Yugoslavia
12.	Dr. Savanonda, N.	Atomic Power Division Energy Technology Department Electricity Generating Authority of Thailand, Nonthaburi 11000 Thailand
13.	Dr. Prillinger, G.	Institut fuer Kernenergetik der Universitaet Stuttgart Pfaffenwaldring 31 D-7000 Stuttgart 80 Fed. Rep. of Germany
14.	Dr. Piksaikin, V.	Nuclear Data Section International Atomic Energy Agency Wagramerstrasse 5 P.O. Box 100 A-1400 Vienna Austria
15.	Dr. Reffo, G.	C.R.E.E. Clementel E.N.E.A. Via Mazzini 2 I-40138 Bologna Italy
16.	Dr. Thomas, A.F.	Rolls Royce & Associates P.O. Box 31 Raynes Way, Derby DE2 8BJ United Kingdom
17.	Dr. Zijp, W.L.	Netherlands Energy Research Foundation (ECN) P.O. Box 1 NL-1755 ZG Petten The Netherlands